Determining grain size distribution of pneumatically conveyed granular media using the passive acoustic measurement method

Doctoral Thesis

to be awarded the degree
Doctor of Engineering (Dr.-Ing.)

submitted by

M.Sc. Hamid Amrollahi

from Isfahan, Iran

approved by

Faculty of Energy and Management Science,

Clausthal University of Technology

Date of oral Examination

07th December 2016

Chairperson of the Board of Examiners:	Prof. Dr. rer. pol. W. Pfau
Chief Reviewers:	Prof. Dr.-Ing. habil. H. Tudeshki
	Prof. Dr. rer. nat. habil. B. Lehmann

To my parents,

my brothers,

and my wife, Maryam.

Komm, weil der Hoffnung Schlösser
so leicht und luftig sind,
Bring Wein! denn das Gebäude
des Lebens ruht auf Wind.

Dem Hochgesinnten dien ich,
der unterm blauen Dom
Frei hält sein Herz von jedem
verstrickenden Gebind'.

O Königsfalk', hochblickend
von Edens Zedern einst!
Dein Nisteplatz ist hier nicht
im Kummertalgewind'.

Von Paradieses Zinnen
sie rufen laut dir zu:
An diesem Ort der Netze,
was taumelst du so blind?

O mahn an festen Bund nicht
die ungebundne Welt!
Die alte Braut, sie wechselt
die Freier gar geschwind.

Ergib dich ins Gegebne,
und runzle nicht die Stirn!
Verschlossen mir und dir ist
die Tür der Wahl, o Kind.

Kein Glaub' ist bei dem Lächeln
der Rose, kein Verlaß;
Klag, Nachtigall! Stoff hast du
zu klagen ungelind.

Warum, o schlechter Reimer,
beneidest du Hafis!
Wohllaut und Sinnes Anmut
ist Himmels Eingebind'.

- Hafis
(übersetzt von Friedrich Rückert)

Abstract

Granular materials are present everywhere. Grain size distribution is the major property of each granular material. In practice, this property is determined mostly by sieve analysis. Sieve analysis has numerous disadvantages and limitations. Other available methods are not being used widely, often due to their shortcomings. Applying the passive acoustic measurement method for different purposes has been developed through the last decades. However, applying this method for quantifying grain size distribution has been rarely studied. The present research work experimentally investigates the use of the passive acoustic method for determining grain size distribution of granular materials. Sand has been selected as test material in this study. Extensive experimental programs have been conducted with different laboratory–scale pneumatic test rigs. Thereby, the effects of key parameters have been studied and the optimum experimental setup for grain size analysis has been determined. Parallel with that, in addition to suitable signal processing techniques, Partial Least Square Regression (PLSR) modeling has been applied for predicting the grain size distribution of tested sand samples using recorded acoustic data. Based on the obtained findings, a prototype laboratory device has been set up and tested over a longer period. The collected data from the prototype, together with the corresponding laboratory sieving results, have been used for PLSR modeling. The PLSR models have been verified using both full cross validation and data-splitting methods. Promising results with fair accuracy have been obtained. However, the results suggest that the current system must be further improved to become a reliable device for quantitative grain size analysis.

Zusammenfassung

Granulare Stoffe sind ubiquitär und die Korngrößenverteilung ist die Haupteigenschaft jedes granularen Materiales. Diese Eigenschaft wird in der Praxis normalerweise mittels der Siebanalyse bestimmt. Die Siebanalyse hat mehrere Nachteile und Beschränkungen, wie auch weitere vorhandenen Methoden, welche jedoch selten genutzt werden. Die Anwendung der passiven akustischen Messtechnik wurde in den letzten Jahrzehnten für verschiedene Einsatzgebiete entwickelt. Der Einsatz dieser Messtechnik ist allerdings kaum zur Bestimmung der Korngrößenverteilung von granularen Stoffen erforscht worden. Die vorliegende Forschungsarbeit untersucht experimentell die Weiterentwicklung der passiven akustischen Messtechnik zur Bestimmung der Korngrößenverteilung von granularen Stoffen. Sand wurde als Versuchsmaterial ausgewählt und umfangsreiche Versuchsprogramme wurden mit verschiedenen pneumatischen Laborversuchsanlagen ausgeführt. Hierbei wurden Einflüsse der Hauptfaktoren untersucht und die optimalen Versuchsbedingungen zur Bestimmung der Korngrößenverteilung festgelegt. Partial Least Square Regression (PLSR) sowie geeignete Signalbearbeitungsmethoden, wurde eingesetzt, um einen quantitativen Zusammenhang zwischen Korngrößenverteilung und akustischen Daten zu bilden. Basierend auf den gewonnenen Ergebnissen wurde anschließend der Prototyp eines Laborgerätes gebaut und über einen längeren Zeitraum evaluiert. Die aufgenommenen akustischen Datensätze, zusammen mit den entsprechenden Siebergebnissen, wurden zur PLSR-Modelbildung angesetzt. Die PLSR-Modelle wurden mittels full cross validation und data-splitting verifiziert. Vielversprechende Ergebnisse mit ausreichender Genauigkeit wurden erzielt. Die Ergebnisse zeigen, dass das vorgestellte System weiter optimiert werden sollte, um ein zuverlässiges Gerät zur routinemäßigen Bestimmung der Korngrößenverteilung zu erhalten.

Contents

List of Figures

List of tables

1 Introduction

The present Chapter briefly outlines the thesis scope as well as problem statement and motivation of the research. Aims of the study, its methodology, together with the structure of the thesis are summarized in this Chapter too.

This experimental research work has been carried at department of surface mining and international mining of the TU Clausthal.

The scope of the thesis involves using the passive acoustic measurement method (‘listening’) for determining grain size distribution of conveyed granular materials in a pneumatic line in laboratory–scale. Sand has been selected as test granular material. The thesis focuses on experimental programs conducted with different laboratory–scale pneumatic test rigs. Within the experimental programs, various parameters have been optimized and the effects of major factors have been investigated. Following the obtained findings, a prototype laboratory device has been set up and tested in long-term. Along with the experimental programs conducted with different laboratory–scale pneumatic test rigs as well as the prototype laboratory device, suitable signal processing techniques and statistical modeling method have been established to convert acoustic data into grain size distribution of tested granular materials.

Problem statement and motivation of the research work are summarized as the following into two main issues:

Firstly, the passive acoustic measurement method has outstanding advantages and vast applicability. However, employing this method for determining grain size distribution of granular materials has been so far rarely studied.

Secondly, current available grain size analysis techniques, particularly sieve analysis, are associated with limitations and drawbacks. Consequently, seeking for alternative grain size analyzing methods is important and appealing.

The above two issues motivated studying the passive acoustic measurement method with the aim of analyzing grain size distribution of granular materials.

The objectives of this research work are:

1) Generally, by presenting versatile practical findings, this study attempts to contribute to the current state-of-the-art of the passive acoustic measurement method.

2) Specifically concerning the thesis scope, it is intended to identify the major effective parameters and examine their influences on the results, document and discuss the obtained results, and draw valuable conclusions. Thus, the

aim of the study is providing comprehensive insight into the specified subject, which would be useful for future research works.

3) Considering the above mentioned motivation, this study attempts to experimentally evaluate the potential of acoustic method for grain size analysis and, identify its limitations as well.

4) Also, the aim of this study is to evaluate the performance of the established statistical multivariate modeling technique for estimating grain size distribution of granular materials using passive acoustic data.

To achieve the above mentioned goals, extensive experimental programs were conducted with various pneumatic test rigs in laboratory–scale. Primarily, a very simple provisional pneumatic test rig was used for the initial experiments. Afterwards, a horizontal test rig and then a vertical test rig were respectively used. The obtained results and findings from each experimental program were taken into consideration for setting up the next experimental program or test rig. This investigation methodology provided the possibility of systematically optimizing the specified condition(s) and simultaneously studying major parameters (objective 2). Additionally, valuable experimental results and practical findings were thereby attained (objective 1). Eventually, based on the conducted experimental programs with the test rigs, a prototype laboratory device was set up and tested in long-term. By this latter part of the study, the third and fourth objectives were also very well met.

In addition to the current Chapter, this thesis is comprised of 8 further Chapters. In the following, the content of each Chapter is briefly outlined:

Chapter 2 includes introductory subjects about granular materials. Grain size distribution is defined and its importance, as well as the methods for determining it, are presented.

Chapter 3 initially deals with the passive acoustic method. Basic physical concept, various operating components of a passive acoustic measurement system, together with the corresponding data analysis techniques are introduced. Furthermore, Chapter 3 introduces the statistical modeling method, which has been investigated within the present research work, and its related concepts.

The previous application cases of the passive acoustic method are reviewed in Chapter 4. In this Chapter, following the literature review, the most outstanding applied issues about the method are summarized and discussed.

Chapter 5 deals with the initial experimental programs. In this Chapter, the conducted experimental programs with the provisional pneumatic test rig are chronologically

described and thereby, the optimization steps of the sensor positioning, as well as other findings are reported.

Chapter 6 concerns the horizontal test rig. The conducted experimental programs with this test rig, which include the independent studies of air flow velocity and mass flow rate, are presented in this Chapter. Moreover, statistical modeling for estimating grain size distribution of the tested granular materials using recorded acoustic data is established and described in detail.

Chapter 7 is designated to the vertical test rig. The advantages of the vertical test rig over the horizontal one are outlined. The conducted experimental programs with the vertical test rig are chronologically presented.

Chapter 8 is dedicated to the prototype laboratory device. In this Chapter, the design parameters and components of the prototype as well as its long-term utilization are chronologically documented. The developed statistical models are evaluated in terms of their performances and the obtained results are statistically analyzed and discussed.

The main points concluded from the entire study are outlined in Chapter 9.

2 Granular materials

A granular material is commonly defined[1] as a collection of discrete, solid macroscopic grains. Characteristic feature of a granular material is energy loss as a result of interaction between its grains (e.g. collision). The size of a grain is regarded to vary from 1 μm to the size of asteroids. In the literature granular materials are also called granular media or matter (see e.g. [1]).

Granular materials are ubiquitous in our daily lives. Sugar, coffee, salt and cereals are a few instances just from our daily consumed foodstuffs. Granular materials are abundant in nature too. Many natural phenomena deal with granular materials. For example, amongst various geological activities, dune migration, erosion/deposition processes, landslides, *etc*. can be named. In terms of tonnage, granular materials are the second most manipulated material by man after water [2]. In mining, each year billion tons of sand and gravel, crushed and milled rock and mineral concentrate are handled and transported. Also in other industries such as construction, agriculture, food and pharmacy, chemistry, metallurgy *etc*., granular materials (powder, pellets, pills, beads *etc*.) are especially important.

Amongst various granular materials, sand and gravel is especially considerable in regards of its availability and applications. Every person in Germany, through his 70 years of life, needs 324 tons of sand and gravel [3]. This common granular material is the most needed raw material in Germany, even more than petroleum, lignite, steel *etc*. The reported statistics in Table 1 highlight the importance of sand and gravel in Germany. This huge amount of production is mainly used for concrete, foundation, water treatment, sport and playground, asphalt *etc*.

Table 1. Sand and gravel industry in Germany from the year 2011 [4].

Companies	Quarries/processing plants	Production (10^6 ton)	Turnover (billion €)	Employed
1130	2250	253	1.5	15800

Therefore, sand, known as a very common and frequently used granular material, was selected as test material in this research work.

[1] The common definition of granular materials can be found in numerous publications, e.g. [1] [126] [127] [128].

In this Chapter, grain size distribution, as the key property of every granular material is defined. Afterwards, different methods of determining this property are introduced. Moreover, some introductory concepts about pneumatic transport of granular materials are briefly presented.

2.1 Grain size distribution

Granular materials are often described by their grain size distribution. Grain size distribution represents the relative amount of material as a function of grain size. The relative amount of material is defined either by the number of grains, their mass, volume or surface area [5].

Grain size distribution is crucial when dealing with granular materials. It is important because almost every other property of a granular material is dependent from that. This property is essential for understanding and predicting different physical/chemical behaviors of a granular material. For example, reactivity of a granular material in chemical reactions is dependent from its grain size distribution. Also, this factor is a prerequisite for analyzing a system, in which granular materials are involved. Slope stability analyses in mining and construction can be named here as an instance.

Grain size distribution is a deciding factor for handling, packaging, transporting and storing the granular materials. For example, when a granular material becomes compacted in a silo, or is transported in a pneumatic/hydraulic line, this factor should be considered.

The quality of a product is highly influenced by grain size distribution of the granular materials, which it is made of. In this case, the production process itself is also affected by this factor. In many industries, such as powder metallurgy, concrete, ceramic, cosmetics, pharmacy *etc*., grain size distribution of raw granular materials should be therefore strictly monitored and controlled.

When speaking about a granular material as a product, its grain size distribution is particularly important. The selected test material in this thesis (i.e. sand), take as an example, is widely used for filtration, pavement, casting and, sports and recreational facilities. In all these areas, grain size distribution determines the performance and quality of the sand product. It is also important for controlling and optimizing the extraction and production processes of this granular material.

Due to the unique role of grain size distribution in various disciplines, measuring this parameter has been always of utmost importance and interest. Different available methods for determining this parameter are introduced in the following part.

2.2 Determining grain size distribution

2.2.1 Sieve analysis

The oldest and yet the most popular method for determining grain size distribution is sieve analysis which has changed very little over the past few decades. A sieve, in the most general sense, is a device designed to retain grains larger than a designated size, while allowing smaller grains to pass through it [6]. Within sieve analysis, a sample of granular material is separated through a stacked series of sieves, each sieve having smaller openings than the one above. The separation is usually succeeded through shaking the stacked series of sieves. Alternatively, the sample may be washed through with a non-reacting liquid (often water) or blown through with an upward air draft (air-jet sieving).

Figure 1 schematically shows how grain size distribution of a sample is determined by sieve analysis. In this Figure, part (a) includes stacked series of n sieves and a pan which is placed underneath them. From top to bottom, the sieves have decreasing opening length, i.e. $l_1 > l_2 > \ldots > l_i > \cdots > l_{n-1} > l_n$. After the sample was separated through the sieves, the retained mass on each sieve, as well as on the pan, is weighed (part (b) in Figure 1). From top to bottom, the retained masses are denoted with $m_1, m_2, \ldots, m_i, \ldots, m_{n-1}, m_n, m_p$. Afterwards, the measured masses are summed up from top to bottom (part (c) in Figure 1). The obtained cumulative masses, from top to bottom, are shown with $M_1, M_2, \ldots, M_i, \ldots, M_{n-1}, M_n, M_T$; where M_T corresponds to the total mass of the sample. The passing percentage of the i^{th} sieve with opening length of l_i is calculated as:

Equation (2.1)

$$\%\, Passing = \frac{M_T - M_i}{M_T} \times 100$$

As shown in part (d) of Figure 1, grain size distribution of the sample is then represented by plotting the passing percentage of each sieve against its opening length. Here, the opening length is considered as grain size. In general, representation of grain size distribution can also be as retaining percentage.

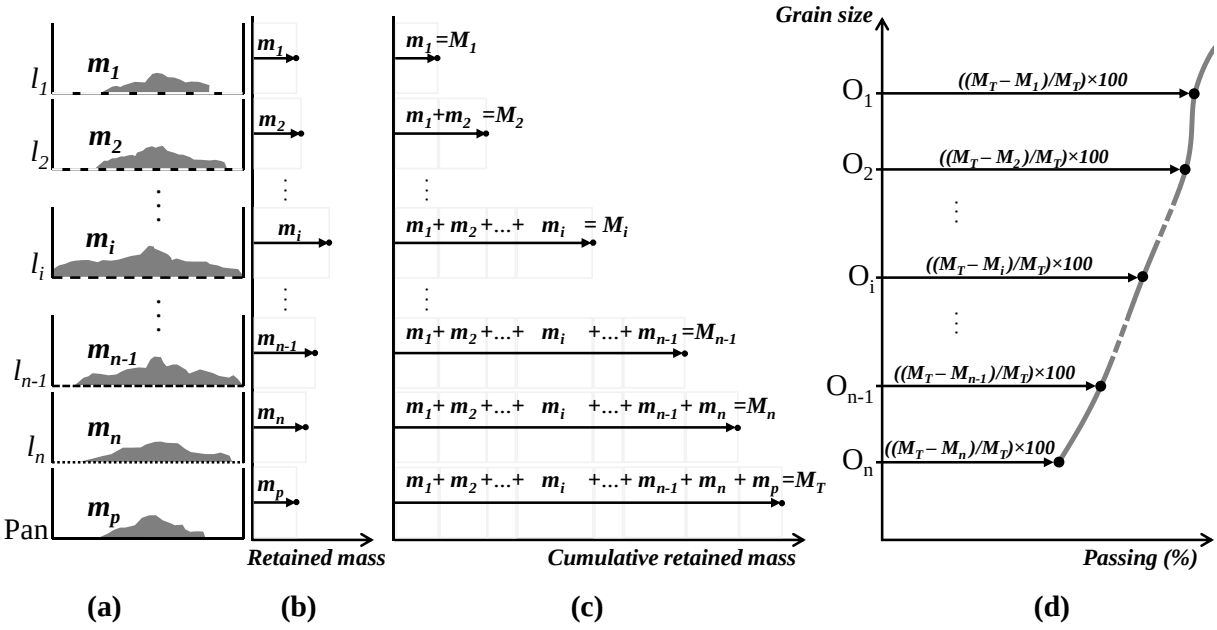

Figure 1. Schematic illustration of sieve analysis.

Relative simplicity, low capital investment and low level of technical expertise required in application, are advantages of sieve analysis [6]. Also, this method is applicable for a relative broad range of grain size. This range depends on the test material and field of application. For instance, according to the standard DIN 18123, sieve analysis can be adopted for determining grain size distribution of soil samples in the range of 0.063 mm to 63 mm [7].

Sieve analysis is currently for the selected test material of this study (i.e. sand), like many other granular materials, the most common method of determining grain size distribution.

However, this method has several drawbacks. The sieving results are strongly influenced by grain shape. Since, the size of a grain is described by its shortest diameter – i.e. the opening length of the sieve that the grain passes through.

In the case of a poorly graded material, a large amount of material is retained on one or two sieves. Thus, the sieve openings tend to become clogged; thereby, preventing finer grains from passing through. Even a material whose grain size is relatively well distributed could still clog the sieve openings.

Sieving results depend on the duration and method of shaking and also, type and number of the sieves that are used. This time-consuming method is physically cumbersome, noisy, dusty and exposes the technician to some potential dangers (e.g. in case of hazardous materials). Sieving does not provide information about the variation in grain size between the sieve sizes. This method is not capable of continuous and/or real-time

grain size analysis, which is required in almost every industrial practice. This shortcoming is even more highlighted when granular materials are treated in large volumes, where online monitoring of grain size is very important and also appealing.

Further disadvantages of sieve analysis and also various sources of error in this method were presented by National Institute of Standards and Technology (NIST) of United States in 2001 [6].

The fact that the most common method of determining grain size distribution is associated with numerous shortcomings and limitations, has brought about the motivation for seeking alternative techniques. Few techniques have been already developed. There are even commercial devices for grain size analysis, which operate based on these techniques. However, none of them has fully replaced sieve analysis in practice. The reason mainly lies within the limitations of these techniques. Therefore, attempts for optimizing these present techniques and above all, developing new methods are being still continued.

Among these alternative methods, image analysis and laser diffraction have the most popular appeal. In the following parts, these two methods are briefly introduced and their limitations and pitfalls are outlined.

2.2.2 Image analysis

Figure 2 is adopted from HORIBA's guidebook published in 2012 [8]. It schematically describes the basic steps of image analysis. As this Figure illustrates, the sample is introduced to a measurement zone, in which images are captured from it by a digital camera (Step I). Step II: individual grains are identified and distinguished from the background (thresholding). Step III: each grain is analyzed for its size (and/or other parameters such as shape) and the result is reported.

Considering how the sample is introduced to the measurement zone, image analysis techniques are basically categorized into two distinct methods: static imaging and dynamic imaging.

In static imaging, the grains of a dispersed sample are placed on a slide, and the slide is moved in order to be investigated by camera and microscope. But in dynamic imaging, the grains flow past one or more cameras.

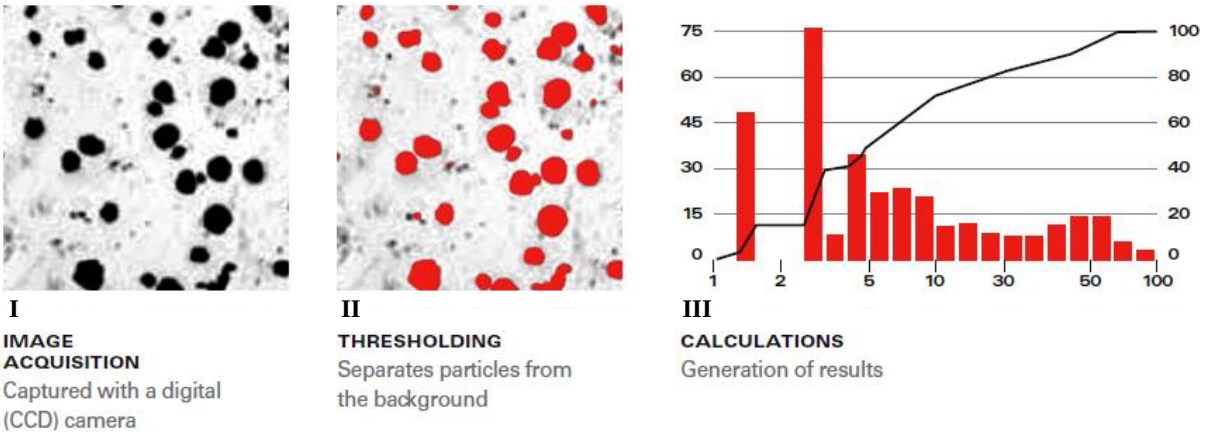

Figure 2. Three basic steps of image analysis [8].

The static method is usually employed only for research and development purposes, rather than for frequent use in quality control. This method is typically suited for powders with grain size range of 0.5 to 1000 µm. However, to cover this range completely, several different magnification levels should be employed. Each magnification level is obtained by using a single microscope objective at a time. Relative complicated sample preparation procedures and trained specialist are required. The size of sample is in the order of milligrams. In static imaging, Morphologi G3 from Malvern [9] and PSA300 manufactured by HORIBA [10] are two commercial products currently popular on the market.

CAMSIZER P4 manufactured by Retsch Technology GmbH [11] is a laboratory device which uses dynamic imaging method for grain size analysis of dry granular samples in the range of 20 µm to 30 mm. In this device, the grains fall between a planar light source and two CCD[2] cameras. The projected grain shadows are recorded and analyzed [11]. CAMSIZER XT manufactured by Retsch Technology GmbH [12] is also a laboratory device which has a function principle similar to CAMSIZER P4, but optimized for finer samples (1 µm to 3 mm) in both dry and wet analyses. In a survey conducted by university of Michigan in 2011 [13], it was claimed that "*CAMSIZER is the best known commercial product in the dynamic category*"; however, "*very small particles tend to agglomerate*" and "*small particles are often occluded behind larger ones, even in free-fall*".

Sysmex FPIA-3000 from Malvern [14] is another commercial device which operates based on dynamic image analysis method. It is suited for grain size analysis only in wet condition. The grain size measurement range doesn't go beyond 300 µm and the size of sample can be maximum 5 ml.

[2] According to Wikipedia, Charge-Coupled Device is a major piece of technology in digital imaging [125].

QICPIC/R from Sympatec [15], which operates based on a quasi-static imaging method, is only suitable for grain size ranges up to about 30 µm.

2.2.3 Laser diffraction

The measurement principle in laser diffraction lies within the fact that the intensity of light scattered by a grain is directly proportional to size of the grain. The grain scatters light at an angle which has an indirect proportionality with size of the grain. Larger grains scatter light at small angles while finer grains cause wider angels of scattering.

Based on this principle, a collection of grains will produce a pattern of scattered light, defined by intensity and angle, that can be transformed into a grain size distribution result [8]. A laser diffraction measurement system is typically consisted of one or more light sources, lenses, and scattered-light detectors. In such a system, projected light is scattered by flowing grains, the scattered light is collected by the detectors, and analyzed to determine size distribution of the grains. In Figure 3, major components of a commercial grain size analysis laboratory device (HORIBA, type LA-950) are schematically presented. The numbered components in this layout are: (1) light sources, (2) lenses, (3) flow cell, in which interaction of grains and light occurs, (4) back scattered-light detectors, (5) side scattered-light detectors, (6) mirror, and (7) small angle light detector.

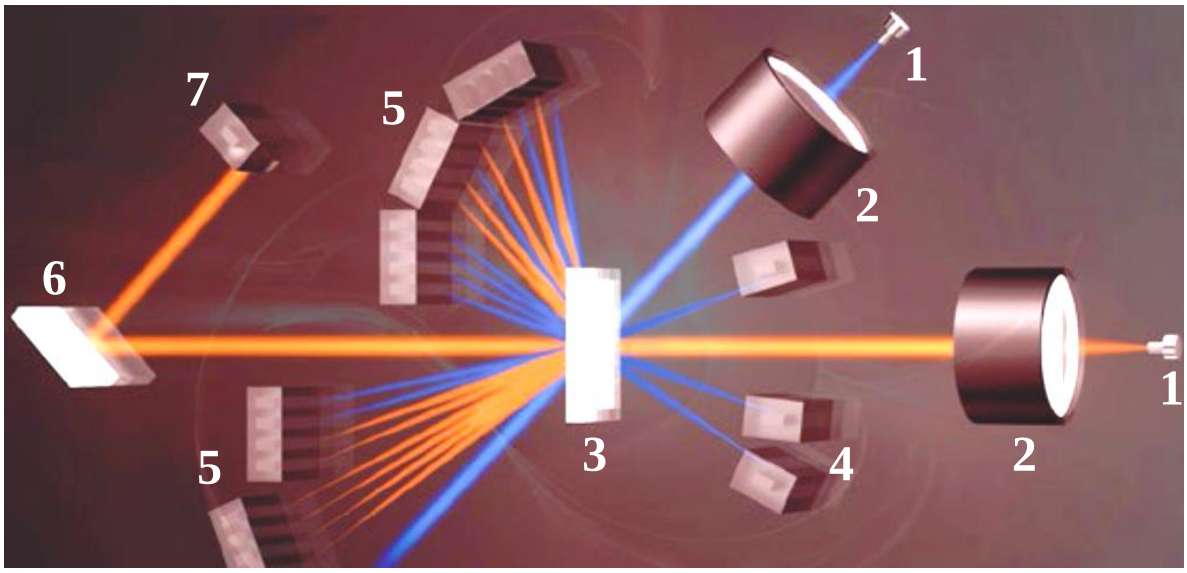

Figure 3. Layout of a laser diffraction grain size analysis device (after [8]).

Among currently available commercial devices, Mastersizer series from Malvern [16], HELOS from Sympatec [17], LS series from Beckman Coulter [18], and LA series from

HORIBA [19] are used the most widely. The grain size measureable by these laboratory devices typically ranges from nanometers to millimeters (max. 5 mm). Sample handling may be in dry or wet (by help of a diluent) condition.

In this method, the complex refractive index of the sample and diluent must be known for optimum accuracy [8]. The assumed optical properties for the sample and diluent, the applied correction factors, and the selected optical model are some issues which often cause inconsistency between the results from laser diffraction and other methods. Assuming the grains as spherical objects is another cause of inconsistency.

In 2012, Stojanović and Marković in their review paper [20] demonstrated that "*the method is not a routine one and the measurement procedure is not limited to entering a sample into the dispersion unit and pressing the button*", and "*the results conclusively depend on the physical and chemical properties of the analyzed material*". Kelly and Etzler, in their critical review titled "*what is wrong with laser diffraction*", outlined several further pitfalls of this methods [21].

2.2.4 Other methods

In addition to image analysis and laser diffraction, there are other methods for determining grain size distribution of granular materials. These methods, however, are less widespread; often due to their narrow ranges of measureable grain size or other limitations.

In accordance with the standard DIN 18123 [7], grain size distribution of soil samples can be determined by using sedimentation method in the range of 1-125 µm. Further size analysis techniques such as dynamic light scattering, cover even more limited grain size ranges. Other available techniques such as electrical sensing zone, are used usually for very specific purposes.

2.3 Pneumatic transport of granular materials

One of the qualities of granular materials is that they can be transported pneumatically very well. Pneumatic transport is known as a quite simple and eminently suitable method for conveying granular materials in different situations (e.g. industrial plants, drilling technology, truck unloading *etc*.). In the current thesis, the experimental investigations include pneumatic handling and transport of granular samples. This kind of sample handling was selected because of its simplicity and flexibility.

The requirements of a pneumatic conveying system are a source of compressed gas, a feed device, a conveying pipeline and a receiver to disengage the conveyed material and carrier gas [22]. In the present research work, the source of carrier gas is air. Vibratory

feeder is selected as feed device. A commercial pre-separator and later on a combination of collection bin and cyclone are used to disengage the conveyed material and air. A normal PVC hose and later on aluminum pipes are employed as conveying pipelines. In this study, vacuum cleaner is responsible for providing air flow with negative pressure in the pneumatic line. Thereby, the conveyed granular material doesn't come into contact with any moving parts.

2.3.1 Gas flow velocity and mass flow rate

Flow velocity of carrier gas and mass flow rate of transported material are the most important and deciding parameters of a pneumatic conveying system.

As an accepted universal rule in pneumatic conveying, superficial gas flow velocity is taken into consideration as gas flow velocity [22]. Superficial gas flow velocity is defined as the velocity of carrier gas while transported material is not present in the conveying pipeline. The velocity of the grains, which are suspended in the conveying gas, is lower than that of the gas. It is a difficult and complex process to measure grain velocity, and apart from research purposes, grain velocity is rarely measured [22]. In summary, it is generally only superficial gas flow velocity which is ever referred to in pneumatic conveying. In the present research work, this parameter is simply expressed as air flow velocity (in m/s). It should be noted that air flow velocity may not be constant along the length of a conveying pipeline. That is due to the variations in cross-sectional surface of the pipeline and/or pressure loss as a results of material transport. Therefore, in this thesis the reported values of air flow velocity correspond only to the position of the impacting head.

Mass flow rate of transported material, unlike gas flow velocity, remains invariable along the length of a conveying pipeline. In this research work, this parameter is expressed in g/s and is calculated simply by dividing the total mass of the sample (in g) by the time of passing of the sample through the pneumatic line (in seconds).

2.3.2 Mode of conveying

Mode of pneumatic conveying refers to how materials are transported through a pipeline. Conveying modes, also known as flow patterns, vary according to gas flow velocity, material mass flow rate and some other parameters such as the properties of the pneumatic line and the transported material.

If a high air velocity is used to convey any material such that it is conveyed in suspension in the air, then it is conveyed in dilute phase (also known as suspension phase). In this case, if the gas velocity is sufficiently high that the particles are well mixed and maintained in a nearly homogenous state, by the absence of both radial and axial solids

segregation, then it is transported in homogenous dilute flow pattern. Figure 4 (a) shows a homogenous flow in a horizontal pneumatic transport. Dilute phase systems constitute the most widely used of all pneumatic conveying systems [23].

Reduction in the gas flow velocity results in a non-uniform distribution of materials over the cross-section of the conveying pipeline. In this case, as a result of low gas flow velocity the material is conveyed in a non-suspension mode, which is known as dense phase conveying. The dense conveying in a horizontal pipeline takes place with a certain proportion of the materials flowing through the upper portion of the cross-section of the pipe together with a highly concentrated material stream, corresponding to an expanded moving layer. This moving layer progresses at a lower velocity in the lower portion of the cross-section [23]. In dense phase, if the material is conveyed in dunes on the bottom of the pipeline, or as a pulsatile moving bed, then it is called dune flow or moving bed flow. This flow pattern is illustrated in Figure 4 (b). The other flow pattern of the dense phase happens when the material is conveyed as the full bore plugs are separated by air gaps. This flow pattern is called slug or plug flow and is presented in Figure 4 (c). In this pattern, there are alternate regions where grains have settled and where they are still in suspension [24].

Finally, with further reduction in gas flow velocity, the granular material completely fills the pipe and becomes packed in it. Meanwhile, the gas flows through the space between the grains. This condition is termed as packed bed and depicted by Figure 4 (d). It is believed that in packed bed pneumatic transport ceases to exist [24].

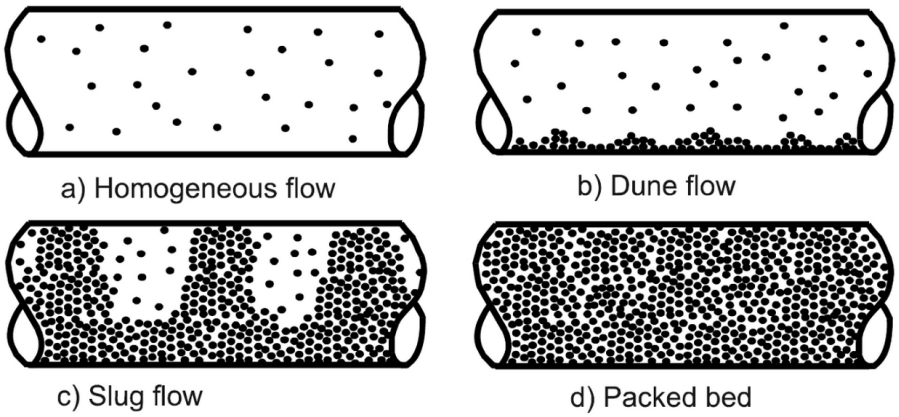

Figure 4. Flow patterns in horizontal pneumatic transport [24].

In the current thesis, all of the experimental programs are conducted in homogenous dilute conveying mode. This is succeeded through properly adjusting the air flow velocity and mass flow rate, as well as other parameters such as width of pipeline.

2.4 Summary

The significance of granular materials was highlighted in this Chapter. Grain size distribution was mentioned as the key property of every granular material. In many areas, this property is still determined by sieve analysis. Sieving has numerous limitations and drawbacks. Commercial devices, which operate based on some alternative techniques, were briefly introduced. However, they have also their own limitations and sources of uncertainty. Consequently, sieving is still often the sole method of grain size analysis in practice.

This state-of-the-art review of grain size analysis showed that attempting to set up new methods is of high interest. In this regard, the current thesis focuses on applying the passive acoustic measurement method for grain size analysis. In the next Chapter, the passive acoustic measurement method together with its related topics are introduced.

3 The passive acoustic measurement method

Acoustics is broadly defined as the study of generation, transmission and reception of mechanical waves [25]. Acoustics is generally known as the science of sound. Sound waves, according to definition, are limited to the frequency range of 20 Hz to 20 kHz (i.e. audible range of human). Acoustics, however, not only deals with the waves that we can hear, but also involves the waves with frequencies lower than 20 Hz (infrasound) as well as higher than 20 kHz (ultrasound).

Acoustic measurements are the obvious prerequisite of acoustic investigations [26]. Based on the field of application, acoustic measurements are categorized into various disciplines such as: measurements of building acoustic, machinery noise, acoustic imaging, sound quality *etc*. [27].

Acoustic measurements can be carried out with different objectives. To carry out proper acoustic measurements with an acoustic measurement system, knowledge about the different components of the system is crucial.

In the current Chapter, active and passive types of acoustic measurement methods are introduced. Afterwards, the basic physical concept of the passive acoustic measurement method is briefly described. Then, components of this method are presented. Eventually, the statistical multivariate modeling approach, which has been applied within the current study, is introduced and its related subjects are extensively presented.

3.1 Active and passive acoustic measurement methods

Acoustic measurement methods are generally utilized in two distinctive operating modes: active and passive measurement methods (see e.g. [28], [29] and [30]).

Active acoustic measurement method involves the use of acoustic transmitter(s) and receiver(s) around the object of interest. Acoustic waves (usually ultrasound) are transmitted to the object, influenced by it, and received by the receiver(s). In this case, the effects of the object on the transmitted waves are considered and analyzed.

In contrary to active acoustic measurement method, in the passive technique only receiver(s) (usually piezoelectric sensors) are employed. In this case, the acoustic waves that are received by the receiver(s) come entirely from the object itself. These acoustic waves can be created via various mechanical activities in relation with the object. Activities such as: impact, vibration, friction, deformation *etc*. In the passive technique, these acoustic waves are considered and analyzed. The conducted acoustic measurements in the current thesis belong to the passive type.

3.2 Basic physical concept

This part briefly describes the basic physical concept, which the acoustic measurements in the current thesis are based on. When a grain impacts on the surface of a solid body, then the impact is the *source* of transient elastic waves which propagate through the body and, outward from the location of the *source*. If a sensor is connected to the body, these waves can be observed via the signal given by the sensor. The terms sensor and signal are introduced later on in the following part. The signal is in relationship with the *source*. By analyzing the signal, relevant information about the *source* can be obtained. Examples of experimental works which deal with this concept are [31], [32] and [33].

3.3 Passive acoustic measurement equipment

3.3.1 Impacting head, probe and sensor

In this thesis, the above mentioned solid body is simply called an 'impacting head'. In literature, impacting head has been alternatively called 'sensor head' [33] or 'impacting surface' [32]. The current thesis considers the assembly of the sensor and impacting head as a 'probe'[3].

A sensor is a transducer which converts a phenomenon into a corresponding signal. A transducer is defined the most commonly as a device that converts one form of energy to another form of energy.

Signal has been defined in various contexts in many different ways [34]. A signal can be defined as a function $x(t)$ of an independent variable t (usually time), by which information about a phenomenon can be conveyed. For example, a time-varying voltage signal $v(t)$ is a function of the independent variable time t. The signal $v(t)$ may convey information about a phenomenon in the form of fluctuating voltage with time.

An accelerometer is a sensor which converts mechanical acceleration into a proportional electrical signal – a voltage signal for example. Amongst the various types of accelerometers, piezoelectric accelerometers are used the most commonly – due to their numerous advantages[4]. Based on mechanical configuration, piezoelectric accelerometers are generally classified into three types of design: compression, flexural and, shear. The shear design offers the best overall performance for an accelerometer [35]. In the current thesis, the employed piezoelectric accelerometers had the shear design. In Figure 5, a schematic illustration of a piezoelectric accelerometer with annular shear design is presented. In this configuration, a ring-form piezoelectric crystal is mated

[3] Probe: (sciences) A small device […] used to explore, investigate or measure something by penetrating or being placed in it [124].
[4] To read more about the advantages of piezoelectric accelerometers refer to e.g. [30] [37].

between a mass[5] and a post. The post is connected with the base of the accelerometer's housing. The crystal can be natural (quartz) or man-made (ceramics). When the accelerometer is mechanically accelerated (during vibration, impact *etc.*), the mass m imposes shear force f upon the crystal; since the mass wants to stay still because of inertia. As shown in Figure 5, as the crystal undergoes the force f, negative and positive ions accumulate onto the opposed surfaces of the crystal in an amount that is directly proportional to the applied force f. By this effect (known as piezoelectric effect), a charge output is generated which is proportional to the force f. The force f is equal to the product of the mass m and acceleration a (Newton's 2nd law). Since the mass m is constant, the charge output is then directly related to the acceleration a. The charge output is usually converted to voltage signal by means of integrated electronics in the accelerometer. The given voltage signal is conducted further to external electronic devices for further processing procedures.

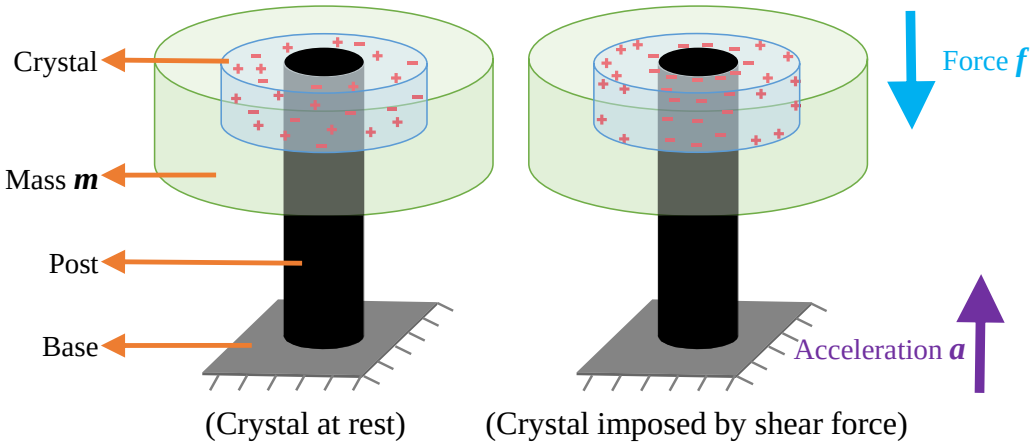

Figure 5. Piezoelectric accelerometer with annular shear design (after [35]).

Sensitivity of a piezoelectric accelerometer is defined as the ratio of the output (voltage signal) to input (mechanical acceleration) and is often expressed in mV/g. For an accelerometer to be useful, the output needs to be directly proportional to the acceleration a. But, this fixed ratio of output to input is only true for a range of frequencies, known as usable frequency range [36]. Usually in order to achieve a wider usable frequency range, the mass m is reduced. However, the lower the mass m, the lower the sensitivity [37].

The utilized sensors in this thesis were uniaxial piezoelectric accelerometers. Uniaxial implies that they were sensitive to acceleration only in one single direction (known as

[5] Also known as seismic mass or proof mass.

the sensitive axis). The sensitivity of a uniaxial sensor in other directions rather than the sensitive axis is typically lower than 5% of the sensitivity in the sensitive axis. The sensitivity in other directions rather than the sensitive axis is called transverse sensitivity.

3.3.2 Data acquisition (DAQ) device

DAQ device is commonly defined as the interface between the digital world (computer) and signals from the real world. Signal conditioning and Analog-to-Digital Converter (ADC) are two main components of this device. Signal conditioning circuitry manipulates a signal into a form that is suitable for input into an ADC. This circuitry can include amplification, attenuation, filtering, and isolation [38].

The output signal of a sensor will be acquired, recorded and further processed by help of digital devices (computers). Therefore, this analog signal, which is continuous, should be represented in discrete form in order to be inputted into computers. Representing an analog signal by a discrete set of its samples is performed by ADC. Amongst the various specifications of an ADC, its sampling rate plays the key role. In the following, sampling rate and related concepts are introduced.

3.3.3 Nyquist–Shannon sampling theorem

The number of samples in one second is defined as sampling rate. Sampling rate deals with the question how fast the analog signal should be sampled. This question can be addressed by Nyquist–Shannon sampling theorem. Nyquist's theorem states that if the highest existing frequency in the signal equals to f_h, then the sampling rate f_s must be $\geq 2f_h$. This sampling theorem is known to be first introduced by the work of Harry Nyquist in 1928 [39]. Half of the sampling rate $0.5f_s$ and twice the maximum existing frequency $2f_h$ are called respectively Nyquist frequency and Nyquist rate. The former and the latter are attributes of the sampling equipment and the analog signal, respectively [40]. Nyquist rate is considered as the minimum required sampling rate for alias-free signal sampling. If a signal be sampled with a rate lower than its Nyquist rate, then aliasing would happen. Aliasing refers to the folding over of the higher frequency components onto the lower spectrum [41]. Consequently, the original frequency components are distorted by the erroneous higher frequencies (the so-called 'alias'). Sampling at higher rates can avoid aliasing and the analog signal would be reconstructed well. But it may result in data redundancy and prove expensive in storage and calculation [41]. Another way to avoid aliasing and make sure that the Nyquist's theorem is satisfied is using an anti-aliasing filter. It is a lowpass filter which filters the analog signal, before

being sampled. Thereby, the frequency components of the analog signal which are higher than the available Nyquist frequency are attenuated to acceptable levels.

3.4 Signal processing

3.4.1 Root Mean Square (RMS)

In literature, RMS value is often considered as one of the most important and commonly used measure in sound and vibration, and electronics. RMS of a time-varying quantity is obtained by: squaring the magnitude at each instant, taking the weighted average of the squared values over the interval of interest, and then taking the square root of this average. In other words, RMS is the square root of weighted average of signal power. RMS averaging function averages the power, or energy, of the signal and reduces signal fluctuations.

The weighting is either linear or exponential. Averaging with linear weighting is used when RMS calculation is to be restricted to a well-defined time interval. Exponential weighting permits continuous tracking of a signal with magnitude that varies with time [42]. Averaging with exponential weighting generates a continuous running average where the most recently sampled magnitude levels have more influence on the average than older ones. It provides a suitable form to examine rapidly changing data with the benefit of some averaging to smooth the data [43]. For a continuous signal $x(t)$, the RMS at time t is calculated by:

Equation (3.1)

$$x_{RMS}(t;\tau) = \sqrt{\frac{1}{\tau}\int_{-\infty}^{t} x^2(t')e^{-\frac{(t-t')}{\tau}}dt'}$$

where τ is the time constant of the exponential average and t' is the dummy variable of the integration [42]. Lower frequency signals require larger τ, whereas higher frequency signals allow shorter time constants. As a rule of thumb, the time constant should be at least as long as one period of the signal. This Equation can be simply implemented for digital signals too.

Quite often, the signal undergoes a frequency weighting filter and/or is divided into frequency bands, before RMS value is determined [44] [45]. Because such a single value does not give sufficient information about the nature of the raw signal, and thus, the RMS is determined in frequency bands or in a frequency filtered signal [44].

3.4.2 Signal-to-noise ratio

Signal-to-noise ratio (SNR or S/N) is a measure that compares the level of a desired signal to the level of background noise [46]. The higher this ratio, the less is the disturbance of background noise (unwanted signal) in proportion to the desired signal (meaningful information). This ratio is often represented on a logarithmic decibel (dB) scale and can be calculated by the following Equation [47]:

Equation (3.2)

$$SNR = 20\log_{10}\frac{RMS\ (signal)}{RMS(noise)}$$

3.4.3 Spectral analysis of a signal using FFT

Spectral (or *frequency*) analysis of a signal involves decomposing the signal into its spectral (or *frequency-domain*) components. This analysis is performed with different objectives. Some of them are: getting representative and relevant information about the vibration source, which are not accessible directly from the time signal; or increasing the selectivity of information; or identifying the dominant frequencies in the signal; or detecting various noises and/or harmonic distortions in the signal.

Spectral analysis can be carried out by means of Fourier transform. Fourier's theorem states that any waveform in time-domain can be represented by a sum of sine waves. Using Fourier analysis, the frequencies constituting a wave can be revealed. Fourier analysis of a digital signal is performed using the Discrete Fourier Transform (DFT). The DFT of a signal with N samples is written as [48]:

Equation (3.3)

$$G(f_n) = \sum_{k=0}^{N-1} g(t_k)e^{-j2\pi nk/N}$$

where $G(f_n)$ represents the discrete Fourier spectrum and $f_n = \frac{n}{N\Delta t}$ is frequency. Δt is the time interval between two successive samples and $n = 0, 1, 2, 3, \dots, N-1$, so that $N\Delta t$ equals the time length of the signal T. Furthermore, $g(t_k) = g(k\Delta t)$ is the sampled signal and j is the imaginary unit. The number of samples N is usually of the form 2^m where m is a positive integer.

The DFT determines sinusoidal 'weights [49]' (coefficients) via the inner product of sinusoids and the signal (see the above Equation). As it is clear from the Equation, the

discrete Fourier spectrum is complex valued. To plot the magnitude spectrum of a signal, the magnitude of each coefficient should be calculated. Assume that a given coefficient is specified by $a + jb$, its magnitude can be determined as $\sqrt{a^2 + b^2}$ [49].

The DFT is considered to be mathematically very complex and too slow to be practical. If the signal has N samples, then $O(N^2)$ [6] arithmetical operations are required by the DFT. Since, as it is seen from Equation (3.3), N coefficients of frequency are related with N samples of time by means of the DFT. In 1965, Cooley and Tukey [50] published their mathematical algorithm which has become known as the Fast Fourier Transform (FFT). This algorithm reduces the number of required arithmetical operations to $O(N \log_2 N)$ by breaking a DFT of size $N = N_1 N_2$ into many smaller DFTs of sizes N_1 and N_2. Dividing the transform into two pieces of $N_1 = N_2 = {}^{N}/_{2}$ at each step, or any factorization of N, is possible. These two cases are called radix-2 and mixed-radix, respectively; and the former is known to be the most common variant of the FFT algorithm [51].

The FFT has been described as "the most important numerical algorithm of our lifetime" [52]. It is worth mentioning that the FFT algorithm developed by Cooley and Tukey in 1965 was later found to be actually a re-invention of an algorithm known to Carl Friedrich Gauss around 1805 (see [53]).

3.4.4 Digital filtering

Signals inherently contain some kinds of noise or other unwanted disturbances. In order to make the signals usable, and extract desired meaningful information from them, these disturbances should be eliminated. It means that, signals should be removed, blocked or attenuated at some specific frequencies. It is often succeeded through filtering. Filtering is defined as the process by which the frequency content of a signal is altered [54].

Analog filtering means that filtering is applied on an analog signal and an analog signal is given as output. Analog filtering is performed by means of electronic devices via signal conditioning, as briefly mentioned in part 3.3.2.

On the other hand, digital filtering has been developed for digital signals. In many practices, analog filtering has been replaced by digital filtering. The reason is numerous advantages of digital filters over analog ones [54].

Digital filters can be categorized in many different ways. Based on the frequency range that digital filters either pass or attenuate, they can be classified into 4 types:

[6] Big O notation (see [123])

- A lowpass filter passes low frequencies but attenuates high frequencies.
- A highpass filter passes high frequencies but attenuates low frequencies.
- A bandstop filter attenuates a certain band of frequencies.
- A bandpass filter passes a certain band of frequencies [54].

In Figure 6, the ideal magnitude frequency response belonging to each of these filters is presented. The magnitude frequency response of a filter is defined as the function which gives the gain of the filter at every frequency [55]. The gain of a filter at a frequency equals to the ratio of the output magnitude to the input magnitude at that frequency. In Figure 6, $f_s/_2$ corresponds to the Nyquist frequency and, the frequencies f_c, f_{c1} and f_{c2} are called cutoff frequencies. In this way, a lowpass filter passes all frequencies below its cutoff frequency f_c, whereas a highpass filter passes all frequencies above its f_c. A bandstop filter attenuates all frequencies between its lower cutoff frequency f_{c1} and its upper cutoff frequency f_{c2}, whereas a bandpass filter passes all frequencies between its f_{c1} and f_{c2}.

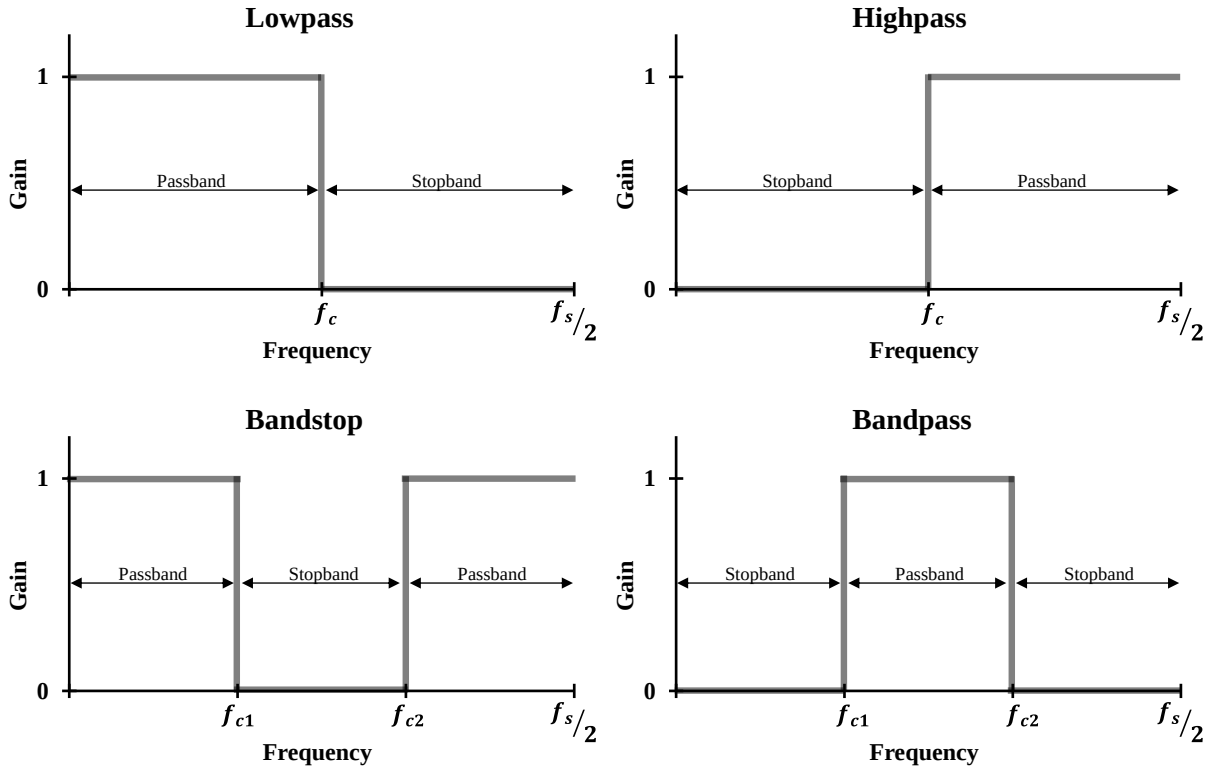

Figure 6. Magnitude frequency responses of ideal filters.

As shown in Figure 6, an ideal filter has a gain of zero at the attenuated frequencies (stopband). Also, the gain of an ideal filter at the passed frequencies (passband) equals

to unity. In practice, however, there is always a finite transition region between the passband and the stopband [54]. In the transition region, the gain of the filter in the passband gradually reduces to its gain in the stopband.

The slope of attenuating in the transition region is called roll-off. Roll-off represents attenuation as a function of frequency and is usually expressed in dB/octave. An octave is equivalent to the frequency range between 10^n Hz and 10^{n+1} Hz, where n is a positive integer [51].

For a filter, there are different types of transfer function that can be used. Amongst them, Butterworth is commonly used and is known to be a maximally flat magnitude filter in both passband and stopband. It means that the magnitude frequency response of this filter is maximally flat at all frequencies and, the ideal gains of unity and zero are given respectively in passband and stopband. Moreover, unlike other filter types, Butterworth filter has a monotonic attenuation in the transition region.[7]

3.5 Statistical methods

3.5.1 Two-sample *t*-test

A two-sample *t*-test is used to determine whether there is statistically significant difference between the means of two populations. The statistical hypothesis of this test is commonly presented in the following form:

Equation (3.4)

$$H_0: \mu_1 - \mu_2 = \mu_0 \quad versus \quad H_1: \mu_1 - \mu_2 \neq \mu_0$$

where μ_1 and μ_2 are the population means and μ_0 is the hypothesized difference between the two population means. The null hypothesis and the alternative hypothesis are denoted by H_0 and H_1, respectively. If $\mu_0 = 0$ then it is called a two-tailed test. In this case, in testing the null hypothesis, i.e. the population means are equal, *t*-value (also known as *t*-statistic or test statistic) is calculated as following:

[7] To read more about Butterworth filter refer to e.g. [54] and [55].

Equation (3.5)

$$t = \frac{\overline{x_1} - \overline{x_2}}{\sqrt{\frac{s_1^2}{N_1} + \frac{s_2^2}{N_2}}}$$

where $\overline{x_1}$ and $\overline{x_2}$ are the sample means, s_1 and s_2 are the sample standard deviations, and N_1 and N_2 are the sample sizes. If the two populations have equal variances[8], then the degrees of freedom equals to $N_1 + N_2 - 2$. Based on the calculated *t*-value, *p*-value (probability value) will be obtained. For further reading about different methods of determining *p*-value and its interpretation refer to [56, 57, 58]. The null hypothesis is rejected in favor of the alternative hypothesis, when the calculated *p*-value is smaller than the acceptable level of significance (α level). By the common convention, the threshold for rejecting the null hypothesis (namely α level) is 0.05 (or equivalently 5%) which corresponds to a confidence interval of 95% [56, 59].

3.5.2 Partial Least Squares Regression (PLSR)

Based on the early works by several researchers (mainly by Wold et al. (1984) [60], Geladi and Kowalski (1986) [61] and Martens and Naes (1989) [62]), PLSR is now known as a very common method in multivariate calibration. The goal of PLS Regression is usually to predict **Y** from **X**, where **X** and **Y** are two matrices containing the independent input variables and the dependent output variables, respectively. Multivariate calibration refers to the fact that each **X** and **Y** include several variables. The independent input and the dependent output variables are respectively denoted as *X*- and *Y*-variables and, are also called predictor and response variables, respectively.

PLSR deals with building a model which describes the common structure of **X** and **Y**. In order to describe both **X** and **Y** simultaneously, PLS Regression decomposes them as following:

Equation (3.6)

$$\mathbf{X} = \mathbf{T}\mathbf{P}^{T} + \mathbf{E}$$

$$\mathbf{Y} = \mathbf{U}\mathbf{Q}^{T} + \mathbf{F}$$

[8] To read about different tests for equal variances refer to the PhD thesis by Nordstokke (2009) [131].

and then performs regression between **T** and **U**. **T** is the *X*-score matrix and **P** is the *X*-loading matrix. Also, **Q** and **U** are the loading and score matrices corresponding to the *Y*-variables, respectively. **E** and **F** are the residual (error) matrices corresponding to the *X*-variables and *Y*-variables, respectively. The decomposition of **X** and **Y** described in Equation (3.6) is graphically presented in Figure 7.

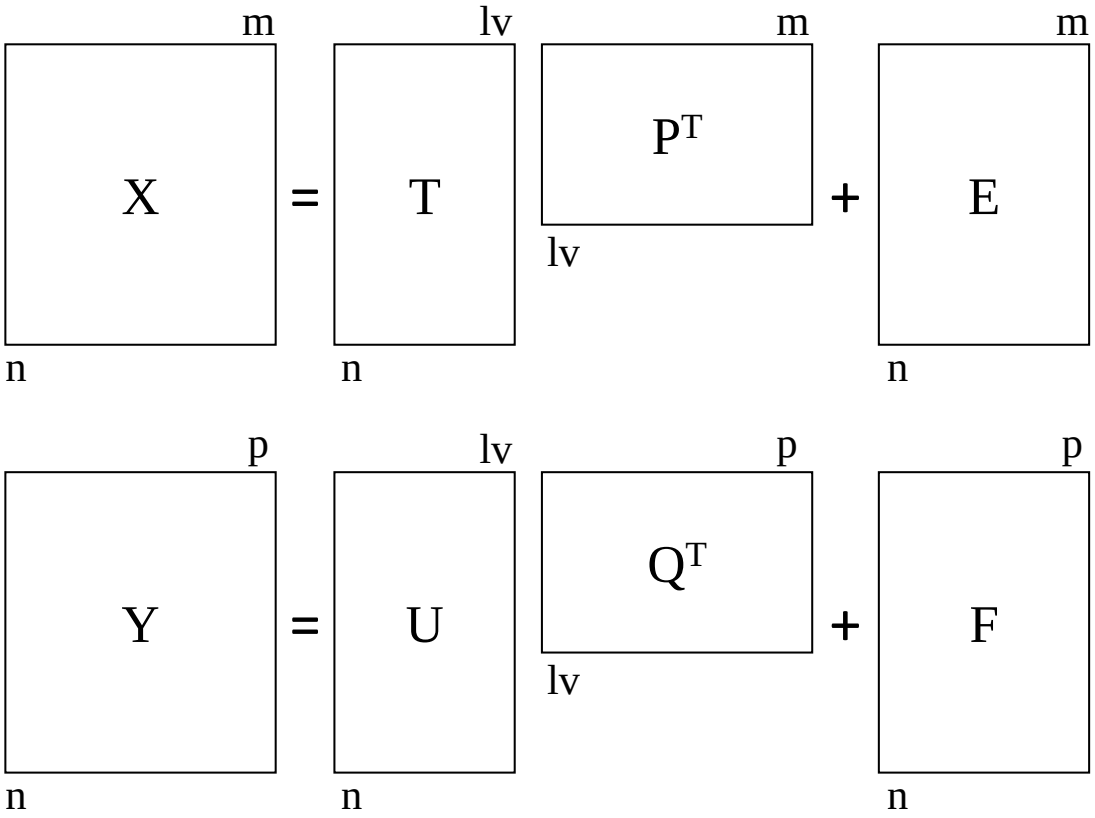

Figure 7. Schematic overview of the matrices involved in PLSR (after [61]).

Different algorithms have been introduced to conduct PLSR (see e.g. [63] [64] [65]). The following algorithm, which is basically built on the properties of the NIPALS[9] algorithm, decomposes the **X** and **Y** blocks by taking information from each other into account:

[9] Non-linear Iterative PArtial Least Squares (for further reading about NIPALS refer to [130])

Equation (3.7)

$$\mathbf{u} \coloneqq \mathbf{y_j} \qquad \text{for some } j \qquad (j = 1, 2, \ldots, p)$$

Loop

$$\mathbf{p} \coloneqq \mathbf{X^T u} \,/\, \|\mathbf{X^T u}\|$$

$$\mathbf{t} \coloneqq \mathbf{X p}$$

$$\mathbf{q} \coloneqq \mathbf{Y^T t} \,/\, \|\mathbf{Y^T t}\|$$

$$\mathbf{u} \coloneqq \mathbf{Y q}$$

Until **t** stops changing

where,

X and **Y** respectively have sizes of $n \times m$ and $n \times p$,

n is the number of samples (observations, objects) in the calibration (training) set,

m is the number of independent variables (X-variables),

p is the number of dependent variables (Y-variables),

u is a column vector of scores for the **Y** block (size $n \times 1$),

t is a column vector of scores for the **X** block (size $n \times 1$),

$\mathbf{y_j}$ is a column vector of features for the dependent variables (size $p \times 1$),

p is a row vector of loadings for the **X** block (size $1 \times m$),

q is a row vector of loadings for the **Y** block (size $1 \times p$),

and $\|\ \|$ is the Fröbenius or Euclidian norm [61].

The above procedure specifies the first set of PLS Principal Components and loadings. In order to find the subsequent components and vectors, it is set:

Equation (3.8)

$$\mathbf{X} \coloneqq \mathbf{X} - \mathbf{t p}^{\mathrm{T}}$$

$$\mathbf{Y} \coloneqq \mathbf{Y} - \mathbf{u q}^{\mathrm{T}}$$

and then the same steps are repeated. After l such steps, two $n \times l$ matrices **T** and **U**, and two $n \times l$ matrices **P** and **Q** are obtained (refer to Equation (3.6)) and, **X** and **Y** become

small. Ideally, the remaining **X** (i.e. **E** in Equation (3.6)) is either almost zero or very small and includes only noise. The remaining **Y** (*Y*-residuals) will be also very small if there is a strong relationship between *X*- and *Y*-variables. In general, meaningfully structured data sets give small residuals (error) both in **E** and **F**.

The number of steps *l* determines the number of PLS Principal Components. The optimal number of steps *l* is usually not the same as the maximum possible number of steps *l*. Because the measured data are never noise-free, choosing the maximum possible number may lead to entrance of noise into the model instead of **E** and **F**. On the other hand, taking too few steps can also result in variances in both *X*- and *Y*-variables to be remained unexplained. Therefore, various methods have been developed and specified to decide at which step to stop. If modeling is performed with the aim of prediction, the optimal number of steps *l* is usually determined by a suitable method. In the context of multivariate calibration, the methods for determining the optimal number of steps *l* are commonly called cross validation (or sometimes simply called validation) methods. For further reading about these methods refer to e.g. [61] [64] [66] [67]. In the current research work, an 'internal' cross validation technique has been employed to determine the optimum number of PLS Principal Components. This technique is introduced together with an 'external' cross validation method later on in the current part.

To establish a regression model relating **X** and **Y**, it suffices to fit *B* for the following:

Equation (3.9)

$$\mathbf{U} = \mathbf{T}B + \mathbf{G}$$

where *B* is an orthogonal matrix which is called the coefficient matrix and has the size of $m \times p$. **G** is the model error matrix with the size of $n \times l$.

By substituting the resulted regression model into the Equation (3.6):

Equation (3.10)

$$\mathbf{Y} = \mathbf{U}\mathbf{Q}^{\mathbf{T}} = \mathbf{T}B\mathbf{Q}^{\mathbf{T}} = \mathbf{X}\mathbf{P}B\mathbf{Q}^{\mathbf{T}}$$

The above described procedure is referred as training or calibration phase of PLS Regression. Also, Equation (3.10) is denoted as PLSR calibration model. After training phase, this model can be used to predict *Y*-variables of new objects. It means, in case of any given new *X*-variable, **P**, **Q** and *B* can be used to compute the corresponding *Y*-variable. This phase is called prediction or verification phase of PLSR modeling.

There are several measures of how good a model is. Amongst the various introduced measures, the followings are the most common:

1) *Model fit* shows how well the model has been fitted to the training data set. However, it doesn't express how well the model will work in predicting *Y*-variables from new *X*-variables.

2) *Prediction error* is an expression of the error which is expected when using a calibration model in future predictions.

3) *Residuals* show how well each individual object is modeled (in the calibration phase) or predicted (in the verification phase). The *residuals* are the differences between the measured and modeled (or predicted) values in each single object. In contrary to *prediction error*, which usually corresponds to several objects, the *residuals* deal with each single object.

4) The correlation between predicted and measured *Y*-variable values is also another approach to see how well the model performs.

In this context, there are alternative measures for these concepts and also many further similar concepts. For further reading refer to the book by Esbensen et al. (2002) [66].

The percentage of variance of *X*- and *Y*-variables which is explained by the model can be used as a measure of *Model fit*. This measure can be employed to estimate how well the **X** and **Y** data have been modeled in the training phase. The percentages of explained *X*- and *Y*-variances are commonly plotted against the number of PLS Principal Components. Thereby, the percentages of *X*- and *Y*-variances made up by each component added to the PLSR algorithm can be represented. In the present thesis, this measure is simply denoted by PCTVAR (according to [68]) and is computed for *Y*-variables as:

Equation (3.11)

$$\mathrm{PCTVAR} = \frac{\sum_{j=1}^{l} q_j^2}{\sum_{i=1}^{n} (y_{i\ measured} - \bar{y})^2}$$

where q_j is the *Y*-loadings. Also, $\bar{y} = \frac{1}{n}\sum_{i=1}^{n}(y_{i\ measured})$ is the mean of the measured *Y*-variable values. The percentage of explained variances of *X*-variables is also calculated using the same procedure. Note that the percentage of explained variances of *X*- and *Y*-variables may be calculated by different approaches (see e.g. [65]). In some

contexts, the percentage of unexplained variances (or sometimes simply called the percentage of residual variances) is instead of PCTVAR calculated and reported.

Root Mean Square Error of Prediction (RMSEP) is a direct estimate of average *prediction error*. This very frequently used measure yields a value which represents the performance of a model when presented with new data. The yielded value by RMSEP is stated in original measurement unit of *Y*-variable. It is simply the mean squared difference between measured *Y*-variable value ($y_{i\ measured}$) and predicted *Y*-variable value ($y_{i\ predicted}$), thus:

Equation (3.12)

$$RMSEP = \sqrt{\sum_{i=1}^{n} \frac{(y_{i\ measured} - y_{i\ predicted})^2}{n}}$$

where n is the number of the prediction samples. In the literature, $y_{i\ measured}$ is also expressed as $y_{i\ reference}$.

There are different methods to validate (test) a model. If cross validation methods are used for evaluating and/or validating the performance of a model, they are called 'external' cross validation methods. There are several various 'external' cross validation methods, e.g. ROC[10] curve, *k*-fold cross validation, MCCV[11], data-splitting and full cross validation. Amongst them, the two most popular model validation methods are data-splitting and full cross validation [69].

In data-splitting, both **X** and **Y** are divided (splitted) into two subsets, thus:

$$\mathbf{X} \rightarrow \begin{cases} \mathbf{X}_{train} \\ \mathbf{X}_{test} \end{cases} \qquad \mathbf{Y} \rightarrow \begin{cases} \mathbf{Y}_{train} \\ \mathbf{Y}_{test} \end{cases}$$

where ($\mathbf{X}_{\text{train}}$, $\mathbf{Y}_{\text{train}}$) and ($\mathbf{X}_{\text{test}}$, $\mathbf{Y}_{\text{test}}$) are called train and test (verification) sets, respectively. The train set is used for model training. The trained model is then verified by the test set. Thereby, it is possible to estimate *prediction error* of the model independent from the model itself. The drawbacks of this simple method however are [69] [70]: it is not suited for (very) small number of observations. Care must be taken

[10] Receiver Operating Characteristic
[11] Monte Carlo Cross Validation

that both subsets of **X** and **Y** involve representative spread of data. Moreover, this method does not fully utilize all the information available. The latter may not be a problem when the number of observations is large enough.

Full cross validation (also known as leave-one-out cross validation) is particularly of interest when the number of objects is (very) small. This 'external' cross validation method employs a statistic measure to evaluate the performance of a model in future predictions. Amongst the different measures, RMSEP and PRESS[12] are very popular. The advantages of RMSEP are: unlike PRESS, it is expressed in the same measurement unit as the measured *Y*-variable. Also, since it is normalized, RMSEP values from different models with varying number of observations can be compared. Therefore, in the present study it was decided to employ RMSEP.

Assume a data set consisting of *n* objects. The first object is left out (withheld) and a sub-model (artificial model) is calibrated based on the remaining *n*-1 objects. Using the first sub-model, the response of the first object, which is left out, is predicted. Then, the first object is put back into the data and the second one is removed. The second sub-model is calibrated based on the remaining *n*-1 objects. This sub-model is then verified using the second object. This procedure is successively repeated for each of the objects. Eventually, *n* sub-models have been built and each object has at some point been eliminated from the modeling process. Each object has been once and only once withheld. Therefore, *n* predictions have been made. The *prediction error* of each *Y*-variable through these *n* predictions is evaluated by means of RMSEP (Equation (3.12)). The advantage of full cross validation over other validation methods is that this method uses more of the available data. However, this 'external' cross validation is computationally demanding, since it requires building *n* artificial models.

If a cross validation method is used for determining the optimum number of steps *l*, then it is referred as an 'internal' cross validation. Amongst the different 'internal' cross validation methods, full cross validation is known as a strict technique. In this method, at each step a leave-one-out cross validation, as described above, is performed. Thereby, a RMSEP value is given corresponding to each step. By performing this 'internal' cross validation method until the last possible step, obtained RMSEP values can be plotted against the number of PLS Principal Components. In this plot, the optimum number of steps can be determined – which corresponds to as few steps as possible and yields the lowest (or almost the lowest) RMSEP. Determining the optimum number of steps (equivalent to the optimum number of PLS Principal Components) is of importance and interest, since it affects the computational costs and model complexity directly. Moreover, taking too many steps may make the model too general. It leads to over-

[12] PREdiction Sum of Squares. For more reading about PRESS refer to [69].

fitting (overtraining) and consequently poor predictive power, because of chance relationships built in the presence of noises[13]. On the other hand, taking too few steps (underfitting) avoids the model to be specific enough to describe the entire desired relationship between **X** and **Y**.

Martens (1997) [71] and Martens and Dardenne (1998) [72] are known due to their outstanding research works on full cross validation. Using both simulated and real data, they showed that full cross validation is superior to other similar methods for determining optimum number of steps as well as estimating *prediction error*.

The measure of relative closeness for evaluating goodness of fit is called the coefficient of determination [73] (or squared multiple correlation coefficient [74]) and is shown by R^2. The value of R^2 is a fraction between 0.0 and 1.0, and has no units. This value quantifies how well the measured data is fitted by the statistical model. Higher values indicate that the statistical model – sometimes simply a line or curve – comes closer to the measured data.

It should be noted that R^2 is not really the square of anything. More specifically speaking, R^2 is not actually the square of correlation coefficient R.

To calculate R^2, the distances between the measured *Y*-variable values and their corresponding modeled (predicted) values are calculated and squared. Sum of these squared differences is called residual sum of squares:

Equation (3.13)

$$SS_{res} = \sum_{i=1}^{n} (y_{i\ measured} - y_{i\ modeled})^2$$

where SS_{res} is the residual sum of squares.

The difference between each measured *Y*-variable value and the mean of the measured *Y*-variable values is calculated and squared. Sum of the squared differences is called total sum of squares:

[13] For further reading on this subject refer to the book by H. Lohninger (1999) [132].

Equation (3.14)

$$SS_{tot} = \sum_{i=1}^{n} (y_{i\ measured} - \bar{y})^2$$

where SS_{tot} is the total sum of squares and $\bar{y} = \frac{1}{n}\sum_{i=1}^{n}(y_{i\ measured})$ is the mean of the measured *Y*-variable values.

SS_{tot} represents the total variation of the measured data. The share of this variation which is unexplained by the model equals to SS_{res}/SS_{tot} [75]. If the model fits the measured data well, SS_{res} will be much smaller than SS_{tot}.

R^2 is then defined as:

Equation (3.15)

$$R^2 = 1 - (SS_{res}/SS_{tot})$$

In the following, a very simple example elucidates the subject further. Consider a set of measured values (y_i) as 1, 4, 2, 4 and 4. In Figure 8, these measured values are included in both diagrams. In the left diagram, the horizontal line corresponds to the mean of the data ($\bar{y} = 3$), and the vertical dotted lines indicate how far each data point from $\bar{y}$ is. These distances squared and then summed together, SS_{tot} is obtained which equals to 8.0. In the right diagram, an arbitrary linear model is fitted to the data. In this diagram, the vertical dotted lines illustrate the distance between each observed data point and the model. These distances squared and then summed together, SS_{res} is obtained which equals to 7.7. In accordance with Equation (3.15), R^2 equals to 0.0375.

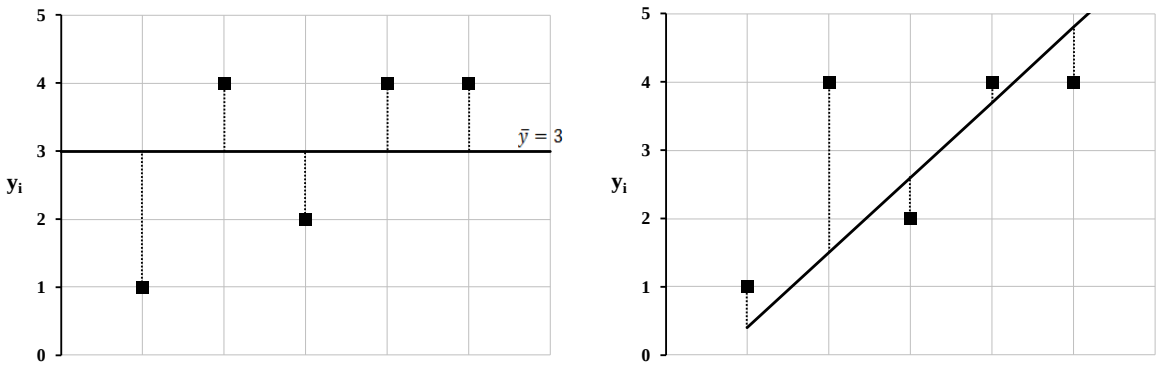

Figure 8. Line of mean value (left) and fitted model (right).

3.6 Summary

In this Chapter, some fundamental terms concerning the (passive) acoustic measurement technique were introduced. In Figure 9, a general layout of the arranged passive acoustic measurement system in the current thesis is schematically presented. The numbered items in Figure 9 are: (1) an impacting grain, (2) impacting head, (3) piezoelectric accelerometer (sensor), (4) analog signal and (5) digital signal. This Figure describes the components of the arranged system, their functions and, the connections between them.

The following briefly describes how the passive acoustic measurement system in the current thesis operated:

A grain impacts on the surface of the impacting head. Transient elastic waves propagate within the impacting head. This imposes mechanical acceleration on the sensor. The sensor gives a voltage signal, which is proportional to the grain's impact. This analog signal is transmitted to the DAQ device. In this device, the signal is prepared and then, digitized. The output digital signal is transmitted to a computer. The data is acquired and recorded by the computer. By help of softwares, the specified signal processing procedures and statistical multivariate modeling method are performed on the data. Finally, the desired information (in this case, size distribution of the impacting grains) is obtained.

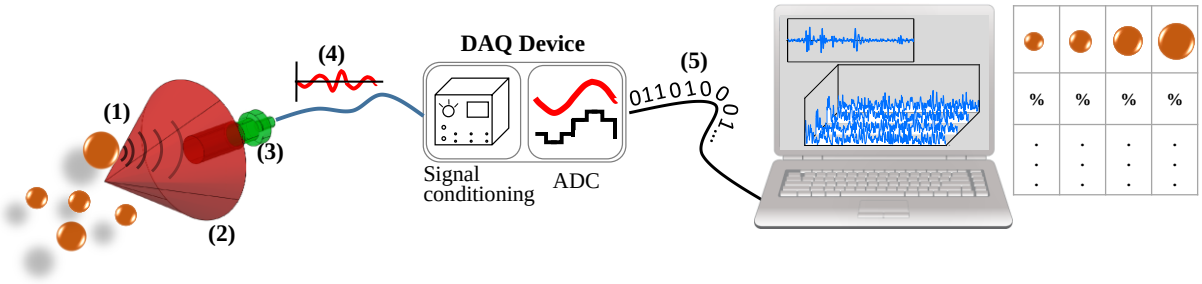

Figure 9. Schematic layout of the acoustic measurement system in this thesis.

4 Literature review

The very first documented acoustic observation is known to have been made in the 8th century by Persian alchemist Jabir ibn Hayyan (born in 721, Tus, Iran). In a book, Hayyan wrote that Jupiter (tin) gives off a *"harsh sound or crashing noise"* when worked, while he described Mars (iron) as *"sounding much"* during forging [76].

Ever since then, the dependency and sensitivity of acoustic waves on different phenomena have made the passive acoustic method an extremely useful tool as measurement, diagnose and monitoring system. In the last three decades, as the development of the digital technology has been bringing up more and more powerful computation facilities to the market, and major progresses have been made in sensor technology and electronic equipment, the passive acoustic method has consequently experienced a significant growth in use. This method is inexpensive, reliable, easy to implement, robust, suitable for real-time measurement purposes and applicable under a very wide range of conditions.

In the present Chapter, through a comprehensive literature review, numerous application cases of the passive acoustic technique within the last three decades are presented. At the end of this Chapter, based on the reviewed previous works, key issues about application of this method are summarized and discussed.

4.1 Overview of previous works

Belchamber et al. (1986) [77] investigated the hydration of silica gel using a piezoelectric transducer (Brüel & Kjær, type 8312) in a purpose built 'AE[14] cell'. As silica gel hydrates, gas is evolved which causes the granules to fracture and produce sound. They showed that the signals were linked in a quantitative manner to three different aspects of the reacting silica gel. These aspects were: weight (0.05-1.00 g), initial water content (0-23%) and mean particle size (0.5-3.0 mm). In the second part of the study, they determined 5 different variables from the acoustic data. They applied these variables as input in a PCA[15]. The PCA indicated that the individual signals can be related to distinct physical processes (e.g. bursting of gas bubbles or fracture of granules) in the 'AE cell'.

Zeng and Forssberg introduced an acoustic sensing system for monitoring the grinding process in both laboratory (Zeng and Forssberg (1992) [78]) and industrial scales (Zeng and Forssberg (1993) [79]).

[14] Acoustic Emission
[15] Principal Component Analysis

In the laboratory study, the vibration waves from a rotating ball mill (D 300 mm, L 300 mm) were picked up by an accelerometer which was fastened on the surface of a bearing under one of the supporting rollers. A dolomite with grain size of <3 mm and solid density of 2.85 t/m^3 was used as grinding feed material. The recorded signals were represented in frequency-domain by using FFT. Relationships between the grinding operating parameters (grinding time, mill speed, powder filling, pulp density and pulp temperature) and the frequency bands were established. They suggested that by observing the changes of the specified frequency bands, an efficient method can be developed for monitoring the grinding process.

The laboratory experiment was later extended to an industrial scale primary ball mill (D 4.2 m, L 5.4 m) [79]. Fine crushed iron ore (<10 mm) was fed to the mill. In addition to a mounted accelerometer on a bearing, a microphone (AKG, type C1000S) was placed 20 cm away from the mill's outside shell. PCA and regression techniques were used to establish models for estimating some grinding operating parameters. They showed that the combination of sound and vibration waves could be used very well for estimating the considered parameters: power draw (in kW), pulp density (in % solid) and particularly, feed rate (in t/h) and 80% passing grain size of the product (in mm).

Williams et al. (1996) [80] were the first to apply acoustic emissions for monitoring hydrocyclone performance. They reported a case study where a piezoelectric sensor was mounted on the exterior of a 50 mm diameter hydrocyclone for monitoring its performance and fault condition. Two silica sand slurries with different grain size distributions were tested. Measurements were performed under a wide range of solid concentrations ranging from 10 to 50 %, as well as feed pressures ranging from about 0.7 to 3.1 bar. The collected data was analyzed quantitatively using PCA and PLS. The results showed that up to 17 different process parameters including solid concentration, flow rate, and density, as well as two common fault operating status of the hydrocyclone (roping and blockage of the underflow) could be estimated.

Esbensen et al. (1998) [81] [82] attempted using ‘clamp-on’ surface mounted accelerometers (Brüel & Kjær, type 4396) to determine the solids mass flow rate (Mf_{solids}) in a pneumatic conveying pipeline (L 21 m, D 53 mm) with a 90° bend. They used 4 different representative types of granular materials: PVC granules, sand, rape seed, and cement with mean particle sizes of respectively 472, 687, 1650 and 15 µm. PLS was employed to establish connections between measured Mf_{solids} by standard instruments (pressure sensors) and frequency spectra of the acoustic data (obtained by FFT). In this way, Mf_{solids} could be estimated very well. In the second part of the study, the effect of sensor position was investigated. As schematically shown in Figure 10, various radial and axial positions were considered. According to their results, they claimed that the bottom combination (C1-C2), and top combination (A1-A2) presented respectively the best and worst accuracy in estimation of Mf_{solids}.

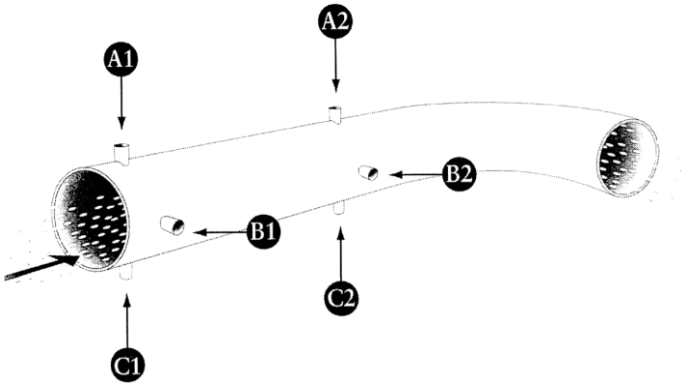

Figure 10. Different sensor positions on the pneumatic transport pipe [82].

As foodstuffs (e.g. breakfast cereals, snack foods and pastas) exit the cooking extruders, the moisture causes pockets of steam to form in the product which burst if they are close to the surface. Elsey et al. (1998) [83] used a microphone to record the sounds emitted from the product exiting a cooking extruder. The study was aimed to determine bulk density and fracture force of the product. In time-domain analysis, they calculated the number of peaks per second and, RMS value of the signal. In frequency-domain analysis, frequency content of the signal was determined by FFT and then PCA was applied to reduce the dimensionality of the data. For both GP[16] and ANN[17] modeling methods, the obtained data from time and frequency analyses was used as input variables, while bulk density and fracture force were outputs. These two properties of the product could be estimated by means of the models very well.

Houlsby and Ruck (1998) [84] mounted a microphone in a standard CPT[18] (from Fugro McClelland Ltd.) to develop an ACPT[19] (see Figure 11a). They conducted acoustic cone penetration tests in a calibration chamber which is illustrated schematically in Figure 11b. Three different sand types were each in three different levels of density (loose, medium and dense) and also in seven different combinations of horizontal and vertical stresses investigated. The frequency coefficients of the acoustic data, together with three common variables from the cone penetration tests, namely tip resistance, friction ratio and vertical stress, were used as input variables into a NN[20]. In this way, detection of sand type was perfectly succeeded. However, exact determination of relative density

[16] Genetic Programming
[17] Artificial Neural Networks
[18] Cone Penetrometer
[19] Acoustic Cone Penetrometer
[20] Neural Network

was not given. It was also concluded that the acoustic data were not strongly dependent on stresses, and so cannot be used to determine stress.

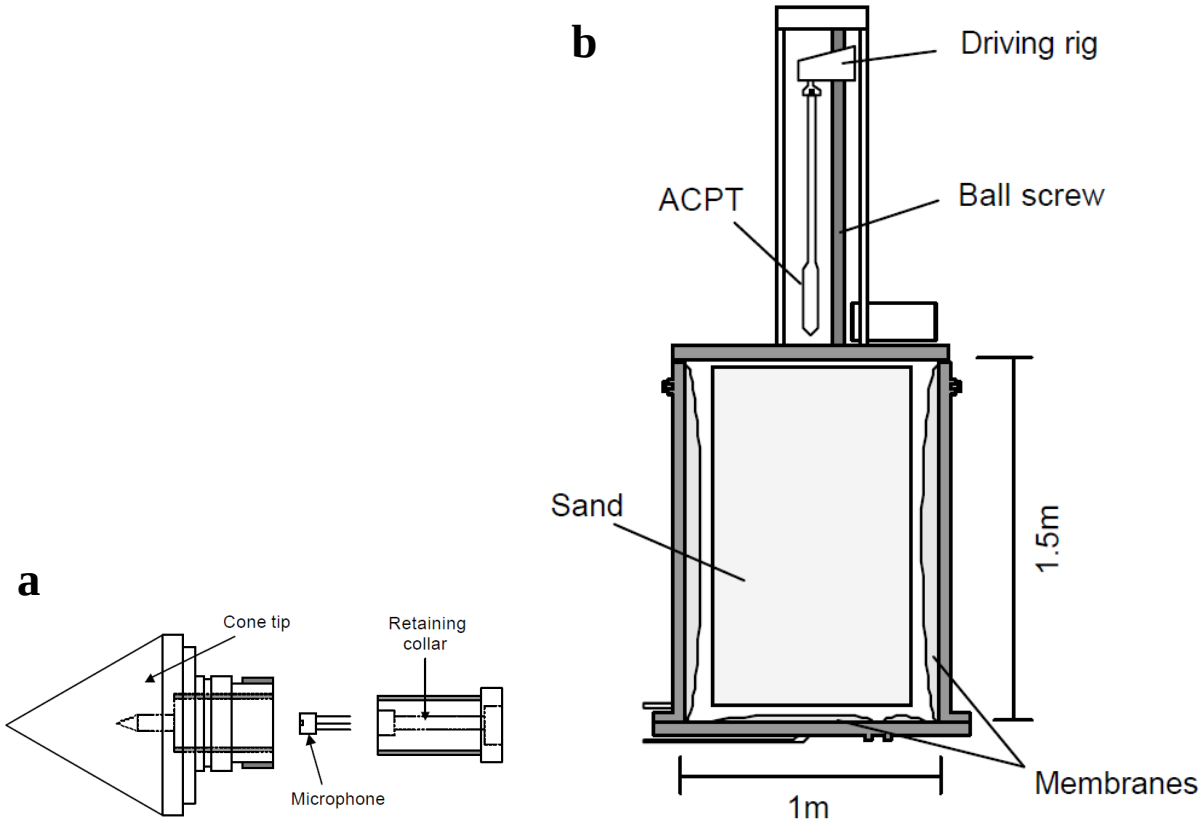

Figure 11. Schematic illustration of (a)ACPT and (b)Calibration chamber [84].

Aldrich and Theron (2000) [85] used two microphones to record the sound emissions from a laboratory–scale ball mill (D_{in} 200 mm, L_{in} 280 mm). The second microphone was intended to record the ambient noise, which could be used to improve the signal of the first microphone. They milled two different types of sulfide ore at different run times (5, 10, 15 … 45 and 50 minutes) and at the end of each run they took samples for sieve analysis. Using FFT, the signals were represented in frequency-domain and the results were then related to grain size distribution by use of a regression method. In Figure 12, for a fine material, as well as a coarse one, grain size distribution obtained by the acoustic method is compared with sieve result. For both materials, significant inconsistency (up to almost 30%) between acoustic results and sieving can be seen.

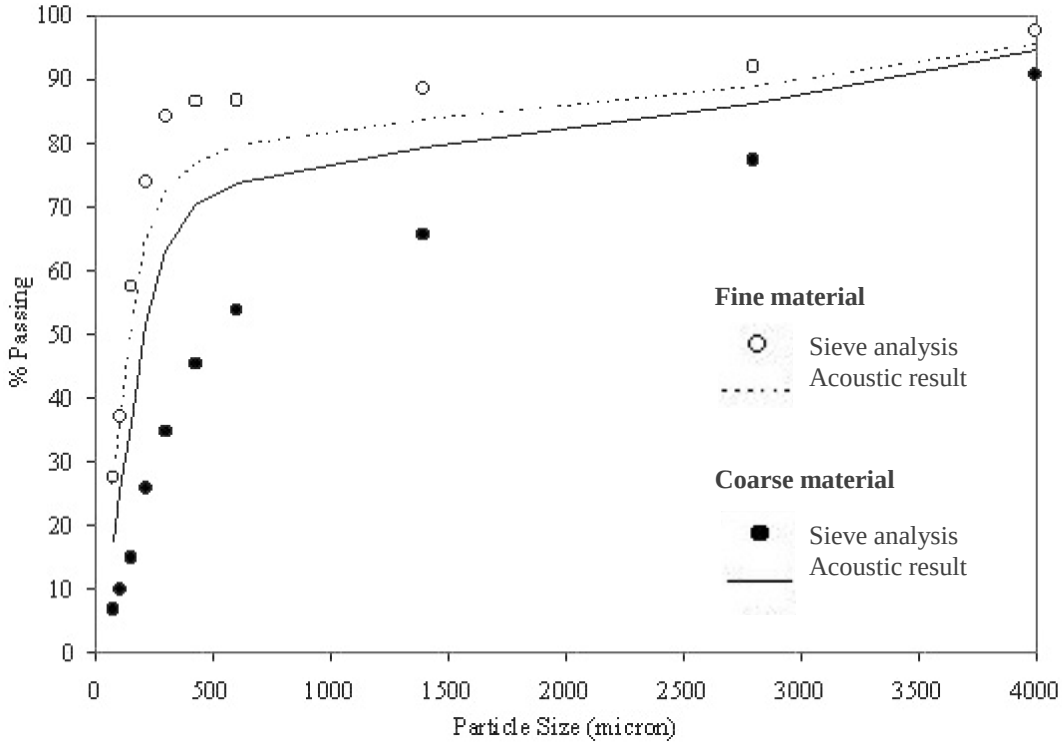

Figure 12. Comparison between acoustic results and sieve [85].

In the review paper of Boyd and Varley in (2001) [29], the passive acoustic measurement method was introduced as a mean of monitoring physico-chemical changes within various chemical engineering processes. They outlined several examples, where acoustic emissions from the processes had been studied. The examples included:

Investigation of bubble sound in gas-liquid dispersions for characterizing and monitoring bubble size and some other factors. Emitted acoustic waves from solid mixing and transport processes had been related to various process parameters. Certain chemical reactions had been shown to emit acoustic waves. These emissions had been used to classify and follow the reactions. Fault detection in a process plant through analyzing the emitted acoustic waves had been also studied.

Boyd and Varley concluded that *"...despite any disadvantages, passive acoustic measurement is potentially a powerful process-monitoring tool, which could allow insight into the physico-chemical state of the process where other techniques such as photography/video are inapplicable or require off-line, time-consuming analysis.*"

Huang et al. (2003) [86] used a technique similar to Esbensen et al. (1998) [82] to estimate the dust fraction of different types of alumina[21] during pneumatic transport in

[21] Aluminum oxide, Al_2O_3

an industrial scaled test rig (max. transport length of approx. 500 m). The dust fraction was defined as the percentage of particles finer than 21 or 42 µm. Based on the earlier findings from [82], they adopted bottom sensor positioning. For each alumina type, 15 runs were conducted and during each run 5 samples were taken. The dust fractions of the samples were measured by laser diffraction method. In each case, the acoustic data together with the laser diffraction results were applied in a PLS model. By using the models, the dust fraction was successfully estimated based on the acoustic data.

Björk and Danielsson (2004) [87] installed an accelerometer (Brüel & Kjær, type 4396) on a refiner in a paper pulp mill. The aim of their study was to determine the fiber length distribution (0-4.5 mm) through analyzing the recorded signals. The process conditions were extensively varied to provide different qualities of paper pulp and also to realize various ambient noises. Parallel with the acoustic measurements, samples were taken and their fiber length distributions were determined in laboratory by image analysis method. A CWT[22] was applied on the signals. The obtained data was then related to the laboratory results. Very good agreement between the results from acoustic measurements and laboratory was reported.

In a similar study, Björk and Danielsson (2006) [88] installed the same accelerometer type on a pipe (D 30 cm) in bleachery of the same paper pulp mill. The aim of the study was to determine three quality factors of the paper pulp; i.e., length distribution, CSF[23] and brightness. Acoustic measurements were conducted and simultaneously samples were taken and their considered quality factors were measured in laboratory. A signal processing algorithm, named WT-MRS[24], was developed and applied on the recorded signals. The derived data together with the laboratory results were applied in PLS modeling. In this way, CSF and brightness were estimated *"fairly good"* and *"as good as can reasonably be expected"*, respectively. However, the fiber length distribution could not be successfully modeled.

Albion et al. (2007) installed non-intrusive microphones on an upward inclined [89] and also a horizontal [28] transport pipe (D_{in} 10 cm) in a pneumatic test rig. They tested three different solids (polyethylene pellets, glass beads and PVC powder) at various solid fluxes and gas velocities. The aim of their study was identifying the two flow regimes (dilute phase and conveying over settled solids) based on the acoustic measurements. Simple analysis of the recorded signals failed to detect the two flow regimes. Some further analyses in frequency-domain did not succeed either. But applying a statistical function (known as V Statistic) on the raw signals provided the possibility of detecting flow regimes. Applying the V Statistic on the filtered signals,

[22] Continuous Wavelet Transform
[23] Canadian Standard Freeness
[24] Wavelet Transform Multi Resolution Spectra

rather than raw signals, provided even better results. In contrary to the results of Esbensen et al. (1998) [81], here no significant difference between acoustic measurements on top, on side or on bottom of the pipe was reported.

Additionally, Albion et al. (2007) [89] used pressure transducers to record pressure signals simultaneously with the acoustic sensors at different locations along the inclined pipe. The analysis techniques which were applied on the acoustic data, together with further processing methods, were tried on the pressure signals. However, detection of the flow regimes, using pressure signals, was not possible.

Bruwer et al. (2007) [90] mounted two accelerometers on the underside of a chute in a snack food production line, as shown schematically in Figure 13. Vibrational waves were created as pieces of product fell from an overhead conveyor belt onto this chute. The frequency spectra of the recorded signals were computed by FFT. The yielded spectra were used in PLS modeling. Based on the models, two desired textural properties of the product, i.e. 'blister level' and 'brittleness', were estimated very well.

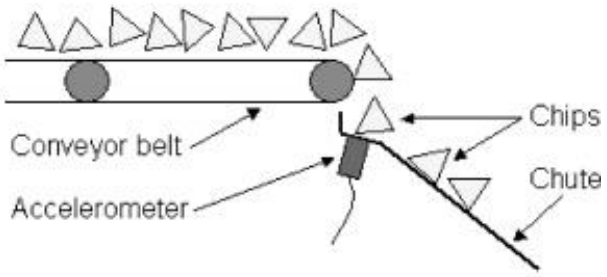

Figure 13. Sensor positioning in a snack food production line [90].

Daniher et al. (2008) [91] investigated the application of acoustic measurements for end-point detection in a high-shear granulator with 10 L capacity. In their study, the end-point of granulation was reached when the granule size had a narrow distribution by 600 μm. They used 5 microphones (PCB, type 130D10) placed on different areas of the granulator, in order to find the optimum location. They also attached an accelerometer (PCB, type 353B34) to the outside wall of the granulator bowl. Samples were taken during the acoustic measurements and their grain size distributions were measured by using a laser diffraction device. Different signal processing techniques were applied on the recorded signals. It was proved that among the different positions, microphone 4 (located in the air exhaust of the granulator) have had the optimum location. Analysis of its data resulted in successful identification of the end-point. The data from the accelerometer, showed some correlation to physical changes during the granulation process, but the end-point could not always be clearly determined.

Briens et al. (2008) [92] installed a microphone (PCB, type 130D10) in the air outlet of a 1.5 m diameter rotary dryer. The dryer was used in the production of molecular sieves (crystallized synthetic zeolite grains). The tested grains had a mean diameter of 3.2 mm. The critical end-point, corresponding to the minimum moisture content of the product before 'over-drying', was detected successfully by analyzing the recorded acoustic signals. In the second part of the study, they used the obtained frequency spectra from FFT, as well as wavelet components, each as input parameters in separate regression models and moisture content as output parameter. They concluded that the moisture content could be determined from both models.

Extensive research work on the passive acoustic measurement method has been carried out in the recent years at department of surface mining and international mining in Clausthal University of Technology. It has covered a wide variety of application fields. The followings are three examples amongst the different fields.

Tudeshki and Hertel (2008) [93] installed piezoelectric sensors (Bosch, type Knock) on a 'sleigh' test apparatus. The test apparatus is shown in Figure 14. With the aim of identifying various geomaterials in an active open-cast mine, the 'sleigh' was pulled over lignite, silt, fine sand and fine gravel for approx. 20 m at two different speeds (i.e. 0.08 and 0.19 m/s). The recorded signals were represented in frequency-domain by using FFT. By comparing the obtained frequency spectra, different materials could be effectively identified. In the second part of the study, the 'sleigh' was pulled over a layer boundary. Also in this case, the layer boundary from lignite to rock vein could be clearly identified through spectral analysis.

Tudeshki and Hertel (2009) [94] utilized the described technique in [93] on a bucket wheel excavator to identify different excavated materials in real-time. As it is shown in Figure 15, they installed the sensor on the bucket by help of a robust housing. The presented results proved that gravel, fine sand and silt could be very well identified and distinguished.

Figure 14. The 'sleigh' test apparatus was used in an open-cast mine [93].

Figure 15. Installation of the sensor on the bucket [94].

Tudeshki et al. (2012) [95] installed a piezoelectric accelerometer in the cone of a standard CPT. Several CPT field investigations were conducted in different regions in Germany. By combining the obtained acoustic data with two variables from the cone penetration tests, namely tip resistance and friction ratio, it was succeeded to perform soil characterization very precisely. Moreover, they were able to detect very thin geological layers (< 5 cm), as well as layer boundaries and single coarse grains.

They also installed sensors on hydraulic pipelines used to transport the cuttings in micro tunneling projects. The aim was continuous detection and characterization of drilled

material. Thereby, adjusting the drilling parameters in accordance with the drilled material type, as well as gapless documentation of the entire drilling progress was made possible.

Albion et al. (2009) [96] installed non-intrusive microphones (PCB, type 130D10) on a 0.05 m diameter hydrotransport pipe. The aim of their study was detecting rocks and oversized materials mixed with the transported slurry of silica sand and water. Ten microphones were used to simultaneously record signals at different locations along the pipeline. The microphone locations on the horizontal line were chosen based on the results of the model developed by Albion et al. (2009) [97]. A variety of rocks with different sizes, shapes and densities were tested in the hydraulic system within various slurry concentrations (10, 20, 30, 40, and 50 %) and velocities (1, 2, 3 and 3.5 m/s). The silica sand had a mean grain diameter of 180 µm. A relative simple analysis method (known as kurtosis) was applied on the signals. Using kurtosis, at all slurry velocities, all rocks were detected and no false indication of rocks was given. Furthermore, the kurtosis of the signals was successfully used to specify the rock size index; as a warning if a rock was oversized. Simultaneous measurements were conducted on top, side and bottom of the pipe. No significant difference between the positions was reported.

El-Alej et al. (2013) [98] used piezoelectric sensors (Physical Acoustic Corporation, type WD) to monitor hydraulic sand transport in a test rig. The experiments were conducted in a three-phase flow (air-water-sand) with various gas velocities (V_{SG}) from 0.2 to 2.0 m/s and superficial liquid velocities (V_{SL}) from 0.2 to 1.0 m/s. In this way, four levels of sand concentration were realized. The studied sand had an average grain size of 200 µm. The energy of each signal was calculated and then quantitatively related to sand concentration, V_{SG} and V_{SL}. Thereby, these three parameters were estimated successfully from the acoustic data.

Ren et al. (2013) [99] proposed a method to determine the critical speed N_f of a impeller in a gas-liquid stirred tank. As schematically shown in Figure 16, N_f corresponded to the regime transition between flooding and loading. They fixed a piezoelectric sensor on the exterior wall of the tank and then analyzed the signals in frequency-domain. The energy content of a specified frequency component increased significantly with increasing impeller speed until N_f was provided, where the energy reached its maximum and then remained nearly constant. This finding was verified under different conditions of flow rate (0.011-0.028 m^3/s), static liquid height (700 and 800 mm) and impeller fixed height.

In a similar study, Ren et al. (2008) [100] applied the same method to determine the impeller critical speed N_{js} in a solid-liquid stirred tank. When the impeller speed reached N_{js}, all the solid particles were completely suspended and no particle rested on the bottom of the tank any more. They conducted experiments on water-glass beads with

various particle diameter (0.5 and 0.7 mm) and solid concentrations (0.8-3.2×10^{-2} g/ml). Increasing the impeller speed led to reduction of energy in the characteristic frequency component. Reaching N_{js} was successfully indicated as energy remained constant.

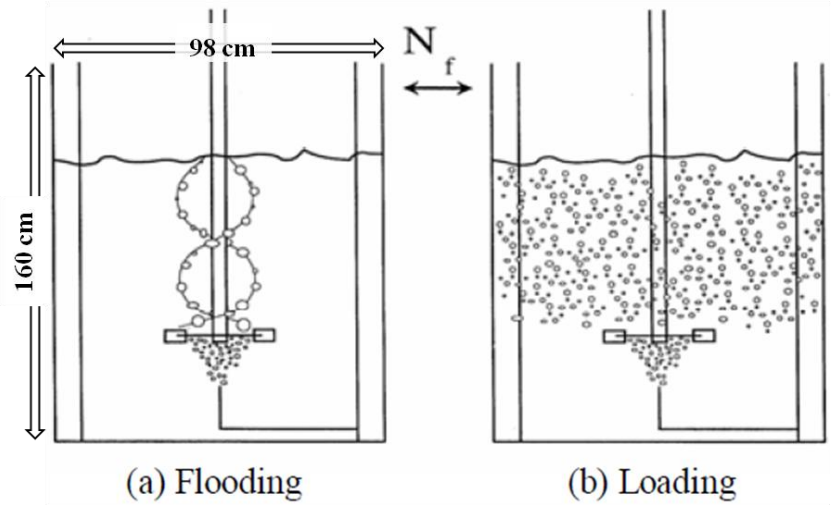

Figure 16. Impeller speed reaches N_f, flow transits from flooding to loading [99].

4.2 Discussion and concluding remarks

4.2.1 Categorization of acoustic measurements

Based on the type of application, one may currently categorize the passive acoustic measurement technique into three groups: monitoring the condition of (a) equipment, (b) process, and (c) product.

An example for the first category is the studies of Fowler (1988 and 1992) [101] [102] and Fowler et al. (1989) [103] in chemical industry. Their studies indicated that the implementation of acoustic measurements could give an early warning of developing structural flaws in in-service vessels. The application of acoustic monitoring on metal tanks, pressure vessels and fiber reinforced plastic equipment led to a significant improvement in performance under various service conditions.

The comprehensive paper of Esbensen et al. (1999) [104] provides a typical example for the second category: measurement of volume flow rate, multi-component mixture concentrations, as well as density and other physico-chemical parameters of the liquid mixtures flows in pipelines. As the second example for this category, Ihunegbo et al. (2012) [105] used passive acoustic for on-line quantitative characterization of dry matter content as an important process control parameter in the bioconversion application field. Third example is the recently published paper by Wagner et al. (2013) [106], where they determined varying concentration levels of the extraneous material (plastic pellets) in

each pneumatic flow of wheat flour and alumina. Several other examples of this category were earlier reviewed in the present Chapter.

The third category represents perhaps the most ambitious use of acoustic waves from a process, namely property determination of the product. This is akin to 'soft sensor' technology ([90] [107]). For example, Halstensen and Esbensen (2000) [33] used the vibrations generated by powder grains falling onto a surface to estimate the grain size. Their idea was using additional grain segregation to make coarse and fine grains come out of the transport system at different times. Their results were based on a laboratory experiment, with the ultimate goal to implement the technology in an industrial process. As another example, Eggen et al. (2004) [108] patented a method and apparatus for measuring viscosity of polymers flowing in a conduit using a constriction and recording acoustic emissions. The patented apparatus for determining the type of paper material, carried on a conveyor belt, by Walter et al. (1997) [109] is another typical example. Further examples belonging to this group were presented in the previous part.

The spectrum of application fields can be considered certainly even broader than the above categorization. For example, in field of seabed sediment transport, the research works of Throne (1985 and 1986) [110] [111] can be named. Thorne (1985) [110] measured the acoustic emissions, due to grain collisions, generated in a water-filled rotating drum with a hydrophone above glass spheres with diameters ranging from 0.36 to 30 mm and masses from 50 to 3000 g. He related the recorded acoustic data to the mass of glass particles. Thorne (1986) [111] continued his laboratory experiments with natural sediments (0.31-25 mm) and reported similar findings. In the same paper, he presented development of a marine system, based on the laboratory results, to study bedload transport at sea. At the end, he came to this conclusion: *"The marine work has shown the technique capable of measuring the fine details of sediment transport and thereby providing a deeper understanding of the mechanisms underlying the movement of coarse sediments"*. Another example is continuous monitoring of sediment transport (since 1986) in the Erlenbach stream in Switzerland, as reported by Rickenmann and McArdell (2007) [112].

4.2.2 Advantages of the passive acoustic method

The passive acoustic method is inherently simple, low costing, robust and independent of various environmental conditions (e.g. light, weather and dust). It hardly needs maintenance and spare parts.

One of the outstanding capabilities of this measurement method is continuity in monitoring the phenomenon being studied. It means that this method can be very well utilized as a monitoring system in real-time. In case of monitoring a process in real-time, the provided information by this method are much more representative, compared with

sample analysis, where the results merely rely on taken samples from the process. Acoustic monitoring has obviously many further advantages over the traditional method of sample analysis. In contrary to some other measurement methods, utilizing the passive acoustic technique doesn't disturb the process, needs hardly any alteration to be made to the process and the process could be in its any possible operating condition. Passive acoustic monitoring systems could be easily installed/uninstalled.

Hou (1998) [30] concluded in his PhD thesis: "*It is evident that a detailed understanding and knowledge of the process to be investigated are indispensable for successful implementations of this methodology*". However, in contrary to his conclusion, "*infer the micro-dynamic structure*" [30] of the phenomenon being studied has not been essential in any of the above reviewed successful cases. Detailed investigations of physical/chemical aspects of the phenomenon might help to optimize the utilization of the acoustic technique, but are totally unnecessary. Additionally, such investigations would be obviously very complicated, as Hou (1998) [30] states: "*the revelation of acoustic origins is basically difficult and complex*".

Therefore, one of the advantages of the passive acoustic method is that this method can be used effectively, without necessarily knowing detailed properties of the phenomenon being studied. Boyd and Varley (2001) [29] also supported this opinion: *"…research is moving away from the fundamental understanding of the physics behind the acoustic emissions towards using these emissions as 'fingerprints' describing a specific set of conditions without necessarily knowing or understanding their cause"*.

The passive acoustic method, as the name suggests, deals with the signal which is entirely produced by the studied phenomenon itself, in contrary to the active acoustic methodology where a signal is transmitted to the phenomenon. This implies that, passive acoustic systems would be used mainly for 'acoustically active' phenomena; i.e. where distinctive sound or vibration waves are available. Nonetheless, the present extensive literature review showed that the passive technique has been already used successfully under a very wide range of conditions, including relative 'quiet' processes (e.g. [77] and [83]) and high-noise environments (e.g. [79] and [85]). One may conclude that this method can be practically utilized for any kind of process accompanied by sound and/or vibration waves to get valuable information about it. Thanks to diverse developments made in the components of the passive method (measurement equipment, signal processing *etc.*), which have made this flexibility of the method possible.

4.2.3 Implementation of acoustic measurements

The decisions such as in which frequency range to measure, what kind of sensor to use and how or where to install it, which signal processing and statistical methods to apply *etc.* are not always straightforward. The choices are made usually in accordance with

the conditions of the studied phenomenon and the objectives of the study, rather than following some pre-defined regulations. In this part, a few technical issues concerning implementation of passive acoustic measurements are discussed.

Table 2 presents sampling rate f_s (or maximum frequency f_h) in some of the above reviewed studies. This Table shows that the employed sampling rate f_s (or the highest frequency of interest f_h) has been very various in different studies. In general, passive acoustic measurements can be conducted in quite different ranges of frequency.

The investigated frequency range is sometimes confined to the 'audible range' (i.e. lower than 20 kHz). However, there may be valuable information in the higher frequency ranges. But, the higher the frequencies recorded, the greater the demands on the data acquisition and processing system (with associated increase in cost). Furthermore, as highlighted by Esbensen et al. (1998) [82], the 'higher frequencies' often call for a somewhat different data analytical approaches. On the other hand, in some cases, e.g. the study of Bruwer et al. (2007) [90], it is beforehand known that the desired acoustic signatures with useful information could be intuitively heard. In these cases, needless to say, the 'audible range' would be preferred.

Table 2. Sampling rate f_s (or max. frequency f_h) in some of the reviewed studies.

Belchamber et al. (1986) [77]	Esbensen et al. (1998) [81] [82]	Elsey et al. (1998) [83]	Houlsby and Ruck (1998) [84]
f_s 10 MHz	f_h 25 kHz	f_h 13 kHz	f_s 100 kHz
Aldrich and Theron (2000) [85]	Huang et al. (2003) [86]	Björk and Danielsson (2004) [87]	Björk and Danielsson (2006) [88]
f_s 11 kHz	f_h 25kHz	f_s 80 kHz	f_s 200 kHz
Albion et al. (2007) [89]	Bruwer et al. (2007) [90]	Daniher et al. (2008) [91]	Briens et al. (2008) [92]
f_s 40 kHz	f_h 21kHz	f_s40 kHz	f_s 40 kHz
Ren et al. (2008) [100]	Albion et al. (2009) [96]	Ren et al. (2013) [99]	El-Alej et al. (2013) [98]
f_h 100kHz	f_h 40kHz	f_h 200kHz	f_s 5 MHz

In order to study a phenomenon by means of the passive acoustic method, the sensor(s) can be positioned intrusively as well as non-intrusively in respect with the studied phenomenon. For example, to study the flow parameters in a hydraulic pipeline, a sensor can be simply mounted on the pipeline (non-intrusive) or positioned inside it (intrusive) by help of a probe. Boyd and Varley (2001) [29] highlighted in their review paper: *"The advantage of acoustics is that unlike other techniques, direct contact with the process under investigation is not required so intrusion can be kept to a minimum"*. This advantage is very appealing in many fields of application, e.g. chemical, pharmaceutical or food industries, where it is imperative to employ non-intrusive (non-invasive) measurement systems. In addition to the acoustic method, there are a few methods that can be implemented non-intrusively too. But those methods have often considerable limitations. As an example, Nordon et al. (2006) [113] implied that: *"Techniques such as NIR*[25] *and Raman spectrometries can also be employed non-invasively, but only if there is a suitable window available. In comparison, acoustic waves can be transmitted through optically opaque materials such as steel or concrete"*.

According to the present literature review, almost in all of the cases it has been preferred to conduct the acoustic measurements non-intrusively rather than intrusively. It has been mainly due to simplicity, low-costing or some limitations such as lack of technical possibilities. In contrary to non-intrusive acoustic measurements, intrusive investigations have been rarely reported and thus, there is currently very limited scientific and technical basis, as well as methodology, about the subject. There are here a few reasons, why invasive studies should be carried out:

- Basically, shifting from non-intrusive to intrusive is expected to enhance the signal quality. The signal would be less influenced by the surrounding noises. More representative and meaningful information about the studied phenomenon would be received, which may be not accessible in the case of non-intrusive.
- There are cases where the passive acoustic method cannot be utilized non-intrusively at all. As an example, developing an ACPT, as described by Houlsby and Ruck (1998) [84], may not be conceivable without intrusion into the soil layers. Therefore, intrusive studies are generally essential to be carried out in order to provide the required knowledge about the subject. The obtained knowledge can be then used in a broad variety of application fields.
- For real-time measurement systems, it would be superior when the sensor is positioned so close as possible to the studied phenomenon, rather than

[25] near-infrared

positioning it non-intrusively in respect with the phenomenon. For example, in pneumatic or hydraulic transport systems, 'clamp-on' sensor positioning allows for recording a very complex signal. This signal typically involves acoustic waves from a large part of the equipment itself in addition to the waves emitted from other undesired positions rather than exactly the measurement position. This signal calls for more complicated analysis methods and, provides poor real-time measurement results. On the other hand, positioning the sensor inside the transport system by help of a probe, which is acoustically isolated from its surrounding objects, can address the complex signal problem and yield more accurate real-time results.

The present literature review showed that some of the employed data analysis techniques have been based on very complicated mathematical and statistical methods. These techniques, e.g. Artificial Neural Networks and Genetic Programming modeling methods, are due to their complexity and high number of required input parameters, quite vulnerable against any minor change in the signal. Numerous experiments usually should be carried out in order to provide the required data for 'training' such a model. A model, which is 'trained' with so much effort, is very case specific and must be re-'trained' for each single case of study.

The literature review showed that the passive acoustic method has been adopted to capture a very broad variety of quantitative or qualitative parameters. However, according to the best knowledge of the author, the use of this method for quantifying grain size distribution of granular materials has been so far scarcely researched. One of the few attempts, published by Aldrich and Theron (2000) [85], reports some experiments with only two types of test materials in a limited grain size range. The obtained results were not particularly satisfactory anyway (see Figure 12). Another attempt, published by Halstensen and Esbensen (2000) [33], deals with some laboratory experiments on only three limited grain size ranges – i.e., fractions 63-125 µm, 250-300 µm, and 425-500 µm. Their results may not be considered as grain size distribution at all; since the fractions were discrete. The rest of the reported investigations have had less challenging aims, rather than determining grain size distribution. Determining this parameter involves quantifying a series of dependent variables, while other so far published studies have been intended to determine one or more qualitative or quantitative parameter(s).

Versatility and many other positive aspects of the passive acoustic method were outlined in this Chapter. In Chapter 2, the necessities of seeking new grain size analysis methods were highlighted. These two Chapters provided the research motivation for the present thesis. This thesis documents an attempt of using the passive acoustic technique for determining grain size distribution of granular materials (sand samples). The entire steps of the experimental study are presented in Chapters 5-8.

5 Initial experiments

The proven enormous potential of the passive acoustic method and its advantages (refer to Chapter 4), and the fact that grain size distribution is a deciding factor of granular materials which should be quantified properly (refer to Chapter 2), provided the motivation to experimentally investigate the basic concepts from part 3.2 of Chapter 3. This experimental investigation included examining the relation between grain size and properties of the obtained signal.

Initial investigations were carried out with the aim of characterizing this relation and eventually setting up a methodology for determining grain size distribution. In this Chapter, these primary experiments are chronologically presented and their results are discussed.

5.1 Test materials

Among the different products from a sand and gravel quarry in Netherlands, four screened sand fractions were selected as test materials for the initial investigations. These four sand types (sand 1, sand 2, sand 3 and sand 4) have a solid density of 2.64 g/cm^3. Their nominal ranges of grain size are reported in Table 3 (in passing percentage). In this Table the commercial names of sand types 1-4 are additionally reported in parentheses. In Figure 17, photos from the samples of sand types 1-4 are presented.

Table 3. Nominal grain size distributions of sand types 1-4.

	Sand 1 (Fractie 0-250)		Sand 2 (Fractie 250-500)		Sand 3 (Fractie 500-2)		Sand 4 (Fractie 2-4)	
Grain size (µm)	Min	Max	Min	Max	Min	Max	Min	Max
63	0	5	0	0	0	0	0	0
125	0	10	0	0	0	0	0	0
250	40	50	0	15	0	5	0	0
500	100	100	80	95	10	25	0	5
1000	100	100	100	100	60	80	0	10
2000	100	100	100	100	90	100	5	25
4000	100	100	100	100	100	100	75	90
5600	100	100	100	100	100	100	100	100
8000	100	100	100	100	100	100	100	100

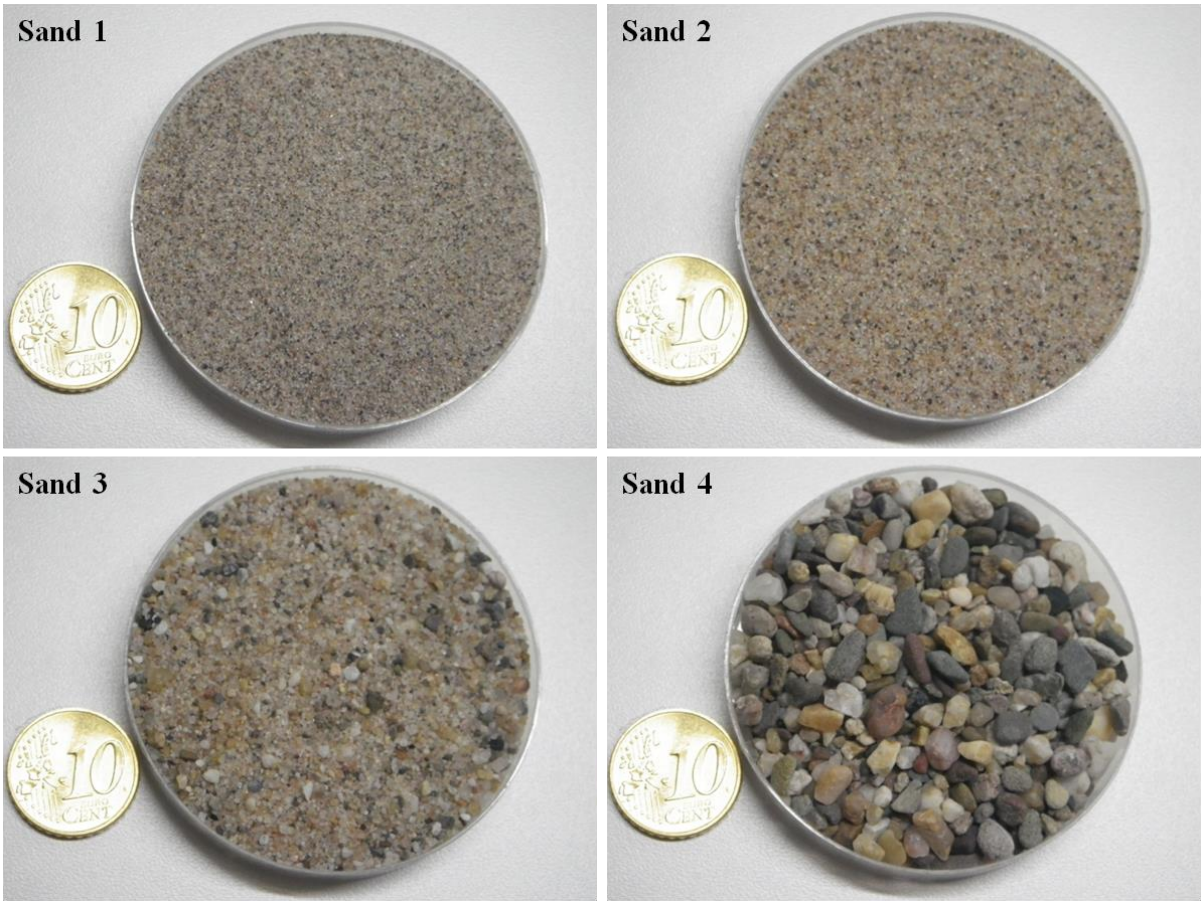

Figure 17. Sand types 1-4.

From each sand type, one sample was considered as test material for the initial experiments. The sieving results of the test materials are summarized in Table 4. Adequate amount of each homogenized test material was supplied. In this way, performance of several different experiments with the same test material was possible.

Table 4. Sieve results of the test materials for the initial experiments.

Grain size (µm)	Sand 1	Sand 2	Sand 3	Sand 4
63	0.2	0	0	0
125	1.9	0.3	0	0
250	42	16	1	0
500	100	93	15	0
1000	100	100	82	1
2000	100	100	99	9
4000	100	100	100	75
5600	100	100	100	100
8000	100	100	100	100

5.2 'Clamp-on' sensor positioning

A photo from the primary test rig is presented in Figure 18. The numbered components in this photo are:

1) Vacuum cleaner (Kärcher, type A 2054 Me),
2) Pre-separator (Kärcher, type Basic coarse dirt/ash filter),
3) Sensor,
4) POM[26] mounting,
5) Laptop (Dell, type Latitude E6400),
6) DAQ device consisted of an ADC (NI, type 6215) together with a signal conditioner (PCB, type 682A02),
7) Vibratory feeder (Sympatec, type VIBRI),
8) Induction regulator.

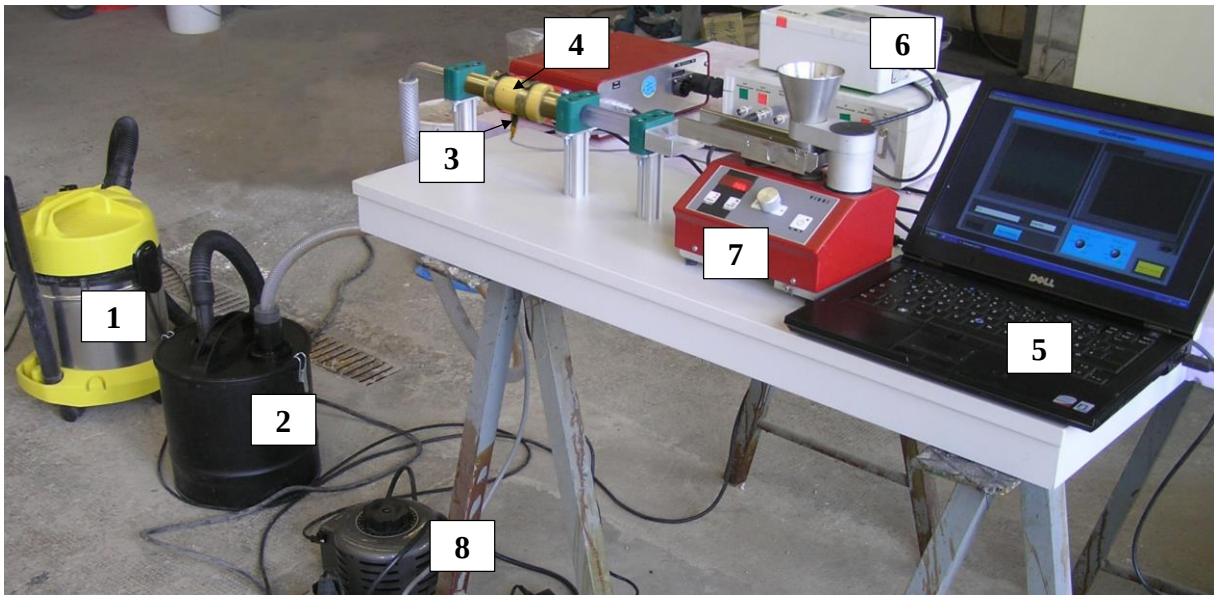

Figure 18. The 'clamp-on' test rig.

The sensor was a 10 mV/g piezoelectric accelerometer (PCB, type 353B18) [114], which was installed on a steel pipe (D_{in}=15 mm) by help of the POM mounting. The

[26] Polyoxymethylene

vacuum cleaner was used to provide air flow in the pneumatic line. The Pre-separator was responsible for collecting the transported sand and preventing it from being sucked further into the vacuum cleaner.

The intention of using the induction regulator was to provide the possibility of changing the supplied voltage for the vacuum cleaner. Thus, by varying the input voltage of the vacuum cleaner, different air flow velocities would be realizable.

Samples of sand types 1, 3 and 4 were fed into the pipe by using the vibratory feeder. The measurements were conducted with sampling rate f_s of 50 kHz and binary data was recorded on the laptop using LabView™ 2010 (NI) [115] software. The data was recorded in both *.*wav* and *.*tdms*[27] formats.

The data in *.*wav* format was in the form of voltage fluctuations with time. This data, considered as raw signals or time signals, was in FAMOS 5.0 software (imc Meßsysteme GmbH) [116] depicted. In this way, the recorded data of each tested sand type was represented in time-domain by a signal. From each signal, a 30-second long segment was selected. In Figure 19, one second of each segment is presented.

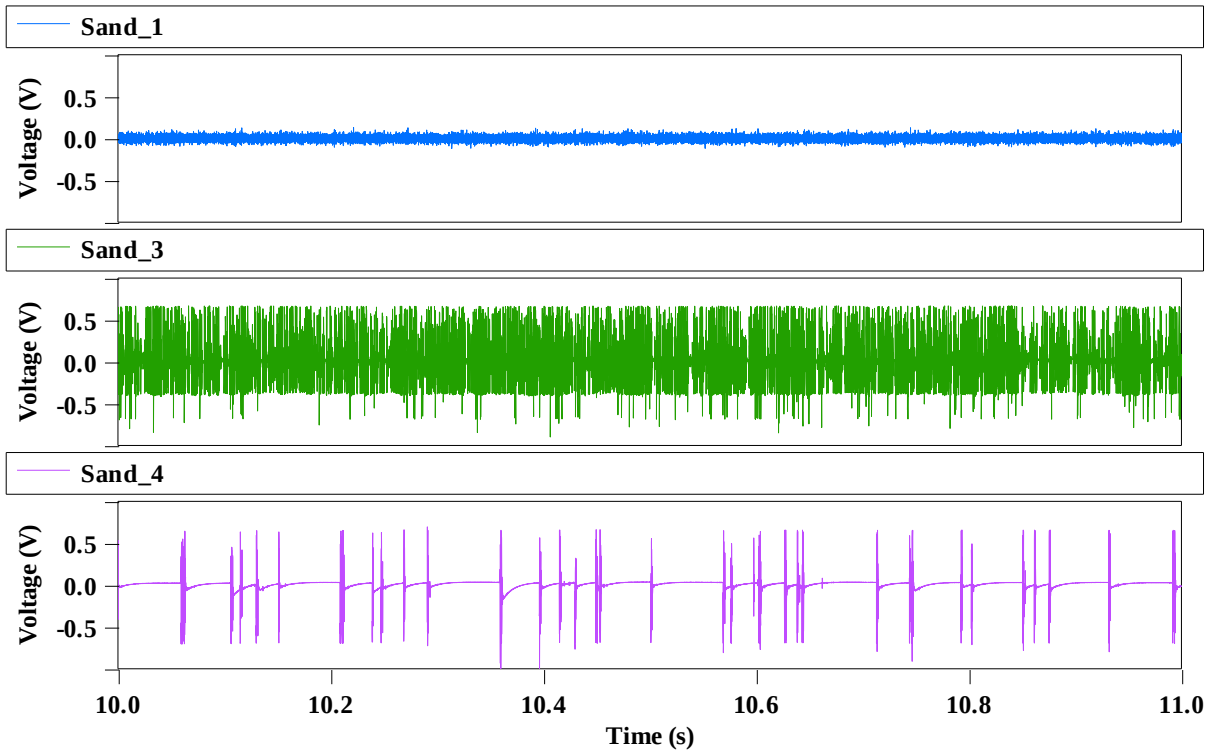

Figure 19. Raw signals from the 'clamp-on' test rig.

[27] Technical Data Management System (TDMS)

In FAMOS 5.0, the spectral analysis of each 30-second long segment was succeeded through using radix-2 variant of FFT (see part 3.4.3). Hanning windowing function with 1024 (=2^{10}) data points for each time window, without overlapping, was applied. Each resulted magnitude spectrum was over its spectra arithmetically (linearly) averaged. Thereby, averaged magnitude spectrum of each 30-second long segment was obtained. Figure 20 shows all the obtained averaged magnitude spectra. In this Figure, the recorded data from each sand type is represented in frequency-domain by a magnitude spectrum. Bearing in mind that the analog signals were sampled with a rate of f_s=50 kS/s [28], according to Nyquist theorem (see part 3.3.3) the correct representation of the data in frequency-domain was up to a maximum of $0.5f_s$=25 kHz possible.

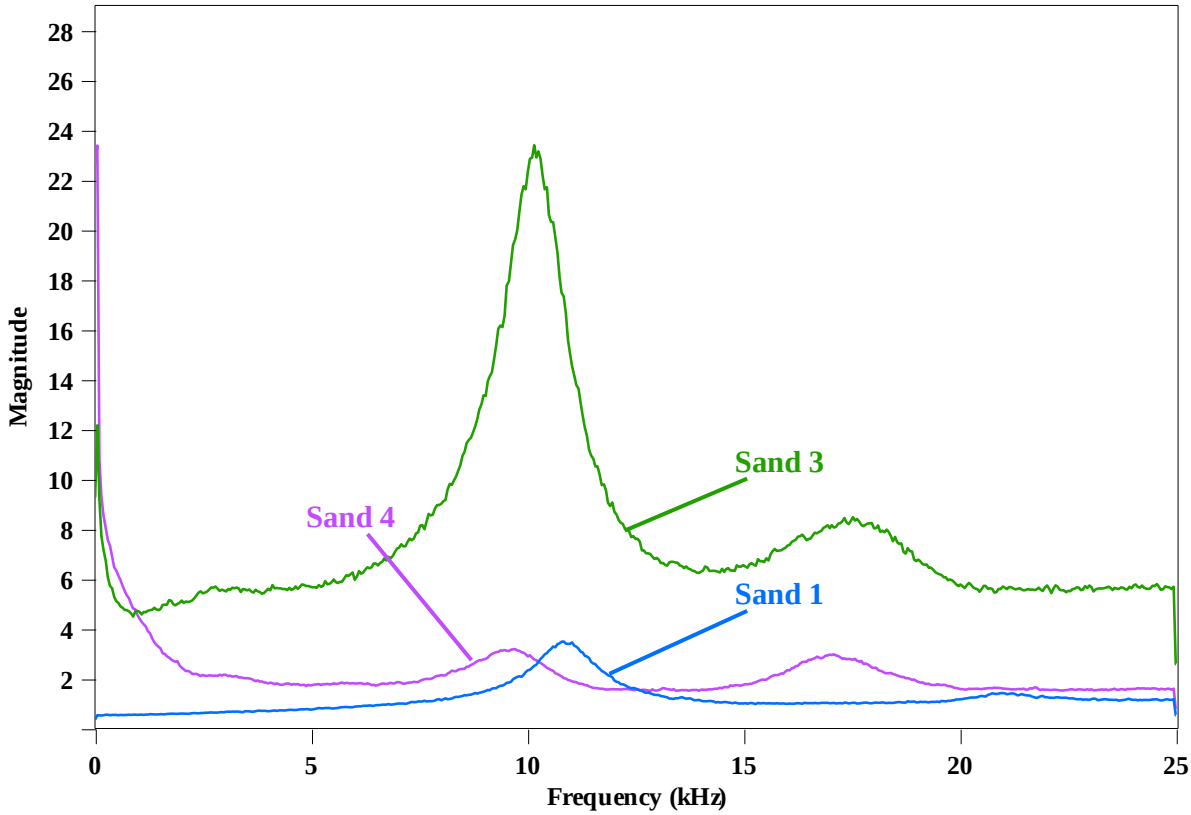

Figure 20. Averaged magnitude spectra from the 'clamp-on' test rig.

Considering the sieve results of the tested sand types (Table 4), sand 3 is finer than sand 4 and coarser than sand 1. Figure 19, however, suggests that the proportionality between grain size and voltage has not been successfully captured in time-domain. Since, the level of signal voltage in sand 3 is obviously higher than sand 1 but not much different from sand 4. In Figure 19, the individual peaks of sand 4 are unexpectedly not much

[28] kilo samples per second

‘stronger’ than those from sand 3. Also, it can be seen from Figure 20 that the tested sand types have some noticeable differences in their frequency patterns. As an instance, the position of the predominant peak around 10 kHz is not the same for all the three tested sand types.

The two above mentioned issues might be resulted from ‘clamp-on’ sensor positioning. In this case, the velocity of a sand grain in the pneumatic line, as well as its transportation regime, may have been dependent from its size. Consequently, at the sensor position, the various tested sand types may have passed by very differently; which literally means, at this position the various sand types have collided with the pneumatic line very differently. The collisions may have been different in mode and frequency of occurrence. Therefore, the expected proportionality between grain size and voltage has not been given and, the tested sand types have some differences in their frequency patterns.

Moreover, there are obvious gaps in the raw signal of sand 4; which is not the case for sand types 1 and 3. This phenomenon suggests that, although all the three sand types have been transported with the same mass flow rate, nevertheless, sand 4, due to its coarser grain size, has not collided with the sensor position so frequent such as the other two sand types. In an equal mass of each sand type, the number of grains has an indirect relation with grain size. This fact explains the occurrence of these so-called ‘air gaps’ between the peaks of sand 4 in time signal.

The ‘air gaps’ phenomenon shows its influence in frequency-domain too. In Figure 20, in almost the whole frequency spectrum the magnitude of sand 4 is unexpectedly comparable to sand 1, which both are much lower than sand 3.

Understanding the motion of grains and their collisions with the sensor position and other related issues in the current case, with the aim of establishing a quantitative relation between grain size and voltage, if at all possible, may require quite complicated analyses which did not cope with the scope and aim of this research work.

5.3 Sensor positioning in 90° bend

It was believed that, in the case of ‘clamp-on’ sensor positioning, though using a uniaxial accelerometer with very low transverse sensitivity, the signals were much more influenced by the surrounding different conditions, rather than the case, where the sensor would have been positioned inside the pneumatic line.

The other issue about ‘clamp-on’ sensor positioning was that the sensor’s sensitive axis was not oriented toward the motion of sand grains, but perpendicular to it. In this case, it was believed that the sensor would have been receiving a relatively complex acoustic emission, created by sand grains inter-collisions, as well as friction and collision with

the pipe and also other various existing vibrations in the pipe. This would have led to recording an erroneous signal. Thus, finding and establishing an applicable relation between grain size and voltage seemed to be rather more complicated than the case, where grains could be transported simply toward the sensitive axis.

The above stated issues brought about the idea of connecting the sensor to an impacting head and positioning the probe (see part 3.3.1) inside the pneumatic line. It was succeeded through making a 90° bend in the pneumatic line and positioning the probe at this bend. Figure 21 shows different photos from this positioning. The photo at top shows the rubber stud which was adopted as the impacting head. The sensor was connected to the impacting head, additionally wrapped by a rubber shell, and positioned at the bend as shown in the photo at bottom left. The bend was held fixed by means of an airproof POM element (see the photo at bottom right).

Also, instead of the steel pipe from part 5.2, a PVC hose (D_{in}=16 mm) was selected for the pneumatic line. The aim of using the rubber shell and PVC hose (made from vibration damping materials) was to acoustically insulate the probe from the surrounding periphery; and thereby, to minimize the transmission of unwanted vibrations towards the sensor. The rest of the test rig (described in part 5.2) remained unchanged. The same experimental program of part 5.2 was conducted.

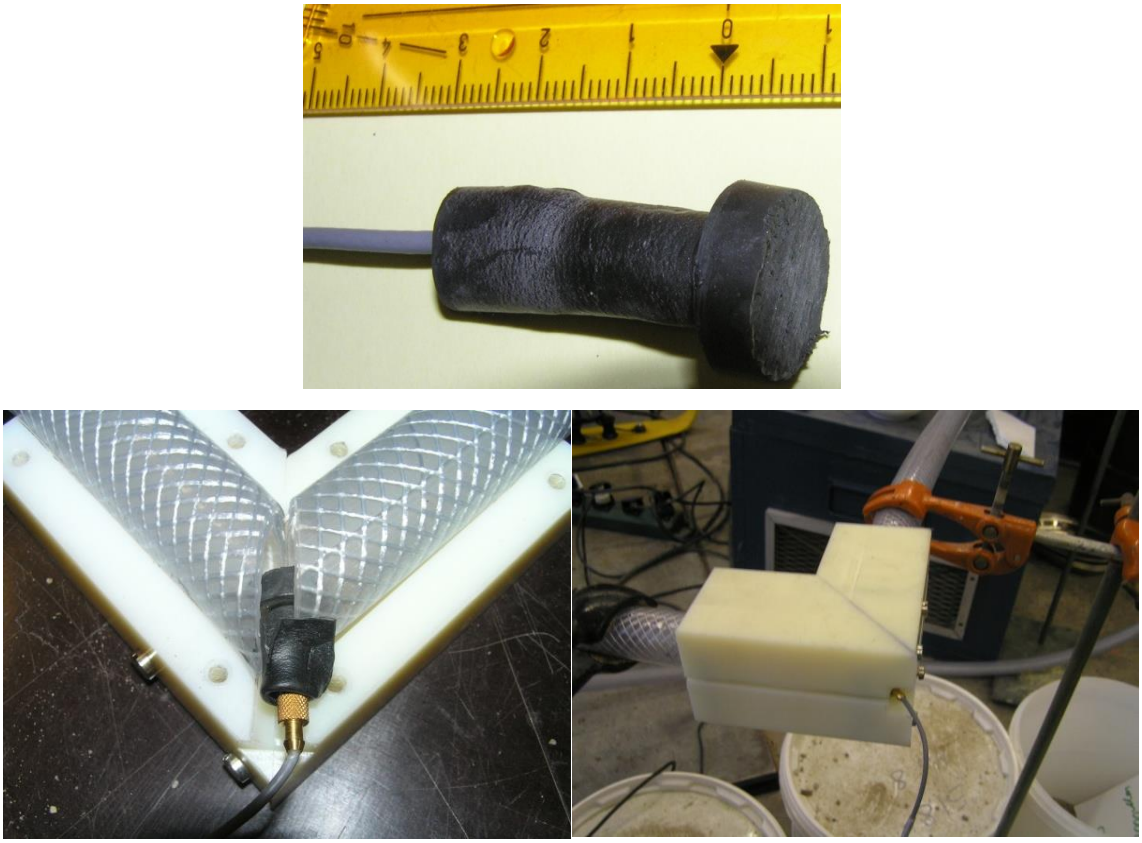

Figure 21. The 90° bend test rig.

In FAMOS 5.0 software, the identical procedures described in part 5.2, were carried out. In Figure 22 and Figure 23, one second of each raw signal segment and the obtained averaged magnitude spectra are presented, respectively.

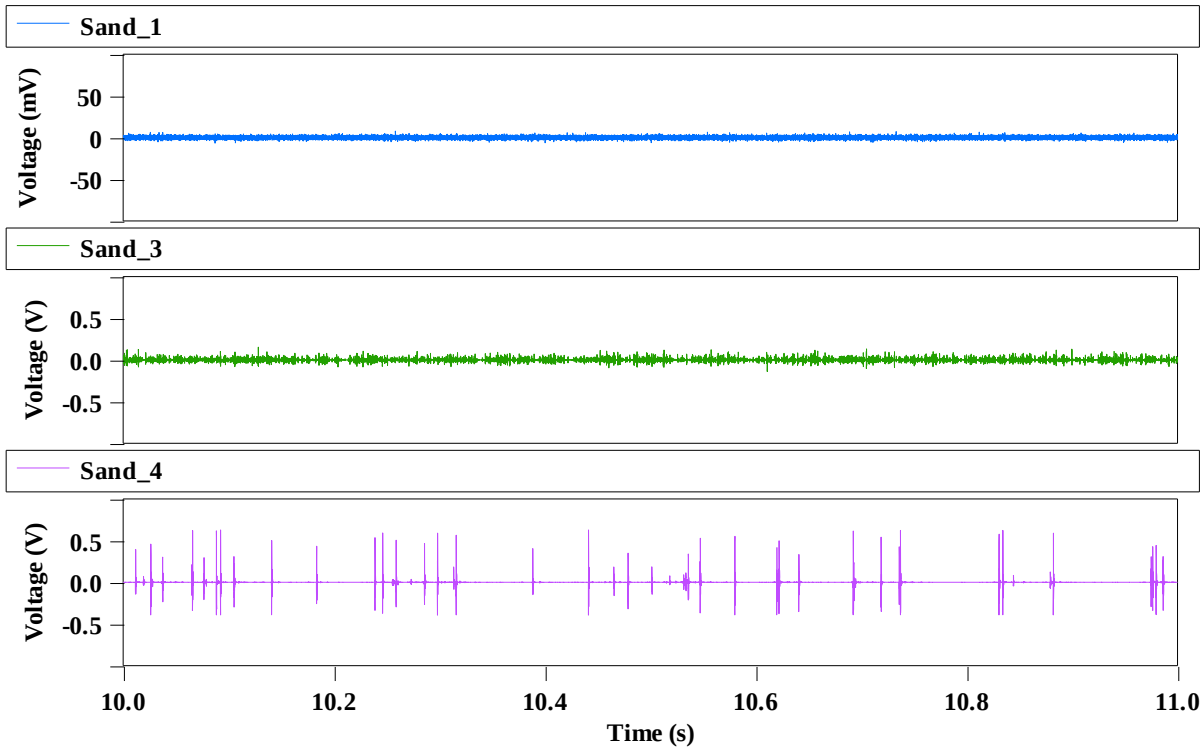

Figure 22. Raw signals from the 90° bend test rig.

Compared to the ‘clamp-on’ sensor positioning, the recorded raw signals in 90° bend have generally lower levels of voltage. In simple words, the signals have become ‘quieter’. That’s because of using a probe made of rubber, in which the induced vibrations would be attenuated much more rather than steel. Also, the effective impact surface of the probe has been smaller than the ‘clamp-on’ case.

In contrary to the ‘clamp-on’ sensor positioning, the correct qualitative proportionality between grain size and voltage is yielded. However, ‘air gaps’ can be still obviously observed in the case of sand 4.

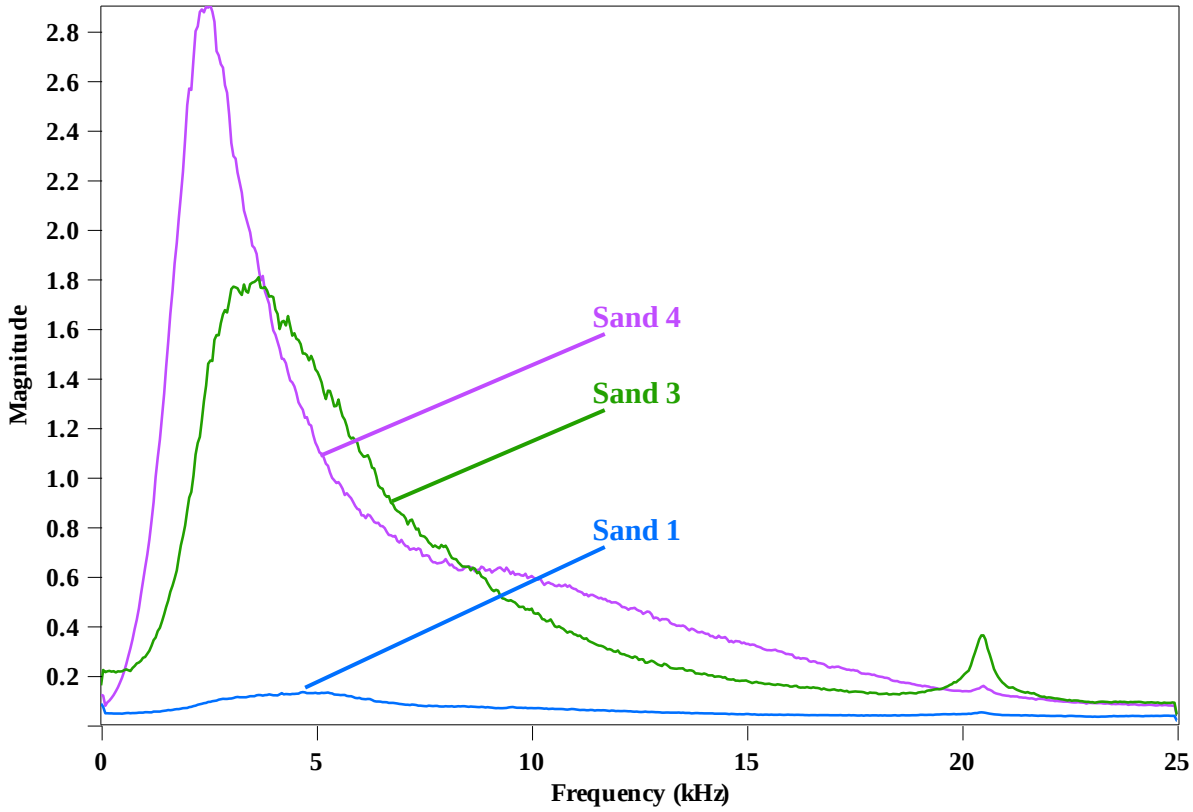

Figure 23. Averaged magnitude spectra from the 90° bend test rig.

Comparing Figure 23 with Figure 20 reveals that changing from 'clamp-on' sensor positioning to 90° bend, not only reduces the magnitude, but also alters the form of the frequency spectrum. However, similar to the 'clamp-on', here also the obtained averaged magnitude spectra prove that the sampling rate of 50 kHz has been fast enough to capture all the present frequencies in the signal; since almost all the signal energy is represented in frequencies lower than 20 kHz.

According to Figure 23, the correct proportionality between grain size and magnitude is not valid through the whole frequency spectrum, but partially in 0.5-4 kHz and 9-19 kHz. In spite of stronger peaks of sand 4 (compared to the other sand types) in the raw signal, the 'air gaps' has caused the drop of sand 4 magnitude in Figure 23.

The results showed that, positioning the sensor at the 90° bend, though the sensor axis was not yet completely aligned towards the sand grains flow, has certain advantages over 'clamp-on' sensor positioning. However, it was still questionable if a representative fraction of each sand type could collide with the probe. Since the probe is positioned marginally in the pneumatic line, rather than centrally. The next part presents a new configuration, by which positioning the probe centrally in the pneumatic line was given.

5.4 Centrally positioned probe inside the pneumatic line

Figure 24 shows a photo of the new element, in which the probe was centrally positioned. Thereby, the probe consisted of a sensor, impacting head made of steel and probe housing made of rubber. The probe was fixed and centered inside the element by means of three supporting arms. The element itself was made of POM.

The ‘Clamp-on’ element from part 5.2 was replaced by this element. The rest of the test rig (shown in Figure 18) remained unchanged. In addition to sand types 1, 3 and 4, sand 2 was also tested in this part of the study.

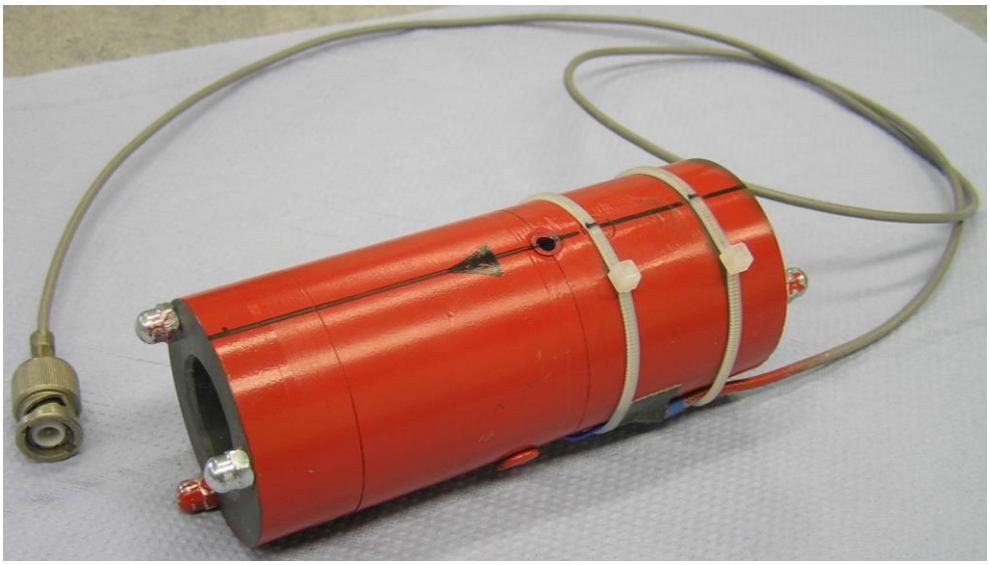

Figure 24. The element containing the probe.

The data processing was similar to the two previous parts. In Figure 25 and Figure 26, one second of each raw signal segment and the resulted averaged magnitude spectrum of each 30-second long segment are presented, respectively.

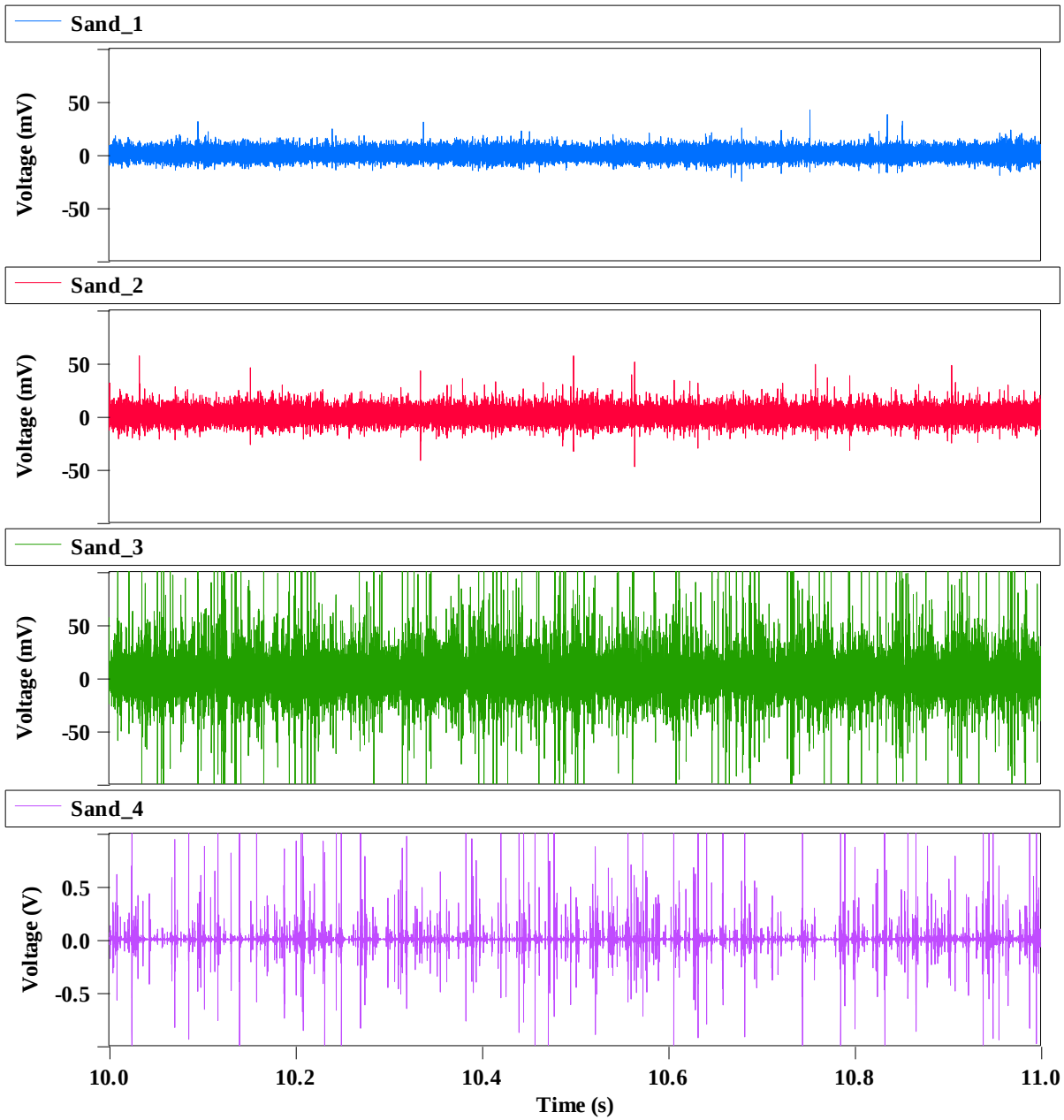

Figure 25. Raw signals from the centrally positioned probe test rig.

Figure 25 claims that a direct relation between grain size and voltage has been obtained. Furthermore, this Figure shows that centrally positioning the probe inside the pneumatic line, instead of 'clamp-on' and 90° bend, has significantly reduced the 'air gaps'. Since in case of sand 4, the number of impacts within time-unit is clearly higher

According to Figure 26, the form of frequency spectrum given by this new sensor positioning is not similar to any other two previously tested positions. In addition to the raw signals (Figure 25), the expected proportionality between grain size and magnitude can also be verified in frequency-domain (Figure 26).

Similar to ‘clamp-on’ and 90° bend, here also Figure 26 suggests that the rate of 50 kHz has been sufficient for sampling the analog signals. Since the magnitude at the highest frequencies is drastically low. Most of the signal energy is concentrated in frequencies of 0-5 kHz and 15-20 kHz.

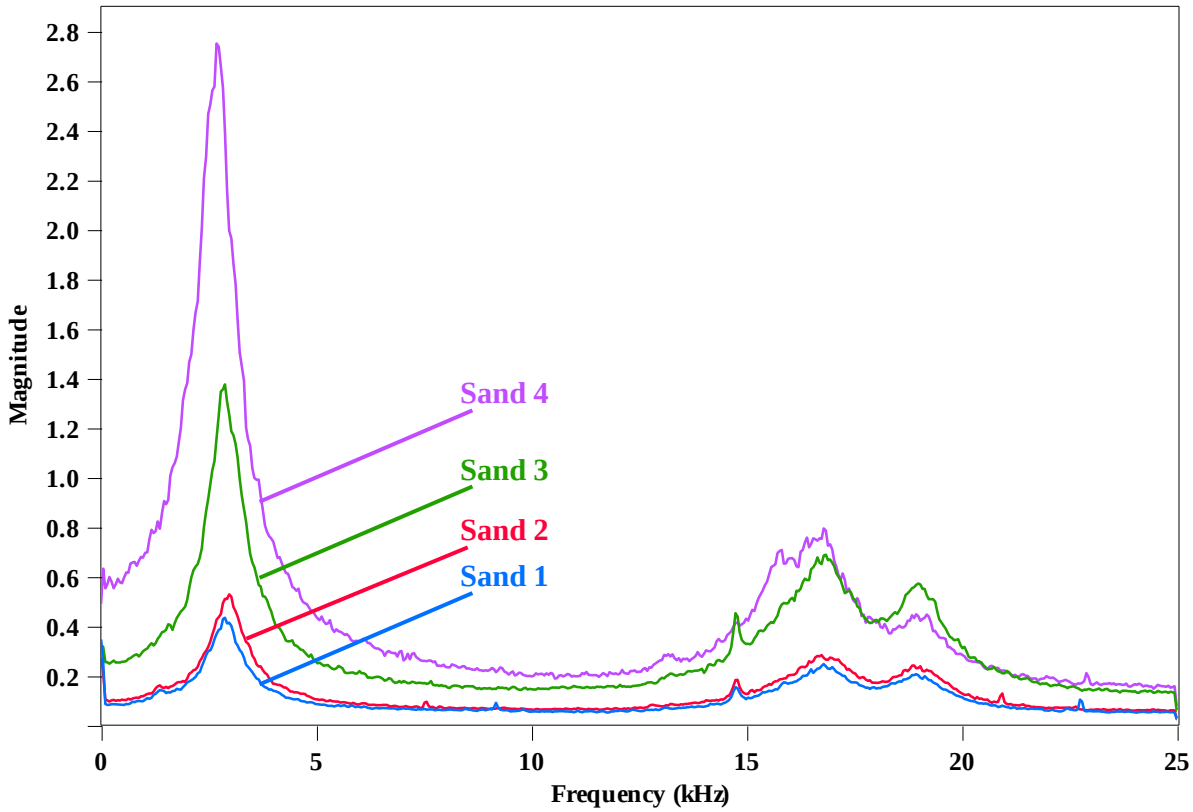

Figure 26. Averaged magnitude spectra from the centrally positioned probe.

5.5 Concluding remarks on the initial experiments

The proportionality between grain size and voltage was attempted to be investigated experimentally. Using a provisional pneumatic test rig, two modes of sensor positioning (namely ‘clamp-on’ and 90° bend) were found to be not proper. The third sensor positioning (centrally positioning the probe inside the pneumatic line) yielded promising results. These primary results verified the – not yet quantified – relation between sand grain size and voltage. These two variables were found to be directly proportional.

Based on the obtained findings from the initial experiments and promising results from part 5.4, a new pneumatic test rig was prepared and called horizontal test rig. With the aim of quantifying the above mentioned relation, diverse experimental programs were conducted with the horizontal test rig and, corresponding signal processing procedures, as well as statistical methods, were set up. These attempts are reported in the following Chapter.

6 The horizontal test rig

Similar to parts 5.3 and 5.4, a PVC hose (D_{in}=16 mm) was employed as the pneumatic line. The same steel impacting head was also used for the horizontal test rig. The rest of the test rig remained identical to part 5.4.

A very large sample (about 6 kg) from each sand type was provided. From each homogenized sample, 3 representative subsamples were taken. The grain size distribution of each subsample was determined by laboratory sieve analysis. For each sand type, the obtained 3 sieve results were averaged. The averaged sieve results of sand types 1-4 are reported in Table 5. The averaged sieve result of each sand type was assigned as its reference grain size distribution. The reference grain size distribution of each sand type is graphically demonstrated in Figure 27. In this Figure, each reference grain size distribution is represented by plotting the passing percentage of each sieve against the opening length of that sieve. The opening length is considered as grain size (in µm) and constitutes the horizontal axis. The horizontal axis in Figure 27, like in any other common demonstration of grain size distribution, is logarithmically scaled for better visualization.

Further representative subsamples were taken from the same large samples and were used for conducting the acoustic measurements in different experimental programs with the horizontal test rig.

In each experimental program, each sand type was tested three times, i.e. each experimental program included 12 trials. The data recording was similar to the initial investigations (see part 5.2).

Table 5. The reference sieve analysis of each sand type.

Grain size (µm)	Sand 1	Sand 2	Sand 3	Sand 4
63	0.0	0.0	0.0	0.0
125	1.6	0.1	0.0	0.0
250	37.0	0.7	1.2	0.0
500	100.0	93.0	9.0	0.0
1000	100.0	100.0	82.3	0.1
2000	100.0	100.0	98.4	6.5
4000	100.0	100.0	100.0	71.8
5600	100.0	100.0	100.0	99.8
8000	100.0	100.0	100.0	100.0

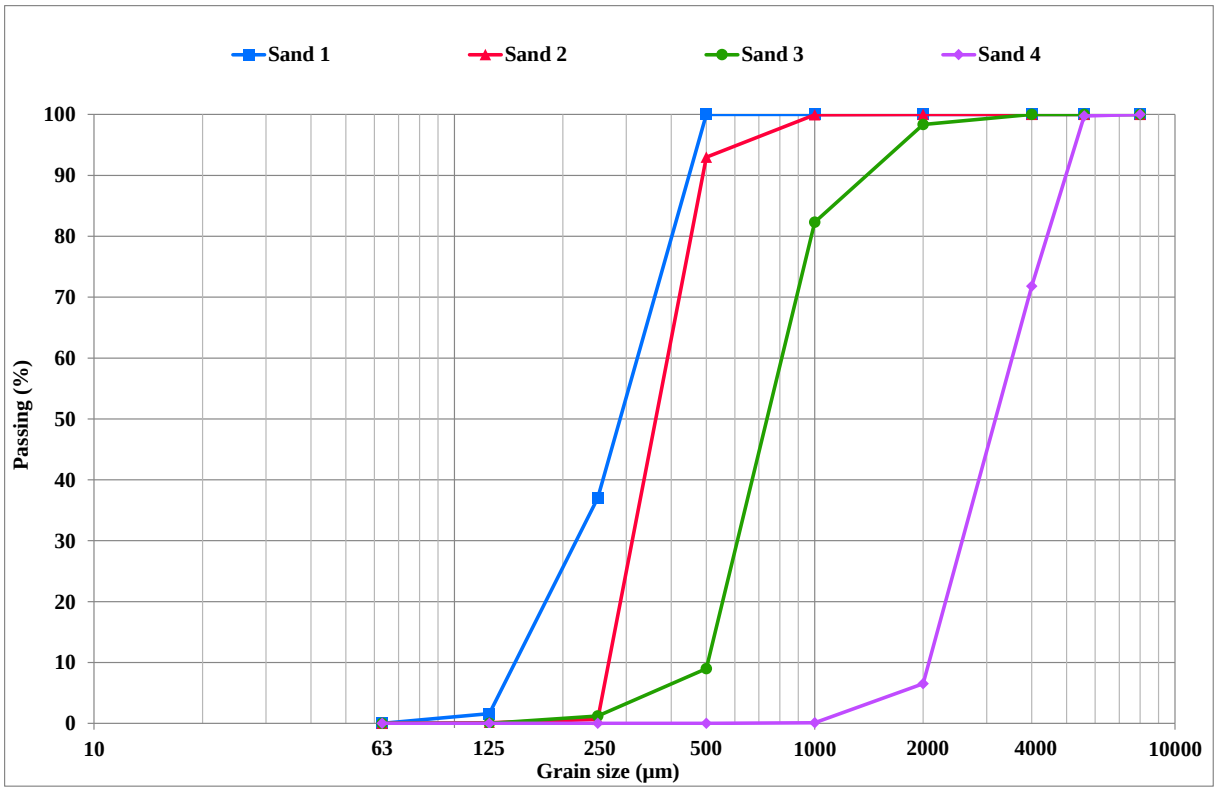

Figure 27. Sieve results of sand types 1-4.

6.1 First experiment with the horizontal test rig

6.1.1 Experimental setup

By adjusting the induction regulator to 220 volt, air flow velocity of 106 m/s (at position of the impacting head) was given. Air flow velocity measurements were succeeded by using a micro-manometer (TSI, type PVM620) [118]. The measured air flow velocity values were validated through the comparison made with the provided fact-sheet by the vacuum cleaner manufacturer [119].

Generally, the air flow velocity measurements in the current thesis were conducted only when vacuum cleaner was running and sand was not fed into the system yet. By introducing sand into the pneumatic line, air flow velocity would has obviously deviated from the measured values. In the present thesis, as mentioned earlier in part 2.3.1, superficial air flow velocity is used to describe the air flow and is expressed simply as air flow velocity (in m/s).

The vibratory feeder was adjusted with 9 mm and 70% for funnel height and vibration intensity level, respectively. With this adjustment, the vibratory feeder was able to provide a mass flow of about 27 g/s. For this experimental program, each trial was conducted by using 350 g sand.

6.1.2 Signal processing

From each trial, 10 seconds of the recorded raw signal was selected as the corresponding representative segment. Averaged magnitude spectrum of each 10-second long segment was calculated through the same procedure described in part 5.2. Figure 28 presents all the obtained averaged magnitude spectra.

The reproducibility in the 3 trials of each sand type can be proved in Figure 28. In this Figure, all the 3 spectra belonging to the same sand type are certainly comparable. Furthermore, the expected proportionality between grain size and magnitude in frequency-domain can be also observed – but not quantified yet.

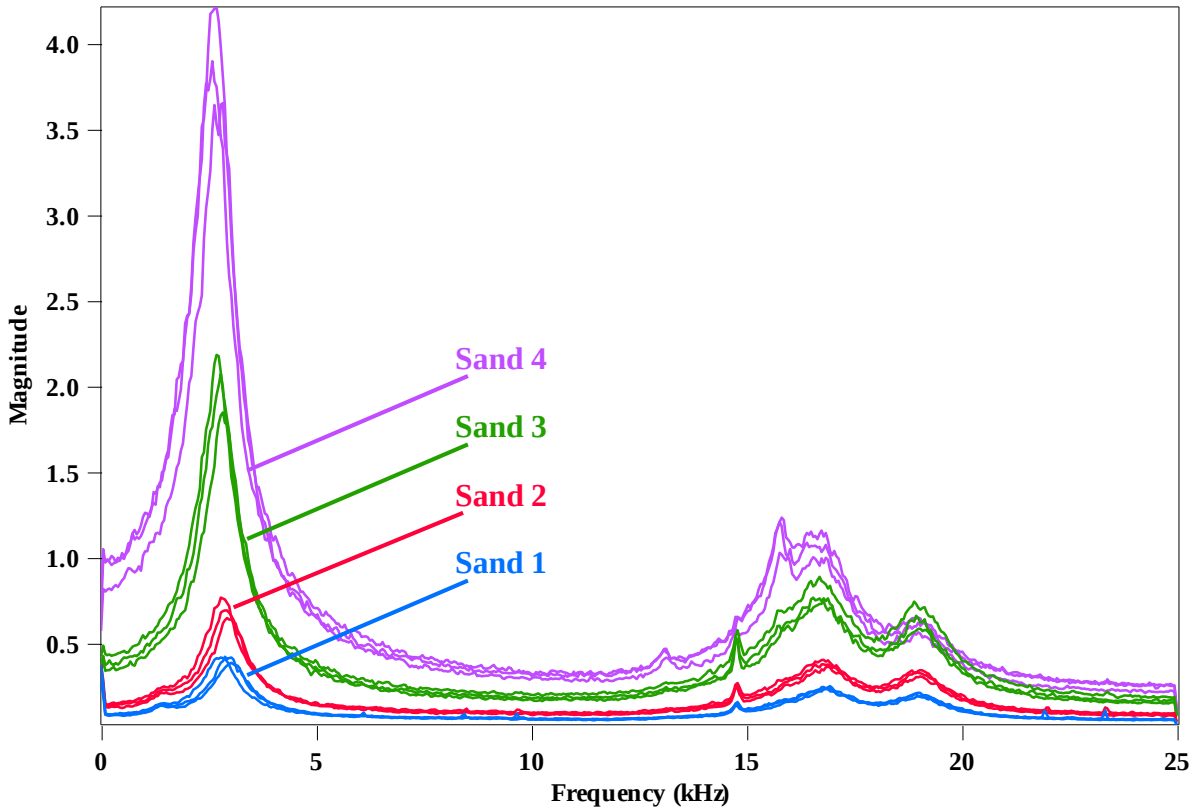

Figure 28. Averaged magnitude spectra from the first experiment.

The second trial of sand 4 was selected at its entire length. Figure 29 shows the resulted magnitude spectrum of this trial. Three time periods are marked in this diagram: (a) sand feeding is not started yet; (b) sand is being fed, and (c) sand feeding is finished. This Figure clearly shows that in presence of sand flow in the pneumatic line, the highest magnitude values belong to the lower frequency components, namely <5 kHz. It implies that the emitted signal from impacting sand grains has its highest share of energy at this frequency range. Needless to say, the same observation can be made in Figure 28 for other sand types too. On the other hand, when sand grains don't collide with the

impacting head (time periods a and c in Figure 29), the magnitude in this frequency range remains extremely low. Therefore, it might be mentioned that the components of the signal which have this range of frequency, probably contain the most share of information about the colliding sand grains. In other words, the grain size distributions of the tested sand types can be characterized at its best in this frequency range.

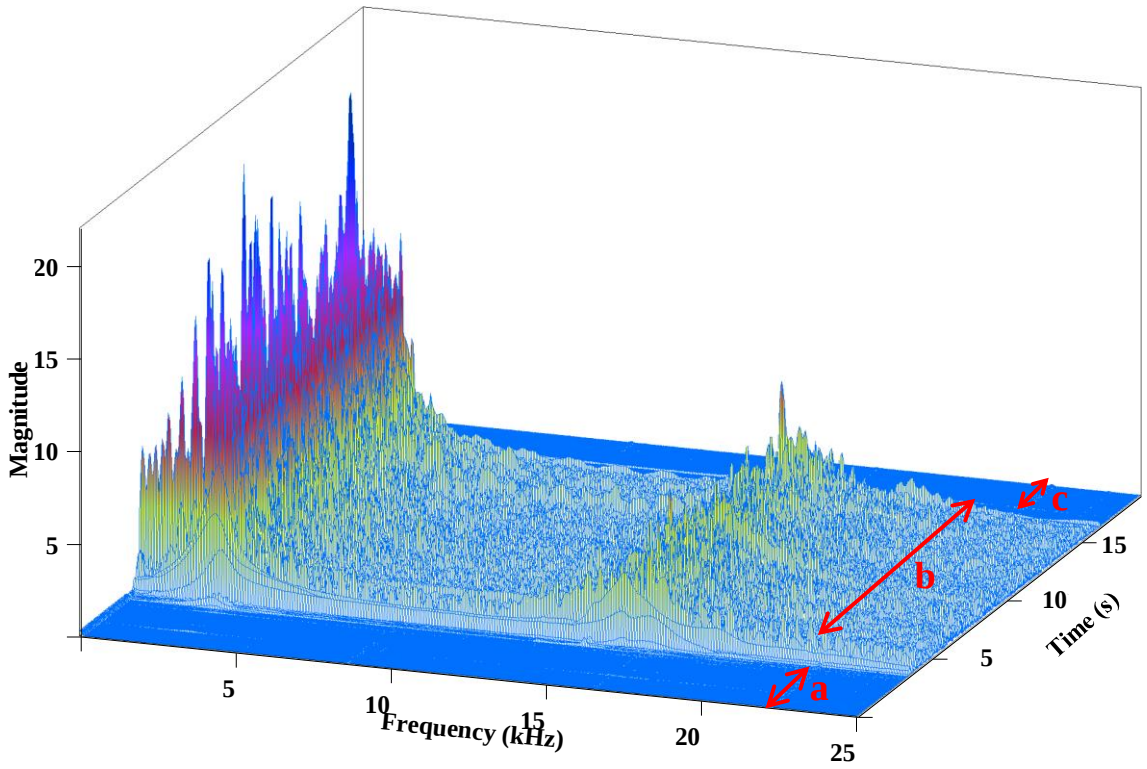

Figure 29. Magnitude spectrum from a trial of sand 4.

A Butterworth bandpass filter was applied on the 10-second long segment of each trial. The applied filter was between 1 and 5 kHz with -12 dB/octave roll-off.

To elucidate the effect of the applied filter, the whole length of the recorded raw signal from the second trial of sand 4 was undergone the same filter. Afterwards, its magnitude spectrum was again calculated. Figure 30 presents the resulted spectrum in three-dimensional demonstration. This Figure shows how effective the bandpass filter has been in attenuating various components present in the signal which have had frequencies rather than 1–5 kHz. Those neglected components were considered as unwanted noises and/or other disturbances which were of no interest. Filtering them allowed for avoiding the entrance of irrelevant information into the next steps of the signal processing procedures; which could otherwise corrupt the establishment of a quantitative relation between grain size and voltage.

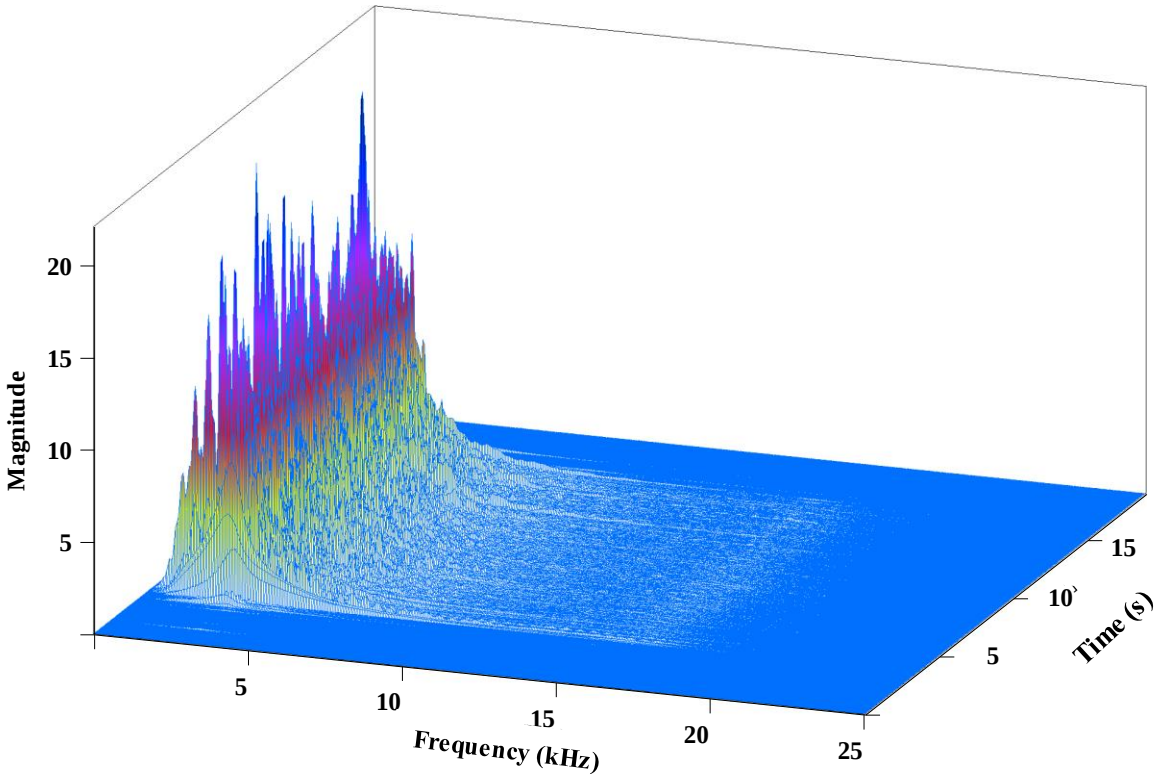

Figure 30. Magnitude spectrum of the filtered signal from a trial of sand 4.

The filtered 10-second long segment of each trial was then inputted to the FFT built-in function in MATLAB R2012b [120]. In this case, each trial was represented by a signal with a total number of $N = 5 \times 10^5$ samples, where $\Delta t = 0.02$ millisecond and $T = 10$ seconds (refer to Equation (3.3) in part 3.4.3). In order to perform the FFT function, a window length of 2^8 samples, equivalent to 5.12 milliseconds, was selected. The window length is the length of the vector which is inputted to the FFT algorithm in each single irritation. The transform length was kept equal to the window length and overlapping remained zero. It means that the length of the FFT function's output, namely the computed DFT, was set equal to its input (for further details see [120]). Thereby, a 1954×256 matrix from each trial was resulted, where the rows and columns corresponded respectively to time and frequency. The number of the columns obviously was equal to the window length, i.e. 2^8 =256; whereas, the number of the rows corresponded to:

$$\frac{(N = 5 \times 10^5) + padding}{window\ length = 256} = 1954$$

In the above calculation, padding means that the FFT algorithm inserted 224 extra zero values at the end of the input data, so that the output would be representable in a matrix with the desired transform length.

Each individual resulted matrix was over its spectra arithmetically averaged. Thereby, each trial was represented by a row matrix with 256 columns. Since the output of the employed FFT function included frequencies from 0 to the sampling rate f_s=50 kHz, therefore only the first half of the row matrix was considered for further processes. The second half was just a reflection of the first half [120], while the first half already represented the whole frequency spectrum up to the Nyquist frequency $f_s/2$. Hence, each trial was then represented by a row matrix with 128 columns.

6.1.3 PLSR calibration process

From each sand type, the obtained row matrix from the first trial was considered. These four row matrices were merged together and a 4×128 matrix was built, whose rows and columns respectively corresponded to sand type and frequency. This matrix, which included the predictor variables (*X*-variables), can be schematically described as following:

$$\mathbf{X} = \begin{bmatrix} x_{1\,1} & \cdots & x_{1\,128} \\ \vdots & \ddots & \vdots \\ x_{4\,1} & \cdots & x_{4\,128} \end{bmatrix}$$

where,

$x_{n\,m}$ stands for DFT values,

$n = 1,2,3,4$ stands for sand type,

$m = 1,2,\ldots,128$ stands for frequency.

On the other hand, the sieve analysis of the tested sand samples (Table 5) can also be represented as a 4×9 matrix, whose rows and columns correspond to sand type and grain size class (or literally the sieve used in laboratory), respectively. This matrix, which included the response variables (*Y*-variables), can be schematically demonstrated as following:

$$\mathbf{Y} = \begin{bmatrix} y_{1\,1} & \cdots & y_{1\,9} \\ \vdots & \ddots & \vdots \\ y_{4\,1} & \cdots & y_{4\,9} \end{bmatrix}$$

where,

$y_{n\,p}$ stands for passing percentage,

$p = 1,2,\ldots,9$ stands for grain size class,

$n = 1,2,3,4$ stands for sand type.

Training phase of the PLSR, as described in part 3.5.12, was performed by a code developed in MATLAB R2012b. The number of PLS Principal Components was chosen as 3. To estimate how well the model has fitted the **X** and **Y** data, the percentage of variance explained by the model for respectively *X*- and *Y*-variables was calculated (see part 3.5.1). The obtained PCTVAR results (in %) are graphically presented in Figure 31. Needless to say, the joining of the points in this graph has no mathematical significance and is merely a visual aid.

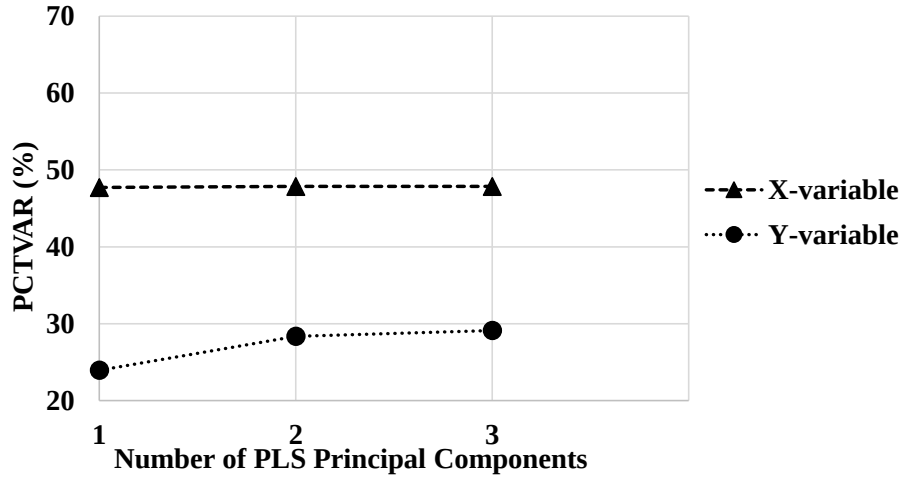

Figure 31. Percentage of variance explained by the model for *X*- and *Y*-variables.

Figure 31 shows that using the maximum possible number of PLS Principal Components, i.e. 3, only about 48% and 29% of variance respectively in *X*- and *Y*-variables has been made up. Taking the relative small number of objects *n*=4 into account, the fact that about 48% of information present in the acoustic data has been already related to 29% of grain size distribution is encouraging. In this stage, as the very first PLSR calibration in this research work was performed, two challenges were

remained to deal with: seek for the reason(s) of not very well fitted model and, find the way(s) to improve its goodness of fit.

6.1.4 PLSR verification process

In accordance with the procedure earlier presented in part 3.5.1, the developed algorithm in MATLAB R2012b was completed to perform the verification phase of the trained PLSR model. For each sand type, the data from second and third trails were prepared each in a 4×128 matrix (similar to the calibration phase) and respectively inputted to the verification algorithm as verification tests 1 and 2. The first and second sets of the predicted *Y*-variables (here passing percentage) were each outputted in a 4×9 matrix.

Since passing percentage in analysis of grain size distribution may neither exceed 100% nor go below 0%, therefore two threshold levels were defined. All the predicted *Y*-variables higher than 100% were replaced by 100%. Also, all the negative predicted *Y*-variables were replaced by 0%. Applying such threshold-based decision rules on predictions of PLS models is a common method to enhance performance of this statistical multivariate modeling method. As an example of thresholding, the paper by Eliseyev et al. (2011) [121] can be named.

In Figure 32, the block of measured *Y*-variables (sieve analysis) is compared with the first and second sets of the predicted *Y*-variables. The joining of the points in this Figure has not any mathematical significance and is merely a visual aid. The first and second sets of the predicted *Y*-variables are simply denoted as ‘Verif.1’ and ‘Verif.2’, respectively. The sieve analysis is expressed as ‘Lab.’. For simplicity, the predicted *Y*-variables in this research work are simply called ‘acoustic results’. In Figure 32, by comparing the ‘acoustic results’ and sieve analysis, suitability of the experimental setup as well as the performance of the model in order to determine (predict) the grain size distribution of the tested samples can be visually evaluated.

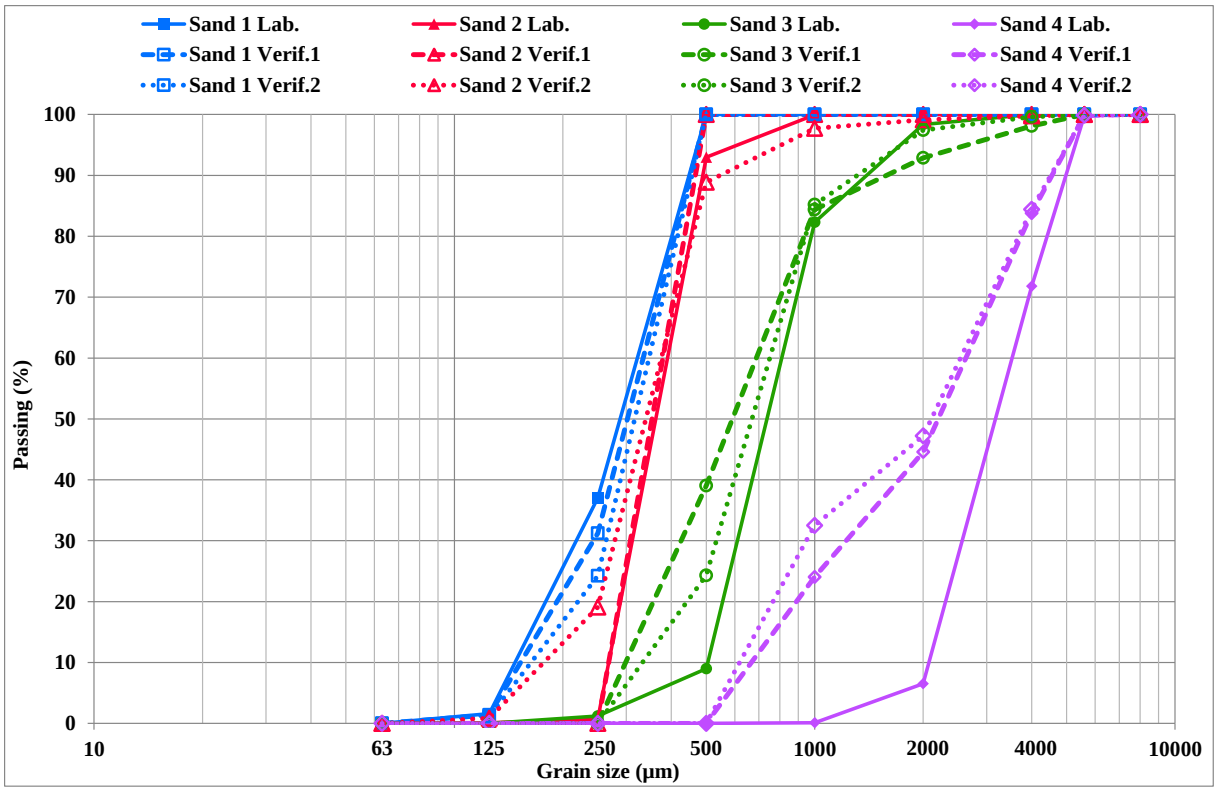

Figure 32. Sieve results (solid lines) vs. verification trials (broken and dotted lines).

6.1.5 Discussion on the results

From Figure 32, a good reproducibility can be seen in the 'acoustic results'. It means that for each sand type, the 'acoustic results' from the two verification trials are consistent. Figure 32 also shows a good general agreement between the 'acoustic results' and sieve analysis. However, the 'acoustic results' of sand 4, especially in two grain size classes (namely 1000 and 2000 µm), are quite different from the sieve result. For this sand type, in 1000 and 2000 µm the passing percentages from the 'acoustic results' are respectively up to 32 and 41% higher than the sieve analysis. In other words, considering these two grain size classes, the 'acoustic results' suggest a finer size distribution for sand 4 – in comparison with the sieve analysis.

In order to provide a quantitative evaluation of the consistency between the 'acoustic results' and sieve analysis, the use of absolute difference was considered. Thus, the absolute difference between each single $y_{i\ measured}$ value and its corresponding $y_{i\ predicted}$ value was calculated. These two values were taken respectively from the sieve analysis and 'acoustic results'. Thereby, each sieve result was compared with its two corresponding 'acoustic results'. As an example, for sand 1 in the grain size 250 µm, the passing percentage from the sieve analysis equals to 37.0, while the corresponding 'acoustic results' from the first and second verification trials equal to 31.2

and 24.2%, respectively. Consequently, the absolute differences were respectively obtained as 5.8 and 12.8%.

The entire calculated absolute differences (all in %) are reported in Table 6. For each sand type, the absolute differences belonging to the first and second verification trials (Verif.1 and Verif.2) are presented. Also, for each sand type, the Average row simply reports the mean values from the Verif.1 and Verif.2 rows. These averaged values represent the general consistency between each sieve result and its two 'acoustic results'. For each sand type the unshaded fields are those grain size classes which represent that sand type the most significantly. The gray shaded fields, however, are the grain sizes where passing percentage is either 0 or 100. It means that the absolute difference is close/equal to zero anyway. In this Table, the maximum absolute difference occurred in each sand type is in Max. column reported. These values determine with which level of accuracy the sieve result of each sand type has been predicted by the model.

Table 6. Absolute differences between the sieve analysis and 'acoustic results'.

Grain size (µm)		63	125	250	500	1000	2000	4000	5600	8000	Max.
Sand 1	Verif.1	0.0	0.2	5.8	0.0	0.0	0.0	0.0	0.0	0.0	12.8
	Verif.2	0.0	0.5	12.8	0.0	0.0	0.0	0.0	0.0	0.0	
	Average	0.0	0.4	9.3	0.0	0.0	0.0	0.0	0.0	0.0	
Sand 2	Verif.1	0.0	0.1	0.7	7.0	0.0	0.0	0.0	0.0	0.0	18.4
	Verif.2	0.0	0.8	18.4	4.1	2.2	0.9	0.2	0.0	0.0	
	Average	0.0	0.4	9.5	5.6	1.1	0.4	0.1	0.0	0.0	
Sand 3	Verif.1	0.0	0.0	1.2	30.0	2.1	5.5	1.9	0.0	0.0	30.0
	Verif.2	0.0	0.0	1.2	15.3	2.9	0.9	0.4	0.0	0.0	
	Average	0.0	0.0	1.2	22.7	2.5	3.2	1.2	0.0	0.0	
Sand 4	Verif.1	0.0	0.0	0.0	0.0	23.9	38.1	12.0	0.1	0.0	40.7
	Verif.2	0.0	0.0	0.0	0.0	32.4	40.7	12.6	0.1	0.0	
	Average	0.0	0.0	0.0	0.0	28.2	39.4	12.3	0.1	0.0	

According to Table 6, sand 1 – with maximum absolute difference of 12.8% – in comparison with the other sand types has presented the best agreement between the sieve analysis and 'acoustic results'. The agreement in sand types 2-3, considering the values in Max. column and Avg. row, has been relatively moderate. However, sand 4 has given a very poor consistency, where absolute difference reaches up to 40.7%. Table 6 also implies that for each sand type, both acoustic trials have yielded comparable accuracies, even in the case of sand 4. This validates again the reproducibility of the acoustic trials.

RMSEP, as a common measure of *prediction error*, was used to evaluate how well the model predicted *Y*-variable values in the verification phase (refer to part 3.5.12). Each individual grain size was considered as a *Y*-variable. RMSEP was then calculated for each grain size using Equation (3.12), while i=1, 2, …, n=8. All of the obtained RMSEP values are reported in Table 7. The RMSEP values were expressed in %, since the measurement unit of *Y*-variable (passing percentage) was percent.

Table 7. RMSEP value of each grain size.

Grain size (µm)	63	125	250	500	1000	2000	4000	5600	8000
RMSEP (%)	0.00	0.33	8.21	12.26	14.32	19.80	6.19	0.05	0.00

The two first grain sizes (i.e. 63 and 125 µm) and the two last grain sizes (i.e. 5600 and 8000 µm) present RMSEP values close to zero. That's because in these grain sizes sieve results are almost equal to 0 and 100%, respectively. On the other hand, the corresponding predicted *Y*-values are also successfully close to 0 and 100%, respectively. Moreover, as mentioned earlier in part 6.1.4, two threshold levels were defined, by which all the predicted *Y*-variables higher than 100% were replaced by 100% and all the negative predicted *Y*-variables were replaced by 0%.

RMSEP is an average error. It is composed of large and small errors altogether. In the current case, each reported RMSEP value in Table 7 involves errors occurred in all of the tested sand types. According to Table 7, the first and second worst consistencies between the sieve analysis and 'acoustic results' belong to 2000 and 1000 µm, respectively. Considering the fact that in these two grain sizes, sand types 1-3 present a very good agreement between the sieve analysis and 'acoustic results' – sand types 1-2 are 100% anyway – it can be claimed that sand 4 has been the most problematic sand type. This sand type has been responsible for the largest *prediction errors* in the current PLS Regression model. It can be interpreted that if new samples of sand types 1-4 were tested, their passing percentages in 2000 and 1000 µm would be predicted by this model with about ±40 and ±28% precision, respectively. The prediction precision is estimated commonly as ±2×RMSEP [29].

The bad performance of the model, particularly for sand 4, was believed to be due to the 'air gaps' effect in this sand type. In part 5.4, based on the investigations made on the raw acoustic signals and frequency spectra, it was concluded that centrally positioning the probe inside the pneumatic line, instead of 'clamp-on' and 90° bend, drastically

[29] To read more about interpreting RMSEP and other measures, refer to the book by Esbensen et al. (2002) [66].

reduced the ‘air gaps’ effect. However, here it was suspected that despite of those former investigations, this effect in this part of the study has not been negligible enough.

It was suggested that the ‘air gaps’ effect has adversely reduced statistical reproducibility of sand 4 data. It means that in contrary to sand types 1-3, the three trials of sand 4 may have not been statistically representative samples from a same population. This has been eventually responsible for large inconsistency in the results of sand 4 in the verification phase. This argumentation was investigated in detail by help of two-sample *t*-test (refer to part 3.5.1). In each sand type, an unpaired (independent) two-sample *t*-test was performed between each two acoustic trials. Thereby, a total number of 12 tests were performed. The essential conditions of this statistical hypothesis test were supported as: the trials were independent from each other, sample variances were equal, samples were normally distributed and had equal sizes. The filtered signal of each trial was considered as a sample (thus, $n=5\times10^5$). Each test was performed with the aim of determining if the difference between the two compared trials was statistically significant. In each of these two-tailed tests, the null hypothesis H_0 and the alternative hypothesis H_1 were respectively set as: the two compared trials are not statistically different, the difference between the two compared trials is statistically significant. Confidence interval of 95% was considered for these tests, thus $\alpha=0.05$. The obtained *p*-values from all of the performed unpaired two-tailed two-sample *t*-tests are reported in Table 8.

Table 8. Obtained *p*-values from the unpaired two-tailed two-sample *t*-tests.

	Sand 1	**Sand 2**	**Sand 3**	**Sand 4**
Trial 1 and Trial 2	0.420	0.594	0.982	0.023
Trial 2 and Trial 3	0.340	0.360	0.527	0.007
Trial 1 and Trial 3	0.884	0.701	0.561	0.020

In Table 8, in cases where *p*-value>0.05 the null hypothesis is approved which means the two compared trials have not been statistically different. Whereas if *p*-value<0.05, the null hypothesis is rejected and it is concluded that the two trials are different at the 0.05 significance level. It can be understood from Table 8 that in each of sand types 1-3, all the three trials have been comparable. Because *p*-value>0.05, thus we fail to reject H_0. Quite the contrary, in sand 4 all the three trials have been statistically different. For example, Table 8 suggests that in confidence interval of 95%, the probability that further samples (new trials) from sand 4 be not statistically different is maximum 2.3%.

In addition to the above discussed reproducibility problem caused by the ‘air gaps’ effect in sand 4, it may also argued that sand 4 has not been measured ‘loud’ enough, compared

to the other sand types. The suitable qualitative proportionality between grain size and voltage was already given in this part of the study. In simple words, the coarser the sand type, the higher the voltage of acoustic data. However, because of the present ‘air gaps’ effect, the proportionality between grain size and voltage provided by sand 4 is not the same as the one which applies for sand types 1-3. Consequently, in the calibration phase, the model was able to relate only about 48% of acoustic information to just 29% of grain size distribution.

In conclusion, in order to improve the consistency of sand 4 ‘acoustic results’ and the whole performance of the model, it was decided to solve the ‘air gaps’ problem through optimizing the experimental setup.

6.2 Optimizing the experimental setup of the horizontal test rig

Based on the former findings from the initial experiments, the horizontal test rig was set up. The recorded raw signals from the first experimental program with this test rig were undergone signal processing and multivariate calibrations procedures. The obtained results were compared with the sieve analysis and were analyzed statistically. The comparison proved the reproducibility of the ‘acoustic results’ as well as their general consistency in regard with the sieve analysis. However, the consistency of sand 4 results, particularly in two grain sizes, was very poor.

The current part deals with the further various experimental programs which were carried out with the horizontal test rig. The aim of these programs was to find the optimized experimental setup under which the sieve results of the sand types 1-4 could be represented correctly by the ‘acoustic results’.

Amongst the different parameters of the experimental setup, air flow velocity and mass flow rate were known to be the key factors. In order to study the effects of these factors on the results and also to find an optimized test condition under which sand 4 results would be consistent too, these two factors were independently varied through several experimental programs. In the following, these experimental programs are presented.

6.2.1 Study of air flow velocity effect

The first experimental program with the horizontal test rig was conducted while the vacuum cleaner was supplied with 220 volt and as a result, the air flow had a velocity of 106 m/s (refer to part 6.1.1).

By means of the induction regulator an input voltage of 150 volt was supplied for the vacuum cleaner. Thereby, air flow velocity of 72 m/s was measured at position of the impacting head. Having this air flow velocity and keeping the rest of the test conditions

identical to the first experiment, an experimental program was conducted. Similar to the first experiment, this experimental program also included 12 trials – 3 trials for each sand type. By decreasing the input voltage from 150 to 100 volt, air flow velocity was reduced to 48 m/s. Another experimental program was conducted while air flow had a velocity of 48 m/s and the rest of the test conditions were kept identical to the first experimental program. Therefore, two experimental programs were documented which were identical to the first experiment in every aspects of the experimental setup except the air flow velocity.

In each of the experimental programs 48, 72 and 106 m/s, the averaged magnitude spectrum of 3 trials belonging to each sand type was produced. Thus, each sand type in each experimental program was represented by means of a spectrum. Figure 33 shows the averaged magnitude spectra of sand types 1-4 in the experiments 48, 72 and 106 m/s.

In accordance with Figure 33, reduction of air flow velocity has not caused any significant alteration in the form of the frequency spectra. In this regard, in the experiments with 48 and 72 m/s – likewise the first experiment with 106 m/s – the major peak can be observed in lower frequency ranges (<5 kHz). Additionally, in all of the three experiments, a significant part of the signal energy is concentrated in the frequencies between 15 and 20 kHz.

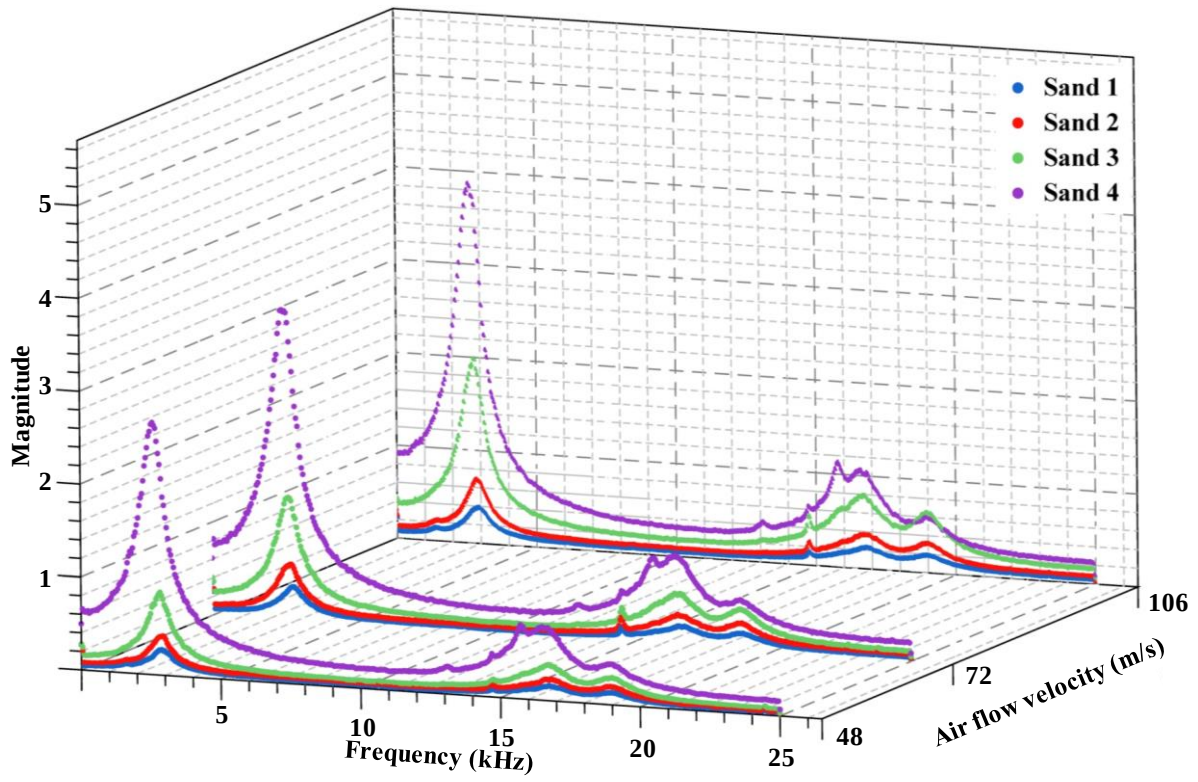

Figure 33. The effect of air flow velocity on magnitude spectra.

The qualitative proportionality between grain size and acoustic signal magnitude in the cases of lower air flow velocities is similar to the first experiment. In other words, by reducing the air flow velocity from 106 m/s to 72 and 48 m/s, the sand types (considering their magnitude levels) remain in the correct order. On the other hand, Figure 33 shows that the air flow velocity obviously influences signal magnitude. Decreasing the air flow velocity has caused reduction in signal magnitude for sand types1-4 in the whole frequency spectrum.

The recorded signals from the experiments 48 and 72 m/s were filtered identical to those from the first experiment. In the first experiment program with the horizontal test rig (106 m/s), as well as in the 72 and 48 m/s programs, the filtered 10-second long segment of each trial was undergone a RMS averaging function with an exponential weighting (see part 3.4.1). Considering that the applied bandpass filter had a lower cutoff frequency of 1 kHz, it was decided to use a time constant (τ) of 1 millisecond for this averaging function. This very fast averaging (and without any data reduction) was found to be suitable for tracking the very quickly varying voltage levels, while still able to smooth the data.

In the first experiment with the horizontal test rig, for the second trial of sand 4, Figure 34 compares the result of the exponential RMS averaging function against the corresponding filtered signal.

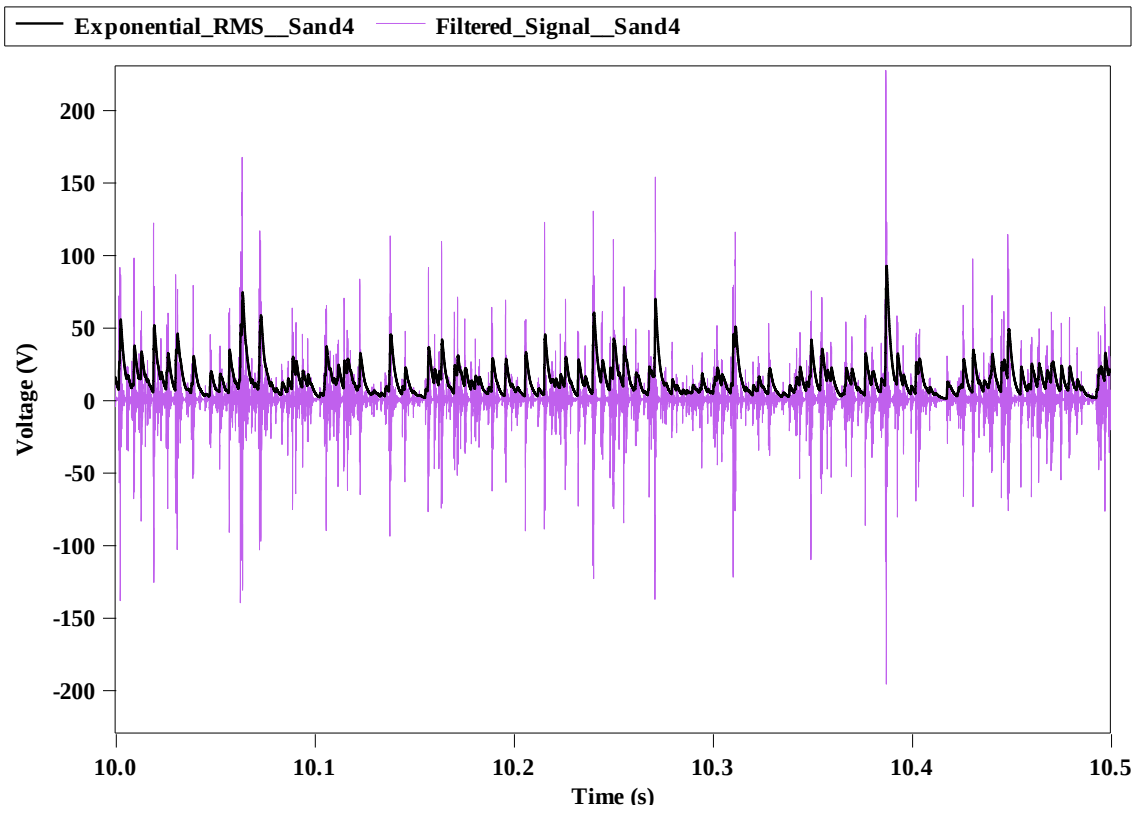

Figure 34. Filtered signal overlaid by exponential RMS average.

Through the exponential RMS averaging function, the square root of averaged power has been derived from the zero-mean filtered signal. Figure 34 shows how the square root of the exponential time-averaged power (in simple words: exponential RMS averaging), reduces the signal fluctuations and smoothes the data.

In Figure 35, one second of the exponential RMS average from 4 trials, each trial belonging to a sand type, is illustrated. All the trials belong to the first experiment with the horizontal test rig. Figure 35 shows that after performance of the exponential RMS averaging function, not only the desired proportionality between grain size and voltage was still preserved but also, the voltage levels were characterized of course by positive values (not zero-mean anymore).

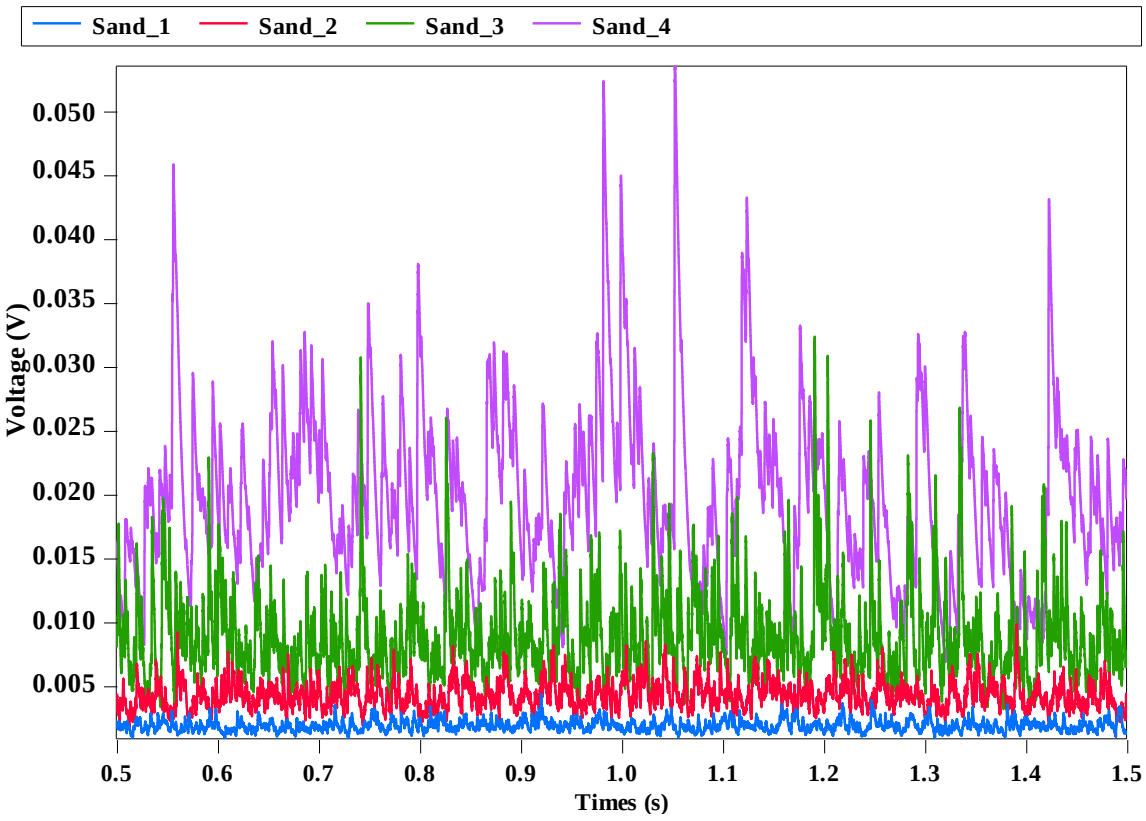

Figure 35. 1 s of exponential RMS average in each sand type.

In the first experimental program with the horizontal test rig (106 m/s), as well as in the 72 and 48 m/s programs, the obtained exponential RMS average of each single trial was arithmetically (linearly) averaged. Thereby, 10-second long segment of each trial was represented by an individual value. The obtained mean values from each three relevant trials were averaged together. Therefore, each experimental program was represented with only 4 mean values, each value corresponding to a sand type. All of the obtained mean values from the experimental programs 106, 72 and 48 m/s are demonstrated in

Figure 36. In this Figure, each single data point represents the data of three trials; i.e., 1.5 million values. Figure 36 literally presents the effect of air flow velocity on signal magnitude. The percentage of signal magnitude reduction caused by reducing air flow velocity in each step is also reported in this Figure.

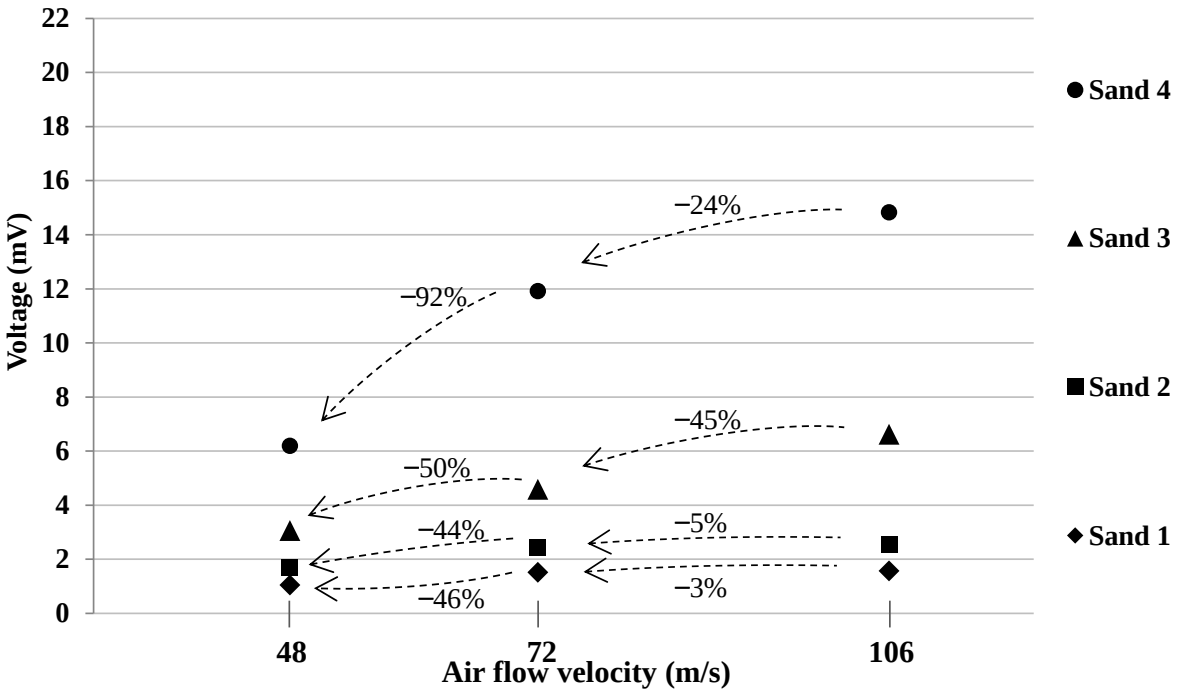

Figure 36. The influence of air flow velocity on signal magnitude.

The earlier discussion concerning Figure 33 can be verified through Figure 36: signal magnitude has a direct relation with air flow velocity and it applies for all of the tested sand types. Moreover, according to Figure 36 this relation is not identically the same in all of the sand types. The percentage of signal magnitude reduction, resulted by reducing velocity, is clearly different in various sand types. As an instance, reduction of velocity from 106 to 72 m/s has reduced signal magnitude of sand types 1-2 only 3 and 5%, respectively; whereas, this percentages for sand types 3-4 are respectively up to 45 and 24%. It implies that although decreasing the air flow velocity generally results in reduction of signal magnitude in all of the sand types, however, this effect differs quantitatively in various sand types and in different velocities. In other words, how much air flow velocity influences signal magnitude depends on grain size distribution and level of air flow velocity.

A PLSR model was trained for each of 48 and 72 m/s experiments. The calibration phase of each of these two models was performed identically to the first experimental program (refer to part 6.1.3). The percentage of variance explained by each of these two models

for both *X*- and *Y*-variables was computed. The obtained PCTVAR values – by three PLS Principal Components – of 48 and 72 m/s models are compared with those from the first experiment (106 m/s) in Table 9.

Table 9. PCTVAR values (in %) of 48, 72 and 106 m/s models.

Air flow velocity (m/s)	48	72	106 (first experiment)
X-variable	59	80	48
Y-variable	29	29	29

According to Table 9, no meaningful straightforward influence of reducing air flow velocity on PCTVAR for *X*- and *Y*-variables can be recognized. In all the three models, only about 29% of variance in **Y** has been explained by 3 PLS Principal Components. Meanwhile, by reducing velocity the explained percentage of variance for *X*-variable increases from 48% to 80% and then drops again to 59%.

The verification phase for each of 72 and 48 m/s models was performed identically to the first experiment (106 m/s). The obtained 'acoustic results' from air flow velocities 72 and 48 m/s are compared with the sieve analysis in Figure 37 and Figure 38, respectively. The calculated absolute differences between the sieve analysis and 'acoustic results' in correspondence with Figure 37 and Figure 38 are reported respectively in Table 21 and Table 22 of the Appendix. For sand types 1-4, Figure 39 illustrates the calculated absolute differences in each grain size at air flow velocities of 48, 72 and 106 m/s. In this Figure, each column represents an averaged absolute difference from two corresponding verification trials. Figure 39 shows the effect of air flow velocity on the agreement of 'acoustic results' with the sieve analysis.

Comparing Figure 32 (106 m/s), Figure 37 (72 m/s) and Figure 38 (48 m/s) shows that in sand types 1-3, in all the 3 tested air flow velocities the 'acoustic results' are generally consistent with the sieve analysis. Furthermore, this general consistency has not been meaningfully influenced by varying air flow velocity. Figure 39 also shows that the absolute differences in sand types 1-3 are relatively small and in the worst case go up to 22.7%. Also, in these sand types the obtained absolute differences do not suggest a noticeable relation with air flow velocity. In conclusion, it implies that although air flow velocity influences signal magnitude, nevertheless, for sand types 1-3 the desired proportionality between voltage and grain size has been successfully modeled at each of these velocities.

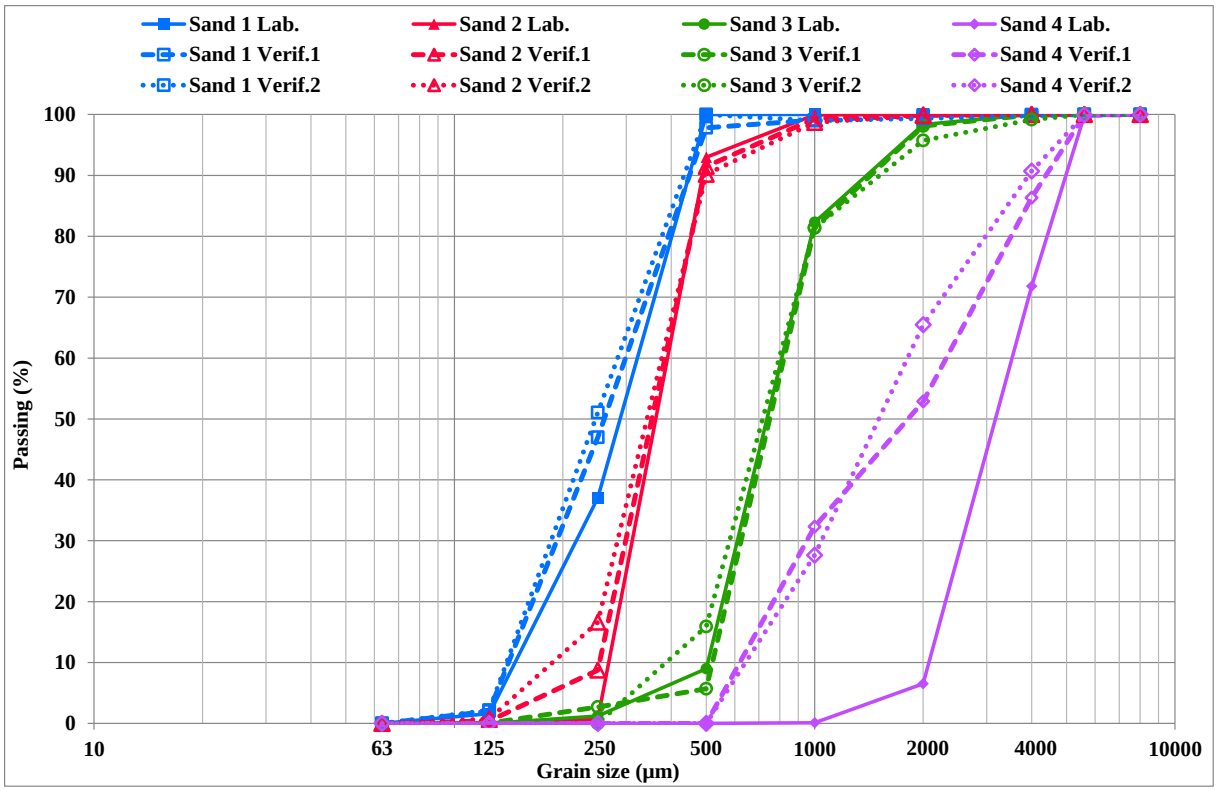

Figure 37. Sieve results (solid lines) and verification trials (broken and dotted lines) at air flow velocity of 72 m/s.

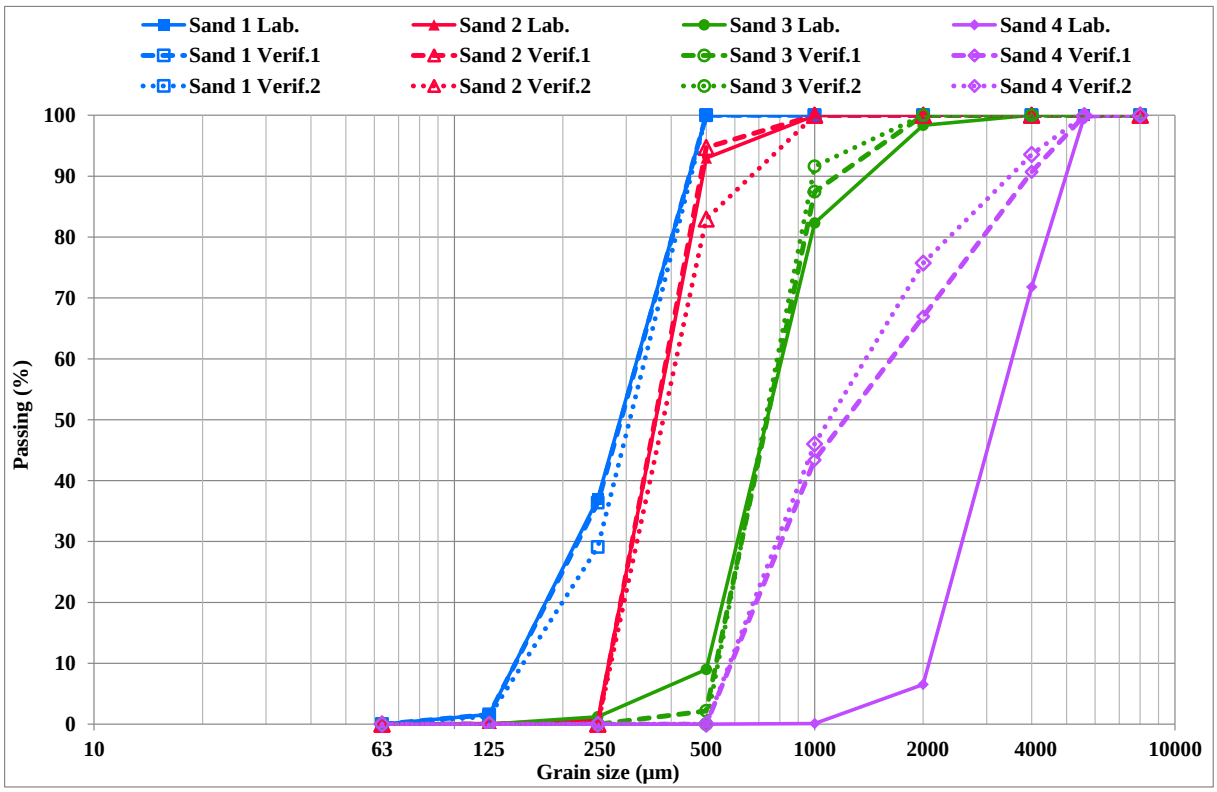

Figure 38. Sieve results (solid lines) and verification trials (broken and dotted lines) at air flow velocity of 48 m/s.

In contrary to sand types 1-3, in sand 4 consistency between the ‘acoustic results’ and sieve analysis in grain sizes 1000, 2000 and 4000 µm is very poor. This inconsistency gets even worse by reducing air flow velocity. For example, as velocity decreases from 106 m/s to 72 and 48 m/s, absolute difference in 2000 µm rises from 39.4 up to 52.7 and 64.8 %, respectively.

Similar to the first experiment, *prediction error* of each 72 and 48 m/s models was evaluated by help of RMSEP. The obtained RMSEP values of 48, 72 and 106 m/s experiments are altogether illustrated in Figure 40. This Figure literally presents the effect of air flow velocity on *prediction error* in each individual grain size.

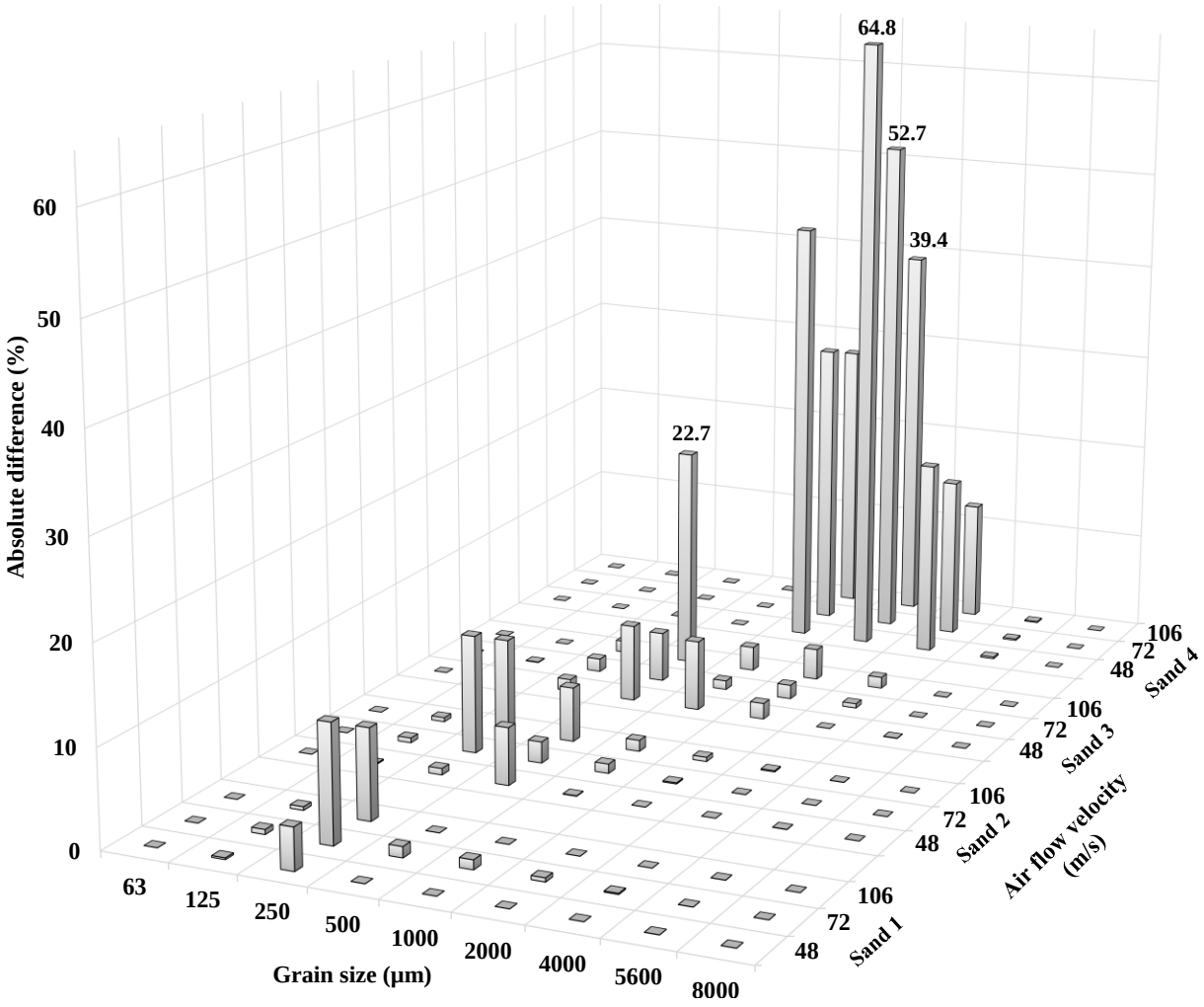

Figure 39. The effect of air flow velocity on absolute difference.

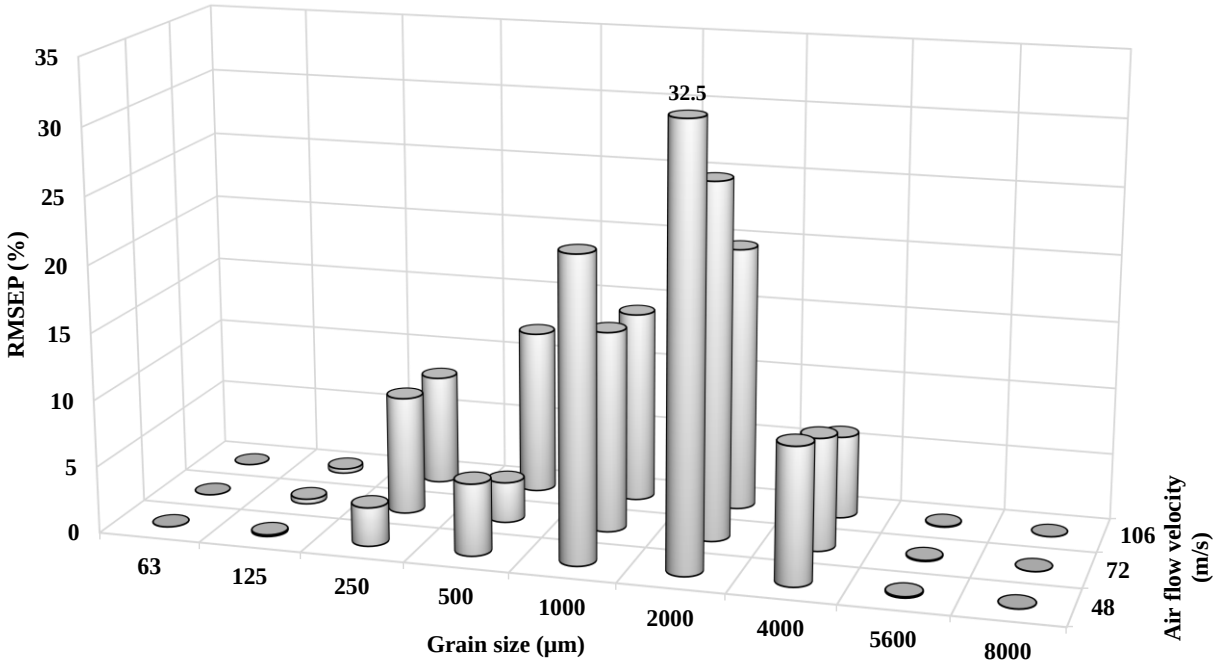

Figure 40. The effect of air flow velocity on *prediction error*.

In accordance with Figure 40, the resulted RMSEP values in grain sizes 250 and 500 µm are relatively small and do not show a recognizable relationship with air flow velocity. On the other hand, *prediction error* in grain sizes 1000, 2000 and 4000 µm is relatively large. As a fact, the highest RMSEP values have occurred in these three grain sizes, which clearly originate from the inconsistencies of sand 4 (refer to Figure 39). As an example, if new samples of sand types 1-4 were tested at 48 m/s, their passing percentages in 2000 µm would be predicted by the corresponding model with about ±65% precision. Moreover, it can be understood from Figure 40 that *prediction error* is in an indirect relationship with velocity, which also copes with the earlier discussions on Figure 39.

In conclusion, it was proved that reducing air flow velocity doesn't significantly affect *model fit*. However, it drastically worsens the general performance of PLSR model, specifically due to sand 4. Reduction of velocity not only doesn't improve accuracy of 'acoustic results' in sand 4, but also intensifies the problem associated with the 'air gaps' effect. Therefore, it was decided to conduct the further experiments with the horizontal test rig while supplying the vacuum cleaner with 220 volt (i.e. 106 m/s air flow velocity).

6.2.2 Study of mass flow rate effect

The first experimental program with the horizontal test rig was conducted while the vibratory feeder was adjusted with 9 mm and 70% for funnel height and vibration

intensity level, respectively. This adjustment provided a mass flow rate of approximately 27 g/s. For each trial 350 g sand was used (refer to part 6.1.1).

Having all of the test conditions of the first experiment constant, the vibratory feeder was adjusted with 11 mm and 80% for funnel height and vibration intensity level, respectively. Thereby, a mass flow rate of about 33 g/s was given. An experimental program was conducted with 33 g/s. Afterwards, while keeping the whole experimental setup constant, the funnel height and vibration intensity were increased to their maximum possible levels; namely 15 mm and 100%, respectively. This adjustment realized a mass flow rate of about 46 g/s. An experimental program was then conducted with 46 g/s. In the experimental programs of 33 and 46 g/s, respectively 400 and 550 g sand for each trail was used. Likewise the first experiment, in both 33 and 46 g/s experiments air flow velocity was 106 m/s.

Similar to the previous part (study of air flow velocity effect), the averaged magnitude spectra of sand types 1-4 in 33 and 46 g/s experiments were obtained. Figure 41 compares the averaged magnitude spectra of these two experiments with those from the first experiment.

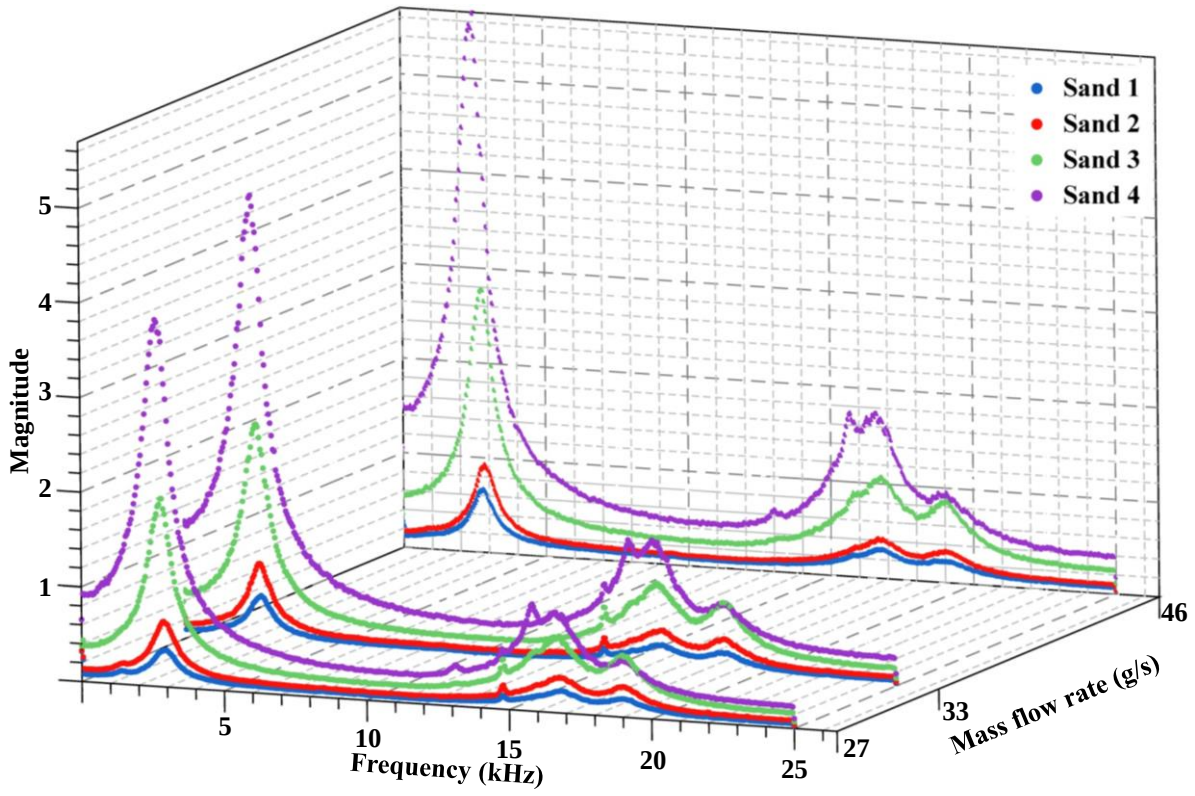

Figure 41. The effect of mass flow rate on magnitude spectra.

According to Figure 41, the increase of mass flow rate has not caused any significant change in form of the frequency spectra. Variation of mass flow rate has not changed the frequency range of the major peak, namely about 1-5 kHz. At each of the 3 tested mass flow rates, through the entire frequency spectrum the order of magnitude levels of sand types 1-4 is in agreement with their grain size. At last but not the least, increasing mass flow rate has amplified the magnitude level in each sand type in the whole frequency spectrum.

Similar to the previous part, the same signal processing procedures (including filtering and exponential RMS averaging function) were performed on the signals of 33 and 46 g/s experiments. The averaged results are illustrated in Figure 42, where each data point represents three trials.

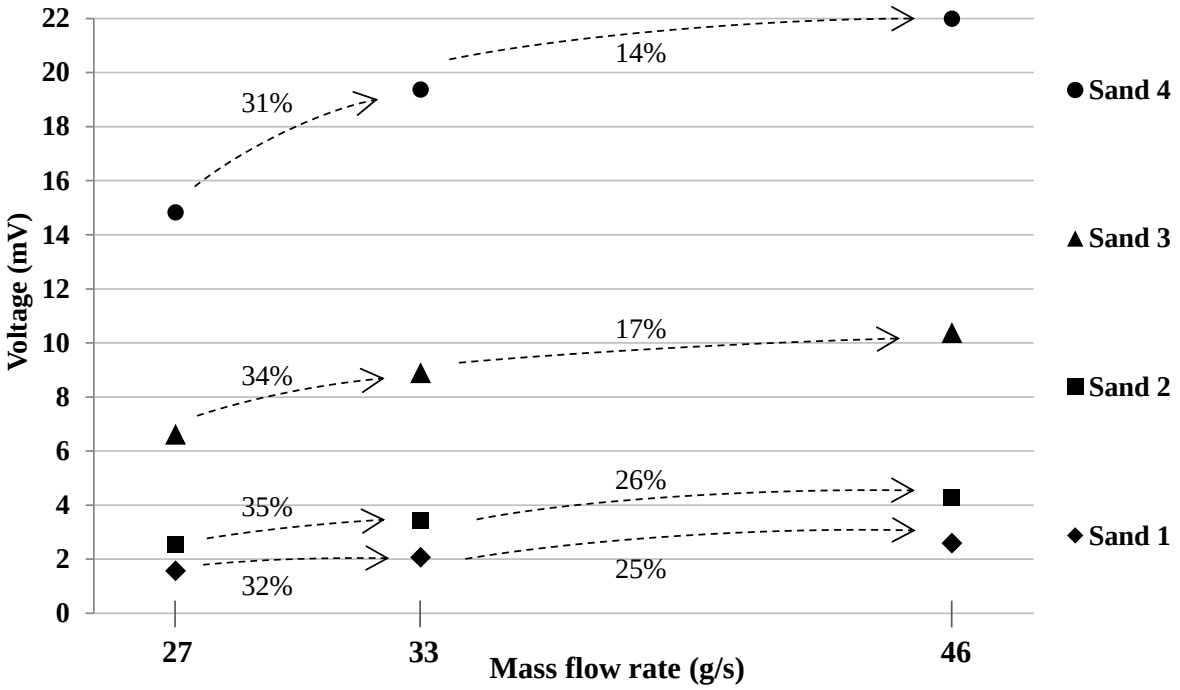

Figure 42. The influence of mass flow rate on signal magnitude.

Likewise Figure 41, Figure 42 also suggests a direct relationship between signal magnitude and mass flow rate in each sand type. This relationship, in contrary to the relation between signal magnitude and air flow velocity, has almost the same tendency in different sand types. Changing mass flow rate from 27 to 33 g/s has increased the signal magnitude in each of the sand types in the range of 31-35%. Further increase of mass flow rate from 33 to 46 g/s affects various sand types not significantly different. It suggests that the amount of variation in signal magnitude as a result of mass flow rate change may not be strongly dependent on grain size distribution. However, in each sand

type this amount of variation depends on the level of mass flow rate. Generally, the influence of mass flow rate on signal magnitude has an indirect relation with the level of mass flow rate. Take sand 3 as an example, increase of mass flow rate from 27 to 33 g/s (22% increase) causes up to 34% rise in signal magnitude. But, further increase from 33 to 46 g/s (39% increase) leads to only 17% rise in signal magnitude.

A PLSR model was calibrated for each of 33 and 46 g/s experiments. The percentage of variance explained by each of these two models for both *X*- and *Y*-variables was computed. The obtained PCTVAR values – by three PLS Principal Components – of 33 and 46 g/s models are compared with those from the first experiment (27 g/s) in Table 10.

Table 10. PCTVAR values (in %) of 27, 33 and 46 g/s models.

Mass flow rate (g/s)	**27 (first experiment)**	**33**	**46**
X-variable	48	50	51
Y-variable	29	35	33

As it can be seen from Table 10 increasing mass flow rate has improved *model fit* for both **X** and **Y**, although the improvement is limited to a few percent. It reveals that increasing mass flow rate from 27 to 46 g/s has enhanced the explained percentage of variance for *X*- and *Y*-variables respectively from 48 to 51% and from 29 to 33%.

The verification phase for each of 72 and 48 m/s models was performed identically to the previous models. Figure 43 and Figure 44 compare the sieve analysis with the ‘acoustic results’ of 33 and 46 g/s experiments, respectively. Table 23 and Table 24 of the Appendix respectively report the absolute differences between the sieve analysis and ‘acoustic results’ of 33 and 46 g/s experiments. The entire averaged absolute differences from 33 and 46 g/s experiments as well as the first experiment (27 g/s) are graphically demonstrated in Figure 45.

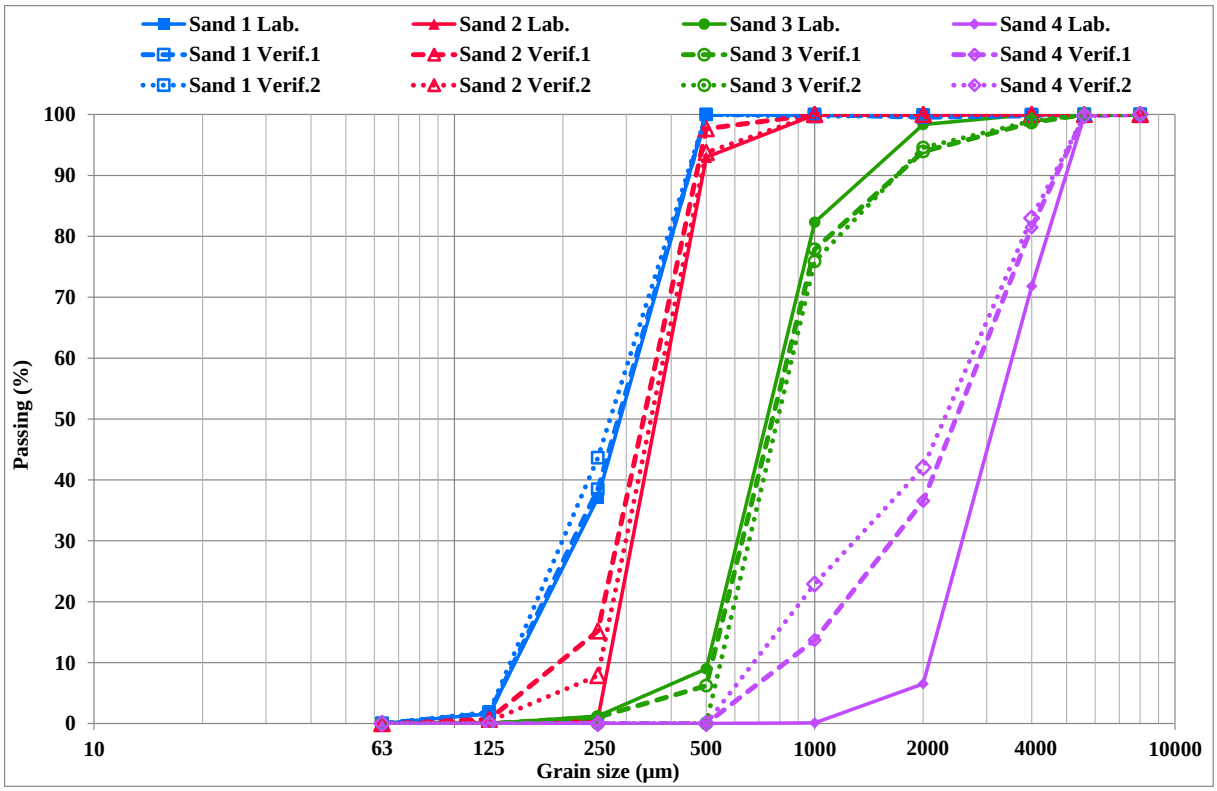

Figure 43. Sieve results (solid lines) and verification trials (broken and dotted lines) at mass flow rate of 33 g/s.

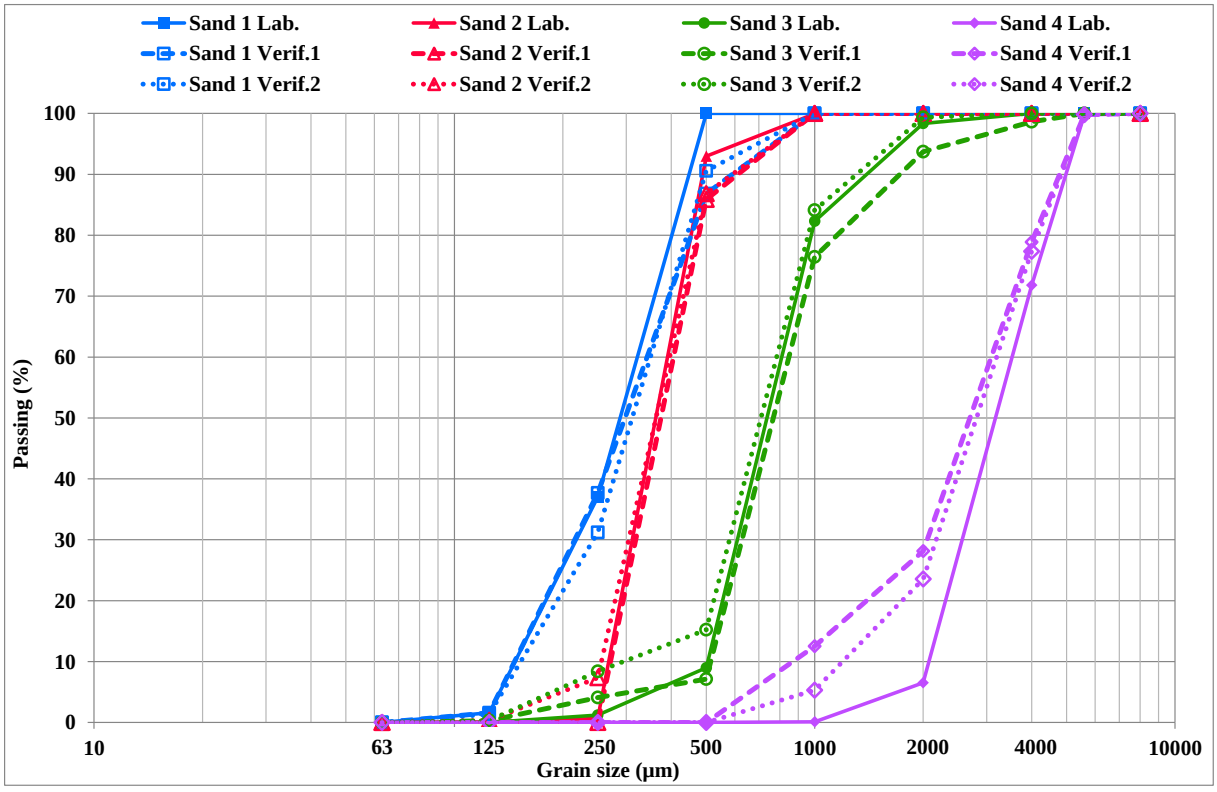

Figure 44. Sieve results (solid lines) and verification trials (broken and dotted lines) at mass flow rate of 46 g/s.

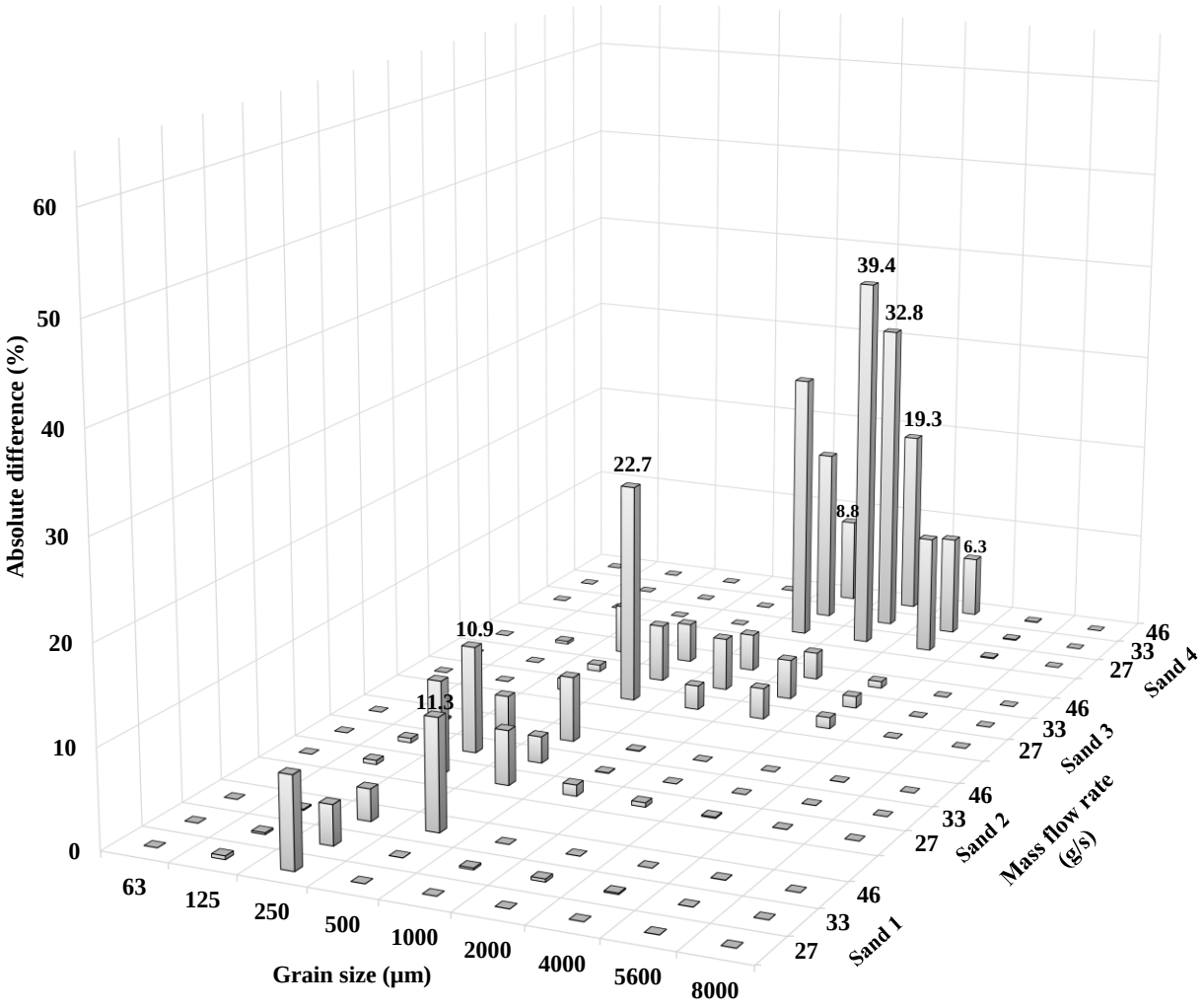

Figure 45. The effect of mass flow rate on absolute difference.

Likewise the previous experimental programs, here also Figure 43 and Figure 44 respectively show that in 33 and 46 g/s experiments the 'acoustic results' of sand types 1-3 are generally consistent with the sieve analysis. Variation of mass flow rate has not significantly affected this general consistency. This can be seen also from Figure 45, where no meaningful tendency between absolute difference and mass flow rate can be recognized for sand types 1-3. Also, this Figure shows that the inconsistencies in sand types 1-3 are relatively small, compared to sand 4. According to Figure 45, the averaged absolute differences in sand types 1-3 reach beyond 10% only in three cases. Therefore, the sieve analysis of sand types 1-3 has been predicted by acoustic data through PLS Regression modeling in each mass flow rate with relative good accuracy. Although, similar to the effect of air flow velocity, here also signal magnitude is significantly influenced by mass flow rate variations.

In 33 and 46 g/s experiments – similar to the earlier experimental programs – the 'acoustic results' of sand 4 do not agree with the sieve analysis well. In Figure 45, the absolute differences in sand 4 are noticeably larger than those in sand types 1-3.

According to this Figure, in grain sizes 1000, 2000 and 4000 µm, absolute differences of sand 4 are only in two cases lower than 10%. However, the inconsistency of sand 4 results has an indirect relation with mass flow rate. Comparing Figure 32, Figure 43 and Figure 44 shows that increasing mass flow rate has clearly improved sand 4 results. It can be seen also from Figure 45, where differences of sand 4 are obviously reduced by increasing mass flow rate. For example in 2000 µm, increasing mass flow rate from 27 g/s to 33 and 46 g/s has respectively improved the absolute differences from 39.4 to 32.8 and 19.3 %.

Similar to the previous experimental programs, *prediction error* of each 33 and 46 g/s models was evaluated by help of RMSEP. The obtained RMSEP values of 27, 33 and 46 g/s experiments are altogether illustrated in Figure 46. In comparison with grain sizes 1000, 2000 and 4000 µm, the resulted RMSEP values in grain sizes 250 and 500 µm are relatively small and do not present a recognizable relationship with mass flow rate. The high *prediction errors* in grain sizes 1000, 2000 and 4000 µm are caused obviously by inconsistencies of sand 4 results. Similar to absolute difference, RMSEP is also reduced by increasing mass flow rate.

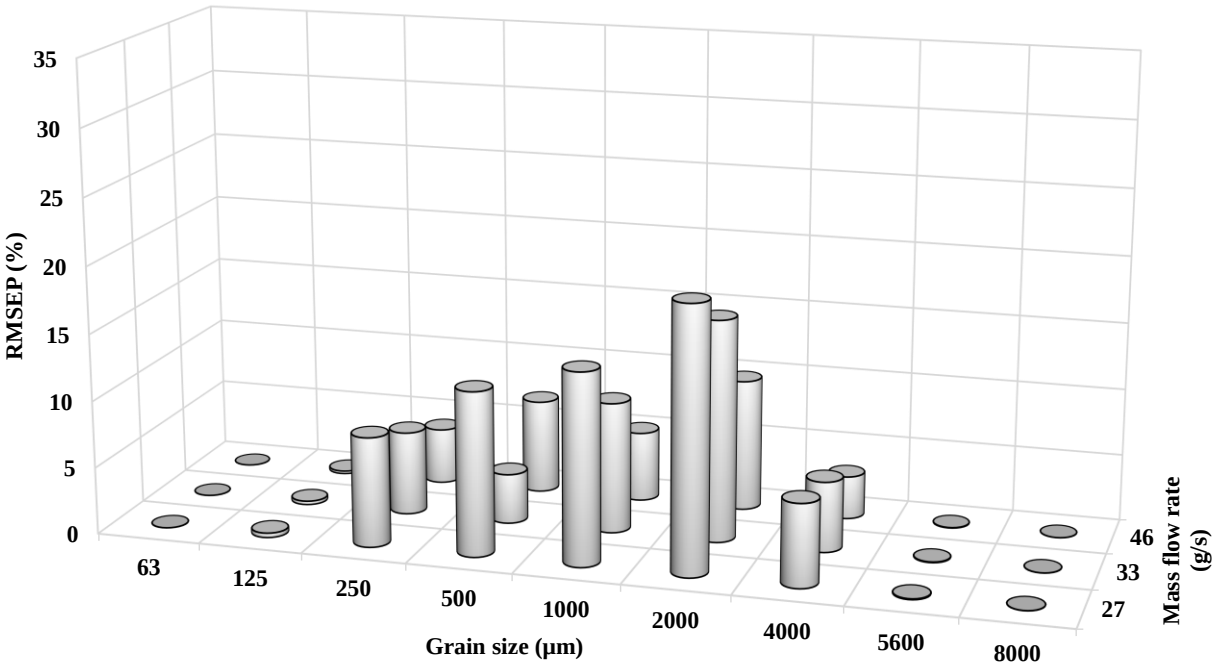

Figure 46. The effect of mass flow rate on *prediction error*.

Increasing mass flow rate improved *model fit*, absolute differences between the sieve analysis and 'acoustic results', and *prediction errors*. These improvements were believed to be because of lower occurrence of 'air gaps' in sand 4 at the higher mass flow rates. During an 'air gap', the energy level of the existing transient elastic waves

within the impacting head would drastically fall. These waves tend to attenuate. Consequently, magnitude of the recorded signal would drop too. In order to present the 'air gaps' effect visually, sand 4 raw signals from 27 and 46 g/s experiments are shown as instances in Figure 47. A 0.1 second long segment from each signal has been selected. Examining and comparing these two segments shows that the increase of mass flow rate has effectively reduced the occurrence of 'air gaps'. At 27 g/s, there are obvious 'air gaps' between impacts of sand 4 grains. At 46 g/s, compared to 27 g/s, the number of impacts within time-unit is considerably higher. This explains reason of the above mentioned improvements.

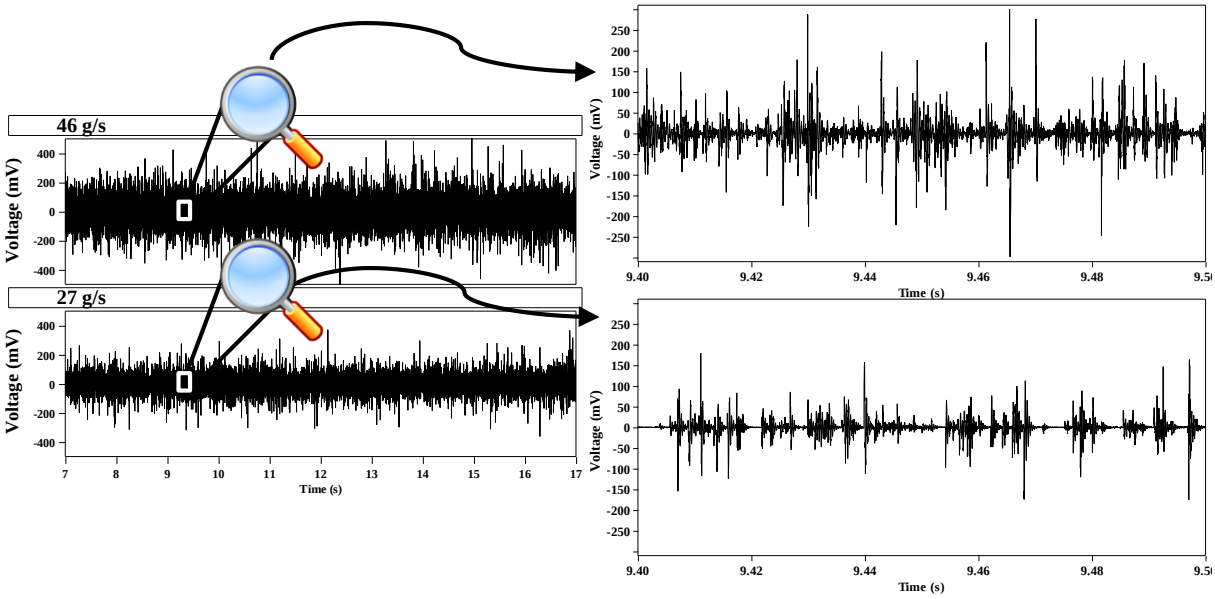

Figure 47. The effect of mass flow rate on the 'air gaps' effect in sand 4.

6.3 Concluding remarks on the horizontal test rig

Based on the obtained findings from the initial experiments, the horizontal test rig was designed and manufactured. In the first experimental program, sieve results of the tested sand types were successfully predicted by the 'acoustic results'. However, the agreement between the sieve analysis and 'acoustic results' was very poor for sand 4. Through the further experiments, the two main parameters of the experimental setup, i.e. air flow velocity and mass flow rate, were varied independently. Reduction of the former parameter from its maximum possible level to two lower levels led to increase of difference between the sieve analysis and 'acoustic results' of sand 4. Increasing the latter parameter up to its maximum possible level resulted in enhancement of agreement between the sieve analysis and 'acoustic results' of sand 4.

In order to investigate the higher mass flow rates, the adopted vibratory feeder (Sympatec, type VIBRI) was replaced by an available larger vibratory feeder (AEG,

type DR 50). However, it was experimentally proved that at higher mass flow rates, the pattern of sand-air flow declined from homogenous dilute conveying mode to dune and even partially slug flows.

Generally, within all the experimental programs in the present thesis, care was taken to have homogenous dilute flow pattern in the pneumatic line. Otherwise, having dune or slug flow patterns, the number and mode of impacts on the impacting head would be adversely affected. In this case, analyzing the recorded signals and deriving meaningful results from them would be quite difficult. Having homogenous flow pattern, it was ensured that the number of impacts within a time-unit would be statistically robust enough to provide a proper representation of the tested sand sample.

Therefore, it was decided to continue the experimental research work by using a vertical test rig with a relative wider pneumatic line and some other optimized aspects. By employing the vertical test rig, investigation of higher mass flow rates, while having homogenous flow, was made possible. The following Chapter documents the conducted experimental programs with the vertical test rig.

7 The vertical test rig

Figure 48 presents a photo of the vertical test rig.

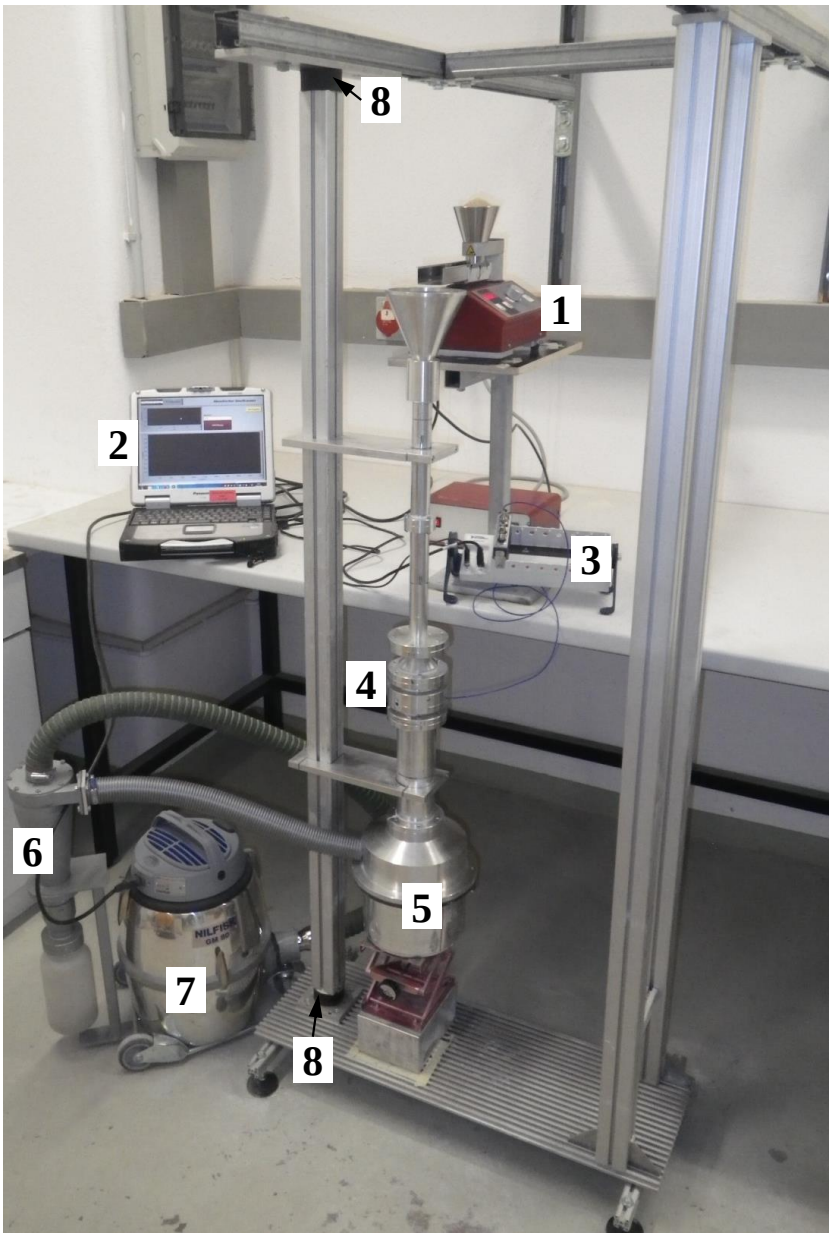

Figure 48. The vertical test rig.

The numbered components in Figure 48 are described as following:

1) Vibratory feeder (Sympatec, type VIBRI),

2) Laptop (Panasonic, type CF-30),

3) DAQ device consisted of an ADC (NI, type 9234 [122]) installed in a chassis (NI, type cDAQ-9172),

4) The element, in which the probe was installed. The probe was equipped with a steel impacting head and a 1 mV/g sensor (PCB, type 352B01),

5) Collection bin,

6) Cyclone,

7) Vacuum cleaner (Nilfisk, type GM 80),

8) Rubber damper.

The major advantage of the employed ADC (NI, type 9234) over type 6215 (which was used in the previous parts) was its anti-aliasing filter (see part 3.3.3). Furthermore, it was compatible with different NI chassis, which made it even more convenient to use. The employed chassis in the current experiments was connected to the laptop via USB cable. By using this DAQ device, the analog signal was sampled with a rate of 51.2 kS/s.

An advantage of the vertical test rig over the horizontal test rig was the possibility of collecting the tested sand sample after each trial in order to using it again. It was succeeded through the collection bin. The sample would be completely collected in the bin and just an absolutely negligible amount of dust would be sucked further into the cyclone. The cyclone was responsible for collecting the dust. Additionally, the vacuum cleaner was equipped with a special textile filter which ensured reliable cleaning of the exhaust air. This set of equipment, i.e. collection bin, cyclone and Nilfisk vacuum cleaner, eliminated any kind of health issues associated with dust.

In contrary to the horizontal test rig, the vertical test rig provided the possibility of having homogenous dilute flows with mass flow rates higher than 46 g/s. That was because of its wider pneumatic line and also, the gravitational force which was in the direction of mass flow. In this case, the sand grains were accelerated not only by means of the vacuum cleaner, but also by the gravitational force. Therefore, for the vertical test rig a vacuum cleaner with a lower power was employed and thereby, the noise level of the test rig was significantly reduced.

As it can be seen from Figure 48, two rubber dampers with vibration absorbing effect, were responsible for avoiding the intrusion of unwanted noises from bottom and top of the test rig towards the probe.

In Figure 49, a schematic drawing of the vertical test rig is illustrated. The dimensions in this drawing don’t necessarily represent the real dimensions of the test rig. The drawing serves merely to show the major components of the test rig as well as positioning of the probe.

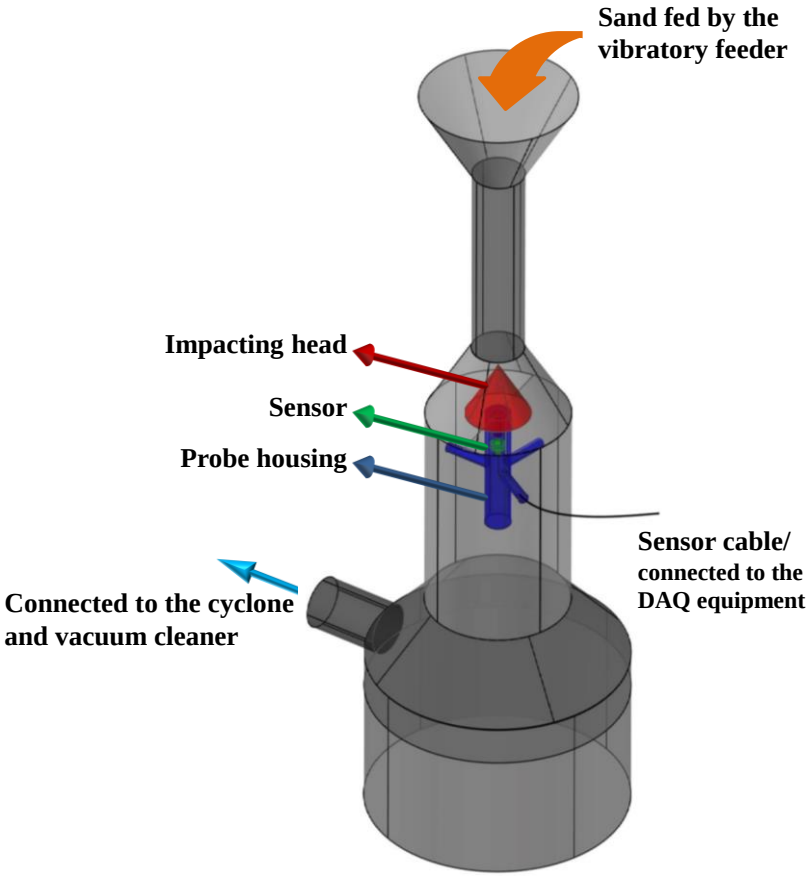

Figure 49. Schematic illustration of the vertical test rig.

From each sand type, one sample with available reference sieve analysis was prepared. Several experimental programs were conducted with the vertical test rig. In each experimental program, three trials were conducted for each sand type. Thanks to the reliable collection bin, the same sand samples were repeatedly used in these experimental programs.

7.1 With and without air flow

From the horizontal test rig it was concluded that increasing mass flow rate, while having the maximum possible air flow velocity, yielded the best results. Considering that conclusion, it was decided to conduct the first experimental program with the vertical test rig, while having both air flow velocity and mass flow rate at their highest possible levels. By supplying the vacuum cleaner with 220 volt, maximum possible air flow velocity at position of the impacting head, i.e. 40 m/s, was reached. Also, the vibratory feeder was adjusted to its maximum possible funnel height and vibration intensity level and a mass flow rate of 46 g/s was given.

On the other hand, the importance of air flow velocity as a deciding parameter and its influence on the results was earlier proved by means of the horizontal test rig. It was shown that at a constant mass flow rate, relative small variations in air flow velocity can lead to significant changes in the results (see part 6.2.1). In contrary to the horizontal test rig, vertical test rig provided the possibility of conducting experiments while the vacuum cleaner was not turned on at all. Another experimental program with the vertical test rig was conducted as the vacuum cleaner was turned off and rest of the test conditions remained identical to the first experimental program. The second experimental program was aimed to investigate if in absence of air flow, the sieve analysis could be properly predicted by the acoustic data. In this case, for the test rig (or eventually the prototype) no vacuum cleaner would be required at all. It would have several advantages, including: elimination of uncertainty about permanent constant air flow velocity; less noise, electricity energy consumption, and space requirement.

Figure 50 shows averaged magnitude spectra of sand types 1-4 in the first experimental program with the vertical test rig. In this Figure, the top diagram represents the recorded signals in frequency-domain during the flow of sand samples in the pneumatic line. The bottom diagram represents the state as sand flow is over and the vacuum cleaner as well as the vibratory feeder still run. Comparison between Figure 50 (a) and Figure 28 reveals that the frequency spectra in vertical and horizontal test rigs have had unlike forms. Differences in type of ADC and dimension of impacting head were considered as major causes for this unlikeness. According to Figure 50, the recorded signals from the vertical test rig represent a peak at lower frequencies (<1 kHz). This peak is in both diagrams present. It implies that independent from the presence of sand flow, a relative large part of the signal energy is concentrated at this frequency range. This peak was then considered to be representative of background noise. Furthermore, it was experimentally proved that the position of this peak may vary unpredictably. On the other hand, at higher frequency ranges (>1 kHz) there is a plateau where magnitude level remains almost constant. In order to eliminate the uncertainties concerning the variation of the peak's position and also to minimize the intrusion of background noises into the analyzed acoustic data, it was decided to apply the bandpass filter at the range of this plateau. The range of 10-20 kHz was considered for the filtering in the current experimental programs. The applied Butterworth bandpass filter had a roll-off of -12 dB/octave. The upper cutoff frequency was selected while considering the frequency range of the sensor. According to the information provided by PCB Group in [117], the employed sensor had a usable frequency range of 1 Hz to 20 kHz (with ±10% tolerance band). It means that, over this frequency range the accelerometer's sensitivity could vary only from 9 to 11 mV/g. Thereby, it was ensured that the bandpass filter was applied at the range with meaningful information. It was however practically proved that as long

as the filter was applied at the plateau, the width of it as well as its lower and upper cutoff frequencies had hardly influence on the eventual results.

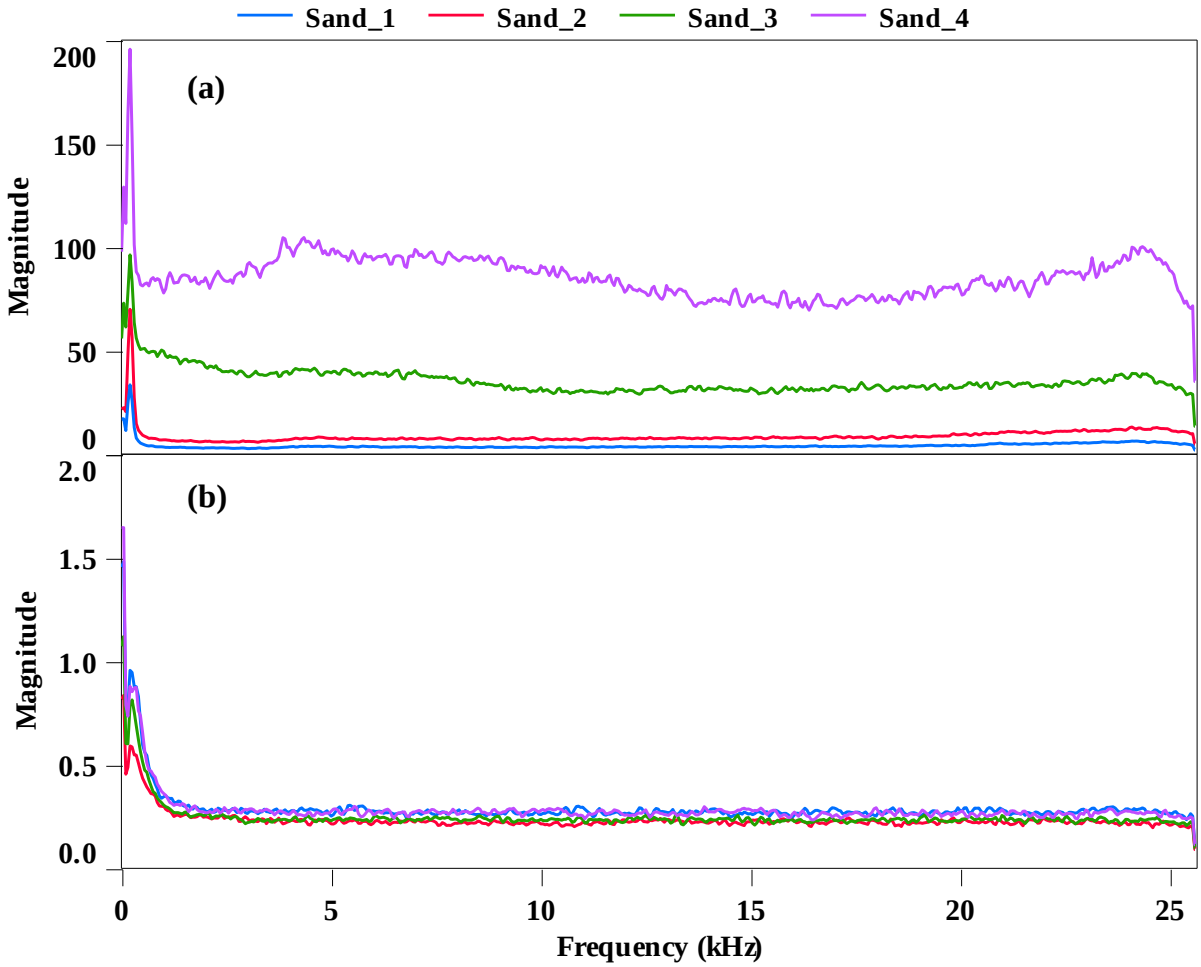

Figure 50. Averaged magnitude spectra: (a)Sand is flowing (b)after the sand flow.

In order to PLSR modeling, the filtered 10-second long segment of each trial was treated identically to the previous experimental programs. The total number of samples in each segment, however, was the only difference. Having a sampling rate of 51.2 kS/s, each trial was represented by a signal with a total number of $N = 512 \times 10^3$ samples. In the FFT function, the same window length of 2^8 samples, as used in all previous experiments, was adopted here too. Thereby, a 2000×256 matrix for each trial was outputted from the FFT function, where the rows and columns corresponded to time and frequency, respectively. In contrary to the previous experiments, no padding was required here to represent the output matrix with the desired transform length, since:

$$\frac{(N = 512 \times 10^3)}{window\ length = 256} = 2000$$

Each resulted 2000×256 matrix was then over its spectra arithmetically averaged. The rest of the procedures were carried out exactly the same as previous experiments – which have been extensively described in part 6.1.3.

For each of the two experiments – namely with and without air flow – a PLSR model was trained. The model for with air flow experiment explained by three PLS Principal Components 50% and 36% of variance in *X*- and *Y*-variables, respectively. The other model (for without air flow experiment) related 53% of information present in the acoustic data to 30% of grain size distribution.

Verification phase of each of the two models was performed identically to the former experiments. The predicted *Y*-variables were compared with measured *Y*-variables. In Figure 51, the obtained 'acoustic results' from the first experimental program (with air flow) are compared with the sieve analysis. The calculated absolute differences between the sieve analysis and 'acoustic results' are reported in Table 25 of the Appendix. The agreement between the 'acoustic results' and sieve analysis in this experiment has not been much different from the former experimental programs with the horizontal test rig. In case of sand types 1-3, 'acoustic results' are generally consistent with the sieve analysis. However, deviation between the 'acoustic results' and sieve analysis of sand 4 is noticeably large. In the worst case, it goes up to almost 30%. In summary, compared to the previous experimental programs, there isn't any significant improvement in the case of sand 4 to be proved. The results of sand types 1-3 have not been worsened either.

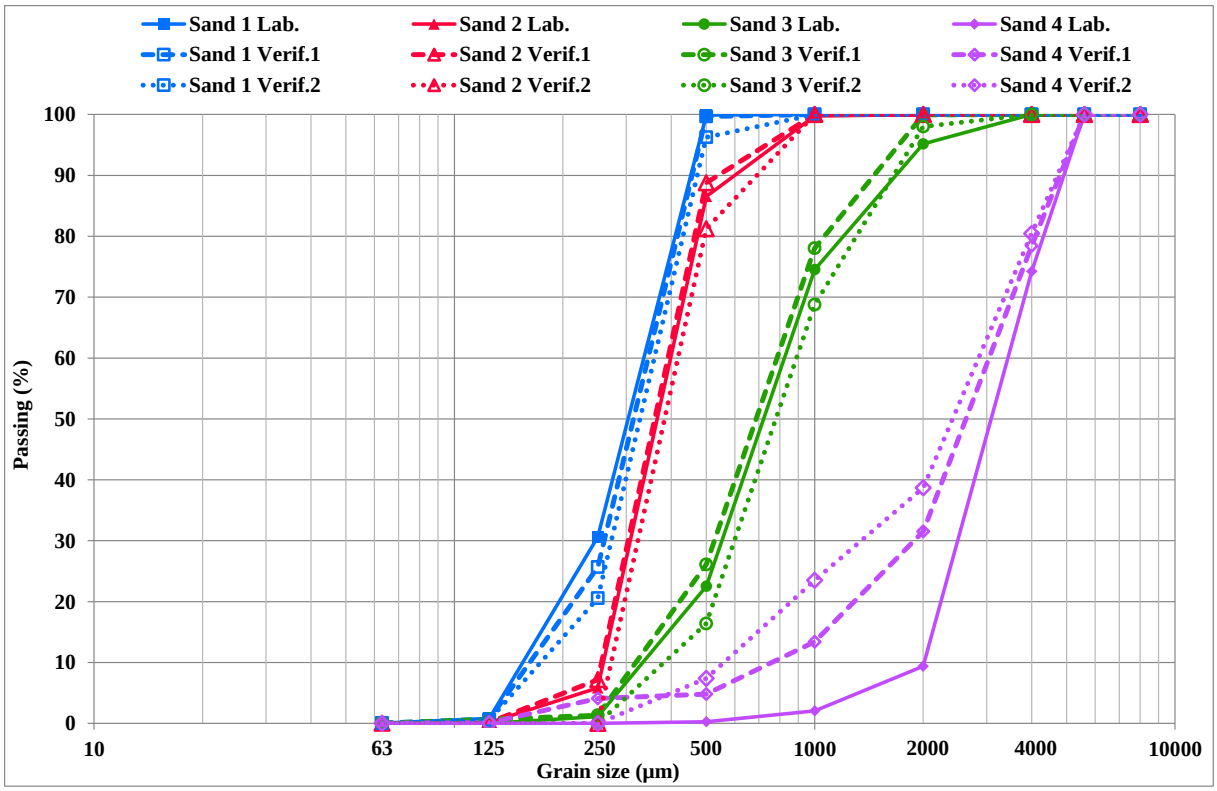

Figure 51. Sieve results (solid lines) and verification trials (broken and dotted lines) in presence of air flow.

Figure 52 compares the 'acoustic results' from the second experimental program (without air flow) with the sieve analysis. The calculated absolute differences between the sieve analysis and 'acoustic results' are reported in Table 26 in the Appendix. Comparison between Figure 51 and Figure 52 shows that omitting the air flow has obviously led to more inconsistency in the 'acoustic results' of sand 4. The maximum deviation between the sieve analysis and 'acoustic result' in 2000 µm increases from 29 to 48%, as a result of turning the vacuum cleaner off. Meanwhile, the results of sand types 1-3 have not been noticeably affected by omitting the air flow. In Table 11, the calculated RMSEP values (in %) from each of the models are reported. According to this Table, the major *prediction error* belongs to grain size 2000 µm. It is the only grain size, in which RMSEP values exceed 10%. Clearly seen from Table 11, by omitting air flow *prediction error* in 2000 µm gets significantly larger.

Table 11. RMSEP (in %) for with and without air flow models.

Grain size (µm)	63	125	250	500	1000	2000	4000	5600	8000
With air flow	0.00	0.26	4.73	4.59	8.89	13.13	2.64	0.00	0.00
Without air flow	0.00	0.06	2.19	3.41	2.34	20.82	7.33	0.00	0.00

It was proved that under a constant condition, omitting the air flow may intensify the 'air gaps' effect in sand 4, which leads to poor *model fit* and model performance. Hence, it was concluded that in order to accelerate sand 4 grains sufficiently, in addition to gravitational force, a reasonable air flow will be also necessary.

Also, from the first experimental program it was concluded that mass flow rate of 46 g/s may have not been sufficient for eliminating the influence of 'air-gaps' on the results of sand 4. Therefore, it was decided to replace the current vibratory feeder by another vibratory feeder (AEG, type DR 50) which was capable of providing mass flow rates higher than 46 g/s. The following parts describe the conducted experimental programs by employing AEG vibratory feeder.

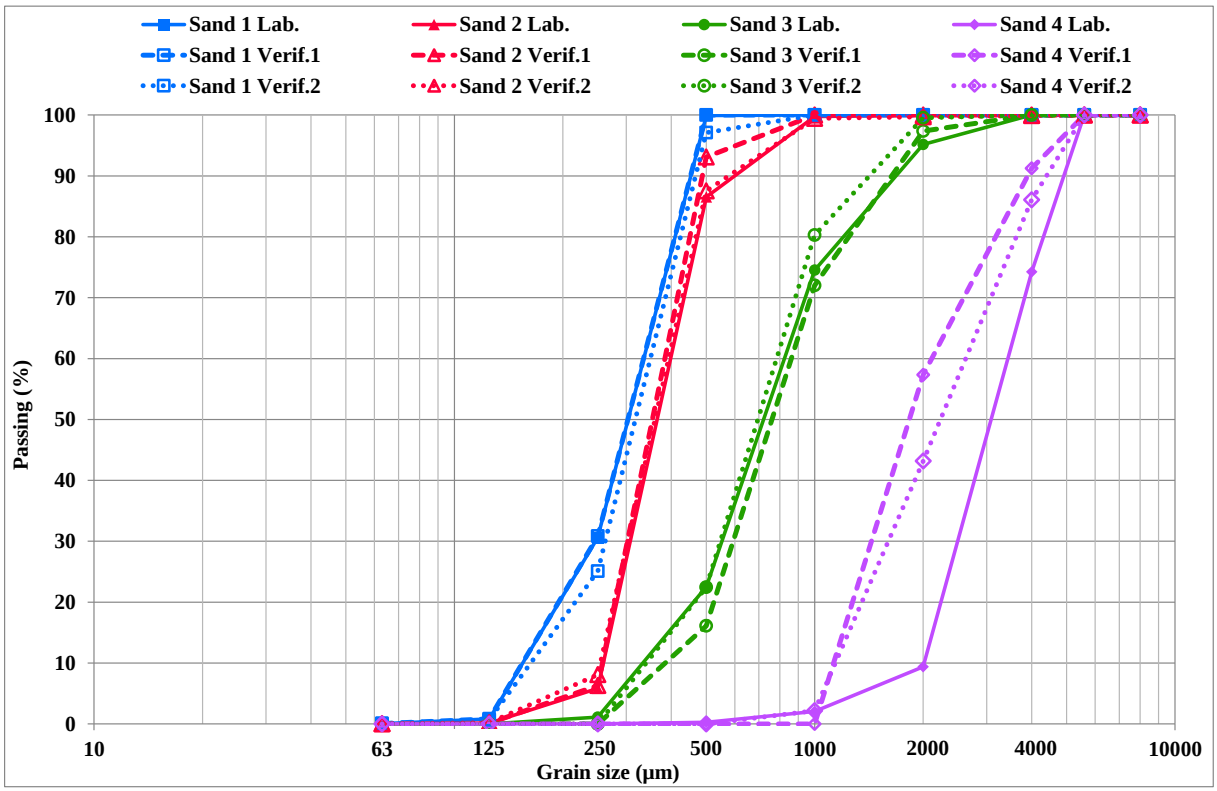

Figure 52. Sieve results (solid lines) and verification trials (broken and dotted lines) in absence of air flow.

7.2 Maximum possible mass flow rate

This part presents the experimental programs which were conducted with the vertical test rig while employing AEG vibratory feeder at its highest levels of vibration intensity and funnel height – i.e. 100% and 5 cm, respectively. The aim was enhancing the consistency in sand 4 results through increasing the number of sand grains colliding with the impacting head within a time-unit.

It was experimentally found out that at this extreme adjustment of the vibratory feeder, the vacuum cleaner had to be supplied with at least 165 volt in order to have homogenous dilute flow in the pneumatic line. By this voltage supply, air flow velocity of about 32 m/s (at position of the impacting head) was given.

It was planned to conduct three experimental programs while having this adjustment of the vibratory feeder. All of the test conditions in these three programs were identical, except air flow velocity. This parameter was varied from 32 to 37 and eventually to 40 m/s. These air flow velocities were obtained as the induction regulator was respectively adjusted to 165, 190 and 220 volt. In these three experimental programs, about 2 kg sand was required for each trial. A representative subsample (2 kg) was taken from each sand type sample and used repeatedly for the entire experimental programs.

For each of the three experiments, a PLSR model was calibrated. In each of these models, *model fit* was evaluated by computing PCTVAR for both *X*- and *Y*-variables. The percentage of explained variance by three PLS Principal Components is presented for 32, 37 and 40 m/s models in Table 12.

Table 12. PCTVAR values (in %) of 32, 37 and 40 m/s models.

Air flow velocity (m/s)	32	37	40
X-variable	63	58	76
Y-variable	37	37	38

It is understood from Table 12 that increasing mass flow rate up to its maximum possible limit has improved the PCTVAR in *Y*-variables to its highest level ever. In the previous experimental programs, the explained percentage of variance in *Y*-variables reached to a maximum of 35% (see Table 10). PCTVAR values corresponding to *X*-variables are also relatively high. According to Table 12, the best *model fit* for both **X** and **Y** has been given at 40 m/s.

Verification phase of each of the models was performed identically to the previous models. The ‘acoustic results’ of 32, 37 and 40 m/s models are respectively compared with the sieve analysis in Figure 53, Figure 54 and Figure 55. Also, Table 27, Table 28 and Table 29 of the Appendix respectively report the calculated absolute differences between the sieve analysis and ‘acoustic results’ of the experimental programs 32, 37 and 40 m/s. The whole averaged absolute differences from the three current experiments are graphically demonstrated in Figure 56. This diagram was produced with the aim of comparing consistency of the results from the current experiments and those from the horizontal test rig. Therefore, the vertical axis in Figure 56 has been scaled similarly to Figure 39 and Figure 45, so that they could be compared conveniently.

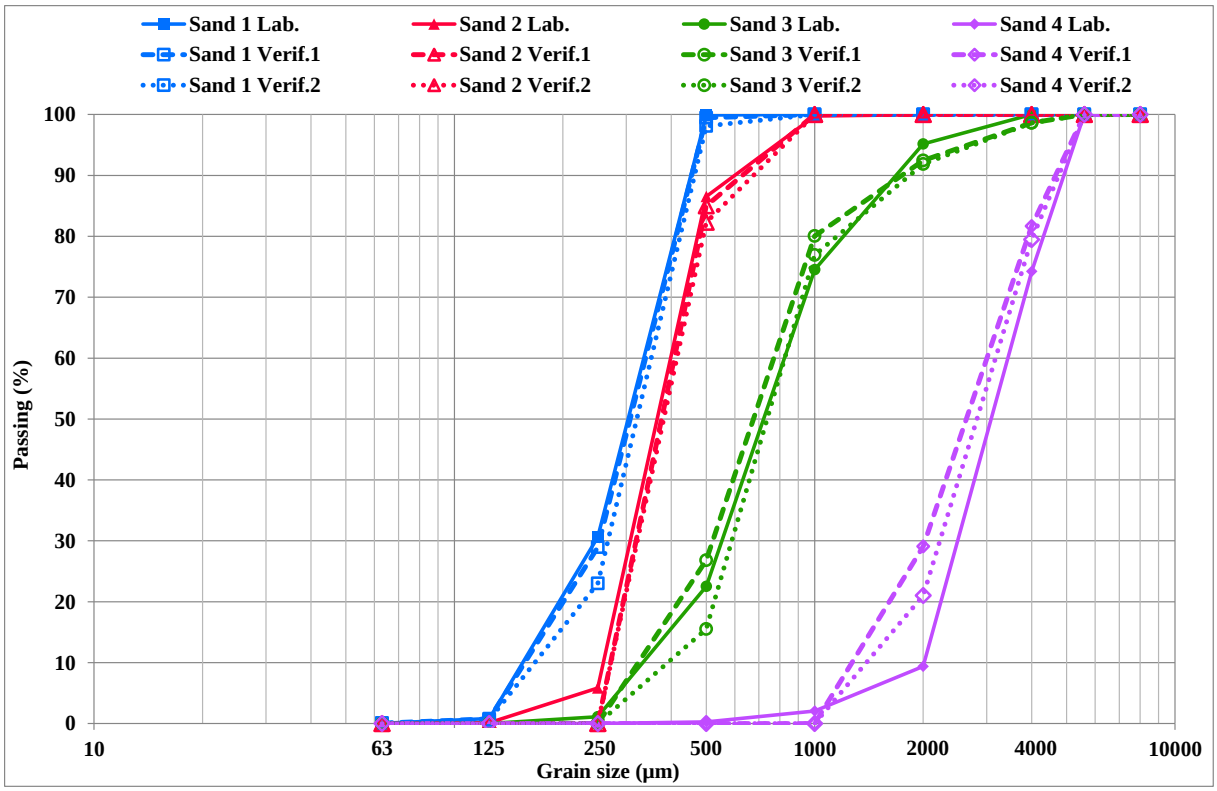

Figure 53. Sieve results (solid lines) and verification trials (broken and dotted lines) at air flow velocity of 32 m/s.

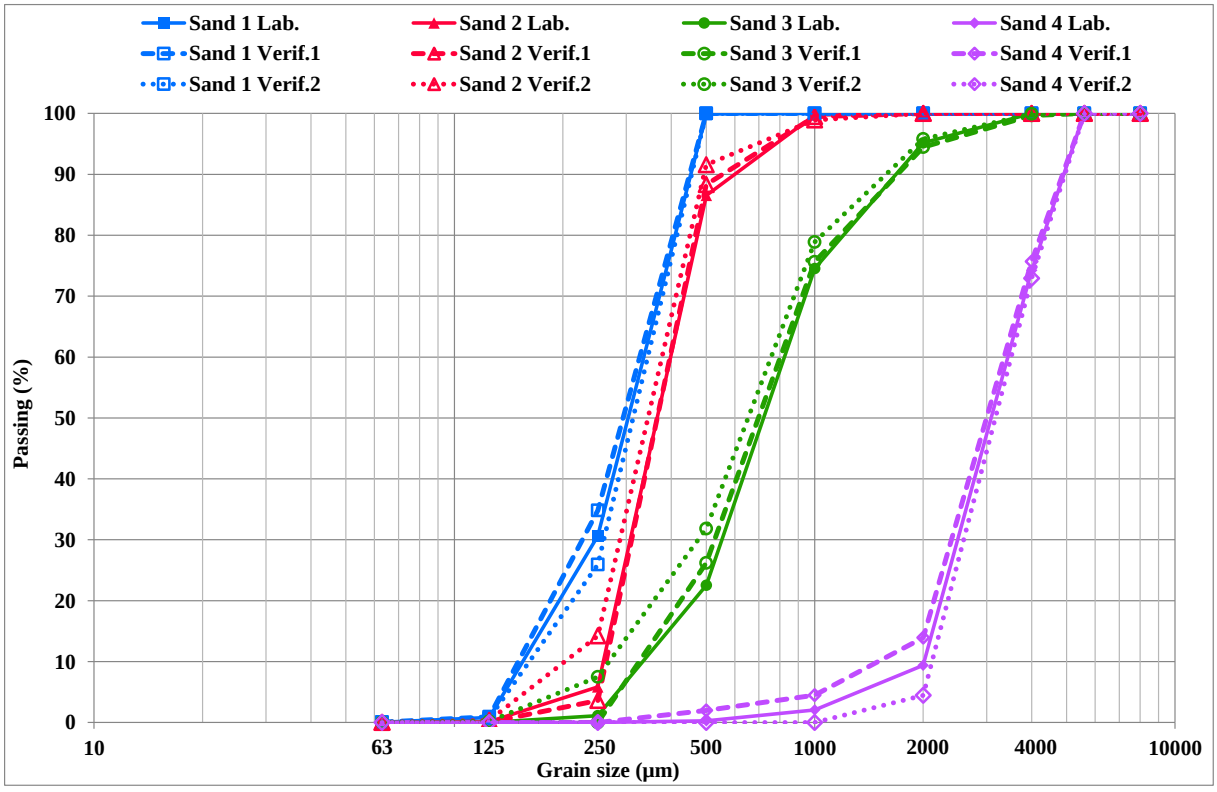

Figure 54. Sieve results (solid lines) and verification trials (broken and dotted lines) at air flow velocity of 37 m/s.

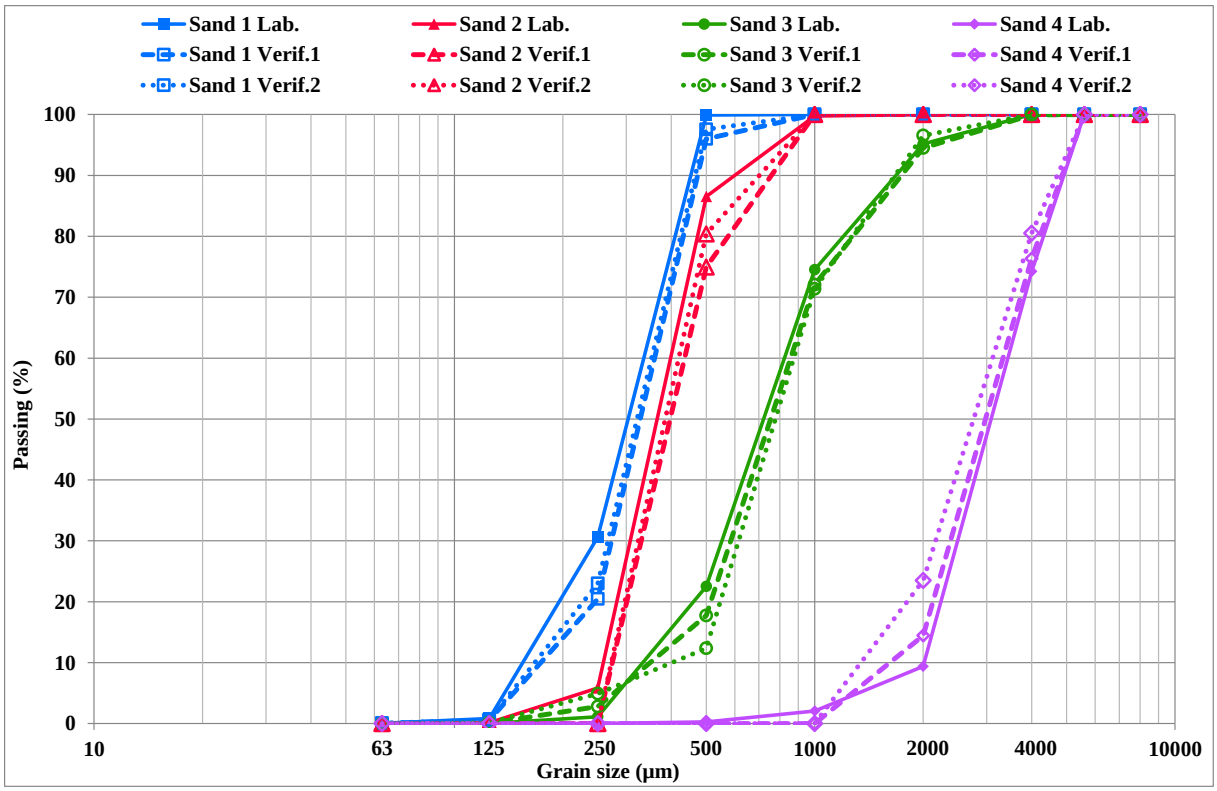

Figure 55. Sieve results (solid lines) and verification trials (broken and dotted lines) at air flow velocity of 40 m/s.

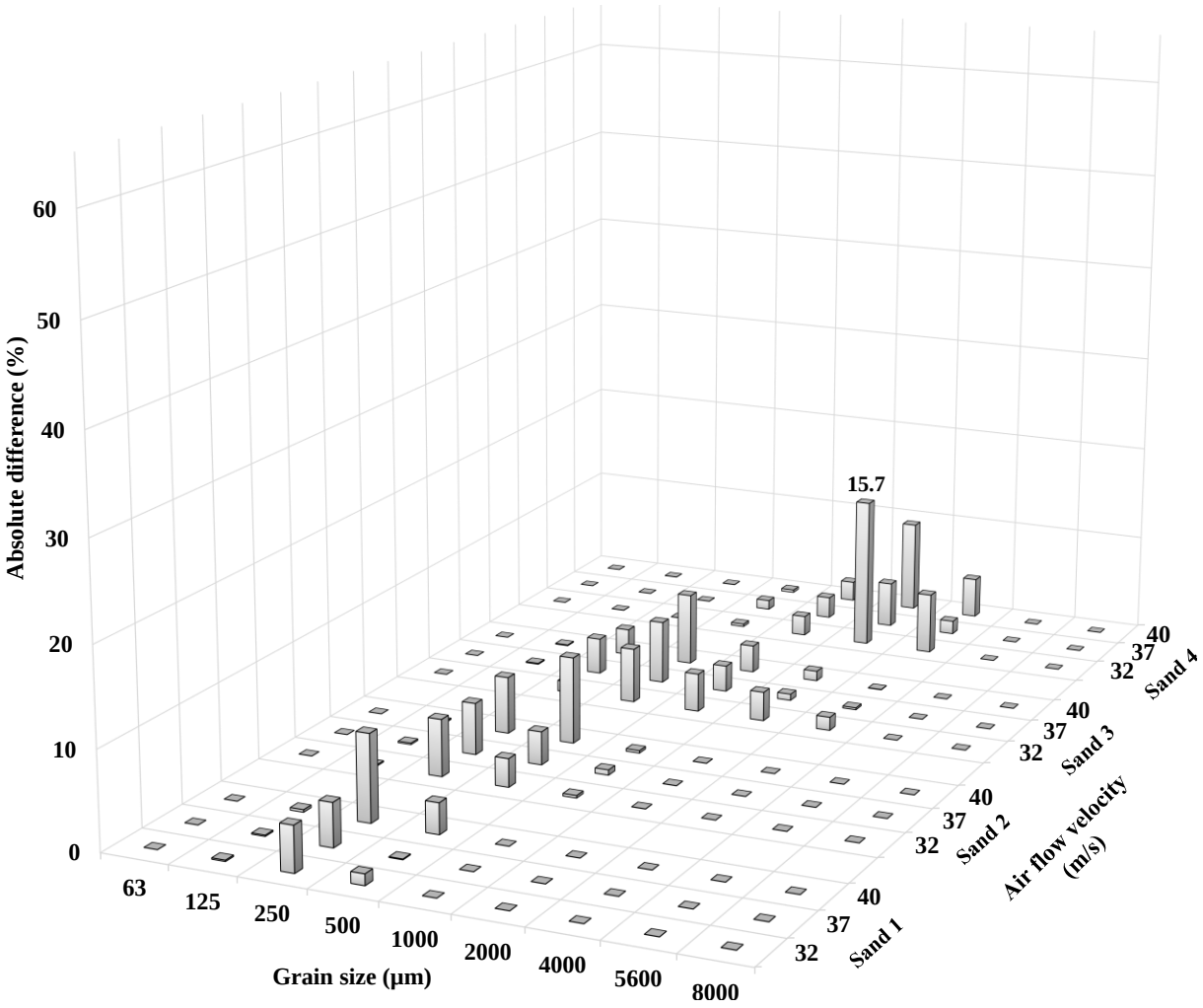

Figure 56. Absolute differences at air velocities of 32, 37 and 40 m/s.

Comparable to previous experimental programs, here also a good consistency can be seen between the sieve analysis and 'acoustic results' of sand types 1-3. No significant deviation can be considered in the results of sand types 1-3 in Figure 53, Figure 54 and Figure 55. According to Figure 56, this general consistency has not been considerably affected by varying air flow velocity.

Compared to all former experimental programs, the 'acoustic results' of sand 4 in the current experimental programs present clearly better agreement with the sieve analysis. Comparing Figure 56 with Figure 39 and Figure 45 simply shows how effective has increasing the mass flow rate up to its maximum limit improved the consistency of sand 4 results. Figure 56 suggests that the highest averaged deviation between the 'acoustic results' and sieve analysis is only about 16%. In this diagram, it is the only value higher than 10% and belongs to the lowest investigated air flow velocity (i.e. 32 m/s).

In contrary to all previous experimental programs, the three present models could predict the sieve analysis based on acoustic data with a relatively good precision. Take 37 m/s

experiment as an example, for each sand type an unpaired two-sample *t*-test was performed between each two acoustic trials. These statistical tests were in detail identical to those mentioned in part 6.1.5, except the sample size *n* which was here equal to 512×10^3 instead of 5×10^5. Table 13 reports the obtained *p*-values from the *t*-tests performed for 37 m/s experimental program.

Table 13. *p*-values from the unpaired two-tailed two-sample *t*-tests at 37 m/s.

	Sand 1	**Sand 2**	**Sand 3**	**Sand 4**
Trial 1 and Trial 2	0.641	0.491	0.306	0.166
Trial 2 and Trial 3	0.504	0.391	0.751	0.525
Trial 1 and Trial 3	0.258	0.866	0.502	0.427

According to Table 13, in all of the cases *p*-value is larger than 0.05 which means there is no evidence against the null hypothesis H_0 and we fail to reject it. Thus, statistical difference between the trials cannot be proved in any of the sand types. Increasing the mass flow rate up to its maximum possible limit has sufficiently decreased the 'air gaps' effect in sand 4 which eventually has led to statistically significant improvement in its data reproducibility.

In each sand type, the above test failed to prove that the three trials are statistically different. Therefore, at 37 m/s experiment the first trial of each sand type was arbitrarily selected for full cross validation. Through this 'external' cross validation, a data set with n=4 was provided. Four sub-models were built, each with two PLS Principal Components. In the first sub-model, trials from sand types 2-4 were used for training and sand 1 data was left out for verification. Similarly, in the second, third and fourth sub-models the data from sand types 2, 3 and 4 were respectively withheld. Thus, an 'acoustic result' was predicted by each sub-model through its verification phase. The four obtained 'acoustic results' are compared with the sieve analysis in Figure 57. Furthermore, RMSEP of each individual *Y*-variable (grain size) was calculated based on the verification tests of sub-models 1-4. All the obtained RMSEP values from this full cross validation are reported in Table 14.

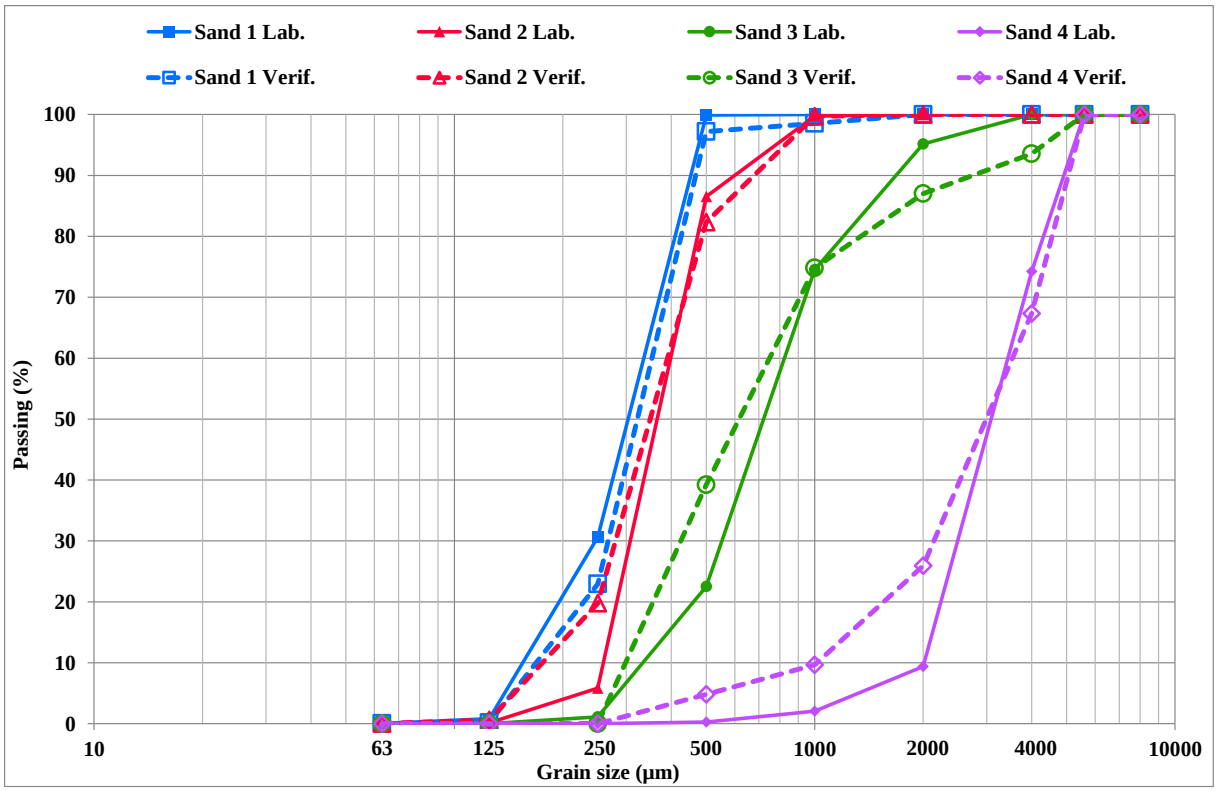

Figure 57. Comparison between the sieve analysis and sub-models predictions.

Table 14. RMSEP values from the full cross validation of first trials at 37 m/s.

Grain size (µm)	63	125	250	500	1000	2000	4000	5600	8000
RMSEP (%)	0.00	0.41	7.97	9.01	3.87	9.23	4.73	0.00	0.00

The adopted model validation method, namely leave-one-out cross validation, validates the good precision of the 37 m/s model in future predictions. In Figure 57 a relatively good consistency can be seen between the sieve analysis and verification results for all of the tested sand types – including sand 4. Also, the obtained *prediction error* values through full cross validation show that in the worst case the sieve analysis would be predicted by the 37 m/s model with a ±18.5% precision. Comparing Table 14 with Figure 40 and Figure 46 reveals that the current model has a better prediction precision than any other previous model.

Rising mass flow rate increases the number of sand grains colliding with the impacting head within a time-unit. This fact applies clearly for all of the tested sand types. In the current part of the study, however, it was experimentally shown that the number of collisions in the case of sand 4 has reached a level where the influence of ‘air gaps’ in the final results was successfully eliminated. It implies that at this high mass flow rate,

the time delay between each two neighboring impacts is short enough to avoid the fall of magnitude level in sand 4 signal.

Although by employing AEG vibratory feeder at its maximum possible capacity the problem associated with the ‘air gaps’ was solved, however, it was found out that sand 4 has had different rate of mass flow compared to sand types 1-3. As an instance, Figure 58 compares the recorded raw signals from sand types 1-4. It can clearly be proved from this Figure that sand 4 has been fed within a longer time period than other sand types; though an equal amount (2 kg) of each sand type has been used.

In Table 15, all the calculated values of mass flow rate (in g/s), which belong to the current experimental programs, are reported. In this Table, the average as well as standard deviation of mass flow rate values from each sand type are presented. Each sand type by itself has had a relative constant mass flow rate, since all of the reported standard deviation values are relatively small. Sand types 1-3 have had comparable rates of mass flow (see the mean values in Table 15). But the mass flow of sand 4 has had significantly lower rates.

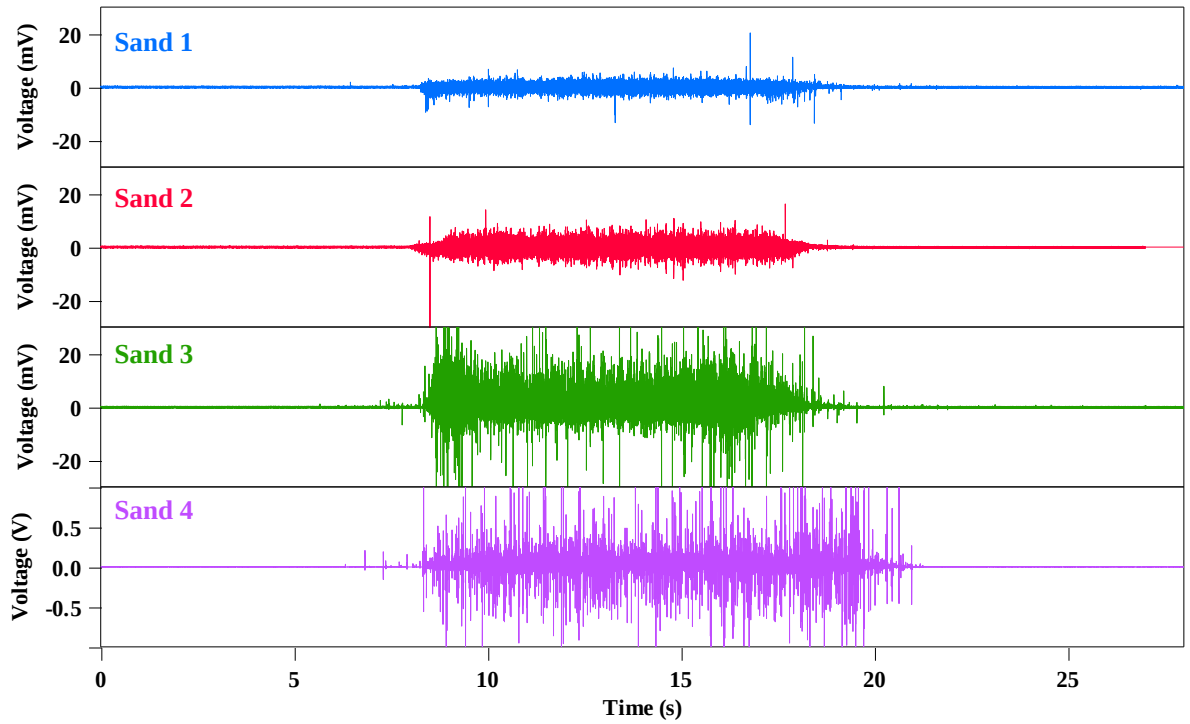

Figure 58. Raw signals recorded while using the feeder at its highest capacity.

Table 15. Calculated mass flow rates (g/s) in different experimental programs.

		Sand 1	Sand 2	Sand 3	Sand 4
32 m/s	Trial 1	200.0	194.2	192.3	163.9
	Trial 2	190.5	185.2	188.7	156.3
	Trial 3	192.3	186.9	190.5	166.7
37 m/s	Trial 1	198.5	192.3	191.8	164.6
	Trial 2	200.0	200.0	196.1	163.9
	Trial 3	190.5	190.5	188.7	169.5
40 m/s	Trial 1	208.3	198.0	192.3	169.5
	Trial 2	200.0	200.0	200.0	162.6
	Trial 3	208.3	190.5	186.9	165.3
Mean		198.7	193.1	191.9	164.7
Standard deviation		6.8	5.4	4.1	4.0

According to Table 15, sand types 1-3 have been fed with an average mass flow rate of 194.6 g/s which is 18.1% higher than the mass flow rate of sand 4 (164.7 g/s). This inconsistency implies that the feed rate of this vibratory feeder would not be independent of sand type, or sand grain size distribution, if it is used at its maximum capacity.

Considering the above discussed inconsistency, the obtained ‘acoustic results’ from the current experimental programs may not be reliable even though they represented the sieve analysis well. Analyzing various sand samples with different distributions of grain size, while being uncertain about the equality of mass flow rate, can lead to inaccurate results.

The feed rate of sand types 1 and 4 was repeatedly (5 times) measured. These measurements were conducted under 9 different combinations of funnel height and vibration intensity of AEG vibratory feeder. The aim of these measurements was to determine an optimum adjustment of the vibratory feeder, under which sand types 1 and 4 would be fed with comparable rates. Table 30 of the Appendix includes the measurement results. Amongst the tested adjustments of the vibratory feeder, 4 cm and 80%, respectively for funnel height and vibration intensity, provided the lowest difference between the feed rates of sand types 1 and 4. The next part concerns the experimental program with the optimum adjustment of the vibratory feeder – i.e. 4 cm and 80%.

7.3 Optimum adjustment of the vibratory feeder

An experimental program was conducted with the vertical test rig while AEG vibratory feeder was adjusted at 4 cm and 80%, respectively for funnel height and vibration intensity. Air flow velocity was kept at 37 m/s. The obtained 'acoustic results' are compared with the sieve analysis in Figure 59.

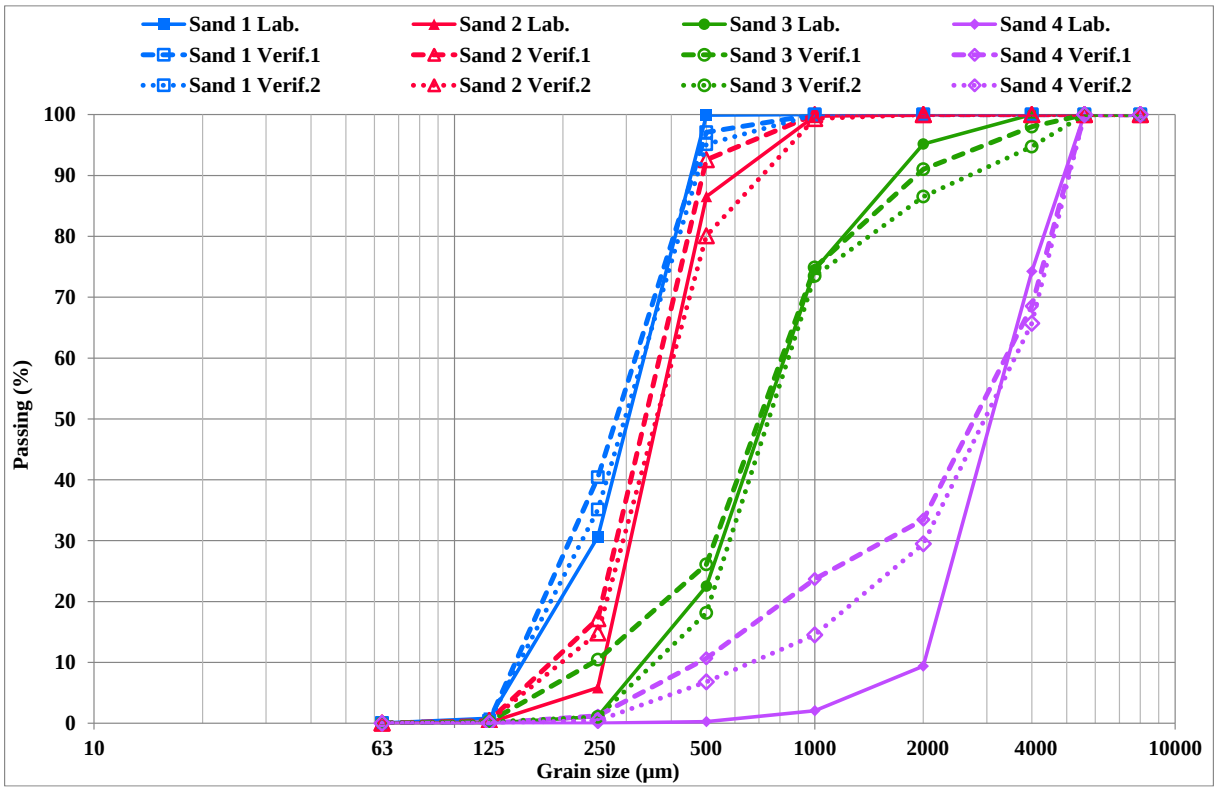

Figure 59. Sieve results (solid lines) and verification trials (broken and dotted lines) at optimum adjustment of the feeder.

According to Figure 59, there is a general agreement between the sieve analysis and 'acoustic results' of sand types 1-3. However, the agreement is relatively poor in the case of sand 4 – particularly in grain sizes 1000 and 2000 µm. In sand 4, the maximum absolute difference reaches about 24%. It implies that at the current mass flow rate (approximately 100 g/s) the presence of 'air gaps' has still influenced the results of sand 4. Although by this adjustment of the feeder sand 4 was fed with a rate very close to sand types 1-3, however under this condition the established model failed to predict the 'acoustic results' of sand 4 accurately.

7.4 Concluding remarks on the vertical test rig

Numerous experimental programs were conducted with the horizontal and vertical test rigs. In most of these experimental programs grain size distribution of sand 4 was estimated by acoustic data inaccurately. This problem was solved by increasing mass flow rate to its highest possible level; i.e. AEG vibratory feeder was employed at its maximum capacity. However, it was proved that sand 4 would be fed more slowly than other sand types when employing the vibratory feeder at this extreme adjustment. In addition to that critical shortcoming, the amount of required sand sample was very high. A 2 kg sample would be required to record a 10-second long raw signal. If a prototype laboratory device were supposed to be manufactured based on this setup, sample preparation (including drying) and handling would be very time-consuming and difficult. Also, utilizing such a noisy, large and heavy vibratory feeder would not be desired. Therefore, it was decided to select the design parameters for manufacturing the prototype laboratory device specifically based on sand types 1-3.

The next Chapter describes the conducted experimental program with the vertical test rig, which was aimed to verify the selected design parameters. Also in the following Chapter, the prototype laboratory device and its components are described. The long-term utilization of the prototype is included in that Chapter too.

8 The prototype laboratory device

8.1 Design parameters for manufacturing the prototype

It was proved earlier in part 7.1 that omitting the air flow didn't affect the 'acoustic results' of sand types 1-3. In that part, advantages of a prototype without vacuum cleaner were outlined too. However, in the current part of the study it was decided to not set up the design parameters of the prototype without air flow. The reason mainly lay in the observation that was made based on signal-to-noise ratio. It was observed that, under constant conditions, eliminating the air flow led to reduction of this ratio. This observation succeeded through conducting two experimental programs, both at mass flow rate of 15 g/s. In the first experimental program, the vacuum cleaner was not turned on at all, while in the second one air flow velocity of 18 m/s was provided. The rest of the test conditions in both experimental programs were identical. Each of sand types 1-3 were tested in each of these experimental programs three times. The recorded data during flow of sand in the pneumatic line was considered as the desired *signal*; while, the data from the period as sand flow was over and vibratory feeder (and vacuum cleaner) was (were) still running was taken as the background *noise*. Using Equation (3.2) from part 3.4.2, the signal-to-noise ratio in each trial was computed. In Figure 60, all the obtained signal-to-noise ratios from these two experimental programs are graphically presented.

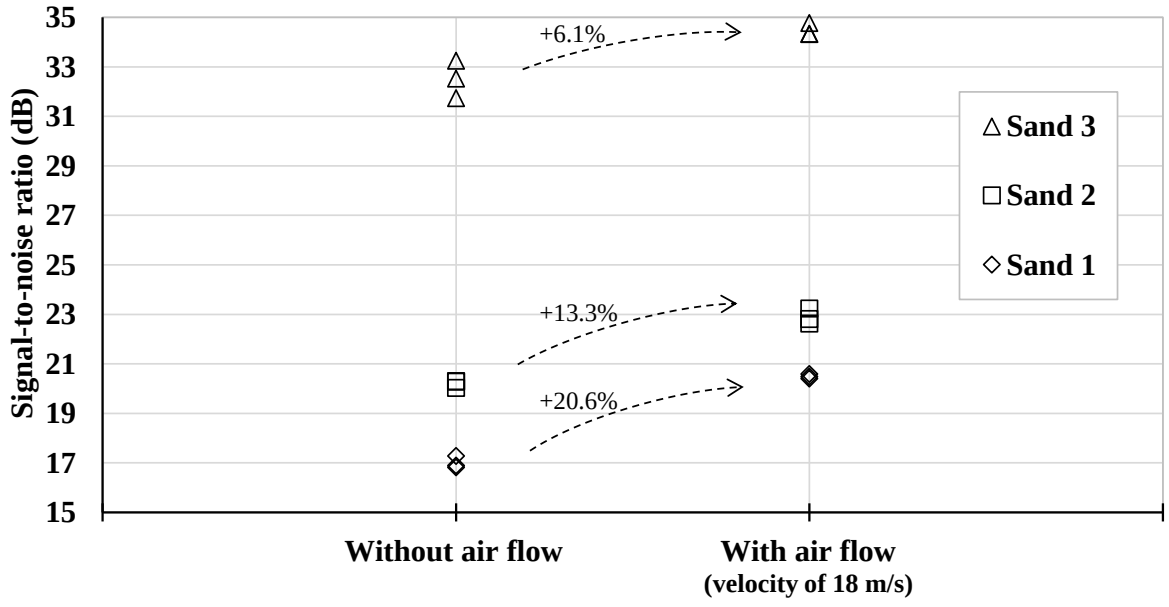

Figure 60. The effect of air flow presence on signal-to-noise ratio.

According to Figure 60, introducing air flow into the pneumatic line has noticeably enhanced the signal-to-noise ratio in each sand type, even though the velocity of air flow has been relative low, i.e. only 18 m/s. Therefore, to keep the signal quality at a reasonable level, it was decided to consider the design parameters of the prototype with presence of air flow.

This part of the study was aimed to verify the design parameters of the prototype. An experimental program was conducted at air flow velocity of 18 m/s. This velocity was obtained as the vacuum cleaner was supplied with 100 volt. This relative low air flow velocity was selected, since utilizing the vacuum cleaner under this condition ensured that the prototype laboratory device would not be unpleasantly loud.

The vibratory feeder (Sympatec, type VIBRI) was adjusted with 8 mm and 50%, respectively for funnel height and vibration intensity. It provided a mass flow rate of about 15 g/s. Thereby, from each sand product only about 250 g was required for each trial. Small amount of required sample was considered as an advantage of the prototype.

In addition to sand types 1-3, three further products from the same sand and gravel quarry in Netherlands were also included in the current experimental program. These three products are actually various mixtures of sand types 1-3. The mixtures are produced in the processing plant of the quarry simply by mixing various proportions of sand types 1-3. In Table 16 nominal grain size distribution of these three mixtures are presented.

Table 16. Nominal grain size distributions of mixtures 1-5.

	Mixture 1 Zand 0-1 (95-30)		Mixture 2 Zand 0-2 (85-20)		Mixture 3 Zand 0-2 (80-10)	
Grain size (μm)	Min	Max	Min	Max	Min	Max
63	0	0	0	0	0	0
125	0	5	0	4	0	1
250	25	35	17	23	8	11
500	68	82	42	52	42	58
1000	90	98	81	89	77	83
2000	98	100	95	100	92	97
4000	100	100	100	100	99	100
5600	100	100	100	100	100	100
8000	100	100	100	100	100	100

Instead of sensor with 1 mV/g sensitivity (PCB, type 352B01), for the current experimental program a sensor with 10 mV/g sensitivity (PCB, type 353B18) was

employed. Grain size range of the sand products, and also the adopted mass flow rate and air flow velocity in the current experimental program allowed to enhance the sensitivity of the sensor without exceeding the measurement range of the ADC (±5 volt, see [122]). Although the frequency range in 10 mV/g sensor was relatively more limited than in 1 mV/g (see [114] and [117]), however, by applying the bandpass filter at the range of 10-18 kHz it was ensured that only meaningful information would be processed. Worthy to mention that the form of frequency spectrum was not significantly affected by enhancing the accelerometer's sensitivity.

A PLS Regression model was trained for the current experimental program. **X** and **Y** were respectively in the form of 6×128 and 6×9 matrices, where the number of observations *n* was equal to 6. The first trial of each sand type was used for training. The second and third trials of each sand type were considered for subsequent model verification. In the calibration phase of the model, full cross validation – as an 'internal' cross validation – was adopted to determine the optimum number of PLS Principal Components. In this regard, model calibration was performed until step *l*=4. In each step, a full cross validation was performed and its corresponding calculated RMSEP value was computed. Each full cross validation consisted of 6 artificial models. This 'internal' cross validation was succeeded by means of an iterative algorithm developed in MATLAB R2012b. This algorithm built a total number of 24 sub-models. For each individual *Y*-variable (grain size), all the four obtained RMSEP values (in %) are plotted against their corresponding step numbers in Figure 61.

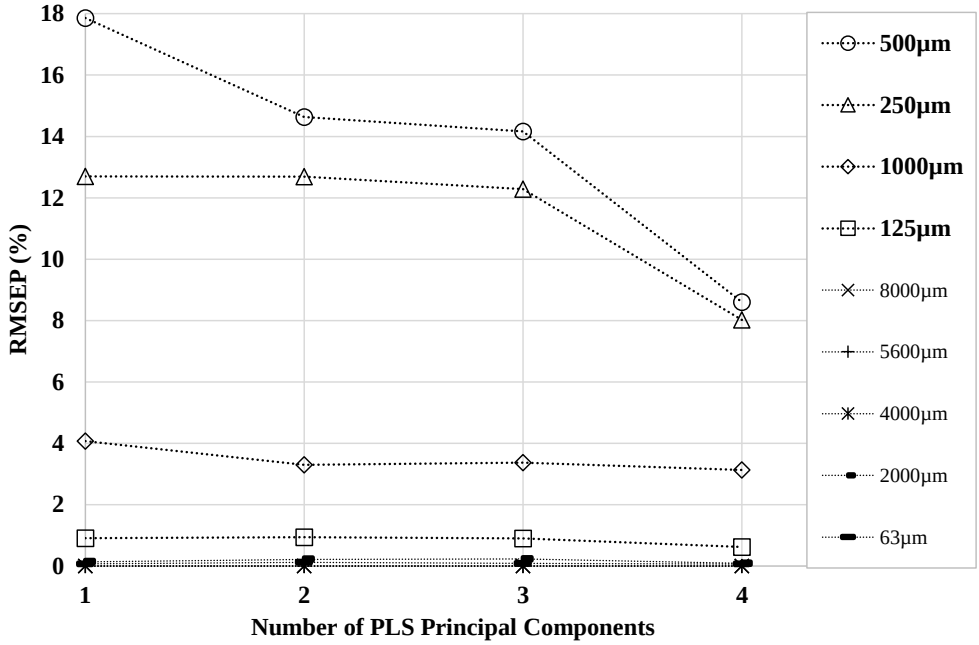

Figure 61. *Prediction error* against the number of PLS Principal Components.

Figure 61 shows that *prediction error* in grain sizes 63, 2000, 4000, 5600 and 8000 µm in all the four steps is almost zero. Because the columns in **Y** which correspond to these grain sizes are filled either with 0 or (almost) 100%. Therefore, the model, even by one Principal Component, is able to predict these *Y*-variables very well. Additionally, as mentioned earlier, the two defined threshold levels replace the predicted values higher than 100% and lower than 0% with 100% and 0%, respectively. On the other hand, RMSEP values corresponding to 125, 250, 500 and 1000 µm decrease noticeably as the number of applied Principal Components increases. Figure 61 suggests that the most suitable number of steps is 4, as this step presents a minimized *prediction error* for all of the *Y*-variables. In the fourth step, all the RMSEP values obtained through the applied 'internal' cross validation are reasonably small – and do not even exceed 10%.

Therefore, the model calibrated with 4 PLS Principal Components was selected to be verified. Likewise earlier experimental programs, here also second and third trials from each sand type were used for the verification phase. The obtained 'acoustic results' from the verification phase are compared with the sieve analysis in Figure 62. In this Figure, each grain size is specified by a color. Some of the grain sizes, namely 63, 4000, 5600 and 8000 µm, are not illustrated in this Figure. Because the passing percentage in these uninteresting grain sizes was either 0 or 100 anyway. The sieve results are shown with □, while ∗ and × respectively represent 'acoustic results' from second and third trials. The calculated absolute differences between the sieve analysis and 'acoustic results' are reported in Table 32 of the Appendix.

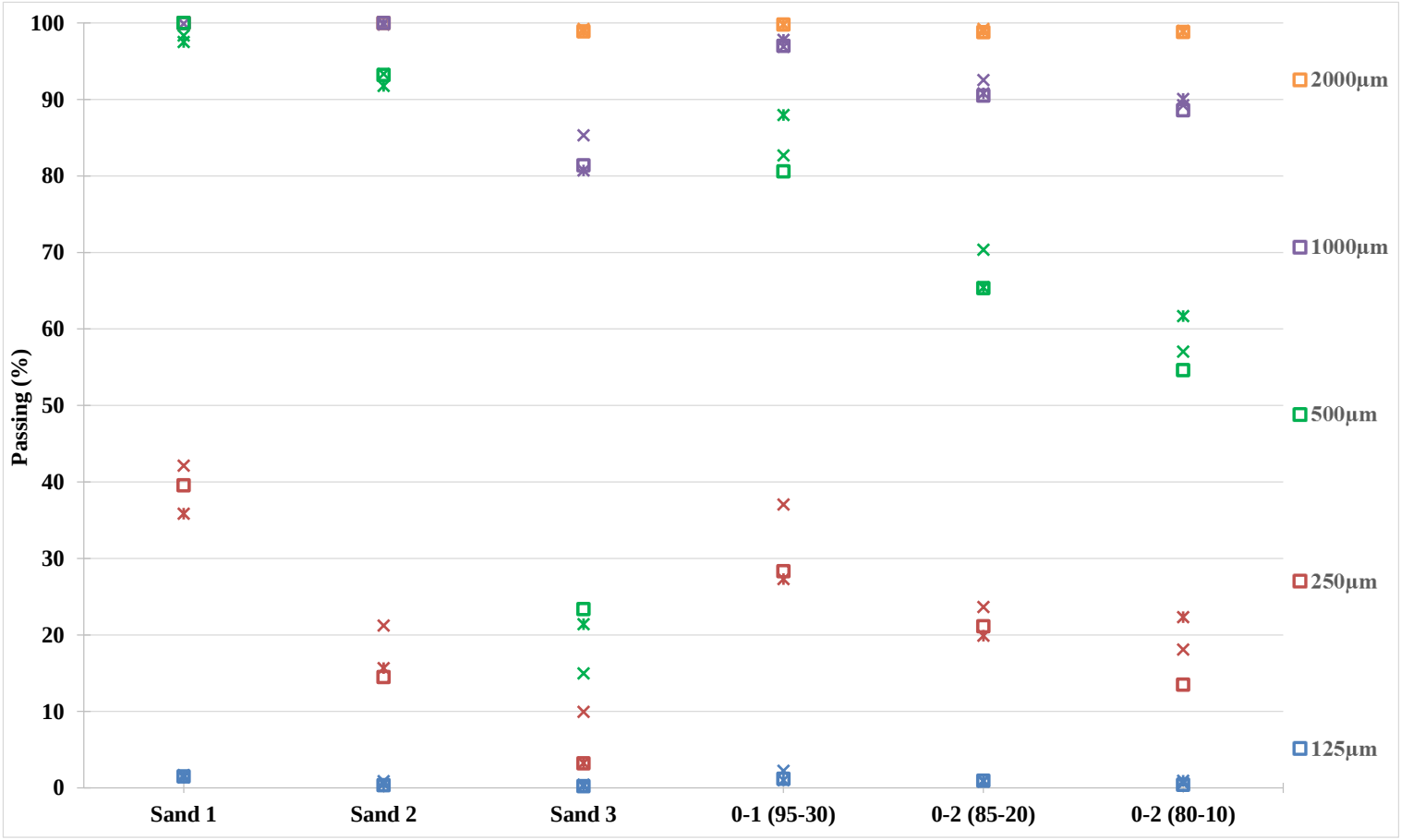

Figure 62. Sieve analysis (□) vs. the first (∗) and second (×) verification trials.

As it can be seen from Figure 62, the 'acoustic results' of the tested sand products fairly agree with the sieve results. Also, in each sand product the first and second verification trials are quite comparable. *Prediction error* of the model was evaluated by help of RMSEP, while i=1, 2, …, n=12 (refer to Equation (3.12) in part 3.5.12). Obtained RMSEP value for each Y-variable (grain size) is reported in Table 17.

Table 17. *Prediction error* in each grain size.

Grain size (µm)	63	125	250	500	1000	2000	4000	5600	8000
RMSEP (%)	0.04	0.39	4.97	4.33	1.40	0.17	0.00	0.00	0.00

According to Table 17, the current model has a much better prediction precision than all the previous models. In the worst case, the prediction precision of this model is about ±10% estimated. The reasons for good performance of this model, compared to the previous models, are: this model doesn't deal with flawed signals of sand 4. Additionally, higher number of observations provided the possibility to perform an 'internal' cross validation; by which the optimum number of PLS Principal Components was determined.

The current experimental program was conducted with 6 sand products under a condition where both mass flow rate and air flow velocity were kept quite low. The model, with specified optimum number of PLS Principal Components, yielded 'acoustic results' with very promising accuracy. Therefore, it was planned to manufacture a prototype laboratory device based on the experimental setup of the current experimental program. The aim was reliability evaluation of the passive acoustic measurement technique for determining grain size distribution of sand products. In the current study, the steps of setting up and optimizing this technique were presented chronologically through the previous Chapters. These steps dealt with measurement equipment, operating parameters and signal processing/statistical methods. Long-term utilization of the prototype in an industrial environment allowed to evaluate all these steps properly. In this way, the accuracy of the 'acoustic results' could be proved very frequently by comparing them to laboratory sieve results. Also, having a much higher number of observations was essential for evaluating PLSR modeling in its different aspects. The next part presents the manufactured prototype as well as its long-term utilization in the sand and gravel quarry (in Netherlands).

8.2 Long-term utilization of the prototype laboratory device

The prototype was fundamentally similar to the vertical test rig. Figure 63 presents a photo of the prototype.

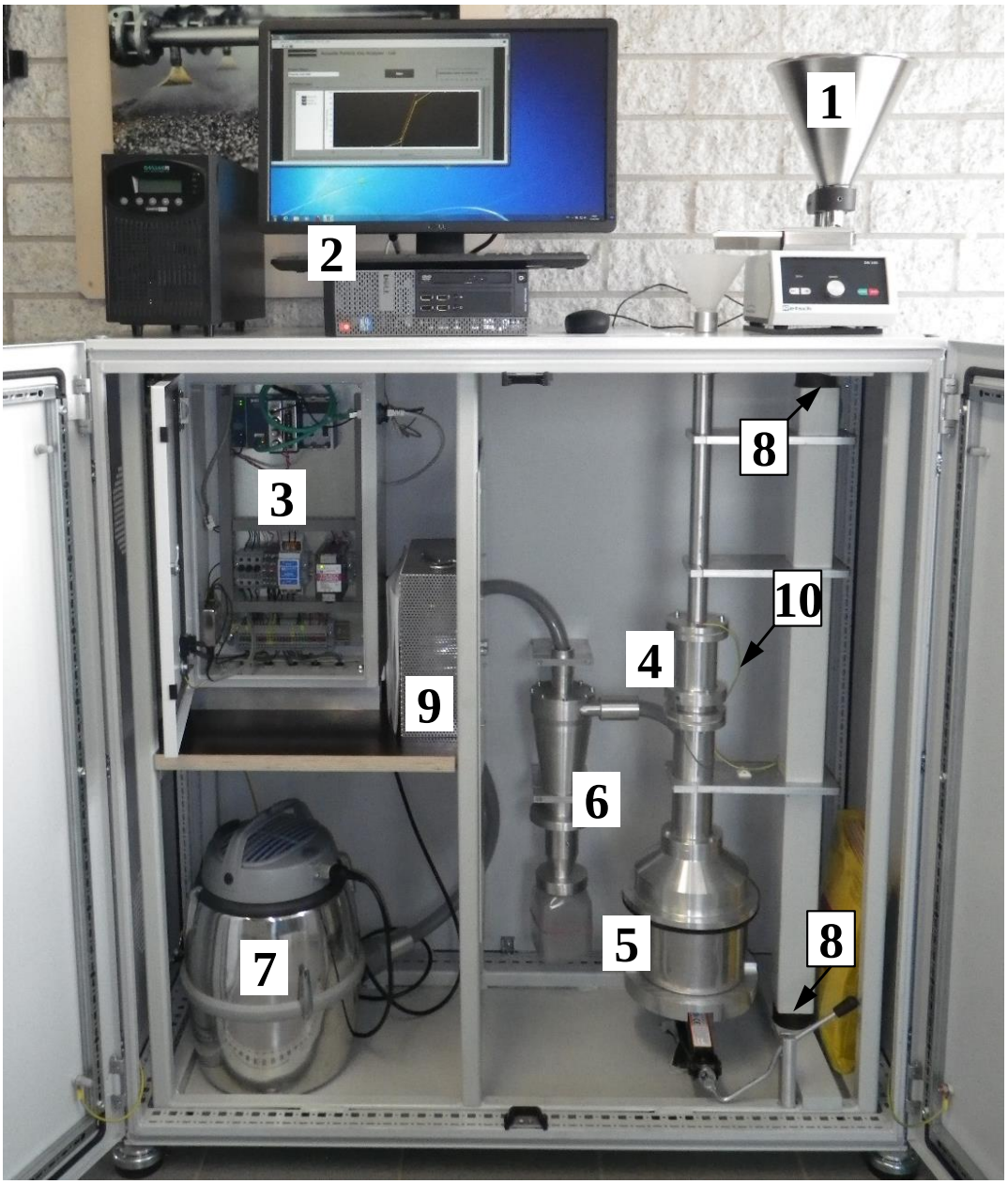

Figure 63. The prototype laboratory device.

The numbered items in Figure 63 are listed as following:

1) Vibratory feeder (Retsch, type DR 100),

2) Computer,

3) DAQ device consisted of an ADC (NI, type 9234) installed in a chassis (NI, type cDAQ-9184),

4) The probe was installed in this element and equipped with a 10 mV/g accelerometer (PCB, type 353B18),

5) Collection bin,

6) Cyclone,

7) Vacuum cleaner (Nilfisk, type GM 80),

8) Rubber damper,

9) Transformer,

10) Earthing cable.

Instead of utilizing the same vibratory feeder (Sympatec, type VIBRI), which was employed in the previous parts, another model of vibratory feeder (Retsch, type DR 100) was considered for the prototype. The reason was relative simplicity of DR 100 vibratory feeder for being controlled via computer. This vibratory feeder was adjusted to 20 mm and 71%, respectively for its funnel height and vibration intensity level. In this way, mass flow rate of about 14 g/s was given. The required size of sand sample for determining its grain size distribution was only about 250 g. From each measurement, a 10-second long segment was considered to be selected for further process. The prototype was utilized for determining grain size distribution of the 6 sand products, which were formerly tested in the previous part.

By means of the transformer, the vacuum cleaner was supplied with a constant voltage of 115 volt. Thereby, air flow velocity of about 18 m/s was achieved.

The entire pneumatic line of the prototype was earthed in order to avoid build-up of static electricity, which could disturb the acoustic measurement results.

By using LabView^{TM} 2010 (NI), a software was programed which was responsible for controlling the vacuum cleaner and vibratory feeder as well as recording the data on the computer.

It was observed that after the above reported experimental programs with the vertical test rig (and also numerous other experiments which were not subject of the current thesis), tip of the impacting head was obviously worn out of shape. In Figure 64, an unused impacting head (left) is compared with the used impacting head (right). Clearly seen from this Figure, tip of the impacting head has been completely worn out though made of steel. Bearing in mind that deformation of the impacting head may affect

properties of the recorded signals, the impacting head of the prototype was ordered to be made of a special hard-wearing sintered metal. Thereby, it was ensured that the impacting head would not be worn out within the long-term utilization. Needless to say, the impacting head of the prototype had the same geometry as the vertical test rig's impacting head.

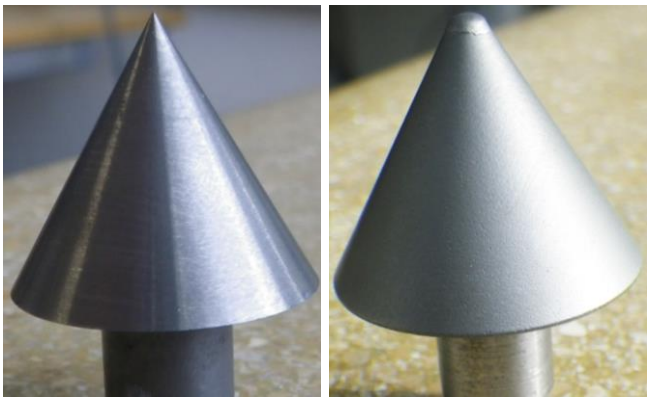

Figure 64. Left to right, an unused impacting head and the used one.

The prototype was transported to the sand and gravel quarry (in Netherlands) and put into operation in the laboratory. It was utilized for over 7 months. During this time, a total number of 300 samples were tested with the prototype. Table 18 summarizes the number of tested sand samples. Parallel with that, grain size distribution of each sample was determined by laboratory sieving. The sieve results of the 300 tested samples are entirely illustrated in Figure 65. This Figure properly shows how each investigated sand product has varied during the long-term utilization in terms of its grain size distribution. Furthermore, the range of grain size distribution which has been investigated through the long-term utilization can be observed from Figure 65. As demonstrated also in Figure 65, it was figured out that none of the 300 samples has had grains coarser than 4000 µm. Therefore, it was decided to ignore 5600 and 8000 µm grain sizes within the long-term utilization of the prototype.

Table 18. Number of tested sand samples in the long-term utilization.

	Sand 1	**Sand 2**	**Sand 3**	**0-1 (95-30)**	**0-2 (85-20)**	**0-2 (80-10)**	
Number of tested samples	66	62	78	16	16	62	**Total:** 300

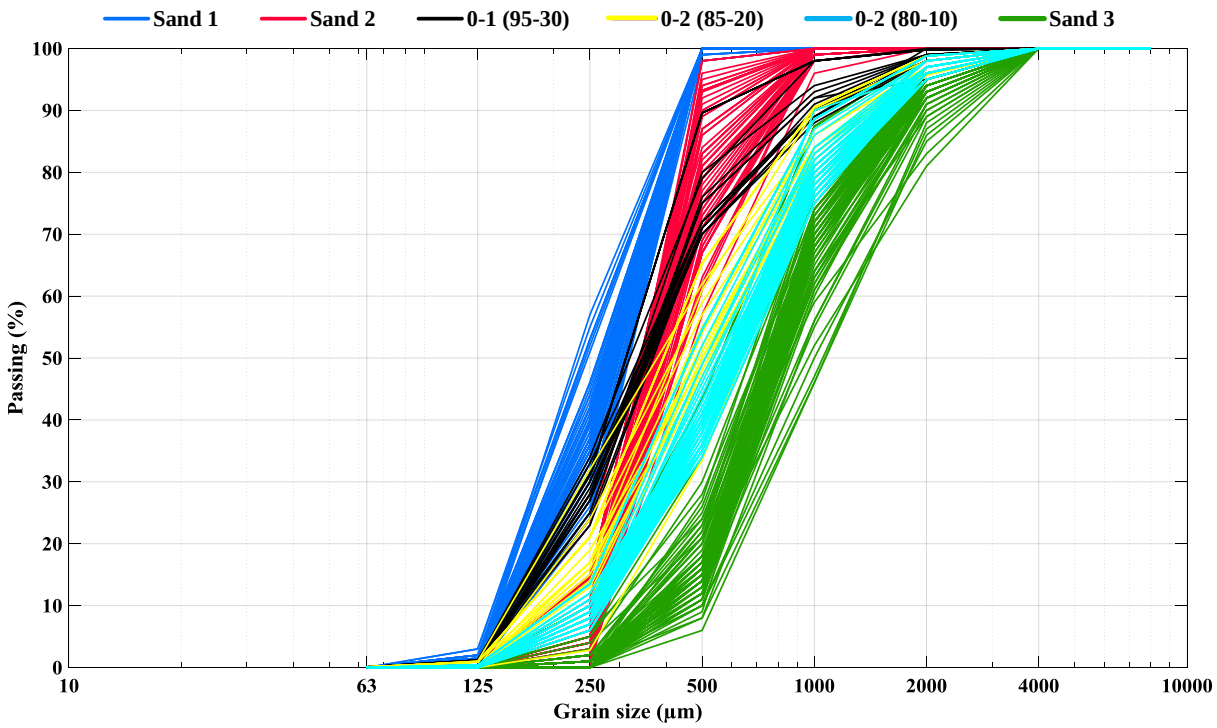

Figure 65. Sieve results of the 300 tested samples within the long-term utilization.

8.3 Determining the optimum number of steps

After the long-term utilization, which lasted over 7 months, the entire recorded acoustic data was collected from the prototype laboratory device. Also, the laboratory sieve results of the 300 tested samples were collected. The 10-second long segment of each acoustic measurement was filtered and then undergone the FFT function identically as discussed earlier within the design parameters of the prototype (part 8.1).

Similar to previous experimental programs, here also the FFT results were stored in a matrix. This matrix, considered as **X**, had 300 rows and 128 columns matrix; thus, n=300. In accordance with **X**, **Y** with 300 rows and 7 columns was built too. A PLS Regression model was calibrated using **X** and **Y**. Full cross validation, as an 'internal' cross validation technique, was employed to determine the optimum number of PLS Principal Components. In this way, model training was continued up to l=12 steps. At each step, a leave-one-out cross validation was performed and its corresponding RMSEP was computed and stored. The 'internal' cross validation procedure involved a total number of 3600 artificial models – 300 artificial models at each step. The whole procedure was carried out by an iterative algorithm developed in MATLAB R2012b. A single run of the algorithm took only a couple of seconds on a dual-core 3.0GHz PC with 8GB RAM running Windows 7. All of the yielded RMSEP values are graphically presented in Figure 66. In this Figure, for each Y-variable (grain size), all the 12 obtained RMSEP values are plotted against their corresponding step numbers.

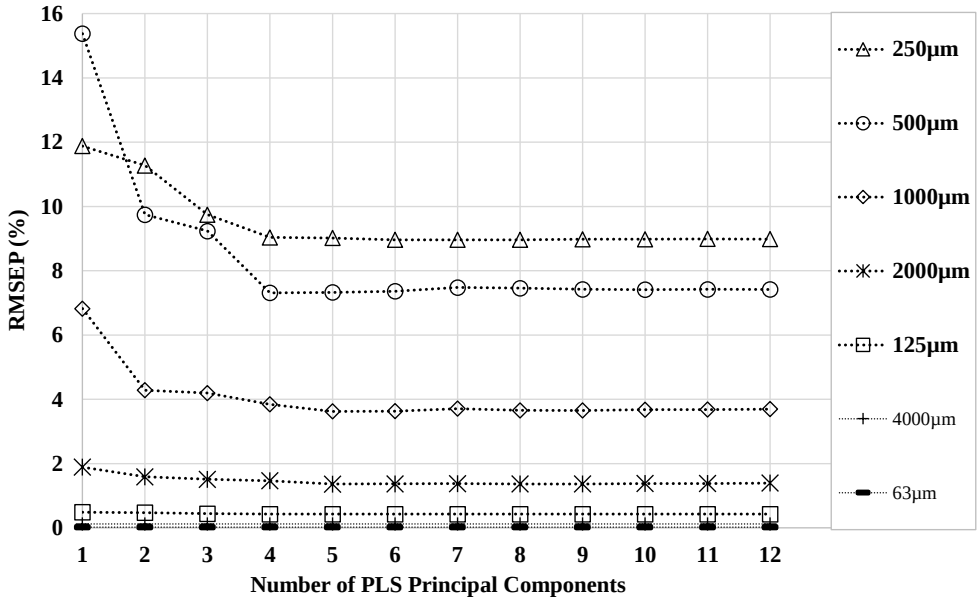

Figure 66. *Prediction error* against the number of PLS Principal Components.

Clearly seen from Figure 66, the optimum number of PLS Principal Components is l=4. l=4 is the smallest number of steps, where RMSEP of every grain size is minimized (or at least relatively minimized). Going beyond 4th step hardly enhances the *prediction error* and may only increase the model complexity. According to Figure 66, the largest RMSEP value at 4th step belongs to grain size 250 µm (about 9%). Generally, RMSEP values of 63 and 4000 µm grain sizes incline to zero and RMSEP of 125 µm doesn't exceed 1%. Comparison between Figure 66 and Figure 61 reveals that the performances of the current model and the one from the very last experiment with the vertical test rig (part 8.1) with 4 PLS Principal Components are quite comparable in terms of their *prediction error*.

Additionally, the above mentioned iterative algorithm computed PCTVAR for *X*- and *Y*-variables at each step. Thereby, the percentage of variance explained by the model for *X*- and *Y*-variables was plotted against the number of PLS Principal Components. The obtained plot is presented in Figure 67. This Figure clearly confirms that the optimum number of steps is l=4. l=4 is the minimum number of required PLS Principal Components, by which the best possible *model fit* can be given. At this step, model has related about 74% of acoustic data present in **X** to about 46% of sieve results existing in **Y**. At steps higher than l=4, the explained percentage of variance would be significantly improved for neither *X*-variables nor for *Y*-variables.

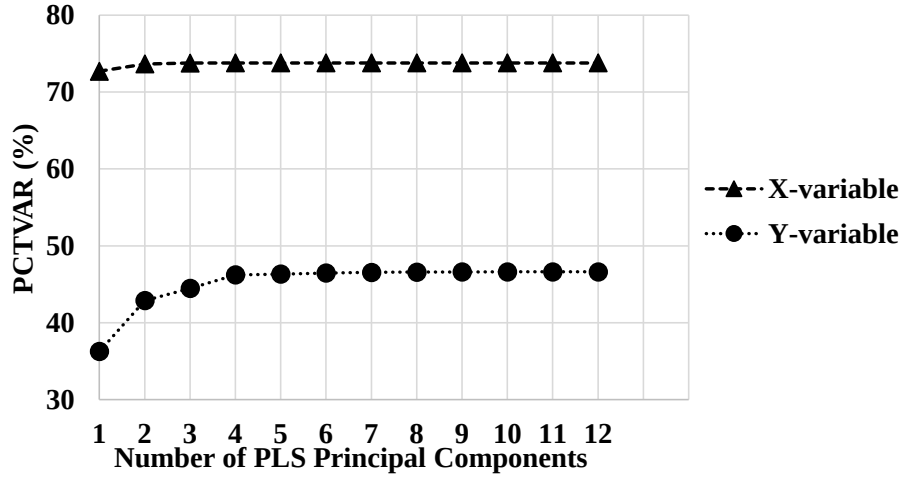

Figure 67. Percentage of variance explained by the model for *X*- and *Y*-variables.

Taking into consideration both *prediction error* and *model fit*, respectively estimated by RMSEP and PCTVAR, it was decided to focus on the model performance with 4 Principal Components. Subsequently, evaluation of model performance was conducted using both full cross validation (as an 'external' cross validation technique) and data-splitting methods. These evaluation methods and their results are presented in the following two parts.

8.4 Evaluating model performance using full cross validation

The predicted *Y*-variables (i.e. 'acoustic results') at the fourth step of the above described 'internal' cross validation were stored and subsequently compared with the corresponding measured *Y*-variables (i.e. sieve results). Thereby, the performance of the model with its optimum number of Principal Components was examined in terms of agreement between the sieve results and 'acoustic results'. The laboratory sieve results from sand types 1-3 are respectively compared with their corresponding prototype results in Figure 79, Figure 80 and Figure 81 of the Appendix. Figure 82, Figure 83 and Figure 84 of the Appendix compare the results from sieving and prototype for mixtures 0-1 (95-30), 0-2 (85-20), and 0-2 (80-10), respectively. In order to provide a better visual presentation in these Figures, 63 and 4000 µm grain sizes were ignored to be demonstrated. Since the passing percentages in these grain sizes were respectively 0 and 100 anyway. The horizontal axis in these Figures represents the sampling days in which samples have been tested by the prototype as well analyzed by laboratory sieving. In accordance with the presented sieve results in these Figures, the variations of grain size distribution in different sand products have been quite extensive. These variations have occurred independently in different sand products.

A relatively good general agreement between the results from the prototype and sieving can be proved from Figure 79-Figure 84 of the Appendix. In sand 2, for example, the sieve results suggest that the passing percentage of grain size 500 µm has had an increasing tendency, which means becoming finer. This variation in grain size distribution has been fairly recognized and represented by the prototype.

According to Figure 79-Figure 84 of the Appendix, in all the analyzed sand products, the prototype results have remained quite steady during the long-term utilization. It means that the results have not shown systematical changes and/or drastic variations without correspondence with sieve results. It proves that the prototype has operated more than 7 months without any immense problems. Otherwise, independent from sieve results, the prototype results would have shown meaningful, systematic tendencies during the long-term utilization.

A statistical summary of calculated absolute differences between the prototype and sieve results is presented in Table 19. In this Table, for each sand product, the minimum, maximum and mean of absolute differences in each grain size are reported. The mean shows how large is the difference on average in each case. According to Table 19, the maximum difference has remained in all of the cases lower than 30%. Also, in almost all of the cases the minimum difference equals to 0%. It implies that in each case at least one full agreement between the sieve analysis and 'acoustic results' has occurred.

Table 19. Absolute differences between the sieve and prototype results.

Product type {No. of analyzed samples}	Grain size (µm)	63	125	250	500	1000	2000	4000
Sand 1 {66}	Minimum	0.0	0.0	0.1	0.0	0.0	0.0	0.0
	Maximum	0.1	2.3	27.9	8.0	5.5	2.7	0.0
	Mean	0.0	0.6	8.7	1.8	0.2	0.1	0.0
Sand 2 {62}	Minimum	0.0	0.0	2.3	0.0	0.0	0.0	0.0
	Maximum	0.0	0.7	22.2	17.6	5.2	0.9	0.0
	Mean	0.0	0.3	11.1	6.0	1.7	0.1	0.0
Sand 3 {78}	Minimum	0.0	0.0	0.0	0.0	0.1	0.0	0.0
	Maximum	0.0	0.5	21.5	24.7	16.3	8.0	0.1
	Mean	0.0	0.1	3.8	8.0	4.4	1.7	0.0
0-1 (95-30) {16}	Minimum	0.0	0.2	1.4	0.1	0.1	0.0	0.0
	Maximum	0.1	0.8	16.4	11.5	6.4	3.3	2.0
	Mean	0.0	0.5	6.2	4.6	2.1	1.1	0.2
0-2 (85-20) {16}	Minimum	0.0	0.0	0.1	1.0	0.1	0.1	0.0
	Maximum	0.1	0.9	10.0	17.3	7.0	2.3	0.1
	Mean	0.0	0.3	5.3	5.6	2.1	0.8	0.0
0-2 (80-10) {62}	Minimum	0.0	0.0	0.1	0.0	0.0	0.0	0.0
	Maximum	0.0	0.5	15.6	20.1	16.5	2.9	0.0
	Mean	0.0	0.1	3.8	5.5	2.8	0.9	0.0

In order to provide a deeper evaluation of consistency between the prototype results and sieve analysis, and thereby a better evaluation of model performance with 4 PLS Principal Components, examining the correlation between measured and predicted *Y*-variables was considered. As Figure 66 and Table 19 respectively proved that *prediction error* and absolute difference in 63 and 4000 µm grain sizes are negligible, therefore examining the correlation was excluded for these two grain sizes. For each *Y*-variable (grain size), the measured values (laboratory sieving) were plotted against their corresponding predicted values ('acoustic results'). In each correlation plot, coefficient of determination (R^2) was also computed to quantify how well the prototype results are correlated with the sieve results. In this way, the passing percentages determined by sieve analysis and prototype were respectively considered as the measured data points ($y_{i\ measured}$) and the modeled values ($y_{i\ modeled}$). The correlation plots of 250, 500, 1000 and 2000 µm are respectively presented in Figure 68, Figure 69, Figure 70 and Figure 71. The fitted PLS Regression line is also illustrated in each correlation plot. This line represents the ideal relationship between measured and predicted *Y*-variables. In other words, R^2 is a statistic measure to describe the deviation of value points from the regression line. Moreover, in each correlation plot, the corresponding RMSEP value is reported. Note that these reported values are the same which were earlier graphically presented in Figure 66 at step *l*=4. It can be understood from correlation plots in Figure 68-Figure 71 that except in 250 µm (where highest RMSEP is given), in other grain sizes large R^2 values (i.e. higher than 0.8) are yielded. Higher R^2 values indicate that the fitted data – here passing percentages obtained from the prototype – comes closer to sieve analysis (the measured data).

Residual value (in %) of each single value point was simply computed as: Residual=Measured-Predicted. In each grain size, obtained residual values were then plotted against their corresponding predicted *Y*-values. Thereby, residual plots were obtained where the prediction made by the model was on the horizontal axis and the accuracy of the prediction was on the vertical axis. In Figure 68-Figure 71, next to each correlation plot, its corresponding residual plot is also presented.

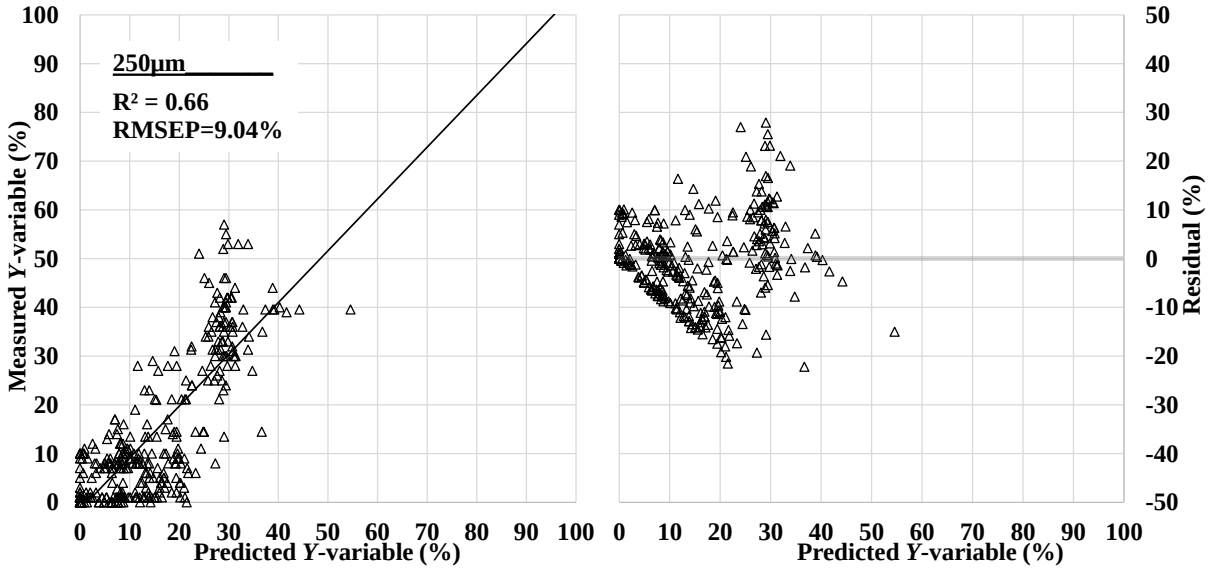

Figure 68. Correlation and residual plots of 250 µm grain size.

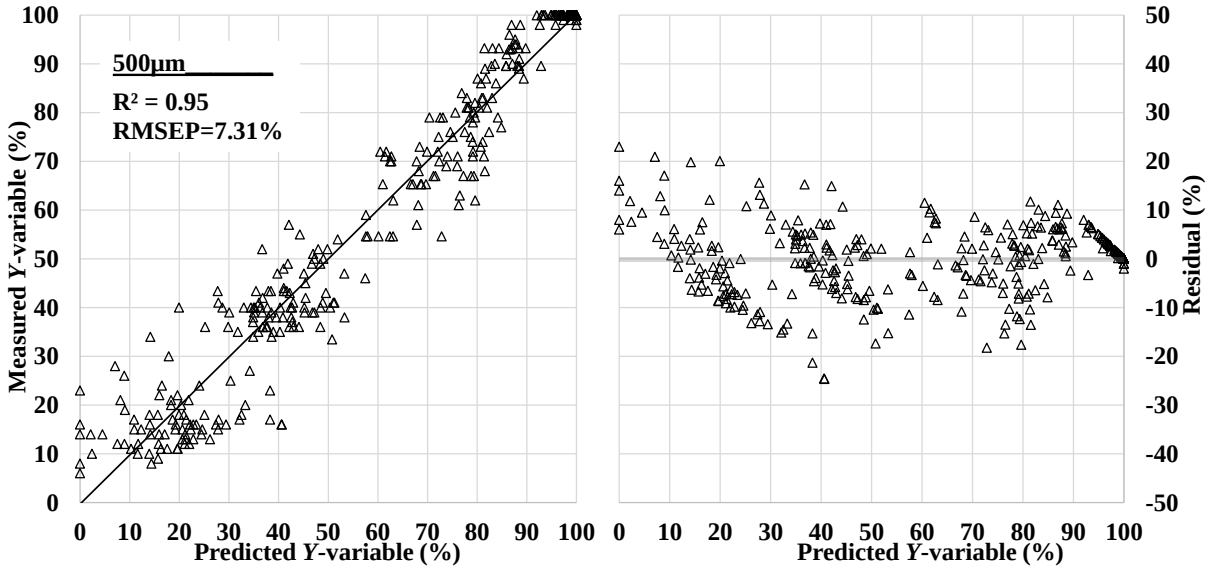

Figure 69. Correlation and residual plots of 500 µm grain size.

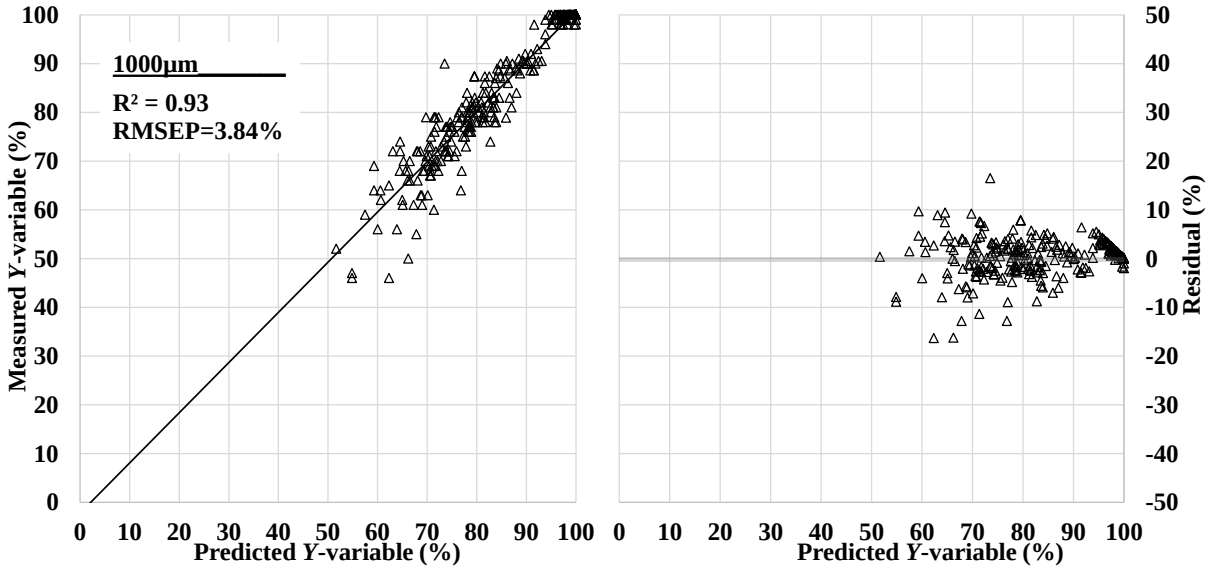

Figure 70. Correlation and residual plots of 1000 µm grain size.

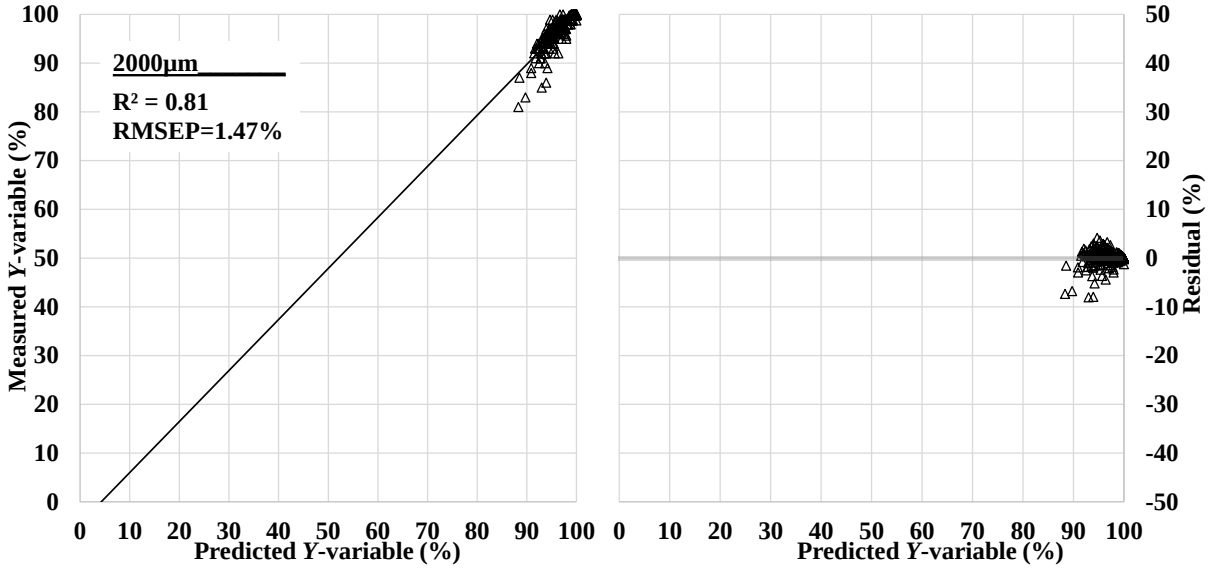

Figure 71. Correlation and residual plots of 2000 µm grain size.

In the residual plots, the distance of each individual value point from the line at 0 is how bad the prediction was for that value. Positive values (above the 0-line) for the residual mean that the prediction was too low, and negative values (below the 0-line) mean that the prediction was too high. Residual values equal to zero mean that the 'acoustic results' have been fully in agreement with the sieve analysis.

The residual plots prove that the model with 4 Principal Components has performed well; because: the value points are scattered randomly and, symmetrically in respect with the 0-line. Also, they are distributed close to the 0-line and have not built clusters away from it. Thus, the residuals are mostly centered on the 0-line throughout the range

of predicted *Y*-values. Particularly, the residuals do not contain any major predictive information. It means that they are not systematically patterned in correspondence with the horizontal axis (i.e. predicted *Y*-values); but, when there is a clear pattern, it originates mostly from the measured *Y*-values. Take 500 µm as an instance, the recognizable four clusters around the 0-line are merely caused by the laboratory sieve results. In this residual plot, predicted passing percentages can be categorized in four ranges: <30%, 30-60%, 60-approx.95% and >95%. These ranges respectively correspond to the sieve results of sand 3, mixtures 0-2 (85-20) and 0-2 (80-10), sand 2 and mixture 0-1 (95-30), and sand 1.

Nevertheless, some deficiencies of the model can also be revealed from the residual plots. Take the same example, in 500 µm the recognizable 'downhill' trend of the residuals in the range of 'acoustic results' >95% is caused by the inaccuracies of the model in predictions of sand 1. In this case, passing percentages of numerous sand 1 samples have been predicted lower than their measured values (refer to Figure 79 of the Appendix). Another considerable example is 250 µm where a clear 'downhill' pattern can be seen when predicted *Y*-values are lower than 20%. This is originated from inconsistencies of sand 3 results, where in many samples the 'acoustic results' of 250 µm are finer than sieve analysis (refer to Figure 81 of the Appendix).

In this part, the applied 'external' full cross validation evaluated the performance of the PLSR model with 4 Principal Components as fairly good. Maximum absolute difference between the measured and predicted *Y*-values did not exceed 30%. *Prediction error* remained lower than 10% and strong correlations between the 'acoustic results' and sieve analysis were proved by large R^2 values. However, some non-random patterns were observed in the residual plots. Bearing in mind that the current model left respectively 26 and 54% of variance in *X*- and *Y*-variables unexplained (refer to Figure 67), these patterns suggest that the model has missed some meaningful information present in **X** and **Y** which has 'leaked' into the residuals. In the following part, the data-splitting technique is employed to evaluate the performance of PLSR model for predicting grain size distribution.

8.5 Evaluating model performance using data-splitting

In order to use the data-splitting technique for evaluating model performance, the acoustic data from each sand product was divided into two halves. Take sand 1 as an example, the first 33 samples (from 27th August to 13th December) were put into the first half (data set 1) and the second 33 samples (from 7th January to 8th April) were designated for the second half (data set 2). Thereby, data sets 1 and 2 respectively contained the first and second halves of acoustic data from each sand product. Corresponding to the acoustic data, the sieve results were also splitted into data sets 1

and 2. In this way, data set 1 was consisted of $\mathbf{X_1}$ and $\mathbf{Y_1}$, where $\mathbf{X_1}$ and $\mathbf{Y_1}$ were respectively 150×128 and 150×7 matrices. Similarly, data set 2 contained 150×128 $\mathbf{X_2}$ matrix and 150×7 $\mathbf{Y_2}$ matrix. In Figure 72, the conducted data-splitting is schematically sketched. This Figure shows how data sets 1 and 2 are built by the first and second halves, respectively. In Figure 72, the numbers next to the columns indicate the number of samples.

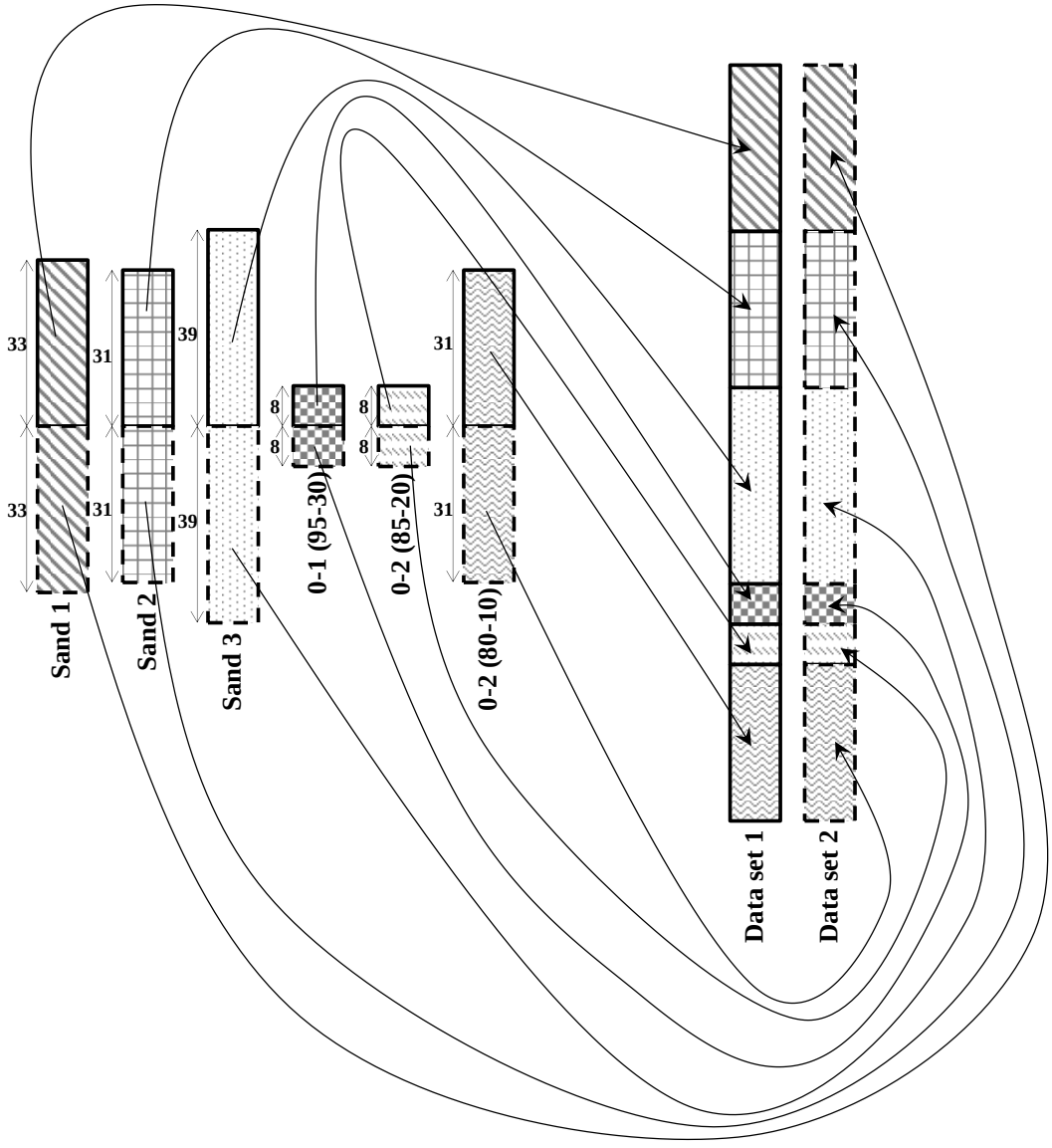

Figure 72. Schematic sketch of data-splitting.

A PLSR model was until step l=4 calibrated, whose acoustic and sieving train data respectively were $\mathbf{X_1}$ and $\mathbf{Y_1}$; thus, n=150. This model, trained by data set 1, respectively explained 68 and 29% of variance in X- and Y-variables. Thus, compared to the model from the previous part, the current model presented poorer *model fit* (refer to Figure 67).

Another PLSR model was calibrated until step l=4, where data set 2 (i.e. $\mathbf{X_2}$ and $\mathbf{Y_2}$) was used for training. The computed PCTVAR values of *X*- and *Y*-variables were equal to 43 and 39%, respectively. Therefore, likewise the first model, this model also yielded poorer *model fit*, compared to the model from the full cross validation part.

In summary, the first model explained 25% more variance of *X*-variables, compared to the second model. While the model trained by data set 2 had a 10%-better *model fit* in regards of PCTVAR value of *Y*-variables. Both the current models left more unexplained variance than the model from full cross validation.

The model trained by data set 1 was then verified by data set 2. Mutually, the second model was tested by data set 1. In this way, each individual measured *Y*-value could be compared with its corresponding predicted value. Figure 85, Figure 86 and Figure 87 of the Appendix respectively present comparison between the 'acoustic results' and sieve results of sand types 1-3. The predicted *Y*-variables of mixtures 0-1 (95-30), 0-2 (85-20), and 0-2 (80-10) are compared with their measured *Y*-variables respectively in Figure 88, Figure 89 and Figure 90 of the Appendix. In Figure 85-Figure 90 of the Appendix, the broken vertical lines represent the boundary between data sets 1 and 2. A general fair agreement between the prototype results and sieving can be seen in these Figures. However, independent from sand product, sieve results of many samples have been predicted with inaccuracies even larger than 20%. Comparison between these Figures and the results from the previous part (i.e. Figure 79-Figure 84 of the Appendix) reveals that the sieve analysis has been predicted more precisely through full cross validation rather than through data-splitting. In data-splitting, there is hardly significant differences between the two sides of the broken vertical line in each Figure. Hence, one may argue that both data-splitting models have performed quite comparably in terms of their prediction precision. Hence, it can be mentioned that splitting the data (both acoustic and sieving) into two halves has been done properly; i.e., both halves have had comparable random data distribution.

To evaluate performances of the current two models, absolute differences between the 'acoustic results' and sieve analysis were computed and statistically analyzed. A statistical summary of the computed absolute differences is presented in Table 20. According to this Table, in several cases the maximum absolute difference has exceeded 20%. Moreover, in two cases it has gone even beyond 30%. Comparing Table 19 and Table 20 confirms that the consistency between measured and predicted *Y*-variables has been stronger in case of full cross validation rather than data-splitting. Nevertheless, likewise Table 19, the minimum absolute differences in Table 20 are also in almost all of the cases very close to zero. It implies that, despite of relative poor accuracy in the data-splitting results, in each case there is at least one sample whose 'acoustic results' and sieve analysis are fully in agreement.

Table 20. Absolute differences between the sieve and prototype results.

Product type {No. of verified samples}	Grain size (µm)	63	125	250	500	1000	2000	4000
Sand 1 {66}	Minimum	0.0	0.0	0.5	0.0	0.0	0.0	0.0
	Maximum	0.1	2.6	34.0	8.2	7.0	5.2	0.2
	Mean	0.0	0.7	11.3	1.9	0.6	0.3	0.0
Sand 2 {62}	Minimum	0.0	0.0	2.6	0.3	0.0	0.0	0.0
	Maximum	0.0	0.8	22.2	18.3	8.6	4.1	0.1
	Mean	0.0	0.3	11.7	5.9	2.0	0.2	0.0
Sand 3 {78}	Minimum	0.0	0.0	0.0	0.0	0.1	0.0	0.0
	Maximum	0.0	0.6	18.5	34.0	25.8	13.2	0.1
	Mean	0.0	0.1	4.6	13.7	8.2	2.6	0.0
0-1 (95-30) {16}	Minimum	0.0	0.2	0.4	0.0	0.3	0.2	0.0
	Maximum	0.1	0.8	20.3	24.8	15.3	6.1	2.0
	Mean	0.0	0.6	8.7	5.4	4.9	2.3	0.2
0-2 (85-20) {16}	Minimum	0.0	0.1	0.3	0.5	0.0	0.1	0.0
	Maximum	0.1	0.9	16.7	27.4	15.8	5.8	0.2
	Mean	0.0	0.4	5.8	7.4	5.9	2.4	0.0
0-2 (80-10) {62}	Minimum	0.0	0.0	0.0	0.2	0.5	0.0	0.0
	Maximum	0.0	0.4	14.5	23.6	18.8	7.8	0.1
	Mean	0.0	0.1	4.0	10.4	5.5	1.6	0.0

The correlation and residual plots of 250, 500, 1000 and 2000 µm grain sizes are respectively presented in Figure 73, Figure 74, Figure 75 and Figure 76. In these Figures, Δ represents the samples where data sets 1 and 2 have been respectively employed for training and verifying; thus, the first model. Also, value points shown by ○ represent the samples where data sets 1 and 2 have been respectively taken for verifying and training; thus, the second model. In Figure 73-Figure 76, in each correlation plot, the regression line as well as R^2 and RMSEP values of each model are demonstrated.

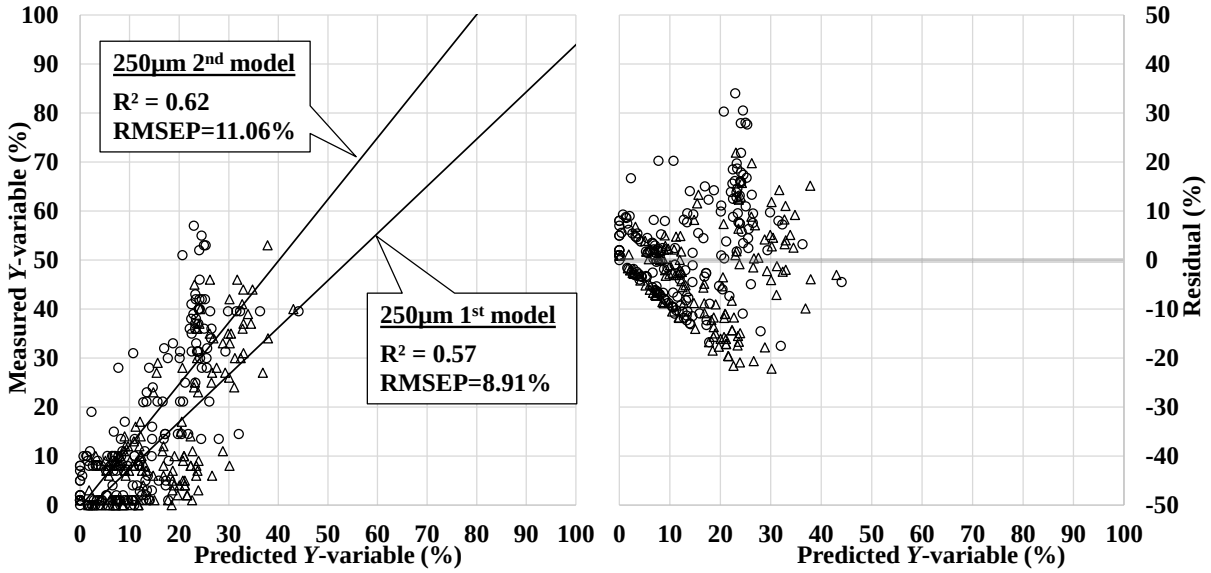

Figure 73. Correlation and residual plots of 250 µm grain size.

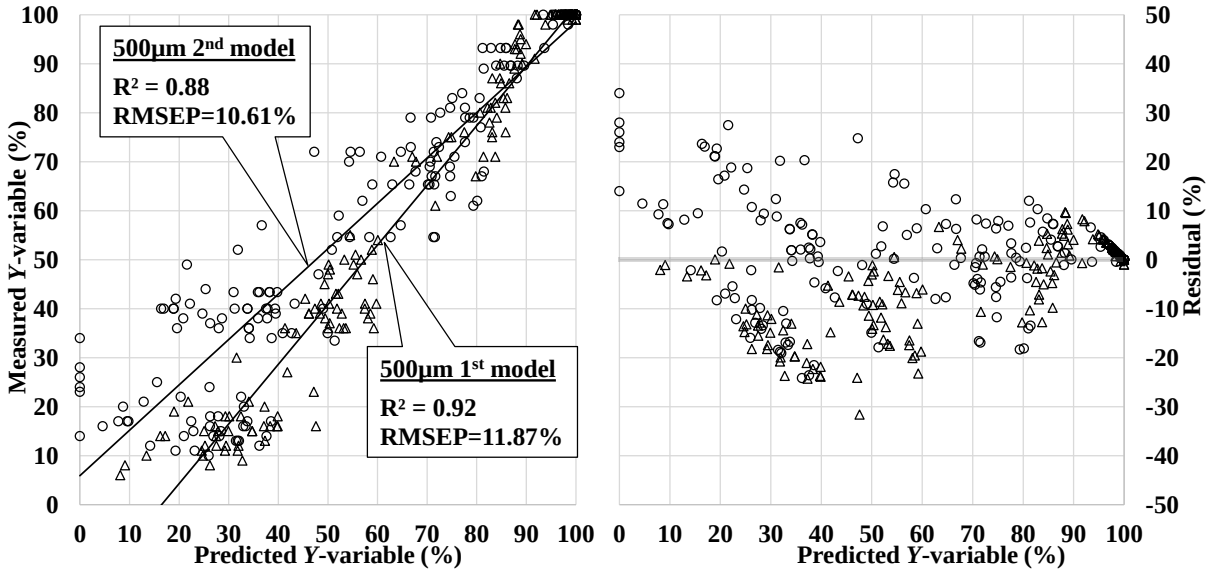

Figure 74. Correlation and residual plots of 500 µm grain size.

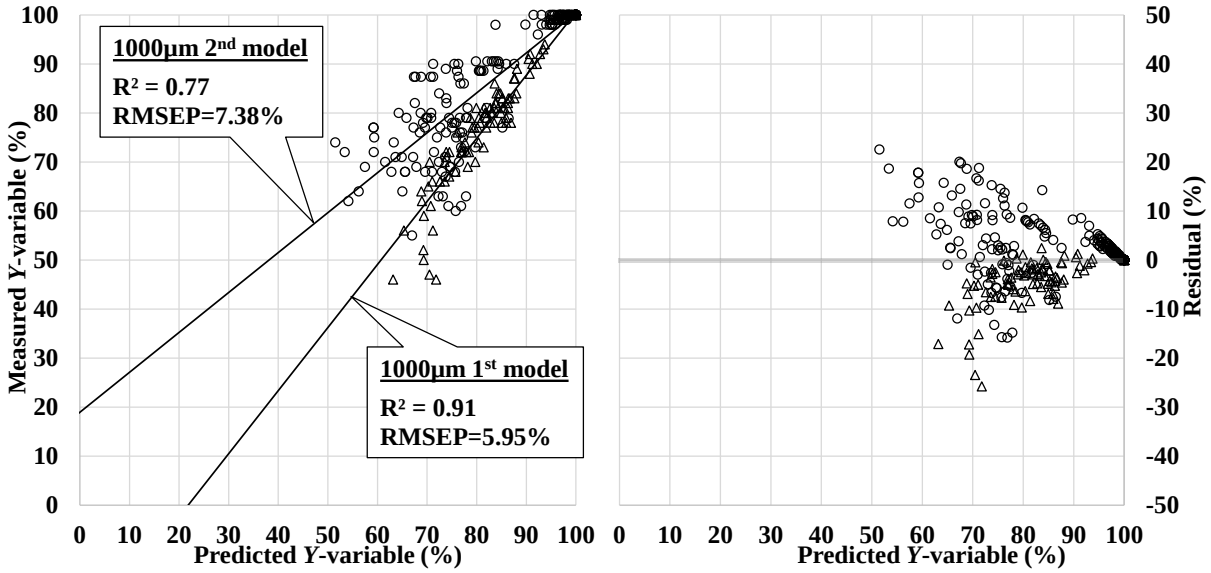

Figure 75. Correlation and residual plots of 1000 µm grain size.

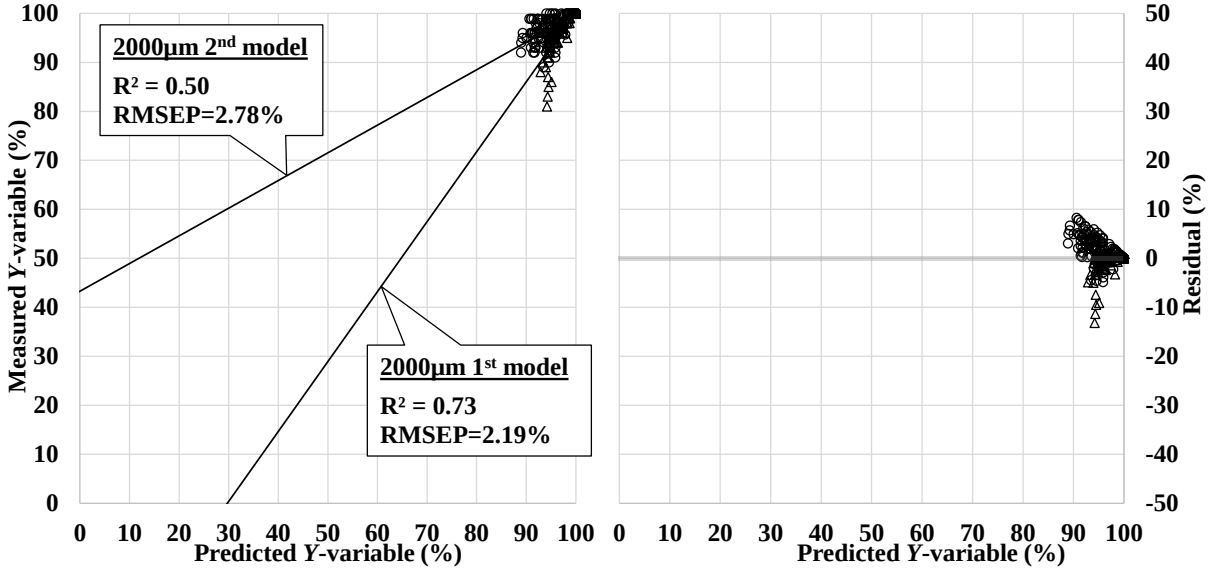

Figure 76. Correlation and residual plots of 2000 µm grain size.

In each correlation plot, R^2 values of the two models do not have significant differences. The same is true for RMSEP values. Additionally, in none of the correlation and residual plots, Δ and ○ are noticeably separated from each other. It confirms that splitting the data into two halves has been conducted correctly, since the obtained value points from the both models are distributed similarly in each correlation and residual plot. Therefore, it confirms that both models have had comparable performances.

The general distribution pattern of value points in each plot is very similar to its corresponding plot in the previous part. The only significant difference, however, is that the value points are more scattered in case of data-splitting, compared to full cross

validation. It can be observed particularly in the residual plots. The higher scattering in data-splitting technique is caused by poorer consistency of its results. Poorer consistency leads to larger distances from the 0-line in the residual plots. In regards of correlation plots, this can be figured out by comparing R^2 values of data-splitting and full cross validation. This comparison reveals that in each grain size, the correlation between measured and predicted *Y*-values is stronger when applying full cross validation rather than data-splitting. Consequently, value points of the correlation plots in data-splitting are more scattered.

Also, in terms of *prediction error*, in all of the *Y*-variables (except 250 µm) the RMSEP values from full cross validation are smaller than their corresponding values from data-splitting. Hence, similar to other measures, RMSEP also shows that full cross validation has predicted the *Y*-values more accurately than data-splitting.

In the following part, the obtained results from the two applied techniques, i.e. full cross validation and data-splitting, are compared and discussed.

8.6 Discussion

For both applied full cross validation and data-splitting methods, Figure 77 and Figure 78 graphically present the obtained RMSEP and R^2 values, respectively. In these Figures, the first and second models of data-splitting are simply denoted as 'First model' and 'Second model', respectively. Furthermore, 63, 125 and 4000 µm grain sizes which were excluded from the correlation and residual plots of the two last parts, are considered in these Figures.

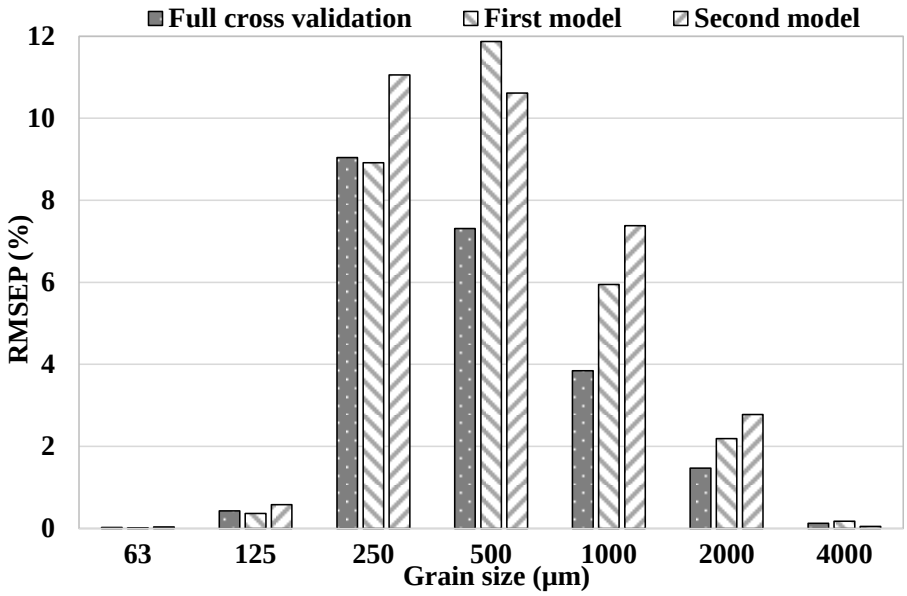

Figure 77. RMSEP values obtained through full cross validation and data-splitting.

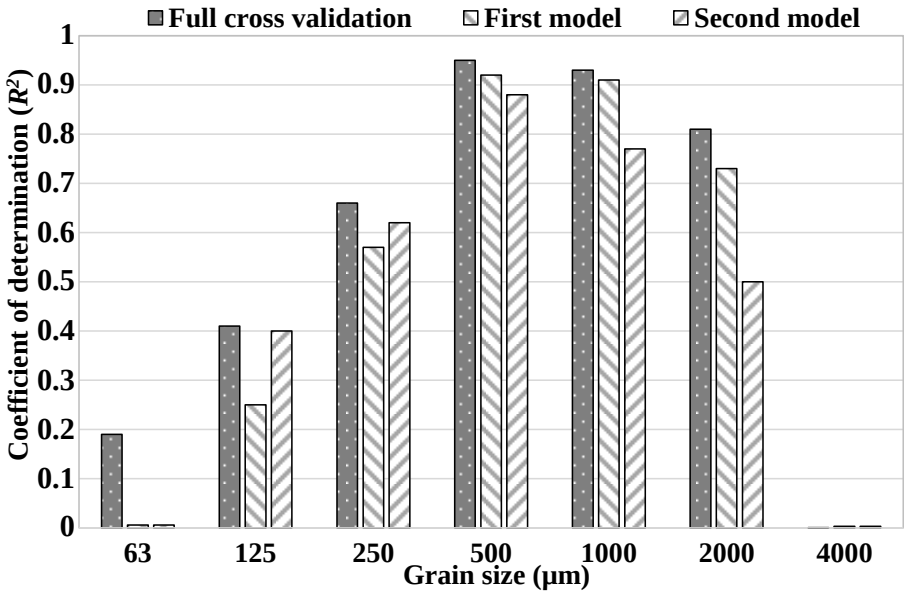

Figure 78. R^2 values obtained through full cross validation and data-splitting.

In accordance with Figure 77, predictions through full cross validation as well as data-splitting have had fairly good precision. In the worst case, i.e. 500 µm of the first model, RMSEP value doesn't exceed 12%. Also, as mentioned earlier in the previous part, in data-splitting *prediction error* has been generally estimated higher than full cross validation.

Figure 78 shows that measured and predicted *Y*-values in both full cross validation and data-splitting techniques are well correlated. In major grain sizes, namely 250, 500, 1000 and 2000 µm, all the R^2 values are above 0.5. Clearly seen from Figure 78, in each grain size, the R^2 value of full cross validation is higher than those from data-splitting.

RMSEP values of the data-splitting models are in each *Y*-variable fairly close to each other. It proves that, as mentioned formerly in the previous part, data-splitting has been carried out properly. Additionally, it also proves that the prototype laboratory device has steadily worked and delivered data for over 7 months. Otherwise, splitting acoustic data into two halves, while it is chronologically sorted, would not have allowed to build two models with similar performances.

Using several different measures – i.e. direct comparison between 'acoustic results' and sieve analysis, absolute differences, *model fit*, *prediction erro*r and R^2 – it was proved that the 'acoustic results' of full cross validation have been more consistent with the sieve results – compared with data-splitting. The reason mainly lies within the number of observations. In full cross validation, each single measured *Y*-value has been predicted by a PLSR artificial model trained by 299 objects. Whereas in data-splitting, each single measured *Y*-value has been predicted by a PLSR model trained by 150 objects. This finding suggests that n=150 is statistically not still large enough for

building a model with predictions as good as those from full cross validation. This conclusion applies for the current research work and its specific **X**, **Y** and further considerations. But it may not be generalized for other PLSR modeling studies.

Worthy to mention, in the present research work it was not attempted to detect and eliminate possible existing outliers in the data. Because this study was aimed to ensure the prediction evaluations as realistic as possible. Omitting outliers may have improved the results though.

In the long-term study, each sand sample was manually divided into two sub-samples, one for the prototype and one for sieving. Presence of human error in dividing a sample into two identical representative sub-samples cannot be ignored completely. Thus, this error may be argued as a contributing factor in occurrence of inconsistency between the prototype and sieve results.

Another source of inconsistency may have been carelessly placing the collection bin. This component of the prototype was designed and manufactured in a way so that an airproof assembly together with other components was given. However, not placing it at its exact position could have prevented it from being airproof within some tests. Not being airproof could have influenced the air flow velocity adversely and deviated it from the desired 18 m/s within those tests. This deviation could have had certainly negative effect on the consistency of the results.

9 Conclusions

9.1 Summary

In Chapter 2, it was concluded that seeking for new grain size analysis techniques is crucial. The passive acoustic measurement method was introduced in Chapter 3. The state-of-the-art of this method was comprehensively presented in Chapter 4. From Chapter 4, it was concluded that application of this method for determining grain size distribution of granular materials has not been properly studied yet. This motivated conduction of the current research work.

Chapters 5-7 involved the entire experimental study which eventually resulted in manufacturing the prototype laboratory device in Chapter 8. Chapters 5-7 documented the experimental research work about employing the passive acoustic measurement method for quantifying grain size distribution of sand samples conveyed in laboratory–scaled pneumatic test rigs. In Chapter 5, the initial experiments provided basic insight into representing grain size distribution of sand samples by using the passive acoustic measurement technique. Amongst the different tested sensor positionings, the centrally positioned probe inside the pneumatic line was proved to be the best for obtaining the desired relation between grain size and voltage.

Based on the concept of centrally positioned sensor, the horizontal test rig was set up in Chapter 6. Suitable signal processing procedures together with PLS Regression modeling were applied on acoustic data from the first experimental program. Thereby, grain size distribution of the tested sand types could be predicted. Various further experimental programs were carried out in order to systematically study the effects of two main factors (i.e. air flow velocity and mass flow rate). Simultaneously, improvement of sand 4 results, through optimizing these two factors, was considered and discussed.

The vertical test rig was manufactured and introduced in Chapter 7. It had several advantages over the horizontal test rig. Through conducting various experimental programs, the appropriate experimental setup, under which sand 4 results were also acceptable, was found. However, due to some limitations and uncertainties associated with this experimental setup, the design parameters of the prototype were defined and tested without considering sand 4.

Chapters 6 and 7 contained a total number of 12 experimental programs, or in other words a total number of 144 trials. Based on the entire obtained findings from the experimental programs within Chapters 6 and 7, in Chapter 8 a prototype laboratory device was manufactured and utilized in long-term (over 7 months) for data collection in an industrial environment. During the long-term utilization, 300 samples (from 6 different sand products) were analyzed. The collected data from the prototype as well as

the laboratory sieving results were used for PLSR modeling. The optimum number of PLS Principal Components was successfully determined by full cross validation method, as an ‘internal’ cross validation. Verification of the PLSR model with the optimum number of Principal Components succeeded through full cross validation method, as an ‘external’ cross validation. Data-splitting method was also employed for verification. It was shown that data-splitting, compared with full cross validation, presented lower prediction power of PLSR modeling.

9.2 Conclusions

The following conclusions were drawn from this thesis:

- The recorded signals were always significantly affected by two key parameters, i.e. mass flow rate and air flow velocity. Signal magnitude was directly proportional to each of these two parameters.

- In the current study, grain size analysis of sand samples with fair consistency was achieved, as these two key parameters were identified and kept constant. Mass flow rate was kept constant through taking a specified fixed adjustment of the vibratory feeder. By supplying the vacuum cleaner with a non-varying voltage, air flow velocity remained constant too. Only under this condition, signal magnitude was dependent merely from grain size. Providing such a condition led to successful establishment of quantitative relations between voltage and grain size in a relative broad range.

  Otherwise, in case of varying mass flow rate and/or air flow velocity, determining grain size distribution would have been a much more complex, meanwhile challenging, task.

- In addition to non-varying mass flow rate and air flow velocity, the flow pattern also was kept always homogenous dilute. Without doubt, conducting the current study, while having other flow patterns rather than homogenous dilute, would have been much more complicated and challenging.

- In Chapters 6 and 7, the number of grain size classes was limited by 9; and by 7 later on in Chapter 8. However, this can be increased with very little effort. Meanwhile, the effect of increasing the number of *Y*-variables on computation time and particularly accuracy of the results should be examined in detail.

- In Chapter 4, it was argued that successfully applying the passive acoustic method doesn't necessarily require detailed investigations about the source(s) of the emitted acoustic waves or other fundamental studies. In the current study, this method was employed for grain size analysis and very promising results were obtained. Meanwhile, detailed studies on subjects such as the impact of the grains on the impacting head or pneumatic flow parameters *etc.* were absolutely unnecessary. In future studies though, taking a closer look at those subjects may shed more light on the application of this method and eventually might help to obtain better results.

- As mentioned earlier in Chapter 4, in a passive acoustic study, the frequency range of interest, type of sensor and DAQ device *etc.* are specified in accordance with the conditions of that study.

  In this study, the measured frequency ranges were slightly over the 'audible range' and good results were obtained though. Extending the study into higher frequency ranges may provide more useful information or even might improve the results. However, it calls for higher computation expenses, special sensors and DAQ devices as well as data analysis techniques.

  Enhancing the sensor sensitivity from 1 to 10 mV/g caused only increase of signal magnitude. Neither the form of frequency spectrum nor the obtained final results were influenced significantly (see part 8.1).

  Subsequent to the horizontal test rig, the vertical test rig as well as the prototype were equipped with a DAQ device which had particular advantages over the DAQ device of the horizontal test rig (refer to Chapter 7).

- The selected air flow velocity for the prototype (i.e. 18 m/s) was optimal. Because, for this relative low velocity the vacuum cleaner was required to be in service only with about half of its suction power. It guaranteed that the prototype was desirably 'quiet'; and also, nothing from the tested samples was sucked further into the vacuum cleaner. The latter was of importance since otherwise dust collection on the vacuum cleaner's filter could have prevented having constant air flow velocity within the long-term utilization.

On the other hand, presence of air flow with this relative low velocity significantly enhanced the signal quality, compared to the condition without air flow (see part 8.1).

– Consider that a grain size analysis laboratory device works based on the introduced technique. It would have then numerous advantages over sieve analysis. In a technical point of view, its results are more accurate than sieving results. Since sieving determines the size of a grain by its shortest diameter, whereas in this technique the acoustic data (signal magnitude) represents the real size of a grain. Moreover, the samples are analyzed easier and quicker, without making noise and dust. The tested samples can be easily collected and analyzed again. In contrary to sieves, there is no wearing part, no moving part and, no maintenance is required either.

  That prospective grain size analysis laboratory device also may have a few advantages over currently common dynamic image analysis and laser diffraction devices. Its results may be more accurate, since in both of these common methods the orientation of a grain as it passes the laser beam/camera is not definitely representative of its real size. But, as mentioned above, in the passive acoustic method the data corresponds to the real size of a grain which impacts on the impacting head. The dynamic image analysis and laser diffraction devices work based on very complex algorithms. As a rule of thumb, these devices currently cost much more than a prospective device which works based on the passive acoustic method.

  However, the long-term utilization of the prototype proved that the results accuracy of the presented system in this thesis may not be good enough to be adopted for grain size analysis in practice. The long-term utilization revealed that in the worst case, RMSEP may reach almost 12% (refer to Figure 77). This realistic performance evaluation of the prototype, as well as of the PLSR models, implies that in the worst case future predictions with ±24% precision should be expected. Therefore, it cannot be concluded from this research work that the presented system is already able to be used as an accurate grain size analysis device.

The present study was focused on determining grain size distribution of pneumatically conveyed sand samples in laboratory–scale by using the passive acoustic method. Considering the importance and abundance of granular materials and versatility of their application fields (Chapter 2) and, unique capabilities of the passive acoustic method (Chapter 4), it is suggested to extend the future studies to cover further granular materials with various grain sizes and physical properties. This wide variety of granular

materials may be handled through other types of processes in both laboratory and industrial scales. Here are some suggestions for the future research works:

- Following the first and second concluding remarks, the future studies may deal with the cases where in contrary to the present study, mass flow rate and fluid flow velocity are not constant and/or flow pattern is not homogenous dilute.

- These studies may preferably examine much broader frequency ranges, with the intention of providing more valuable information and input variables for PLSR modeling.

The future studies may be assisted by fundamental investigations in different areas. Fluid mechanics investigations may elucidate if grains with various sizes impact on the impacting head with equal rate of occurrence. Solid mechanics investigations may address the questions about the emitted acoustic waves as numerous grains simultaneously impact on the impacting head. In order to minimize receiving erroneous signals, originated from reflected waves within the impacting head, the optimal geometry of the impacting head may be determined by acoustical physics analyses.

Appendix

Table 21. Absolute differences at air flow velocity of 72 m/s.

Grain size (µm)		63	125	250	500	1000	2000	4000	5600	8000	Max.
Sand 1	Verif.1	0.0	0.4	10.0	2.2	0.9	0.1	0.0	0.0	0.0	14.1
	Verif.2	0.0	0.6	14.1	0.0	1.0	0.6	0.2	0.0	0.0	
	Average	0.0	0.5	12.0	1.1	1.0	0.4	0.1	0.0	0.0	
Sand 2	Verif.1	0.0	0.3	8.1	1.5	0.7	0.1	0.0	0.0	0.0	16.0
	Verif.2	0.0	0.7	16.0	2.8	1.2	0.2	0.0	0.0	0.0	
	Average	0.0	0.5	12.0	2.2	0.9	0.1	0.0	0.0	0.0	
Sand 3	Verif.1	0.0	0.1	1.5	3.3	0.9	0.2	0.1	0.0	0.0	6.9
	Verif.2	0.0	0.0	1.2	6.9	0.9	2.6	0.9	0.0	0.0	
	Average	0.0	0.1	1.3	5.1	0.9	1.4	0.5	0.0	0.0	
Sand 4	Verif.1	0.0	0.0	0.0	0.0	32.2	46.4	14.5	0.1	0.0	59.0
	Verif.2	0.0	0.0	0.0	0.0	27.5	59.0	18.9	0.2	0.0	
	Average	0.0	0.0	0.0	0.0	29.9	52.7	16.7	0.1	0.0	

Table 22. Absolute differences at air flow velocity of 48 m/s.

Grain size (µm)		63	125	250	500	1000	2000	4000	5600	8000	Max.
Sand 1	Verif.1	0.0	0.0	0.6	0.0	0.0	0.0	0.0	0.0	0.0	7.9
	Verif.2	0.0	0.3	7.9	0.0	0.0	0.0	0.0	0.0	0.0	
	Average	0.0	0.2	4.3	0.0	0.0	0.0	0.0	0.0	0.0	
Sand 2	Verif.1	0.0	0.1	0.7	1.7	0.0	0.0	0.0	0.0	0.0	10.0
	Verif.2	0.0	0.1	0.7	10.0	0.0	0.0	0.0	0.0	0.0	
	Average	0.0	0.1	0.7	5.9	0.0	0.0	0.0	0.0	0.0	
Sand 3	Verif.1	0.0	0.0	1.2	6.8	5.1	1.6	0.0	0.0	0.0	9.3
	Verif.2	0.0	0.0	1.2	9.0	9.3	1.6	0.0	0.0	0.0	
	Average	0.0	0.0	1.2	7.9	7.2	1.6	0.0	0.0	0.0	
Sand 4	Verif.1	0.0	0.0	0.0	0.0	43.3	60.4	18.9	0.2	0.0	69.2
	Verif.2	0.0	0.0	0.0	0.0	45.9	69.2	21.7	0.2	0.0	
	Average	0.0	0.0	0.0	0.0	44.6	64.8	20.3	0.2	0.0	

Table 23. Absolute differences at mass flow rate of 33 g/s.

Grain size (µm)		63	125	250	500	1000	2000	4000	5600	8000	Max.
Sand 1	Verif.1	0.0	0.1	1.5	0.0	0.0	0.4	0.2	0.0	0.0	6.6
	Verif.2	0.0	0.3	6.6	0.0	0.3	0.1	0.0	0.0	0.0	
	Average	0.0	0.2	4.1	0.0	0.2	0.3	0.1	0.0	0.0	
Sand 2	Verif.1	0.0	0.6	14.6	4.7	0.0	0.0	0.0	0.0	0.0	14.6
	Verif.2	0.0	0.3	7.2	0.7	0.0	0.0	0.0	0.0	0.0	
	Average	0.0	0.5	10.9	2.7	0.0	0.0	0.0	0.0	0.0	
Sand 3	Verif.1	0.0	0.0	0.2	2.8	4.4	4.5	1.4	0.0	0.0	9.0
	Verif.2	0.0	0.0	1.2	9.0	6.4	3.8	1.1	0.0	0.0	
	Average	0.0	0.0	0.7	5.9	5.4	4.1	1.2	0.0	0.0	
Sand 4	Verif.1	0.0	0.0	0.0	0.0	13.6	30.0	9.6	0.1	0.0	35.5
	Verif.2	0.0	0.0	0.0	0.0	22.8	35.5	11.2	0.1	0.0	
	Average	0.0	0.0	0.0	0.0	18.2	32.8	10.4	0.1	0.0	

Table 24. Absolute differences at mass flow rate of 46 g/s.

Grain size (µm)		63	125	250	500	1000	2000	4000	5600	8000	Max.
Sand 1	Verif.1	0.0	0.0	0.7	13.2	0.0	0.0	0.0	0.0	0.0	13.2
	Verif.2	0.0	0.3	5.8	9.4	0.0	0.0	0.0	0.0	0.0	
	Average	0.0	0.1	3.2	11.3	0.0	0.0	0.0	0.0	0.0	
Sand 2	Verif.1	0.0	0.1	0.7	7.1	0.0	0.0	0.0	0.0	0.0	7.1
	Verif.2	0.0	0.3	6.7	6.2	0.0	0.0	0.0	0.0	0.0	
	Average	0.0	0.2	3.7	6.7	0.0	0.0	0.0	0.0	0.0	
Sand 3	Verif.1	0.0	0.3	2.9	1.9	5.9	4.7	1.4	0.0	0.0	7.2
	Verif.2	0.0	0.3	7.2	6.2	1.8	1.0	0.0	0.0	0.0	
	Average	0.0	0.3	5.0	4.1	3.8	2.8	0.7	0.0	0.0	
Sand 4	Verif.1	0.0	0.0	0.0	0.0	12.4	21.6	7.1	0.1	0.0	21.6
	Verif.2	0.0	0.0	0.0	0.0	5.2	17.0	5.5	0.0	0.0	
	Average	0.0	0.0	0.0	0.0	8.8	19.3	6.3	0.1	0.0	

Table 25. Absolute differences in presence of air flow.

Grain size (µm)		63	125	250	500	1000	2000	4000	5600	8000	Max.
Sand 1	Verif.1	0.0	0.1	4.9	0.3	0.0	0.0	0.0	0.0	0.0	10.1
	Verif.2	0.0	0.3	10.1	3.7	0.0	0.0	0.0	0.0	0.0	
	Average	0.0	0.2	7.5	2.0	0.0	0.0	0.0	0.0	0.0	
Sand 2	Verif.1	0.0	0.0	1.4	2.2	0.3	0.0	0.0	0.0	0.0	5.8
	Verif.2	0.0	0.1	5.8	5.3	0.3	0.0	0.0	0.0	0.0	
	Average	0.0	0.1	3.6	3.8	0.3	0.0	0.0	0.0	0.0	
Sand 3	Verif.1	0.0	0.6	0.2	3.6	3.5	4.8	0.0	0.0	0.0	6.1
	Verif.2	0.0	0.0	1.1	6.1	5.8	2.9	0.0	0.0	0.0	
	Average	0.0	0.3	0.7	4.9	4.6	3.8	0.0	0.0	0.0	
Sand 4	Verif.1	0.0	0.1	4.1	4.5	11.3	22.1	4.2	0.0	0.0	29.3
	Verif.2	0.0	0.0	0.0	7.1	21.4	29.3	6.2	0.0	0.0	
	Average	0.0	0.1	2.0	5.8	16.4	25.7	5.2	0.0	0.0	

Table 26. Absolute differences in absence of air flow.

Grain size (µm)		63	125	250	500	1000	2000	4000	5600	8000	Max.
Sand 1	Verif.1	0.0	0.0	0.2	0.1	0.0	0.0	0.0	0.0	0.0	5.5
	Verif.2	0.0	0.2	5.5	2.8	0.0	0.0	0.0	0.0	0.0	
	Average	0.0	0.1	2.9	1.4	0.0	0.0	0.0	0.0	0.0	
Sand 2	Verif.1	0.0	0.0	0.5	6.6	0.3	0.0	0.0	0.0	0.0	6.6
	Verif.2	0.0	0.1	2.3	1.0	0.3	0.3	0.1	0.0	0.0	
	Average	0.0	0.0	1.4	3.8	0.3	0.2	0.0	0.0	0.0	
Sand 3	Verif.1	0.0	0.0	1.1	6.4	2.5	2.2	0.0	0.0	0.0	6.4
	Verif.2	0.0	0.0	1.1	0.1	5.7	4.4	0.0	0.0	0.0	
	Average	0.0	0.0	1.1	3.2	4.1	3.3	0.0	0.0	0.0	
Sand 4	Verif.1	0.0	0.0	0.0	0.3	2.1	48.0	17.0	0.0	0.0	48.0
	Verif.2	0.0	0.0	0.0	0.3	0.1	33.8	11.8	0.0	0.0	
	Average	0.0	0.0	0.0	0.3	1.1	40.9	14.4	0.0	0.0	

Table 27. Absolute differences at air flow velocity of 32 m/s.

Grain size (µm)		63	125	250	500	1000	2000	4000	5600	8000	Max.
Sand 1	Verif.1	0.0	0.0	1.7	0.4	0.0	0.0	0.0	0.0	0.0	7.6
	Verif.2	0.0	0.2	7.6	1.8	0.0	0.0	0.0	0.0	0.0	
	Average	0.0	0.1	4.6	1.1	0.0	0.0	0.0	0.0	0.0	
Sand 2	Verif.1	0.0	0.1	5.8	1.6	0.3	0.0	0.0	0.0	0.0	5.8
	Verif.2	0.0	0.1	5.8	4.2	0.3	0.0	0.0	0.0	0.0	
	Average	0.0	0.1	5.8	2.9	0.3	0.0	0.0	0.0	0.0	
Sand 3	Verif.1	0.0	0.0	1.1	4.3	5.5	2.7	1.4	0.0	0.0	7.0
	Verif.2	0.0	0.0	1.1	7.0	2.4	3.3	1.4	0.0	0.0	
	Average	0.0	0.0	1.1	5.6	4.0	3.0	1.4	0.0	0.0	
Sand 4	Verif.1	0.0	0.0	0.0	0.3	2.1	19.7	7.4	0.0	0.0	19.7
	Verif.2	0.0	0.0	0.0	0.3	2.1	11.6	5.2	0.0	0.0	
	Average	0.0	0.0	0.0	0.3	2.1	15.7	6.3	0.0	0.0	

Table 28. Absolute differences at air flow velocity of 37 m/s.

Grain size (µm)		63	125	250	500	1000	2000	4000	5600	8000	Max.
Sand 1	Verif.1	0.0	0.1	4.2	0.1	0.0	0.0	0.0	0.0	0.0	4.7
	Verif.2	0.0	0.1	4.7	0.1	0.0	0.0	0.0	0.0	0.0	
	Average	0.0	0.1	4.4	0.1	0.0	0.0	0.0	0.0	0.0	
Sand 2	Verif.1	0.0	0.1	2.2	1.8	0.3	0.0	0.0	0.0	0.0	8.4
	Verif.2	0.0	0.2	8.4	5.0	0.8	0.0	0.0	0.0	0.0	
	Average	0.0	0.1	5.3	3.4	0.5	0.0	0.0	0.0	0.0	
Sand 3	Verif.1	0.0	0.0	1.1	3.7	1.1	0.7	0.3	0.0	0.0	9.3
	Verif.2	0.0	0.2	6.3	9.3	4.3	0.6	0.1	0.0	0.0	
	Average	0.0	0.1	3.7	6.5	2.7	0.7	0.2	0.0	0.0	
Sand 4	Verif.1	0.0	0.0	0.0	1.7	2.4	4.5	1.5	0.0	0.0	4.9
	Verif.2	0.0	0.0	0.0	0.3	2.1	4.9	1.3	0.0	0.0	
	Average	0.0	0.0	0.0	1.0	2.2	4.7	1.4	0.0	0.0	

Table 29. Absolute differences at air flow velocity of 40 m/s.

Grain size (µm)		63	125	250	500	1000	2000	4000	5600	8000	Max.
Sand 1	Verif.1	0.0	0.3	10.1	3.9	0.0	0.0	0.0	0.0	0.0	10.1
	Verif.2	0.0	0.2	7.6	2.4	0.0	0.0	0.0	0.0	0.0	
	Average	0.0	0.3	8.9	3.1	0.0	0.0	0.0	0.0	0.0	
Sand 2	Verif.1	0.0	0.1	5.8	11.6	0.3	0.0	0.0	0.0	0.0	11.6
	Verif.2	0.0	0.1	5.8	6.2	0.3	0.0	0.0	0.0	0.0	
	Average	0.0	0.1	5.8	8.9	0.3	0.0	0.0	0.0	0.0	
Sand 3	Verif.1	0.0	0.0	1.7	4.8	2.5	0.7	0.1	0.0	0.0	10.1
	Verif.2	0.0	0.1	3.8	10.1	3.2	1.4	0.0	0.0	0.0	
	Average	0.0	0.1	2.7	7.5	2.8	1.0	0.0	0.0	0.0	
Sand 4	Verif.1	0.0	0.0	0.0	0.3	2.1	5.1	2.1	0.0	0.0	14.1
	Verif.2	0.0	0.0	0.0	0.3	2.1	14.1	6.3	0.0	0.0	
	Average	0.0	0.0	0.0	0.3	2.1	9.6	4.2	0.0	0.0	

Table 30. Feed rate in various adjustments of the vibratory feeder.

Funnel height (cm)	Vibration intensity (%)	Sand type	Feed rate (g/s)					Mean (g/s)	Difference between sand types 1 and 4 (%)
5	100	Sand 1	192.6	199.1	199.7	203.4	195.7	198.1	20.8
		Sand 4	161.8	164.9	169.0	162.8	161.4	164.0	
	90	Sand 1	137.4	134.8	133.6	136.1	141.0	136.6	19.4
		Sand 4	116.1	113.1	113.3	115.3	114.1	114.4	
	80	Sand 1	117.1	121.7	117.5	118.1	118.4	118.5	12.9
		Sand 4	103.6	104.9	106.3	105.5	104.5	105.0	
4	100	Sand 1	148.5	145.8	144.1	147.2	146.7	146.4	23.5
		Sand 4	119.4	121.4	122.1	111.9	118.1	118.6	
	90	Sand 1	122.7	125.4	123.4	120.6	122.8	123.0	12.8
		Sand 4	108.6	108.6	108.4	110.3	109.2	109.0	
	80	Sand 1	105.0	103.7	104.7	103.7	105.1	104.5	7.9
		Sand 4	96.1	97.6	96.1	97.2	96.9	96.8	
3	100	Sand 1	120.8	121.7	120.3	117.2	118.3	119.6	16.7
		Sand 4	101.3	102.1	103.3	104.1	101.9	102.5	
	90	Sand 1	110.6	108.3	109.4	112.2	110.7	110.2	15.4
		Sand 4	95.6	96.5	95.1	95.7	94.8	95.6	
	80	Sand 1	93.3	90.0	96.1	94.7	93.0	93.4	10.8
		Sand 4	83.0	84.6	85.7	84.6	83.7	84.3	

Table 31. Absolute differences at optimum adjustment of the feeder.

Grain size (µm)		63	125	250	500	1000	2000	4000	5600	8000	Max.
Sand 1	Verif.1	0.0	0.4	9.8	2.8	0.0	0.0	0.0	0.0	0.0	9.8
	Verif.2	0.0	0.4	4.5	4.8	0.0	0.0	0.0	0.0	0.0	
	Average	0.0	0.4	7.2	3.8	0.0	0.0	0.0	0.0	0.0	
Sand 2	Verif.1	0.0	0.3	11.3	6.0	0.3	0.0	0.0	0.0	0.0	11.3
	Verif.2	0.0	0.3	9.0	6.5	0.4	0.0	0.0	0.0	0.0	
	Average	0.0	0.3	10.2	6.2	0.3	0.0	0.0	0.0	0.0	
Sand 3	Verif.1	0.0	0.3	9.3	3.6	0.3	4.1	2.0	0.0	0.0	9.3
	Verif.2	0.0	0.2	0.1	4.4	1.1	8.6	5.3	0.0	0.0	
	Average	0.0	0.2	4.7	4.0	0.7	6.4	3.6	0.0	0.0	
Sand 4	Verif.1	0.0	0.0	1.2	10.4	21.6	24.1	5.7	0.0	0.0	24.1
	Verif.2	0.0	0.0	0.4	6.5	12.4	20.1	8.6	0.0	0.0	
	Average	0.0	0.0	0.8	8.4	17.0	22.1	7.1	0.0	0.0	

Table 32. Absolute differences from the design parameters of the prototype.

Grain size (µm)		63	125	250	500	1000	2000	4000	5600	8000	Max.
Sand 1	Verif.1	0.0	0.1	3.7	2.5	0.1	0.0	0.0	0.0	0.0	3.7
	Verif.2	0.0	0.2	2.6	1.6	0.1	0.0	0.0	0.0	0.0	
	Average	0.0	0.1	3.1	2.1	0.1	0.0	0.0	0.0	0.0	
Sand 2	Verif.1	0.0	0.1	1.2	1.4	0.0	0.0	0.0	0.0	0.0	6.7
	Verif.2	0.0	0.5	6.7	0.1	0.2	0.0	0.0	0.0	0.0	
	Average	0.0	0.3	3.9	0.8	0.1	0.0	0.0	0.0	0.0	
Sand 3	Verif.1	0.0	0.0	0.1	2.0	0.7	0.1	0.0	0.0	0.0	8.4
	Verif.2	0.0	0.2	6.7	8.4	3.9	0.3	0.0	0.0	0.0	
	Average	0.0	0.1	3.4	5.2	2.3	0.2	0.0	0.0	0.0	
0-1 (95-30)	Verif.1	0.0	0.2	1.0	7.4	0.8	0.0	0.0	0.0	0.0	8.7
	Verif.2	0.0	1.0	8.7	2.1	0.1	0.0	0.0	0.0	0.0	
	Average	0.0	0.6	4.9	4.7	0.5	0.0	0.0	0.0	0.0	
0-2 (85-20)	Verif.1	0.0	0.1	1.2	0.1	0.3	0.1	0.0	0.0	0.0	5.0
	Verif.2	0.0	0.0	2.5	5.0	2.0	0.5	0.0	0.0	0.0	
	Average	0.0	0.1	1.9	2.6	1.2	0.3	0.0	0.0	0.0	
0-2 (80-10)	Verif.1	0.0	0.5	8.8	7.1	1.5	0.1	0.0	0.0	0.0	8.8
	Verif.2	0.0	0.2	4.6	2.4	0.7	0.0	0.0	0.0	0.0	
	Average	0.0	0.4	6.7	4.8	1.1	0.1	0.0	0.0	0.0	

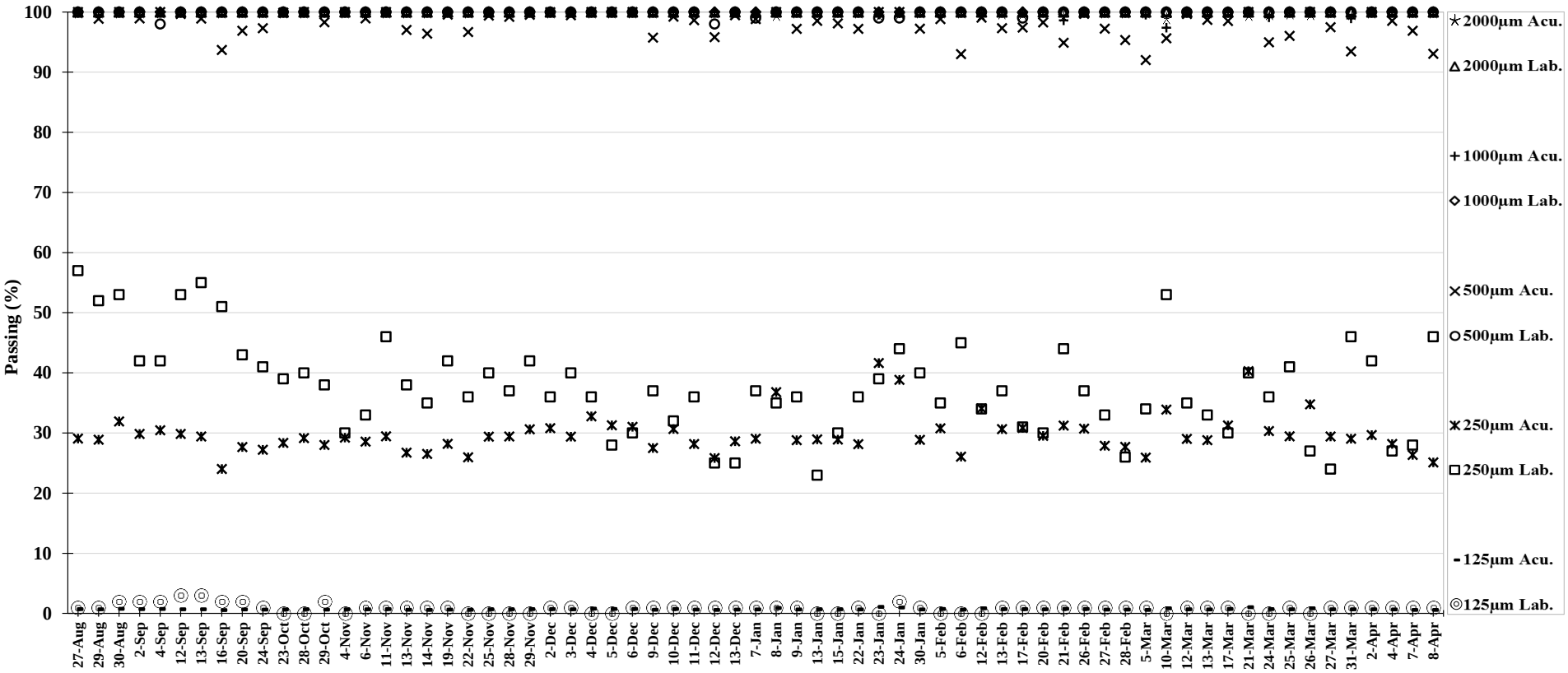

Figure 79. Comparing the results from sieving (Lab.) and prototype (Acu.) through full cross validation for sand 1.

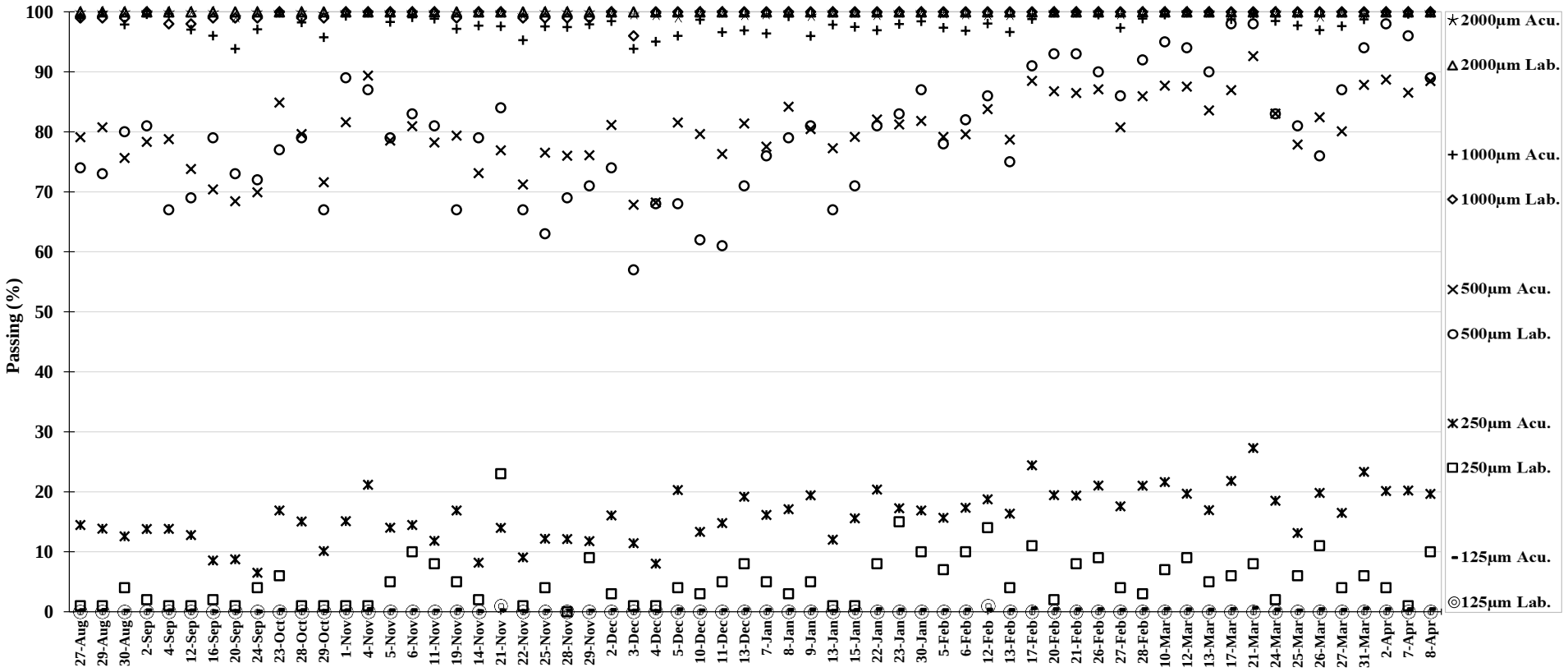

Figure 80. Comparing the results from sieving (Lab.) and prototype (Acu.) through full cross validation for sand 2.

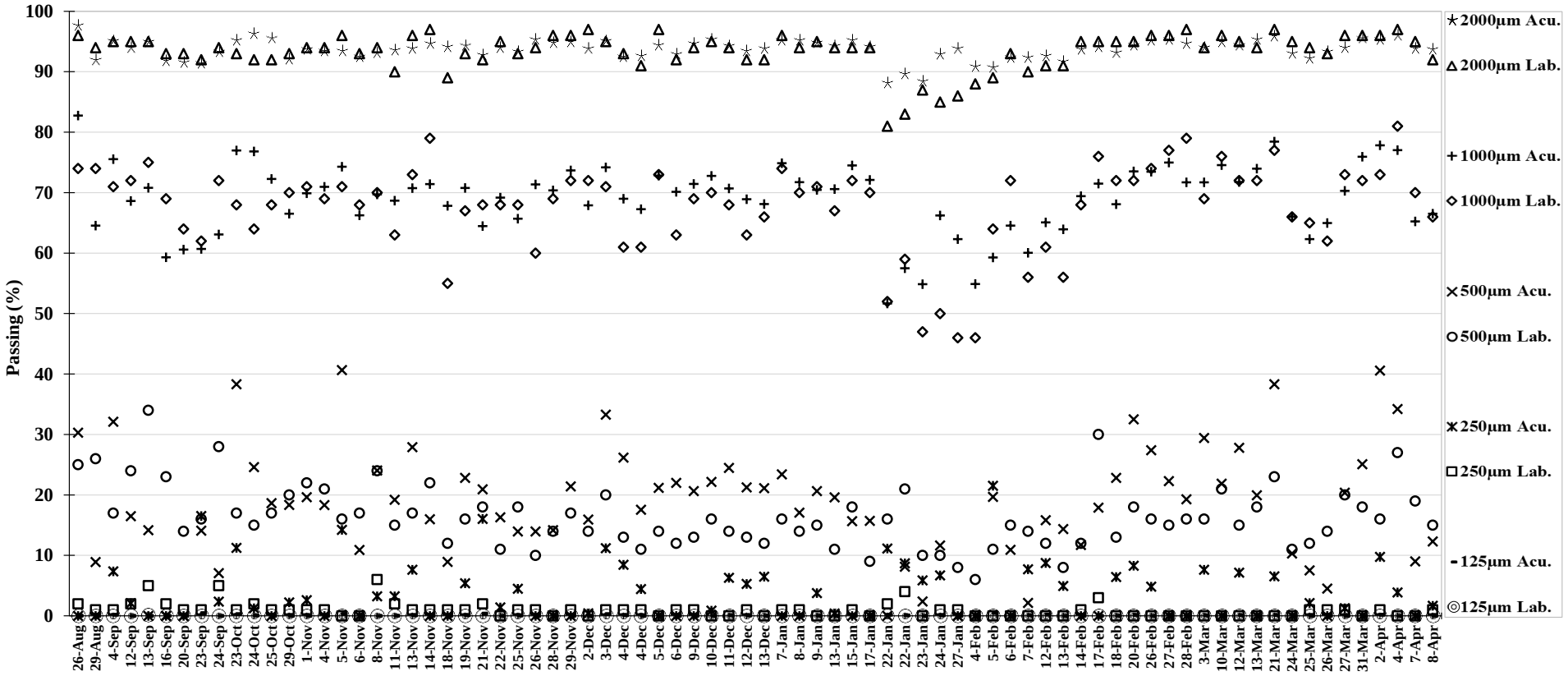

Figure 81. Comparing the results from sieving (Lab.) and prototype (Acu.) through full cross validation for sand 3.

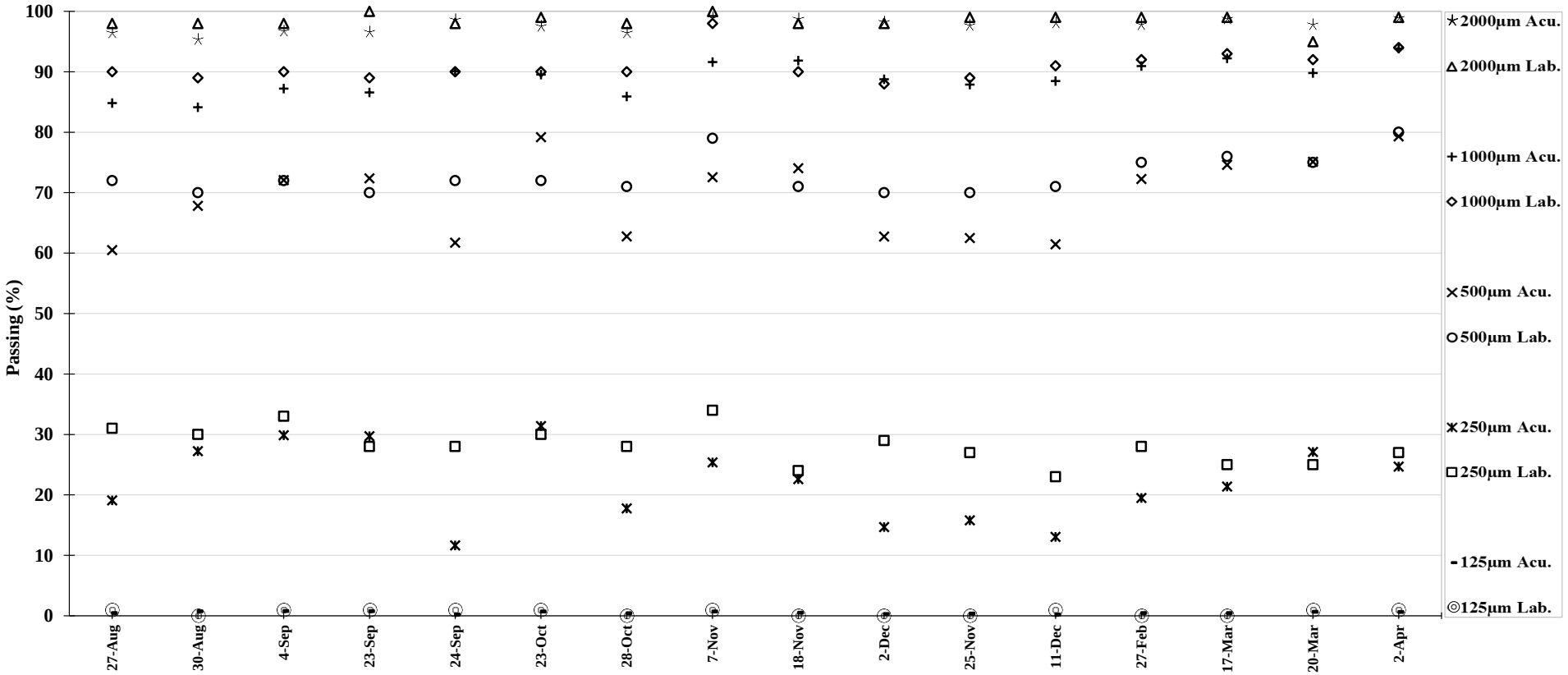

Figure 82. Comparing the results from sieving (Lab.) and prototype (Acu.) through full cross validation for mixture 0-1 (95-30).

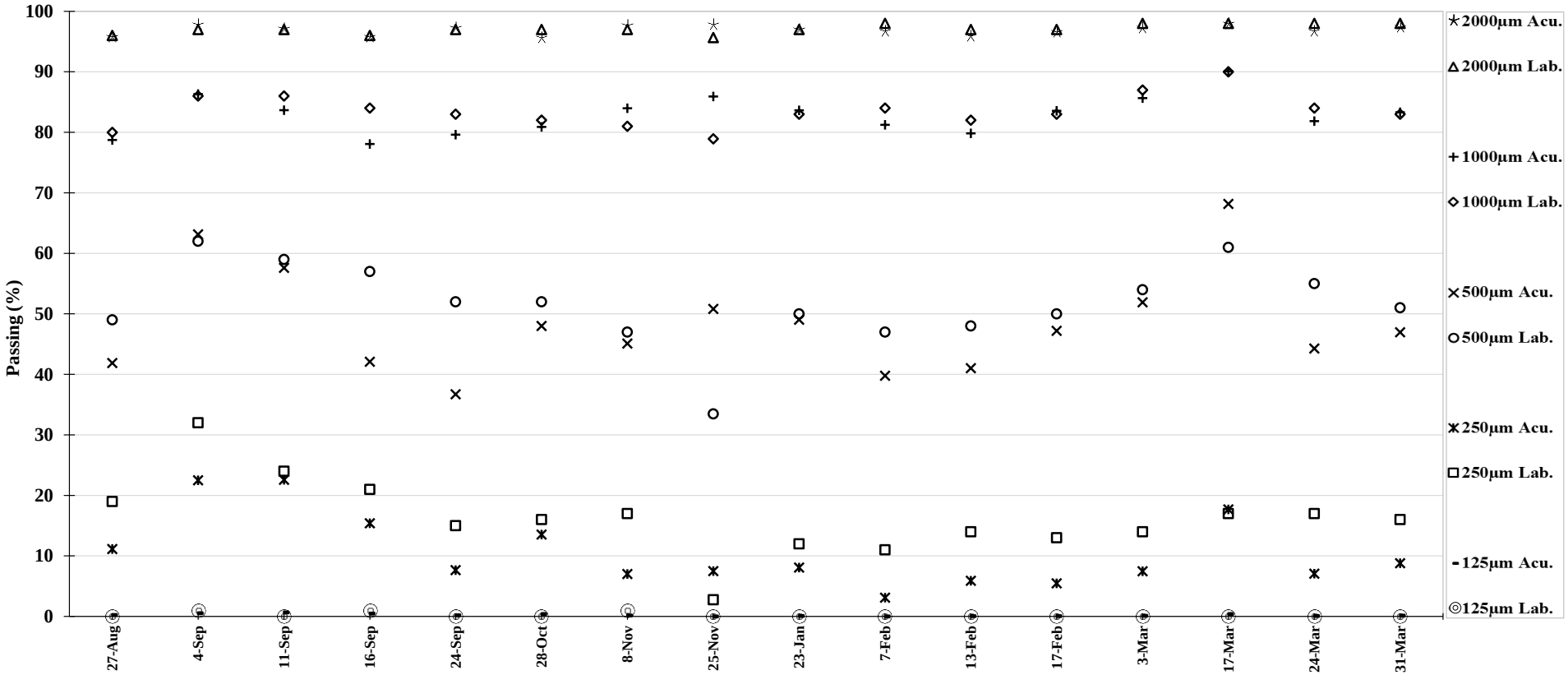

Figure 83. Comparing the results from sieving (Lab.) and prototype (Acu.) through full cross validation for mixture 0-2 (85-20).

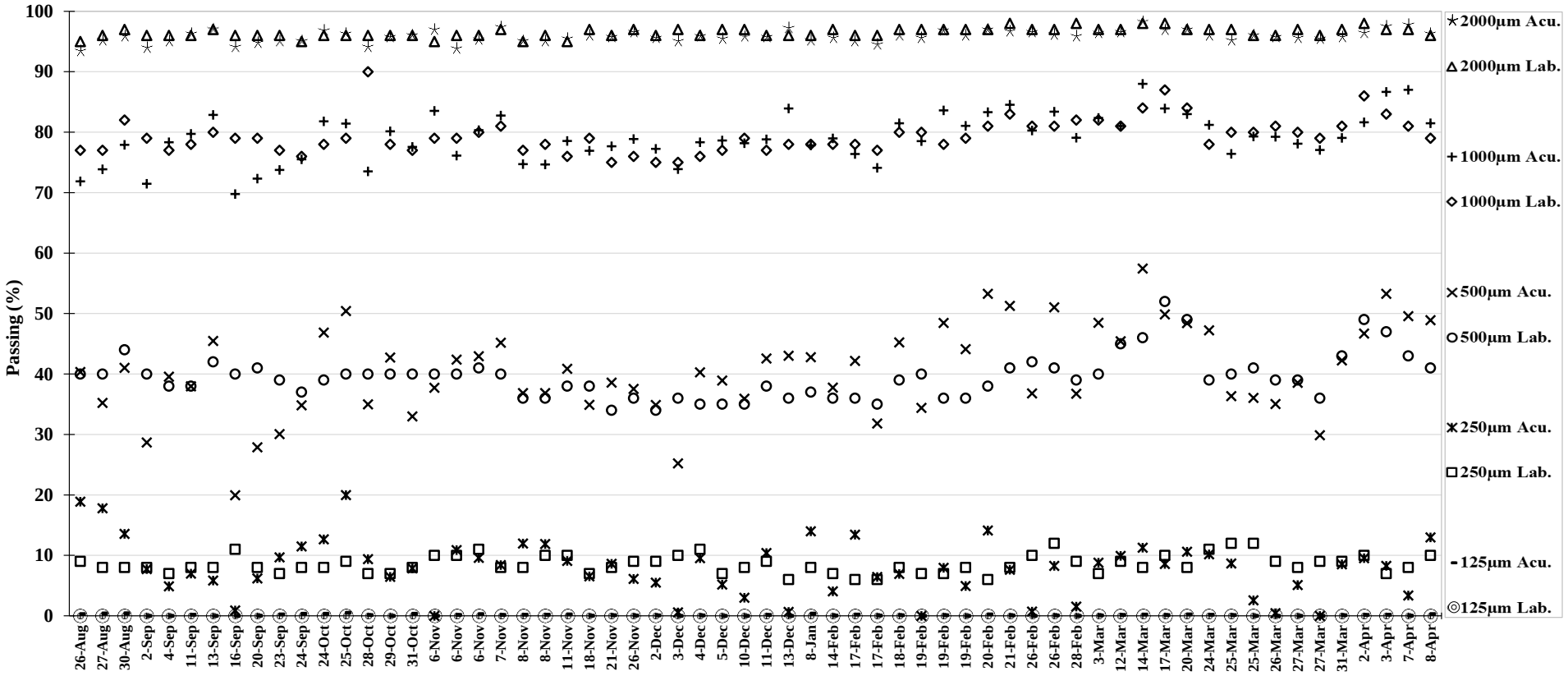

Figure 84. Comparing the results from sieving (Lab.) and prototype (Acu.) through full cross validation for mixture 0-2 (80-10).

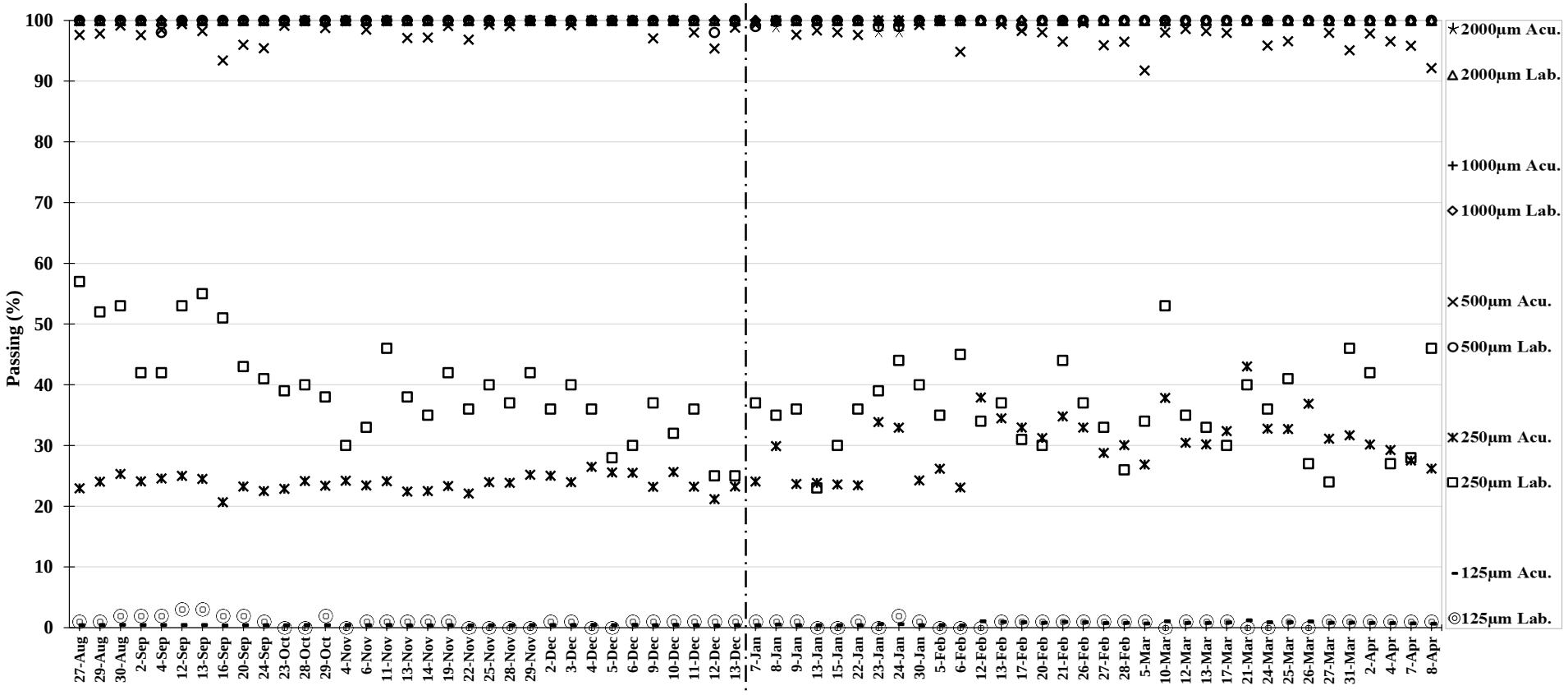

Figure 85. Comparing the results from sieving (Lab.) and prototype (Acu.) through data-splitting for sand 1.

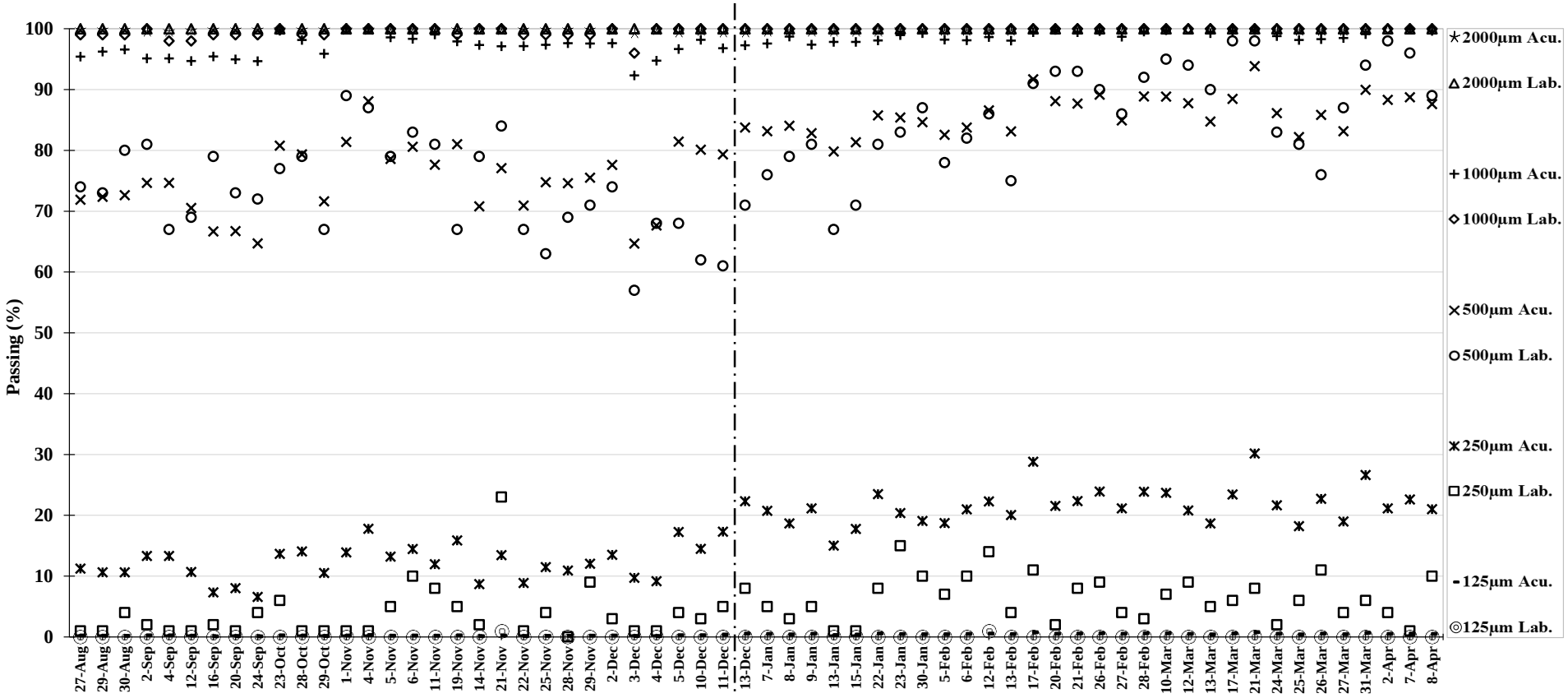

Figure 86. Comparing the results from sieving (Lab.) and prototype (Acu.) through data-splitting for sand 2.

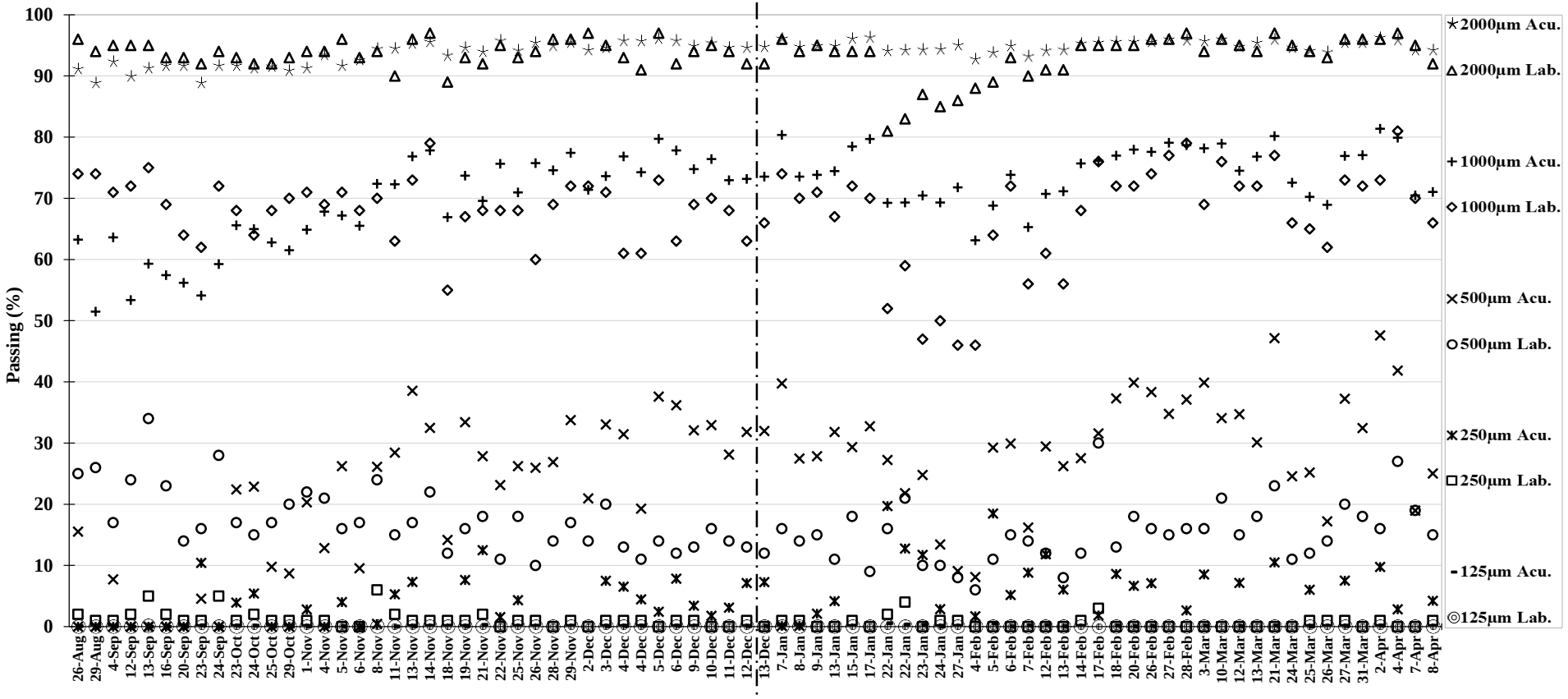

Figure 87. Comparing the results from sieving (Lab.) and prototype (Acu.) through data-splitting for sand 3.

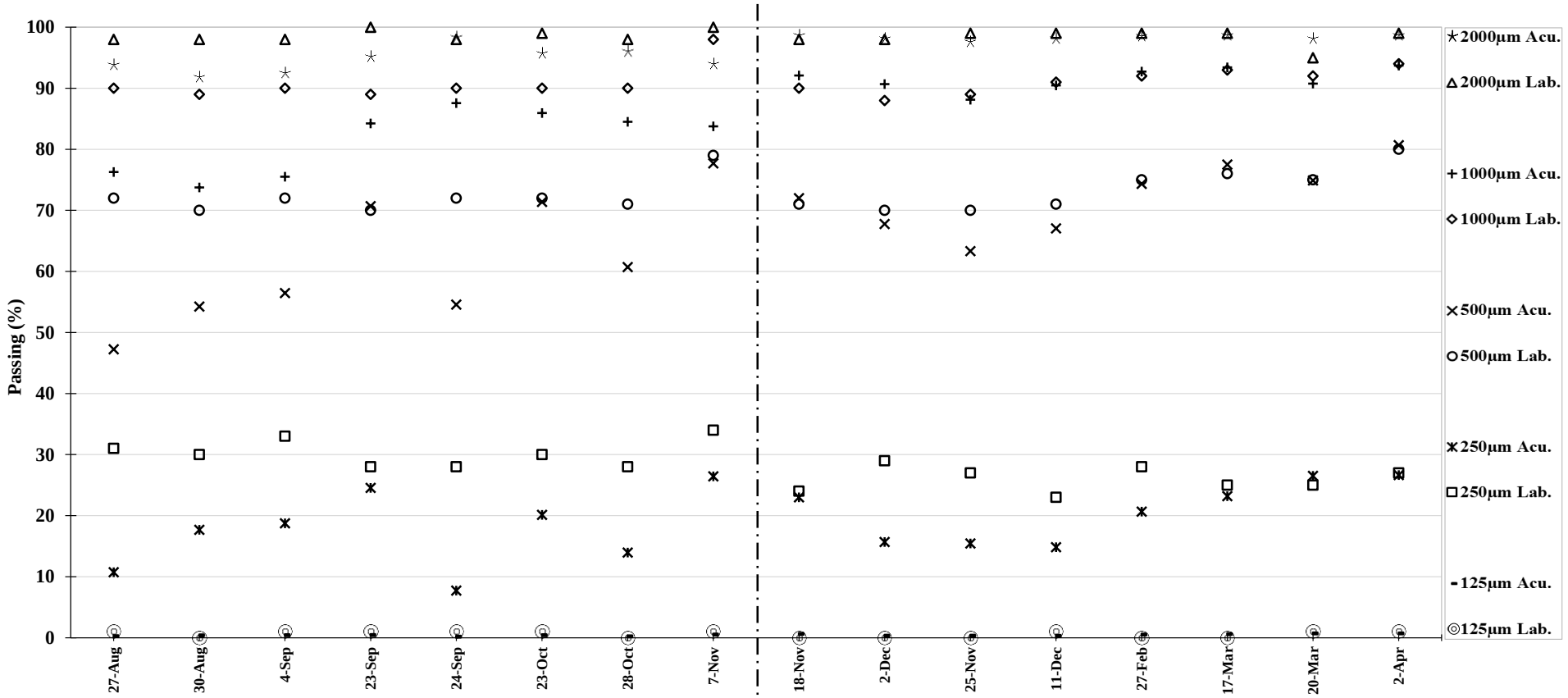

Figure 88. Comparing the results from sieving (Lab.) and prototype (Acu.) through data-splitting for mixture 0-1 (95-30).

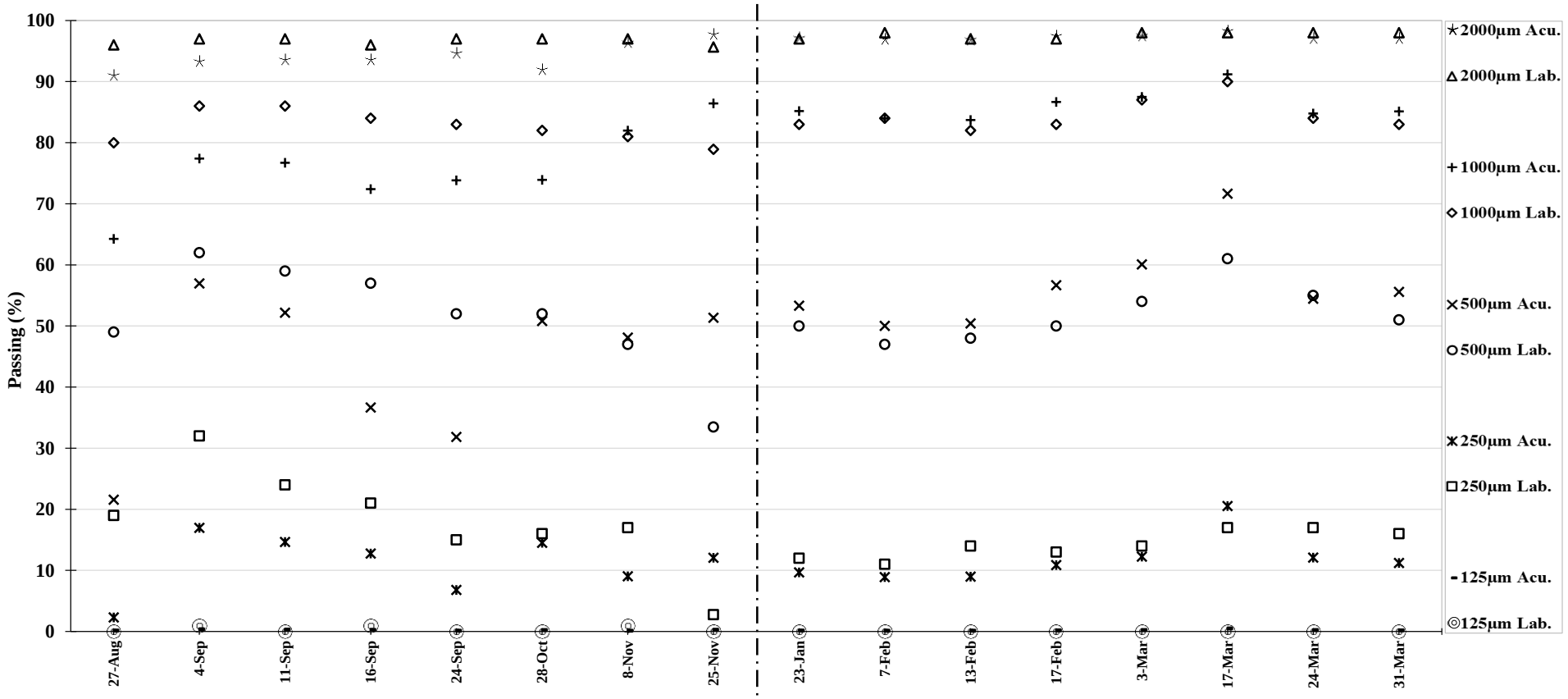

Figure 89. Comparing the results from sieving (Lab.) and prototype (Acu.) through data-splitting for mixture 0-2 (85-20).

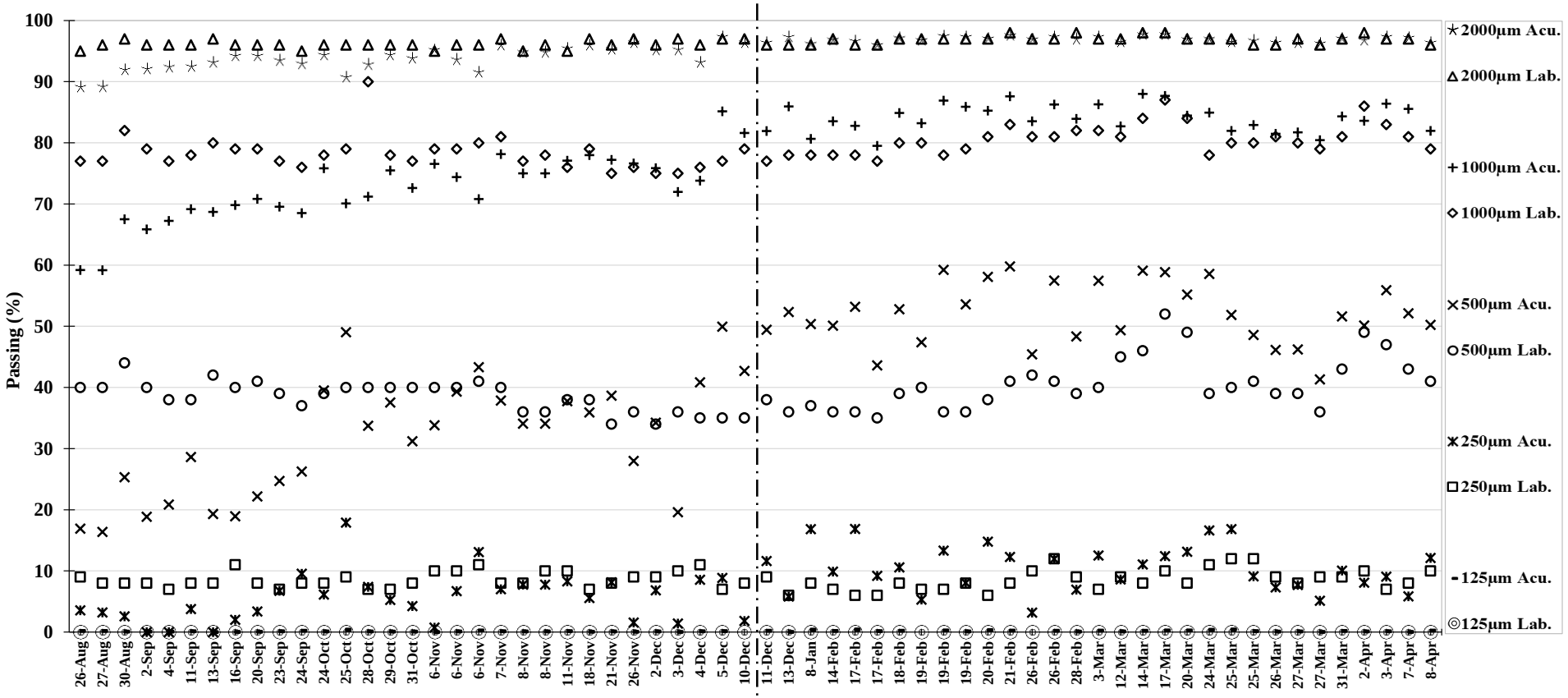

Figure 90. Comparing the results from sieving (Lab.) and prototype (Acu.) through data-splitting for mixture 0-2 (80-10).

References

[1] Jaeger H. M., Nagel S. R. and Behringer R. P., "Granular solids, liquids, and gases," *Reviews of Modern Physics*, vol. 68, no. 4, pp. 1259-73, 1996.

[2] de Gennes P. G., "Granular matter: a tentative view," *Reviews of Modern Physics*, vol. 71, no. 2, pp. 374-82, 1999.

[3] "Industrieverband Steine und Erden e. V., Neustadt/Weinstraße, Fachabteilung Kies und Sand Hessen - Rheinland-Pfalz," [Online]. Available: http://www.verband-steine-erden.de. [Accessed 10 2014].

[4] "Bundesverband Mineralische Rohstoffe e. V.," [Online]. Available: http://www.bv-miro.org/index.php/unsere-industrie.html. [Accessed 4 2015].

[5] Gliński J., Horabik J. and Lipiec J., Encyclopedia of Agrophysics, Springer Science & Business Media, 2011.

[6] Jillavenkatesa A., Dapkunas S. J. and Lin-Sien L., Particle size characterization, NIST special publication 960-1, 2001.

[7] DIN Deutsches Institut für Normung e. V., Baugrund, Untersuchung von Bodenproben – Bestimmung der Korngrößenverteilung, DIN 18123, 2011.

[8] HORIBA Instruments Inc., A guidebook to particle size analysis, 2012.

[9] "Malvern Instruments Ltd. Morphologi G3," [Online]. Available: http://www.malvern.com/en/products/product-range/morphologi-range/morphologi-g3/. [Accessed 07 2015].

[10] "HORIBA, Ltd. PSA300," [Online]. Available: http://www.horiba.com/scientific/products/particle-characterization /particle-size-analysis/details/psa300-604/. [Accessed 07 2015].

[11] "Retsch Technology. CAMSIZER® P4," [Online]. Available: http://www.retsch-technology.com/rt/products/dynamic-image-analysis/camsizer-p4/function-features/. [Accessed 07 2015].

[12] "Retsch Technology. CAMSIZER® XT," [Online]. Available: http://www.retsch-technology.com/rt/products/dynamic-image-analysis/camsizer-xt/function-features/. [Accessed 07 2015].

[13] Nicholas J. B., Hyon-Sohk O., Yong Sub J. and Hryciw R. D., "A review of commercial systems for determination of soil particle size distributions," Department of Civil and Environmental Engineering, University of Michigan, Ann Arbor, MI, 2011.

[14] "Malvern Instruments Ltd. Sysmex FPIA3000," [Online]. Available: http://www.malvern.com/en/products/product-range/sysmex-fpia-3000/. [Accessed 07 2015].

[15] "Sympatec GmbH. System-Partikel-Technik. QICPIC/R," [Online]. Available: https://www.sympatec.com/EN/ImageAnalysis/QICPIC-R.html. [Accessed 07 2015].

[16] "Malvern Instruments Ltd. Mastersizer range," [Online]. Available: http://www.malvern.com/en/products/product-range/mastersizer-range/default.aspx. [Accessed 07 2015].

[17] "Sympatec GmbH. System-Partikel-Technik. HELOS.," [Online]. Available: https://www.sympatec.com/EN/LaserDiffraction/HELOS.html. [Accessed 07 2015].

[18] "Beckman Coulter, Inc. Laser Diffraction Particle Size Analyzers," [Online]. Available: Beckman Coulter, Inc.. [Accessed 07 2015].

[19] "HORIBA, Ltd. Laser Particle Size Analyzer," [Online]. Available: http://www.horiba.com/scientific/products/particle-characterization/particle-size-analysis/. [Accessed 07 2015].

[20] Stojanovic Z. and Markovic S., "Determination of particle size distributions by laser diffraction," *TECHNICS - NEW MATERIALS*, vol. 21, pp. 11-20, 2012.

[21] Kelly R. N. and Etzler F. M., „What is wrong with laser diffraction,“ *A critical review of current laser diffraction methods for particle size analysis*, Undated.

[22] Mills David, Pneumatic conveying design guide, Elsevier Butterworth-Heinemann, 2004.

[23] G.E. Klinzing, F. Rizk, R. Marcus, L.S. Leung, Pneumatic Conveying of Solids: A theoretical and practical approach, Springer Science & Business Media, 2013.

[24] Crowe C. T., Schwarzkopf J. D., Sommerfeld M. and Tsuji Y., Multiphase flows with droplets and particles, Second ed., CRC Press, 2011.

[25] Jain S. D. and Sahasrabudhe G. G., Engineering Physics, Universities Press, 2010.

[26] Vorländer M., "Handbook of Engineering Acoustics," Springer-Verlag Berlin Heidelberg, 2013.

[27] "National Instruments: Acoustic measurements," [Online]. Available: https://www.ni.com/devzone/encyclopedia/acoustics_measure.htm#measurements [Accessed 07 2015].

[28] Albion K., Briens L., Briens C. and Berruti F., "Flow regime determination in horizontal pneumatic transport of fine powders using non-intrusive acoustic probes," *Powder Technology,* vol. 172, pp. 157-66, 2007.

[29] Boyd J. W. R. and Varley J., "The uses of passive measurement of acoustic emissions from chemical engineering processes," *Chemical Engineering Science,* vol. 56, pp. 1749-67, 2001.

[30] Hou R., Acoustic monitoring of particulate processes, University of Exeter: PhD Thesis, 1998.

[31] McLaskey G. C., Stress wave source characterization: impact, fracture, and sliding friction, University of California, Berkeley: PhD Thesis, Spring 2011.

[32] Bastari A., Cristalli C., Morlacchi R. and Pomponi E., "Acoustic emissions for particle sizing of powders through signal processing techniques," *MechanicalSystemsandSignalProcessing,* vol. 25, pp. 901-16, 2011.

[33] Halstensen M. and Esbensen K., "New developments in acoustic chemometric prediction of particle size distribution—‘the problem is the solution’," *J. Chemometrics*, vol. 14, pp. 463-81, 2000.

[34] "Merrian-Webster dictionary: Definition of signal," [Online]. Available: http://www.merriam-webster.com/dictionary/signal. [Accessed 07 2015].

[35] I. PCB Group, "Sensing Geometries for Piezoelectric Accelerometers.," [Online]. Available: http://www.pcb.com/Accelerometers /Sensing_Geometries.aspx. [Accessed 07 2015].

[36] "Honeywell Sensotec: Frequently Asked Questions," [Online]. Available: http://www.alliantech.com/pdf/technique/questions_courantes_capteurs.pdf. [Accessed 07 2015].

[37] Wagner J. and Burgemeister J., Piezoelectric accelerometers: Theory and application, Radebeul, Germany: Metra Mess- und Frequenztechnik in Radebeul e.K., 2012.

[38] "National Instruments Corporation. What Is Data Acquisition?," [Online]. Available: http://www.ni.com/data-acquisition/what-is/. [Accessed 07 2015].

[39] Nyquist H., "Certain topics in telegraph transmission theory," *Trans. AIEE,* vol. 47, pp. 617-44, 1928.

[40] "Nyquist–Shannon sampling theorem, From Wikipedia," [Online]. Available: https://en.wikipedia.org/wiki/Nyquist-Shannon_sampling_theorem. [Accessed 04 2015].

[41] Dhodapkar S. V. and Klinzing G. E., "Pressure fluctuations in pneumatic conveying systems," *Powder Technology,* vol. 74, pp. 179-95, 1993.

[42] Crocker M. J., Handbook of Acoustics, John Wiley & Sons, 1998.

[43] "Gracey & Associates, Acoustic Glossary, Sound and Vibration : Definitions, Terms, Units and Parameters," [Online]. Available: http://www.acoustic-glossary.co.uk/definitions-e.htm#exponential. [Accessed 10 2014].

[44] Jacobsen F., Poulsen T., Holger Rindel J., Gade A. C. and Ohlrich M., Fundamentals of acoustics and noise control, Department of Electrical Engineering, Technical University of Denmark, September 2011.

[45] Brüel & Kjær Sound & Vibration Measurement A/S., "Measuring Sound," September 1984. [Online]. Available: http://www.bksv.com/doc/br0047. pdf. [Accessed 10 2014].

[46] "Signal-to-noise ratio, From Wikipedia, the free encyclopedia," [Online]. Available: https://en.wikipedia.org/title=Signal-to-noise_ratio [Accessed 06 2015].

[47] Drongelen W. V., Signal processing for neuroscientists: An introduction to the analysis of physiological signals, Academic Press, 2006.

[48] Rahman M., Applications of Fourier Transforms to Generalized Functions, Southampton, UK: WIT Press, 2011.

[49] "Music Technology, Schulich School of Music, McGill Uni. Music & Audio Computing II," [Online]. Available: http://www.music.mcgill.ca/ gary/307/week1/spectra.html. [Accessed 4 2015].

[50] Cooley J. W. and Tukey J. W., "An algorithm for the machine calculation of complex Fourier series," *Math. Comput.,* vol. 19, pp. 297-301, 1965.

[51] Björk A., Chemometric and signal processing methods for real time monitoring and modeling using acoustic sensors. Applications in the pulp and paper industry, Royal Institute of Technology, Stockholm, Sweden: PhD Thesis, 2007.

[52] Strang G., "Wavelets," *American Scientist,* vol. 82, pp. 250-55, 1994.

[53] Heideman M. T., Johnson D. H. and Burrus C. S., "Gauss and the history of the fast Fourier transform," *IEEE ASSP Magazine,* vol. 1, pp. 14-21, 1984.

[54] National Instruments Corporation, National Instruments. LabView Measurements Manual, Austin, Texas, USA, 2000.

[55] Julius Orion Smith III, Introduction to Digital Filters with Audio Applications., Center for Computer Research in Music and Acoustics (CCRMA), Stanford University, 2007.

[56] "p-value, From Wikipedia, the free encyclopedia," [Online]. Available: http://en.wikipedia.org/wiki/P-value#Calculation. [Accessed 1 2015].

[57] "The Michigan Chemical Process Dynamics and Controls Open Text Books; Basic statistics: mean, median, average, standard deviation, z-scores, and p-value," [Online]. Available: https://controls.engin.umich.edu/wiki/index.php/ [Accessed 1 2015].

[58] "Cengage Learning EMEA: Computing p-Values Using Minitab and Excel," [Online]. Available: http://www.cengage.com/resource_uploads/downloads [Accessed 1 2015].

[59] "MINITAB® 17 SUPPORT, What is a p-value?," [Online]. Available: http://support.minitab.com/en-us/minitab/17/topic-library/basic-statistics-and-graphs/introductory-concepts/p-value-and-significance-level/what-is-pvalue/. [Accessed 1 2015].

[60] Wold S., Ruhe A., Wold H. and Dunn W.J., "The collinearity problem in linear regression: the partial least squares (PLS) approach to generalized inverses," *SIAM Journal on Scientific and Statistical Computing,* vol. 5, no. 3, p. 735–743, 1984.

[61] Geladi P. and Kowalski B. R., „Partial Least-Squares Regression: a tutorial," *Analytica Chimica Acta,* Bd. 185, pp. 1-17, 1986.

[62] Martens H. and Næs T., Multivariate Calibration, Wiley, 1989, p. 700.

[63] S. de Jong and A. Phatak, "Partial least squares regression," *Recent advances in total least squares techniques and errors-in-variables modeling,* pp. 311-338, 1997.

[64] I. S. Helland, "On the structure of partial least squares regression," *Communications in Statistics - Simulation and Computation,* vol. 17, no. 2, pp. 581-607, 1988.

[65] S. d. Jong, "SIMPLS: An alternative approach to partial least squares regression," *Chemometrics and Intelligent Laboratory Systems,* vol. 18, no. 3, pp. 251-263, 1993.

[66] K. H. Esbensen, D. Guyot, F. Westad and L. P. Houmoller, Multivariate Data Analysis - in Practice: An Introduction to Multivariate Data Analysis and Experimental Design, Camo Process AS, 2002, p. 598.

[67] S. Wold, M. Sjöström and L. Eriksson, "PLS-regression: a basic tool of chemometrics," *Chemometrics and Intelligent Laboratory Systems,* vol. 58, pp. 109-130, 2001.

[68] Lannsjö Fredrik, Forecasting the Business Cycle using Partial Least Squares, Department of Mathematics, KTH, Stockholm: PhD Thesis, 2014.

[69] D. Broadhursta, R. Goodacrea, A. Jonesa, J. J. Rowlandb and D. B. Kell, „Genetic algorithms as a method for variable selection in multiple linear regression and partial least squares regression, with applications to pyrolysis mass spectrometry,“ *Analytica Chimica Acta,* Bd. 348, pp. 71-86, 1997.

[70] B. Xi, H. Gu, H. Baniasadi and D. Raftery, "Statistical Analysis and Modeling of Mass Spectrometry-Based Metabolomics Data," *Methods Mol Biol.,* vol. 1198, pp. 333-353, 2014.

[71] H. Martens, "Determining rank and evaluating performance in regression: independent test sets or cross-validation/cross-regression?," *Proceedings,*, pp. 15-44, 1997.

[72] H. A. Martens and P. Dardenne, "Validation and verification of regression in small data sets," *Chemometrics and Intelligent Laboratory Systems,* vol. 44, p. 99–121, 1998.

[73] Sehroeder L. D., Sjoquist D. L. and Stephan P. E., Understanding regression analysis: An introductory guide, Newbury Park, CA: SAGE Publications, 1986.

[74] Agnew D. and Constable C., Class notes, Geophysical data analysis: Part I, Ch.7, Cecil H. and Ida M. Green Institute of Geophysics and Planetary Physics; University of California, San Diego, Fall 2008.

[75] Andren T., Econometrics - Part II, bookboon.com, 2008.

[76] Drouillard T. F., "A history of acoutsic emission," *Journal of acoustic emission*, vol. 14, no. 1, 1996.

[77] Belchamber R. M., Betteridge D., Collins M. P., Lilley T., Marczewski C. Z. and Wade A. P., "Quantitative Study of Acoustic Emission from a Model Chemical Process," *Anal. Chem.*, vol. 58(8), pp. 1873-77, 1986.

[78] Zeng Y. and Forssberg E., "Effects of Operating Parameters on Vibration Signal under Laboratory Scale Ball Grinding Conditions," *Inter. J. Min. Proc.*, vol. 35, pp. 273-90, 1992.

[79] Zeng Y. and Forssberg E., "Monitoring grinding parameters by signal measurements for an industrial ball mill," *Inter. J. Min. Proc.*, vol. 40, pp. 1-16, 1993.

[80] Williams R. A., Peng S. J., Brown D., Parkinson N. and James P.,, "On-line measurement of hydrocyclone performance using acoustic emission," in *Hydrocyclones '96*, London, 1996.

[81] Esbensen K. H., Lied T. T., Halstensen M., Saudland A., Svalestuen J. and De Silva S., "Acoustic Chemometrics – From Noise to Information," in *Proceedings of 1st International Symposium on On-line Flow Measurement of Particulate Solids*, University of Greenwich, Chatham, UK, 1998.

[82] Esbensen K. H., Halstensen M., Lied T. T., Saudland A., Svalestuen J., de Silva S. R. and Hope B., "Acoustic chemometrics—from noise to information," *Chemometrics Intell. Lab. Syst.*, vol. 44, p. 61–76, 1998.

[83] Elsey J., Barton G. W., Jungk S., Francis G., Sellahewa J. and Chessari C., "Acoustics based on-Line quality estimation," *Computers them. Engng*, vol. 22, pp. S925-28, 1998.

[84] Houlsby G. T. and Ruck B. M., "Interpretation of Signals from an Acoustic Cone Penetrometer," in *Geotechnical Site Characterization*, Balkema, Rotterdam, 1998.

[85] Aldrich C. and Theron D. A., "Acoustic estimation of the particle size distributions of sulphide ores in a laboratory ball mill," *The Journal of The South African Institute of Mining and Metallurgy*, vol. JULY/AUGUST, pp. 243-48, 2000.

[86] Huang J., Ose S., de Silva S. and Esbensen K. H., "Non-invasive monitoring of powder breakage during pneumatic transportation using acoustic chemometrics," *Powder Technology*, vol. 129, pp. 130-38, 2003.

[87] Björk A. and Danielsson L. G., "Extraction of distribution curves from process acoustic measurements on a TMP-process," vol. 105:11, pp. 42-6, 2004.

[88] Björk A. and Danielsson L. G. , "Predicting pulp quality from process acoustic measurements on a medium concistency pulp stream," *Journal of Process Analytical Chemistry,* vol. 10, pp. 1-5, 2006.

[89] Albion K., Briens L., Briens C., Berruti F. and Book G., "Flow regime determination in upward inclined pneumatic transport of particulates using non-intrusive acoustic probes," *Chem. Eng. Process.,* vol. 46, pp. 520-31, 2007.

[90] Bruwer M. J., MacGregor J. F. and Bourg W. M., "Soft sensor for snack food textural properties using on-line vibrational measurements," *Indust. Eng. Chem. Res.,* vol. 45, pp. 864-70, 2007.

[91] Daniher D., Briens L. and Tallevi A., "End-point detection in high-shear granulation using sound and vibration signal analysis," *Powder Technology,* vol. 181, p. 130–36, 2008.

[92] Briens L., Smith R. and Briens C., "Monitoring of a rotary dryer using acoustic emissions," *Powder Technol.,* vol. 181, pp. 115-20, 2008.

[93] Tudeshki H. and Hertel H., „Entwicklung eines akustischen Verfahrens zur echtzeitnahen Detektion von Lockergesteinen und Grenzflächen für die selektive Gewinnungstechnik,“ *Aggregates Int.,* Bd. 3, pp. 18-23, 2008.

[94] Tudeshki H. and Hertel H., "Der akustische Geo-Scanner für die selektive Gewinnung von Kies und Sand," *AMS Online,* vol. 04, pp. 28-34, 2009.

[95] Tudeshki H., Hertel H. and John H. J., „Baugrunderkundung mittels akustischem GeoScanner,“ *bbr Leitungsbau|Brunnenbau|Geothermie,* pp. 40-45, 02 2012.

[96] Albion K., Briens L., Briens C. and Berruti F., "Detection of oversized material in a hydrotransport slurry pipe using a non-invasive acoustic method," *Powder Technology,* vol. 190, pp. 361-71, 2009.

[97] Albion K., Briens L., Briens C. and Berruti F., "Modelling of oversized material flow through a horizontal hydrotransport slurry pipe to optimize its acoustic detection," *Powder Technology,* vol. 194, pp. 18-32, 2009.

[98] El-Alej M., Mba D., Yan T. and Elforgani M., "Monitoring sand transport characteristics in multiphase flow in horizontal pipelines using acoustic emission technology," *World Academy of Science, Engineering and Technology,* vol. 78, pp. 873-79, 2013.

[99] Ren C., Zhou Y., Wang J. and Yang Y., "Determination of flooding/loading transition using acoustic emission method," *Department of Chemical and Bioglogical Engineering,* 2013.

[100] Ren C., Jiang X., Wang J., Yang Y. and Zhang X., "Determination of critical speed for complete solid suspension using acoustic emission method based on multiscale analysis in stirred tank," *Ind. Eng. Chem. Res.*, vol. 47, p. 5323–27, 2008.

[101] Fowler T. J., "Acoustic Emission Testing of Vessels," *Chem. Eng. Progress,* vol. 84, no. 9, pp. 59-70, 1988.

[102] Fowler T. J., "Chemical Industry Applications of Acoustic Emission," *Materials Evaluation,* vol. 50, no. 7, pp. 875-82, 1992.

[103] Fowler T. J., Blessing J. A., Conlisk P. J. and Swanson T. L., "The MONPAC System," *Journal of Acoustic Emission,* vol. 8, no. 3, pp. 1-8, 1989.

[104] Esbensen K. H., Hope B., Lied T. T., Halstensen M., Gravermoen T. and Sundberg K., "Acoustic chemometrics for fluid flow quantifications—II: a small constriction will go a long way," *J. Chemometrics,* vol. 13, p. 209–23, 1999.

[105] Ihunegbo F. N., Madsen M., Esbensen K. H., Holm-Nielsen J. B. and Halstensen M., "Acoustic chemometric prediction of total solids in bioslurry: A full-scale feasibility study for on-line biogas process monitoring," *Chemometrics and Intelligent Laboratory Systems,* vol. 110, pp. 135-43, 2012.

[106] Wagner C., Ihunegbo F. N., Halstensen M. and Esbensen K. H., "Acoustic chemometrics for material composition quantification in pneumatic conveying — The critical role of representative reference sampling," *Powder Technology,* vol. 237, pp. 506-13, 2013.

[107] Kresta J. V., Marlin T. E. and MacGregor J. F., "Development of inferential process models using PLS," *Computers & Chemical Engineering,* vol. 18, no. 7, p. 597–611, 1994.

[108] "Eggen S., Esbensen K. H. and Halstensen M., Viscosity measurement". United States of America Patent G01N 11/00, 2004.

[109] "Walter T., Kirchhoff J., Held H. D. and Uelhoff L., Apparatus for sorting materials". Germany Patent B07C 5/00, 1997.

[110] Thorne P. D., "The measurement of acoustic noise generated by moving artificial sediments," *J. Acoust. Soc. Am.*, vol. 78, pp. 1013-23, 1985.

[111] Thorne P. D., "Laboratory and marine measurements on the acoustic detection of sediment transport," *J. Acoust. Soc. Am.,* vol. 80, pp. 899-910, 1986.

[112] Rickenmann D. and McArdell B. W., "Continuous measurement of sediment transport in the Erlenbach stream using piezoelectric bedload impact sensors," *Earth Surf. Process. Landforms,* vol. 32, pp. 1362-78, 2007.

[113] Nordon A., Carella Y., Gachagan A., Littlejohn D. and Hayward G.,, "Factors affecting broadband acoustic emission measurements of a heterogeneous reaction," *Analyst,* vol. 131, pp. 323-30, 2006.

[114] "PCB Group, Inc. High frequency, quartz shear ICP® accelerometer, Model: 353B18," [Online]. Available: http://www.pcb.com/ Products.aspx?m=353B18. [Accessed 10 2014].

[115] "National Instruments Corporation, NI LabVIEW 2010 Release Details," [Online]. Available: http://www.ni.com/labview/release-archive/2010/. [Accessed 10 2014].

[116] "imc Meßsysteme GmbH, Software zur Messdatenanalyse - imc FAMOS," [Online]. Available: http://www.imc-berlin.de/produkte/messtechnik-software/imc-famos/. [Accessed 10 2014].

[117] "PCB Group, Inc. High frequency, quartz shear ICP® accelerometer, Model: 352B01," [Online]. Available: http://www.pcb.com/ products.aspx?m=352b01. [Accessed 06 20015].

[118] "TSI, Airflow™ Instruments Micromanometer PVM620," [Online]. Available: http://www.tsi.com/airflow-instruments-micromanometer-pvm620/. [Accessed 10 2014].

[119] "Kärcher, A 2054 Me," [Online]. Available: http://www.kaercher-tirol.com/CPE_Katalog_FH_0021-172_07-2006.pdf. [Accessed 3 2015].

[120] "Fast Fourier Transform (FFT), MATLAB, The MathWorks, Inc.," [Online]. Available: http://de.mathworks.com/help/matlab/math/fast-fourier-transform-fft.html. [Accessed 7 2015].

[121] A. Eliseyev, C. Moro, T. Costecalde, N. Torres, S. Gharbi, C. Mestais, A. L. Benabid and T. Aksenova, "Iterative N-way partial least squares for a binary self-paced brain–computer interface in freely moving animals," *Journal of Neural Engineering,* vol. 8, 2011.

[122] "National Instruments. Accelerometer/Microphone (IEPE), 4-Ch. NI 9234," [Online]. Available: http://sine.ni.com/nips/cds/view/p/lang/en/nid/208802. [Accessed 06 2015].

[123] "Big O notation, From Wikipedia, the free encyclopedia," [Online]. Available: http://en.wikipedia.org/wiki/Big_O_notation. [Accessed 11 2014].

[124] "probe, From Wiktionary, the free dictionary," [Online]. Available: http://en.wiktionary.org/wiki/probe. [Accessed 4 2015].

[125] "Charge-coupled device, From Wikipedia, the free encyclopedia," [Online]. Available: https://en.wikipedia.org/wiki/Charge-coupled_device. [Accessed 07 2015].

[126] Rivas Abud N. A., Discrete and continuum descriptions of shaken granular matter, University of Twente, The Netherlands: PhD Thesis, 2015.

[127] Göncü F., Mechanics of granular materials: constitutive behavior and pattern transformation, Technische Universiteit Delft, The Netherlands: PhD Thesis, 2012.

[128] Aranson I. S. and Tsimring L. S., "Patterns and collective behavior in granular media: Theoretical concepts," *Reviews of Modern Physics*, vol. 78, pp. 641-92, 2006.

[129] Kee Siong Ng, „A Simple Explanation of Partial Least Squares," The Australian National University, Canberra, 2013.

[130] S. Wold, P. Geladi, K. H. Esbensen and J. Öhman, "Multi-way principal components and PLS-analysis," *JOURNAL OF CHEMOMETRICS*, vol. 1, pp. 41-56, 1987.

[131] David W. Nordstokke, Investigating tests for equal variances, THE UNIVERSITY OF BRITISH COLUMBIA, Vancouver, PhD Thesis, 2009.

[132] Lohninger Hans, Teach/Me - Data Analysis: Single User Edition, Springer Berlin Heidelberg, 1999, p. 143.

Lebenslauf

Persönliche Daten

Vorname, Name	Hamid Amrollahi
Geboren am	18. September 1984
Geboren in	Isfahan, Iran

Berufserfahrung

07/2016 – heute	**Projektleiter** arccon Ingenieurgesellschaft mbH, Gelsenkirchen
10/2010 – 07/2015	**Wissenschaftlicher Mitarbeiter** TU Clausthal, Institut für Bergbau

Akademische Ausbildung

10/2010 – 12/2016	**Promotion (Dr.-Ing.)** TU Clausthal, Institut für Bergbau Gesamturteil magna cum laude (sehr gut)
09/2007 – 02/2010	**Masterstudiengang (M.Sc.)** Bergbau Ingenieurwesen-Felsmechanik Technische Universität Isfahan, Fakultät für Bergbauingenieurwesen Abschlussnote 1,7
09/2002 – 02/2007	**Bachelorstudiengang (B.Sc.)** Bergbau Ingenieurwesen-Exploration Technische Universität Isfahan, Fakultät für Bergbauingenieurwesen Abschlussnote 2,3